AIR MOTION AND PRECIPITATION DEVELOPMENT IN SEVERE CONVECTIVE STORMS

by

Keith Anthony Browning
Department of Meteorology, Imperial College.

A Thesis submitted for the degree of Ph.D. in the University of London.

1962

Adde parvum parvo magnus acervus erit

— OVID

ABSTRACT

A case study of the 7 convective storms in S.E. England on 9 July 1959 as seen by radar indicates that the individual convective cells comprising the most intense storms persisted the longest and were the most highly organized, new cells forming intermittently on the right flank of existing cells.

The structure and evolution of one of these cells is analysed in particular detail. This was a large, intense and persistent cell which produced widespread large hail in the Wokingham area. Its longevity indicated the existence of a very persistent circulation, and this is demonstrated to have changed from the usual pulsatory kind of circulation to a quasi-steady one during the 30 minutes for which it was at the height of its intensity. Certain characteristic features exhibited by the radar echo throughout this period form the basis of the derivation of a semi-quantitative three-dimensional model of the air-flow within the cell, in terms of which the growth of the observed hail is satisfactorily explained.

The air-flow within a section along the direction of travel of this cell resembles that often drawn to represent an ordinary cold front: it differs from that in previous storm models mainly in that it implies that in the presence of adequate wind shear the up-and-down-draughts can be maintained continuously without serious interference from opposite sides of the storm. The importance of the shear is supported by the fact that on this occasion the latent instability was slight but the shear strong, whereas on an earlier occasion of

considerable instability and little shear there were only short-lived and unorganized storms with scattered hail.

The growth of hailstones is treated in detail and in particular it is shown that their layer structure is consistent with growth within a steady updraught provided there are small fluctuations in the effective water content. Assuming an exponential spectrum of hail size within the updraught and charge separation by the splintering mechanism it is inferred that the region of strong updraught associated with the growth of the large hail was responsible for a negligible proportion of the total charge separated.

CONTENTS

CONTENTS

INDEX TO FIGURES

INDEX TO FIGURES (CONTINUED)

INDEX TO TABLES

INDEX TO APPENDICES

LIST OF SYMBOLS USED IN CHAPTERS IV AND V

a	heat transfer coefficient
A	maximum cross-sectional area of hailstone normal to airflow
b	mass transfer coefficient
C_D	drag coefficient
D	coefficient of diffusion of water vapour in air
E	efficiency of catch of hailstone for droplets
F ,F_D,F	fractional volume swept out per unit-time by all, dry and wet hailstones respectively.
F_S	rate of ice splinter production per unit volume per unit concentration of droplets in the size-range $25 < r < 50\mu$
g	acceleration due to gravity
K	coefficient of thermal conductivity of air
L_f,L_v	latent heats of fusion and vaporisation of water
L ,L_w	factors which give measure of exponential decrease in particle concentration owing to sweeping up by all/wet hailstones
M	mass of hailstone
m_s, M_s	mass of water shed by a/all hailstone(s) within a unit volume of air during its ascent through a unit height interval.
n	concentration of droplets
N	concentration of hailstones
q	average charge separated when accreted droplet (with $25 < r < 50\mu$) shatters
r	droplet radius
R	radius of a spherical (or spheroidal) hailstone
R_1,R_2,R_3	semi-major axes of an ellipsoidal hailstone
R_c	critical hailstone radius
R_e	the equivalent radius of a spherical hailstone of equal volume
R_f	radius of totally frozen core of hailstone
R_e	Reynolds number
S	ice splinter concentration

t	time
T	ambient temperature
T_s	mean surface temperature of hailstone
U_m	profile of vertical velocity along updraught axis
U_x, U_y, U_z	velocity components of air-flow
V	fall-speed of hailstone
W	liquid water content
X	axis/diameter ratio of oblate spheroid
x_s	mean number of splinters ejected when droplet (with $25 < r < 50\mu$) is accreted by dry hailstone
x, y, z	spacial coordinates
Δ	difference
$\bar{\delta}$	mean density of hailstone
μ	micron
ρ	density of air
ρ_v	vapour density
θ_w	wet-bulb potential temperature
η	dynamic viscosity of air

CHAPTER I

INTRODUCTION

1.1 The aims of the present investigation

In the field of cloud physics good progress has been made towards the understanding of the basic microphysical mechanisms involved (Mason 1957): this has been largely the result of laboratory studies during the last decade. On the other hand meso-scale phenomena such as the overall air motions within clouds are not amenable to control and must be studied either by means of mathematical models or in vivo: because of the difficulties inherent in each of these approaches the study of cloud dynamics is by comparison embryonic. This is especially regrettable since the form of the air motion dominates the parameters which control the microphysical mechanisms, so that a dearth of information concerning the dynamics also implies the impossibility of successfully applying the microphysical knowledge to actual clouds. Owing to their greater variability this problem is most acute in the case of convective clouds.

The mathematical treatment of convection in the presence of static instability has so far proved unrewarding as a description of actual atmospheric convection because of its non-linearity and the consequent inseparability of the variables and because of the importance of external influences in determining its mode of organization. However the determination by direct observation of the nature of the air motion within cumuliform clouds — especially cumulonimbus — has been hardly

any more successful owing to the practical impossibility of obtaining airborne observations with an adequate space-time resolution. In fact, at the present time the only model of the structure and circulation within cumulonimbus which is firmly based upon observation is that obtained in 1947 by the Thunderstorm Project (Byers and Braham, 1949) — and this gives only a qualitative and idealized representation of a so-called typical thunderstorm cell. The authors classify the life cycle of such a cell into three stages depending upon the direction and magnitude of the predominating vertical flow. They are:

1. cumulus stage — characterized by updraught throughout the cell, (duration 10-15 min);
2. mature stage — characterized by the presence of both updraughts and downdraughts at least in the lower half of the cell, (duration 15-30 min); and
3. dissipating stage — characterized by weak downdraughts prevailing throughout the cell, (duration about 30 min).

The primary purpose of the present study is the investigation of individual thunderstorm cells, both in relationship to adjoining cells and with respect to the air-flow within and around them. The air-flow within one such cell is described quantitatively and in sufficient detail to enable the growth of the largest precipitation particles within it to be satisfactorily explained. However, this was only possible by virtue of an important difference between the particular cell studied and those of the Florida and Ohio storms of the Thunderstorm Project. Whereas it is clear from the above classification that

the average duration of cells was only 1 hour, the cell selected for detailed study in the present investigation lasted for more than 3 hours, maintaining a persistent and at times nearly steady circulation. Such an organized form of air-flow is far more amenable to quantitative description than are the confused short-lived draughts, with local maxima and minima, which were encountered by the Thunderstorm Project. The present study indicates that this difference is likely to have been due to the different degrees of wind shear in the environment, a strong shear favouring the maintenance of a persistent convective circulation. Now, the air-flow is the controlling factor in the development of precipitation: however it is itself modified by the precipitation, which plays a vital role in organizing the actual air motion. This it does by producing an energy source and sink within the up-and down-draught respectively, whose relative positions can remain fixed for some time in the event of the establishment of a circulation of the kind featured in this investigation. This finding is likely to stimulate theoretical study of severe storms by suggesting that for a start they may sometimes be regarded as steady-state disturbances.

1.2 The observational procedure

Although radar was utilized to some extent in the Thunderstorm Project, it was used neither quantitatively nor intensively; and indeed their model of the structure and circulation was derived largely without its aid. Mainly owing to the development of a simple technique for enabling weather radars to be operated quantitatively (Atlas and Mossop, 1959) it was possible to utilize this tool to far greater advantage in England during the summer of 1959, with the result that a model of the air-flow within a cumulonimbus has been deduced primarily from the analysis of radar data. As will become clear in the subsequent chapter this has entailed an entirely new method of analysis, unprecedented in its intensitiveness.

The observational work during the summer of 1959 which provided the raw-material for this study involved the use of five radars — two 3.3cm radars, one 4.7cm radar (used as a PPI) and 10cm PPI and RHI radars: their characteristics and modes of operation are given in Table 1.2.1. All were based at the Meteorological Office station at East Hill, near Dunstable (Bedfordshire) and had coverage over most of S.E. England — this being the area of the British Isles most susceptible to summer thunderstorms.

Besides the radar and routine synoptic data, special pilot balloon soundings were made at 31 stations in England between 1400 and 1500 and three afternoon reconnaissances were made by the Meteorological Research Flight. About 1500 voluntary observers, mostly within 100 miles of East Hill, reported on the occurrence of hail according to the code in

Table 1.2.2, and about 100 of these gave rather detailed accounts of the surface weather. On the occasion of the severe storm of 9 July a further 400 reports were obtained by interrogating people living in the storm path and, from 13 of these, samples of hailstones were collected for examination. The positions of all of these observations are shown in Figs. 2.4.1. (i & ii).

Data was collected on all convective storms occurring within radar range during the months of June, July and August, but only those on a particular cell within the severe Wokingham storm of 9 July enabled the deduction of the associated air-flow in any detail. This is because it was the only cell which maintained a circulation which was both extensive and persistently intense enough to enable it to retain the characteristic features (cf. section 2.9) which served as vital clues to the nature of the air-flow. Moreover it was the only cell to produce widespread large hail: this has provided a wealth of constraints upon the form of the air-flow by virtue of the need to construct hailstone trajectories in accordance with the distribution of radar echo intensity, the distribution of hail size at the ground, and the internal structure of the hailstones (cf. Chapter 4).

TABLE 1.2.1

Characteristics and mode of operation of radar on 9 July 1959 at East Hill (51°55'N 00°30'W; National Grid Reference 52(TL) 028 248)

Type	Wave-length cm	Beam-width, degrees Hor.	Vert.	Max. display range (statute mi)	Sweep period sec.	Mode of operation
AN/TPS-10	3.3	2.0	0.7	70	1	Set A: manual following of echo column tops, to obtain their rate of rise. Set B: Manual location of most intense echoes, and intensity measurement by reduction of gain.
MPS-4	4.7	4.0	0.8	140	12	Stepwise again reduction during PP1 sweeps at successive fixed elevations (complete cycle time 20 min)
A.M.E.S. Type 13	10 (RHI)	7½	1½	75	10	Manual search for maximum echo heights; intensity measurement by reduction of gain.
Type 14	(PP1)	1¼	6 (centred at 2° elevation)	120	15	Automatic full-gain photograph every 3 min; intermittent stepwise gain reduction

Records were made by photographing the displays, and have been analysed with the help of the written notes and tape-recorded comments of the radar operators.

TABLE 1.2.2 Scale of hailstone size

Code figure	Diameter in inches			Description
0	-	-		No hail
1		¼		Grain; small pea
2	¼	3/8	Hail	Pea
3	3/8	½		Mothball, small marble
4	½	¾		Cherry, marble
5	¾	1		Large marble
6	1	1¼	Large hail	Walnut
7	1¼	1 5/8		Golf ball
8	1 5/8	2		Small egg
9	2	2½	Giant hail	Egg
10	2½	3		Tennis ball

CHAPTER II

CONVECTIVE STORMS IN S.E. ENGLAND ON 9 JULY 1959

2.1 The synoptic situation

Early on 8 July a diffuse cold-frontal region extended from the Irish Sea to just west of Portugal. It advanced slowly eastwards, and on the morning of the 9th extended from the central North Sea, across S.E. England and N.W. France into Spain. In this frontal zone there was a strong horizontal temperature gradient (1°C per 100 mi, or more) throughout practically the entire troposphere, and a corresponding SSW'ly thermal wind of about 3 mi hr^{-1} in each height interval of 1,000 ft. Consequently although the surface wind over S.E. England was NNE'ly about 20 mi hr^{-1} (Fig. 2.1.1 (i)), it had already reversed at 5,000 ft (Fig. 2.1.1 (ii)), and at greater heights it increased nearly linearly from the SSW to reach 75 mi hr^{-1} at the 300 mb level (Fig. 2.1.1 (iii)), and a maximum speed of 80 mi hr^{-1} at the level of the tropopause (37,000 ft). Hodographs of the individual mid-day wind soundings at various stations in S.E. England are shown in Fig. 2.1.2 (i - vii): each of these is plotted as components along and across 210° in Fig. 2.1.3 (i & ii), 210° being the direction of motion of cells within the most severe storms.

The thermodynamic state of the troposphere at 1200[1] is represented in Figs. 2.1.4 and 2.1.5

---

[1] All times in BST.

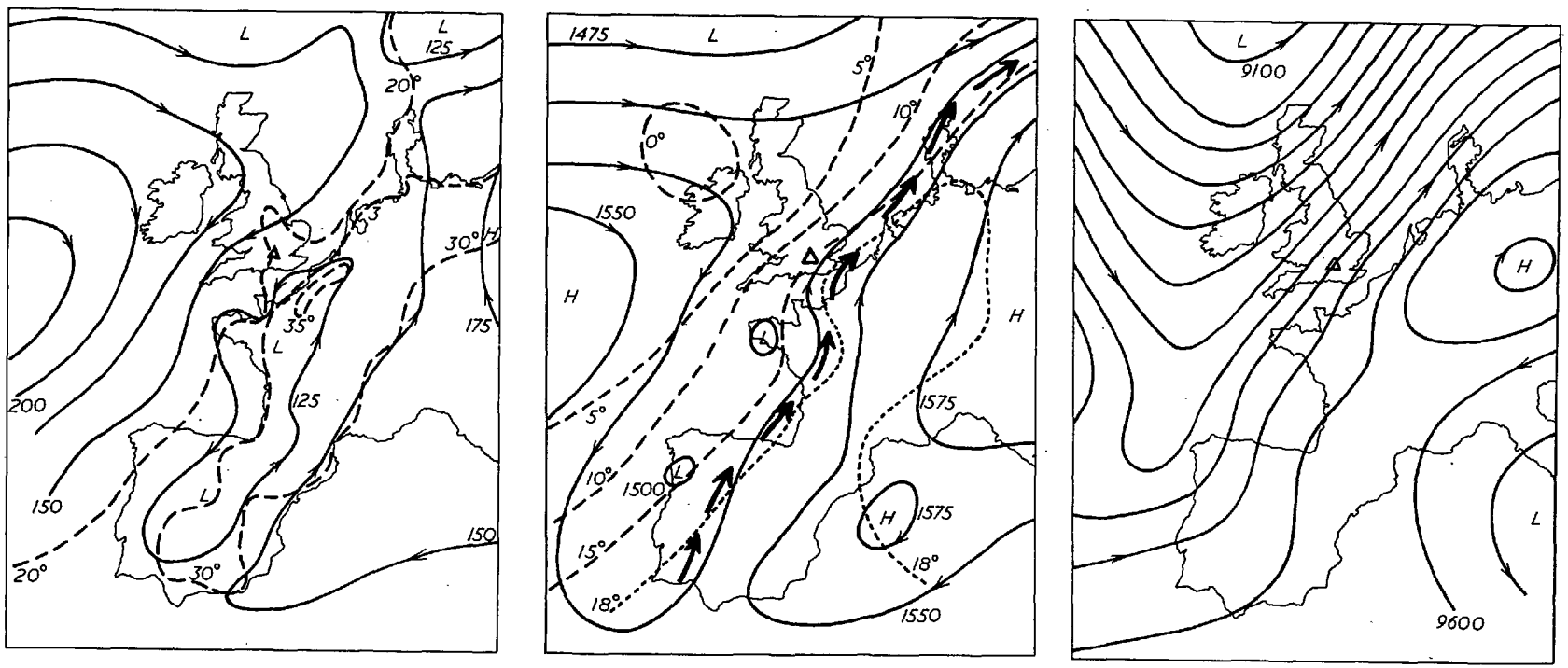

Fig. 2.1.1

Contours (at 25 m intervals) of the 1000, 850 and 300 mb pressure surfaces, 1200 9 July 1959. Arrows show the direction of flow of the geostrophic wind and pecked lines are isotherms (of screen-level temperature on the 1000 mb chart). On the 850 mb chart a chain of black arrows shows a belt in which the wind speed reached or exceeded 20 kt.

The position of the hailstorm over England is shown by the triangular hail symbol.

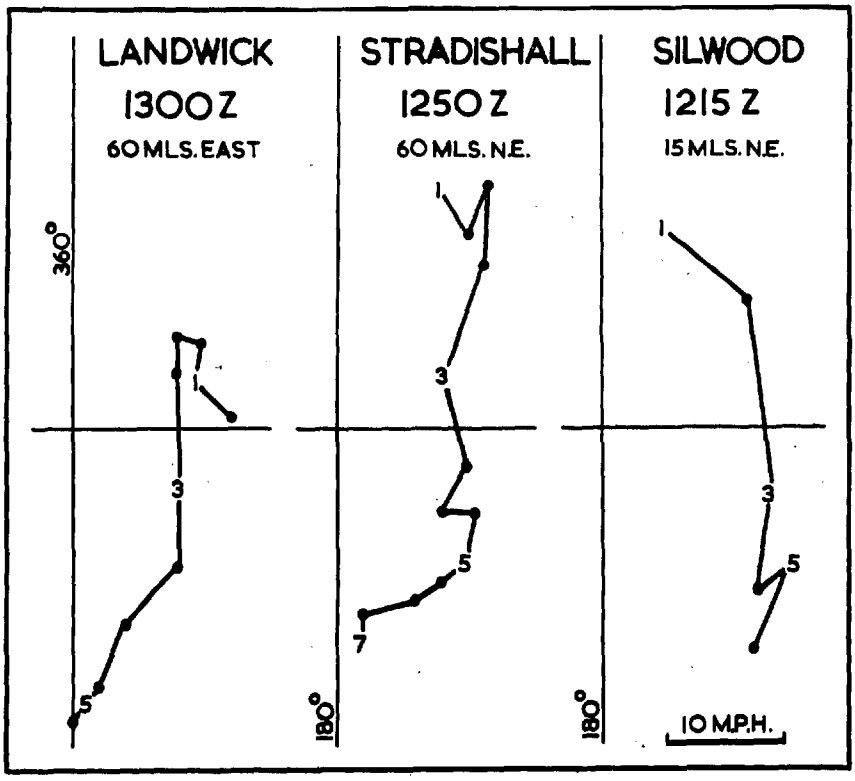

(i) (ii) (iii)

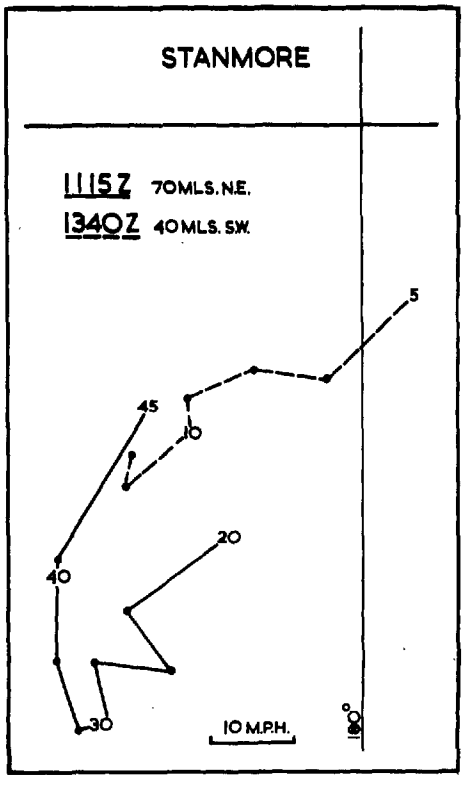

(iv)

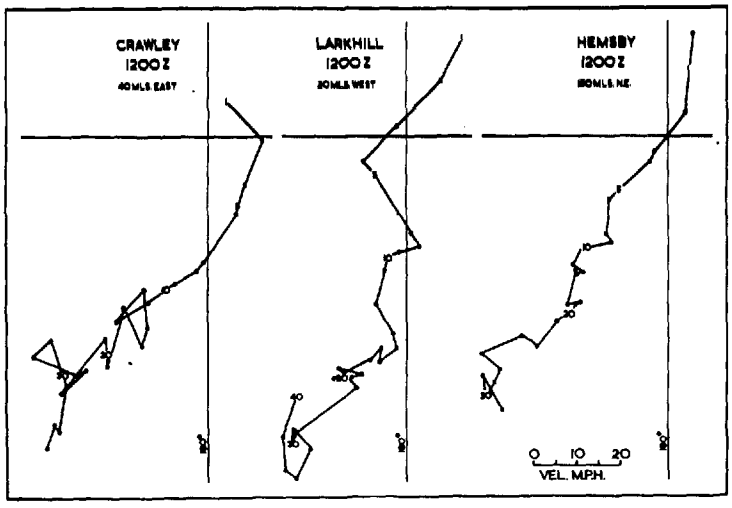

(v) (vi) (vii)

Wind hodographs for 9 July 1959. (The small numbers denote height in thousands of feet.) Also indicated are the distance and direction of each sounding from the core of the main storm (1).

Notice that the Silwood sounding - which was the nearest to the leading edge of this storm - shows a greater wind component from the East in the lowest 6,000 ft.

Fig. 2.1.2

Fig. 2.1.3

Wind components along and across the direction 210° as a function of height at 5 stations. The continuous line drawn through the points denotes the wind profile adopted for the winds around the main storm (1) during its intense phase.

The single additional observation of the component wind speed along 210° at 28,000 ft which is shown in Fig. 2.1.3(c) was derived by following 2 identifiable anvil echo elements for about 15 min. Notice the greater wind components across 210° below 6,000 ft observed at Silwood just ahead of the main storm (1).

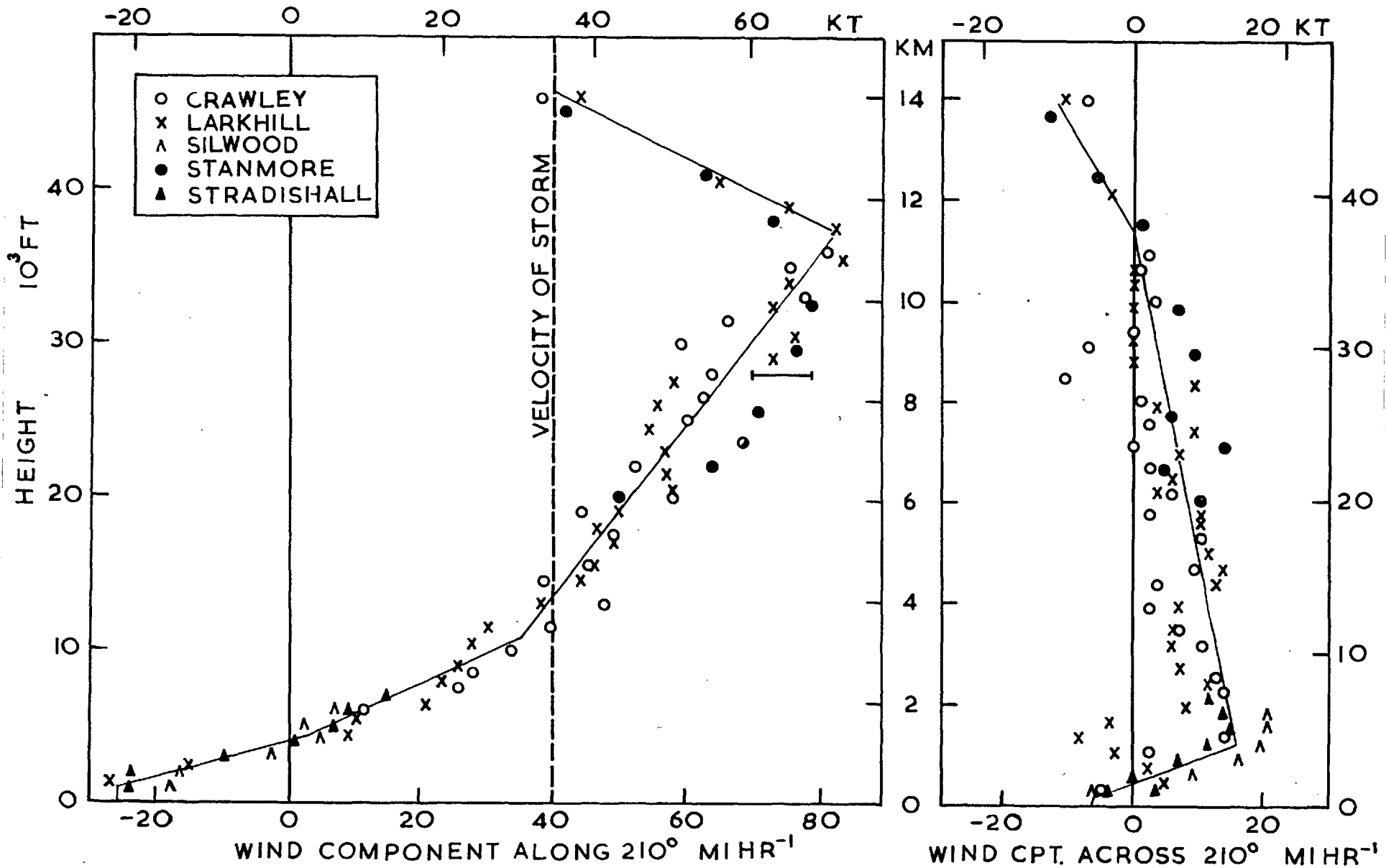
-20
0
20
40
60
KT
CRAWLEY
LARKHILL
SILWOOD
STANMORE
STRADISHALL
VELOCITY OF STORM
HEIGHT
10³FT
0
10
20
30
40
-20
0
20
40
60
80
WIND COMPONENT ALONG 210° MI HR⁻¹
KM
0
2
4
6
8
10
12
14
-20
0
20 KT
-20
0
20
WIND CPT. ACROSS 210° MI HR⁻¹

Fig. 2.1.3

(i)

(ii)

Fig. 2.1.4

Dry- and wet-bulb temperature sounding at Crawley, 1200 9 July 1959, represented on a tephigram. Two (dashed) lines of saturation mixing ratio and the wet adiabatic (pecked) for θ_W of 20°C are included. The energy of air descending in the downdraught from medium levels is derived mainly from the stippled area.

Fig. 2.1.5

Distribution with height of θ_W, the wet-bulb potential temperature, and θ_S, the wet-bulb potential temperature if the air were saturated; from soundings at Crawley and Hemsby, 1200 9 July 1959.

Rising air can become warmer than its environment only if it has become saturated and where its θ_W exceeds θ_S at the new level. Air which has risen from near the ground at Crawley acquires an excess potential temperature of about 1°C between about 9,000 and 23,000 ft on the unmodified sounding (obliquely hatched area), or a maximum of 1 to 3°C if the environment has been cooled and brought to saturation by a general lifting (vertically shaded area). At Hemsby, near the locality in which the storm died out, the possible temperature excess on the unmodified sounding is negligible.

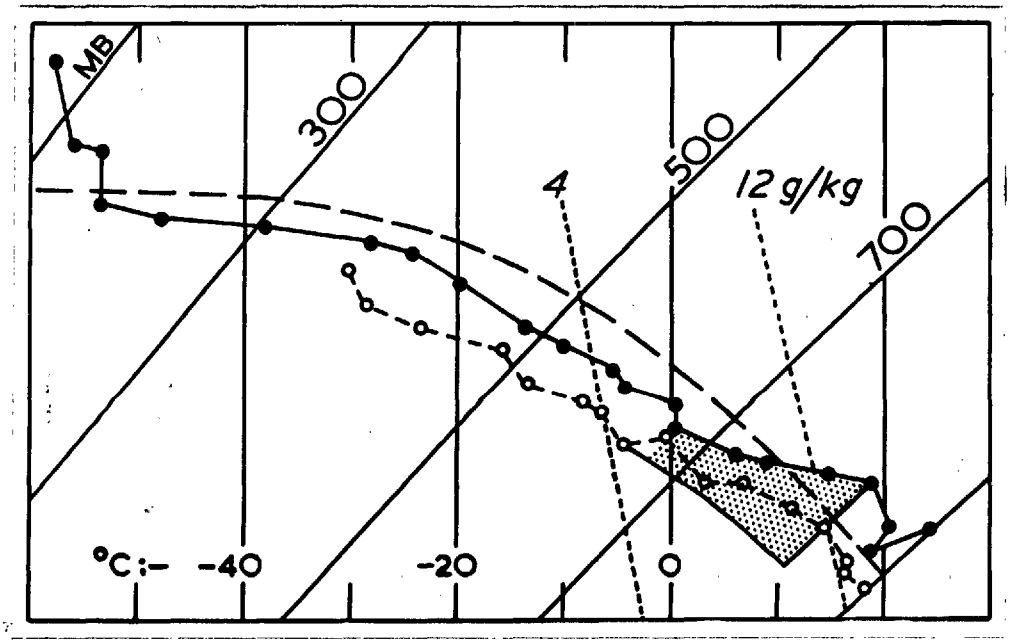

Fig. 2.1.4

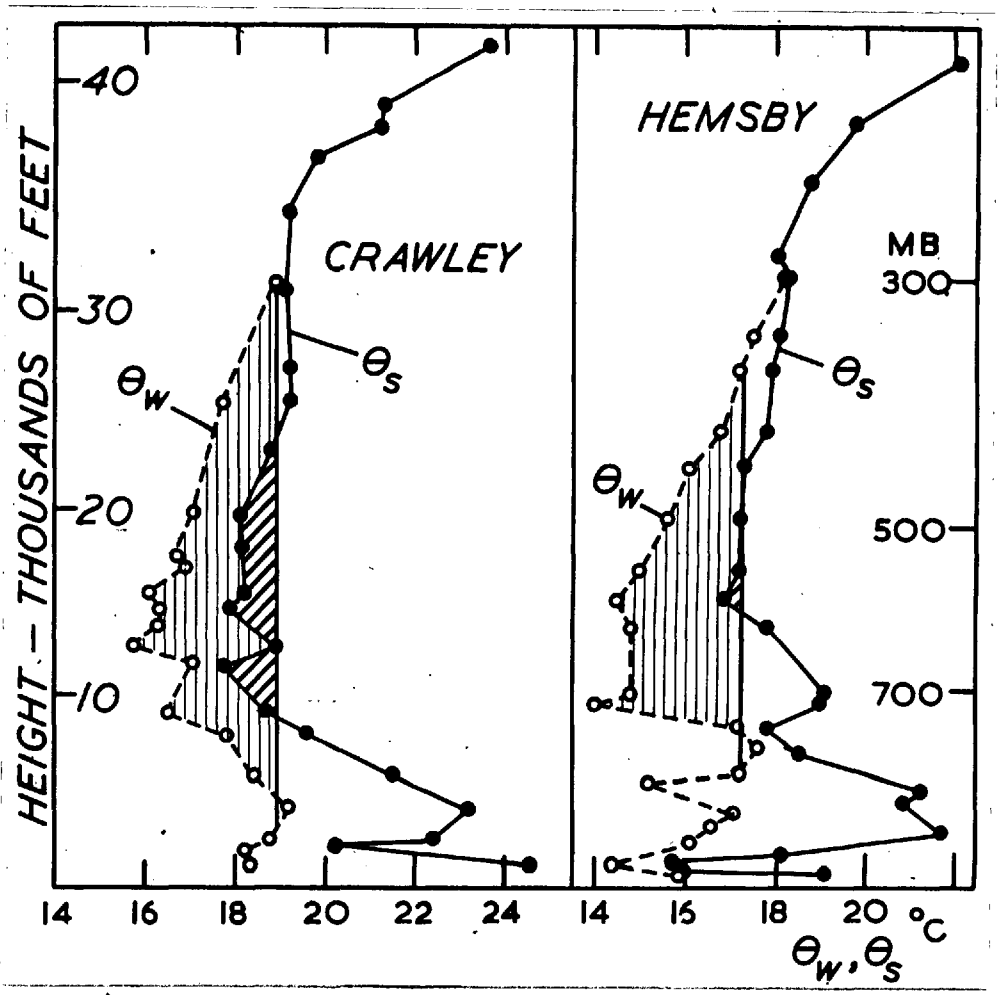

Fig. 2.1.5

2. The general behaviour of the storms

The sferic observations of the British C.R.D.F. network show that during the 8th thunderstorms spread from the west into the Bay of Biscay, and were again active there on the morning of the 9th (Fig. 2.2.1). This activity declined after 0900, but at 0800 a storm was located over the Brest peninsula and, in contrast to the previous storm groups, this region of activity travelled rather rapidly N and then NE across the English Channel, being plotted at 0900 and 1000 as compact clusters of sferic fixes. At 0830 an air observer over Bristol saw developing cumulonimbus tops reaching 32,000 ft south of the Dorset coast, with anvil tops to 40,000 ft farther south-west, and at 0920 a storm was observed as an intense echo about 60 miles SW of Hurn airport radar, directly on the path shown by the sferics (Fig. 2.2.1). Shortly afterwards this storm came within range of the five meteorological radars based at East Hill (near Dunstable); it subsequently crossed S.E. England within the cold front zone. Its development after 1030, as seen on the 10 cm PPI display, is shown in Fig. 2.2.2, where it is labelled storm 1.

The echo-mass[1] of storm 1 was closely followed by another (2): subsequently the development of small cells[1] which formed between them led to the merging of these two echo-masses. At 1200 some sferics were located over the Channel near the Isle of Wight, and soon afterwards a cluster[1] of small cells (3) entered the south of the display. At 1430 (after a power failure had interrupted the radar observations) they and

---

[1] Echo nomenclature is specified in appendix 2.2a.

similar groups (4 and 5) lay in a belt extending southward from storm 1, while two others (6 and 7) had appeared to the NW of East Hill. Judging by the sferics observations, some thundery activity persisted during the afternoon near the W coast of France, (intensifying off-shore in the evening) and also near the NE coast of France. By 1530 all the storms in England were dying out, with the exception of a member within group 4 which became a more severe thunderstorm for a short while after 1600; the sferics at this time (Fig. 2.2.1) located it accurately over the sea near the coast of E. Anglia. Between 1700 and 1800 there was a severe storm on the Dutch Coast but by then all the radar echoes over England had disappeared.

As might have been expected from the times and places of formation of these storms, they were not directly dependent upon solar heating of the ground. Over England the air in the lowest 4,000 ft was stably stratified (Fig. 2.1.5), while on the neighbouring Continent only in the extreme NE of France was the ground heating sufficient to produce cumulus clouds. All the storms appeared in areas where there were extensive altocumulus, and evidently originated as showers from cumuliform developments in these medium-level clouds (mostly to the south of storm 1, near its gust front: see Fig. 2.7.4).

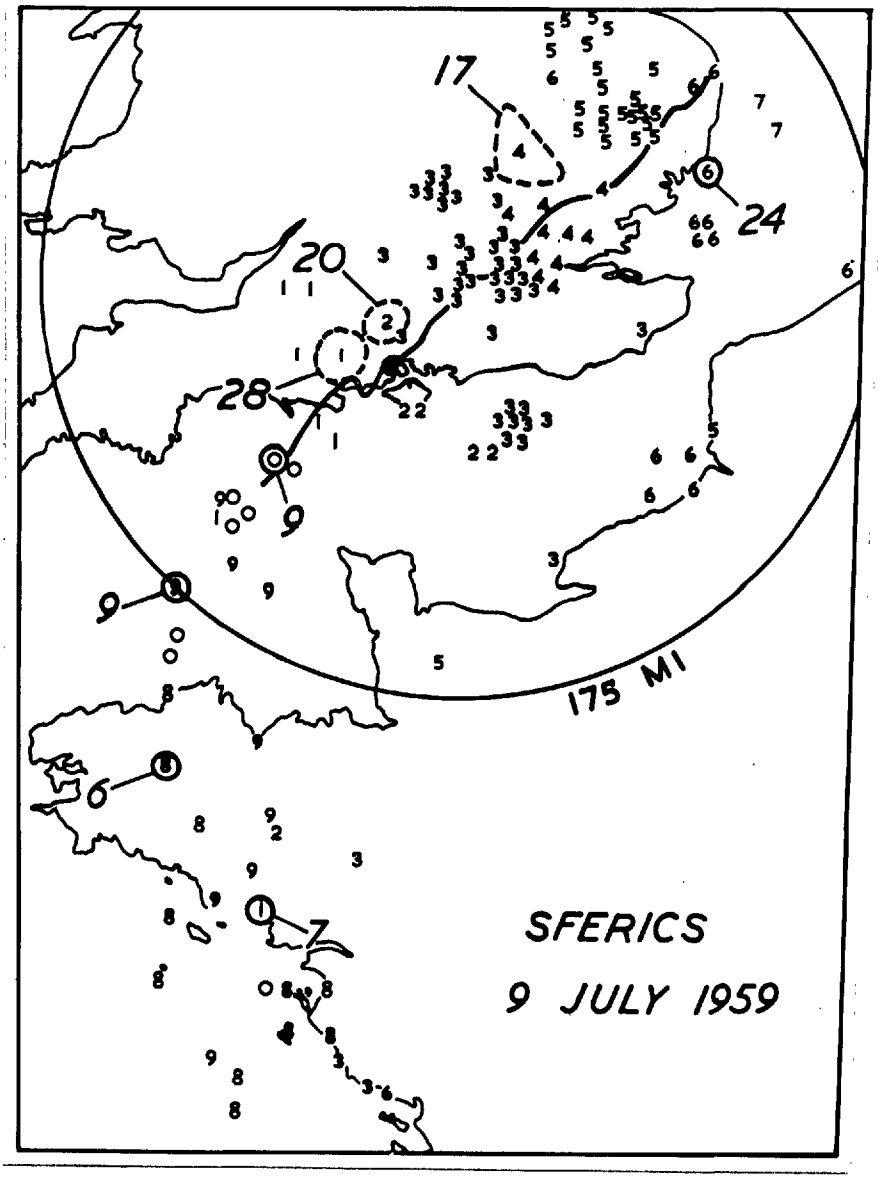

Fig. 2.2.1

Routine SFERICS observations, 0800-1700, 9 July 1959. The locations of lightning sources are shown by numbers representing the last figure of the hour of observation. Observations are made only during the 10 min preceding each hour so that a number '8' refers to the 10 min period prior to 0800 and '7' refers to the 10 min period before 1700. Where a number of sources were detected within a small area, the area is ringed and the total shown by large figures.

It appears that a storm which at 0800 had formed over the middle of the Brest peninsula moved into the Channel and then NE'ward into S. England where it was identified as Storm 1, giving the hail whose distribution is shown in Figs. 6a and 6b. The path of the right-hand edge of the radar echo of this main storm is shown; the extreme SW position is given by reports from the airfield control radar at Hurn and can be seen to be directly in the path of the storm indicated by SFERICS for 0900, 1000 and 1100.

Fig. 2.2.2

Full gain 10 cm PPI photographs at 15 min intervals (with a 90 min break after 1300 owing to a power failure) showing the passage of the 7 separate storm areas across S.E. England.

The range markers are at intervals of 10 miles: azimuth markers are at 20° intervals from 010°.

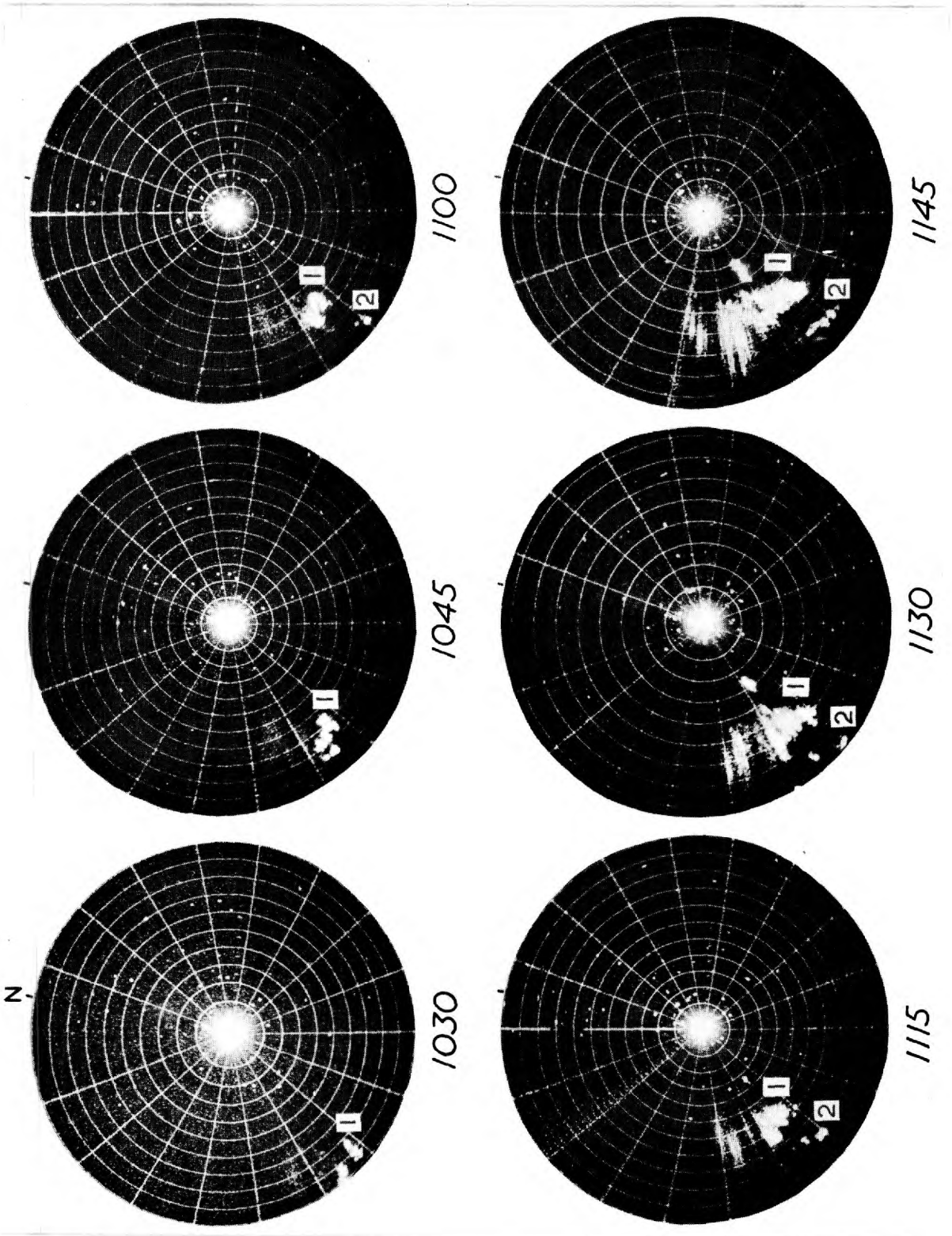

Fig. 2.2.2

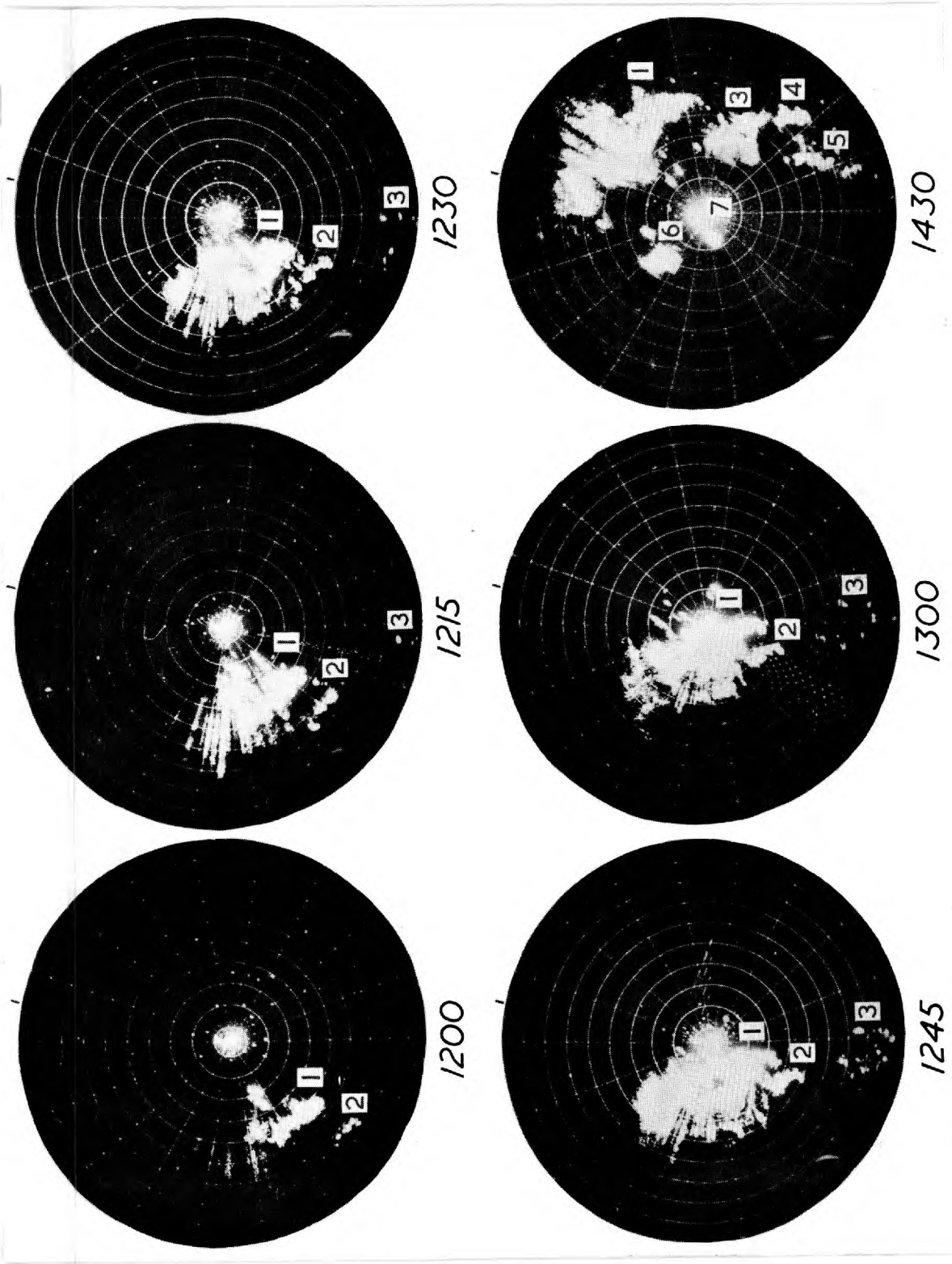

Fig. 2.2.2 (cont^{d})

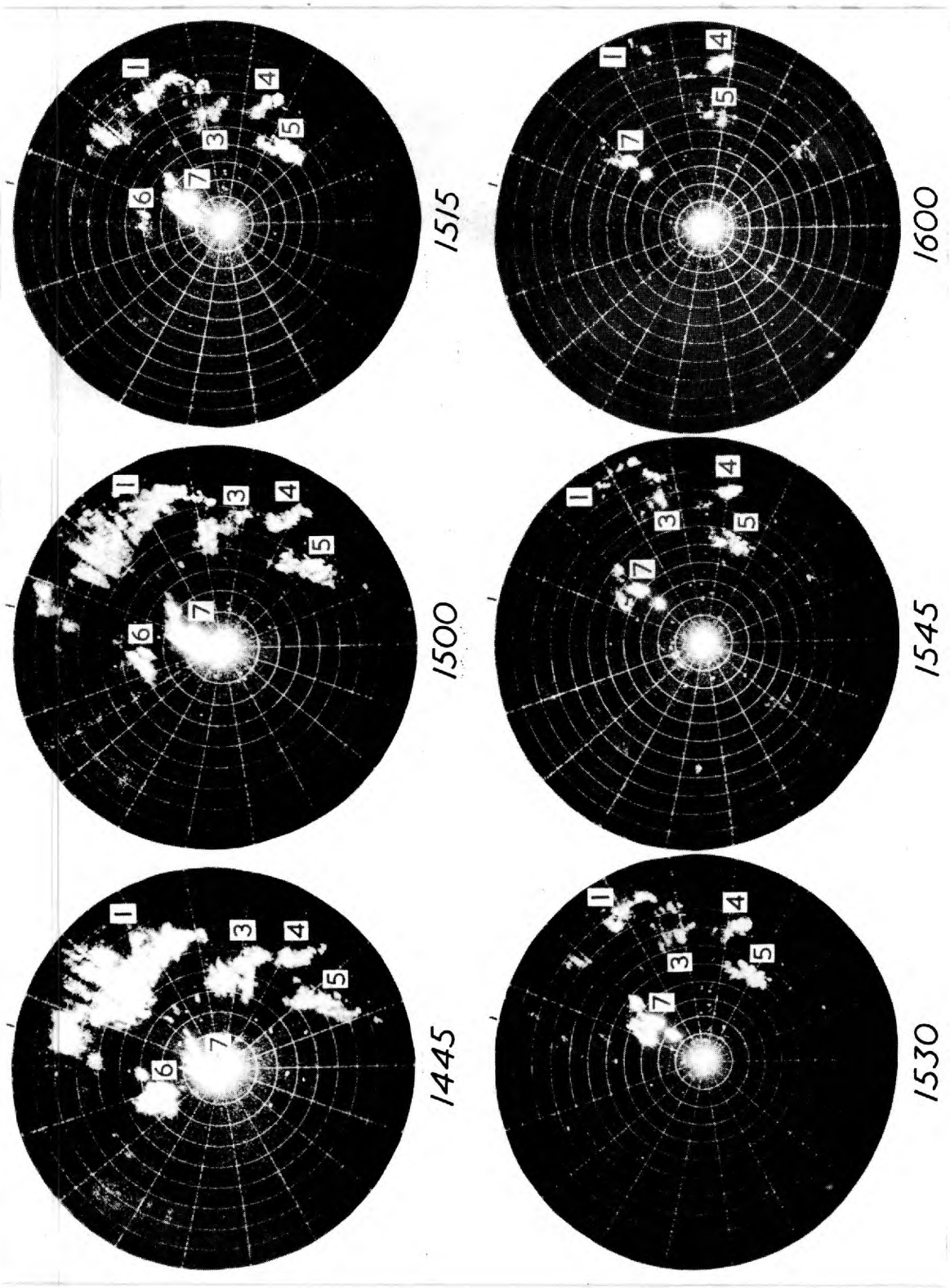

Fig 2.2.2 (cont.d)

Appendix 2.2a: Echo nomenclature

Name	Description	Typical dimensions
Cell	A region of echo which, by virtue of its higher intensity is distinguishable but not necessarily completely detached from neighbouring echo. Probably associated with a single convective cell.	A few miles in diameter
Cluster of Cells	A fairly compact group of separate cells	10 - 30 or more miles across
Supercell	A large cell which cannot be subdivided into smaller units even when viewed at reduced gain: it develops from an amalgamation of smaller cells. It is associated with a single extensive updraught.	About 10 miles in diameter
Column	An echo appearing as an upright column on the usual kind of RHI display, and probably associated with a single updraught.	Columns within cells have a diameter of about 1 mi increasing to 3 mi for the tallest columns. The single column which comprises a supercell may be up to 10 mi across.
Echo-mass	A large region of echo containing some columns at least partly embedded in more diffuse and weaker residual echo from earlier columns.	10 - 100 miles across.

3. The intensity of the storms

Throughout the day measurements of echo intensity were made at all three wavelengths. On the 3.3 cm and 4.7 cm radars attention was concentrated on the storm 1, and so the evolution in the intensity of the other storms has been derived from the 10 cm PPI records, which include frequent series of photographs in which the gain was reduced in a series of steps. At this wavelength errors arising from attenuation are negligible, and so the only correction necessary is that for incomplete filling of the beam (Appendix 2.3a). The resulting distributions of intensity at various times are displayed in Fig. 2.3.1 in which the figure in each 10 km square represents the greatest echo intensity present over any area of at least 4 km^2.

Fig. 2.3.2 shows the trend with time of the maximum intensity in each of the storms; the individual measurements have smoothed curves drawn through them, which are dotted during periods when the storms were over the sea. (Unfortunately the 10 cm PPI radar tended to drift off tune and could not readily be set to a standard brightness, so that the absolute values are rather unreliable. However an approximate estimate of the fluctuation in sensitivity of this radar has been obtained by noting the trend in the amount of noise displayed. This is indicated in Fig. 2.3.2 and has influenced the drawing of the smoothed curves in this figure). Fig. 2.3.2 illustrates some interesting features; in particular

(i) storm 1 was the most persistently intense as well as the largest storm:

(ii) there is no obvious relation between intensity and location over

land and sea:

(iii) while over the Channel, storm 2 was as intense as storm 1 ahead of it but subsequently it weakened greatly while the other was intensifying;

(iv) after 1530 all the storms declined, with the notable exception of storm (4), whose intensification was also indicated by the sferics observations (Fig. 2.2.1);

(v) the storms of groups 3,5,6 and 7, and storm 2 while overland, had intensities which usually were too low to be associated with the occurrence of thunder (Ludlam, 1960): by comparison storms 1 and 4 became very severe.

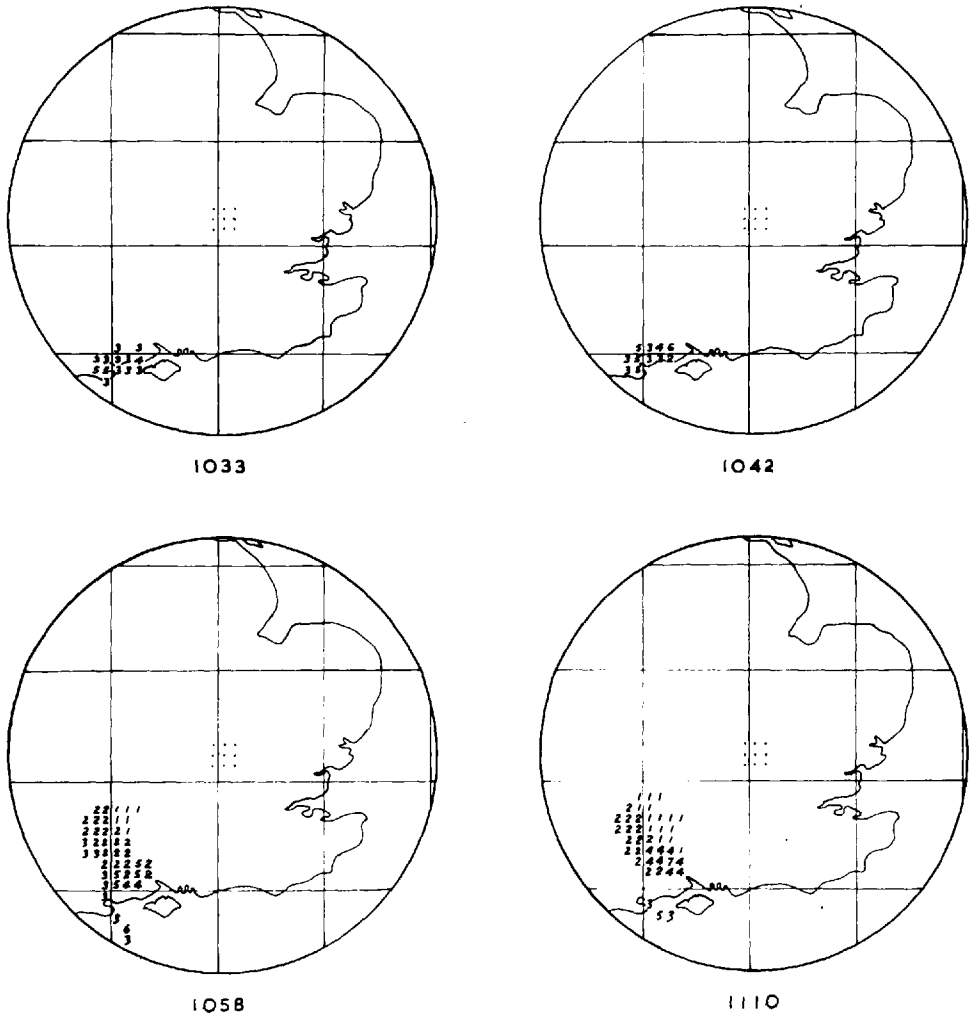

Fig. 2.3.1
The height-integrated echo-intensity distribution at roughly 20 min intervals (with a longer break during the power failure) over a region with the East Hill radar station as centre, deduced from the 10 cm PPI reduced gain series. The grid lines shown are those of the National Grid and divide the area into squares of side 100 km. Each of these is sub-divided into 100 squares, which contain figures representing the greatest echo intensity present over any area of at least 4 km^2 according to the following code:

Code figure	10 log Z_e
0	$\leqslant 25$
1	26 - 30
2	31 - 35
3	36 - 40
4	41 - 45
5	46 - 50
6	51 - 55
7	56 - 60
8	61 - 65
9	66 - 70

The 9 dots in the centre of each diagram indicate those squares which are at least partly obliterated by echoes from ground objects.

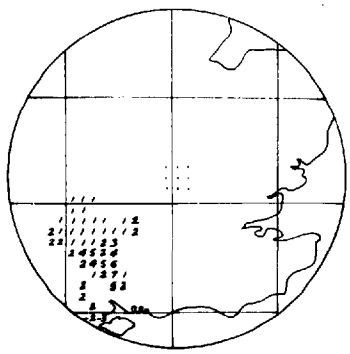

1134

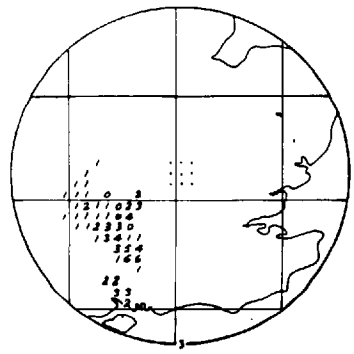

1158

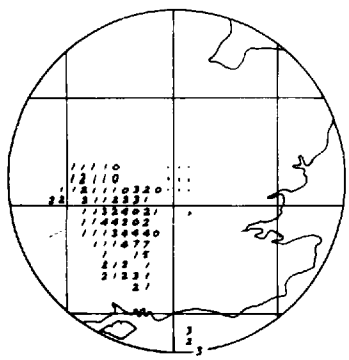

1216

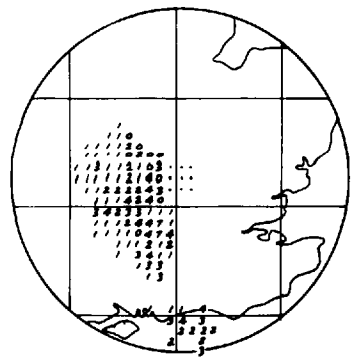

1237

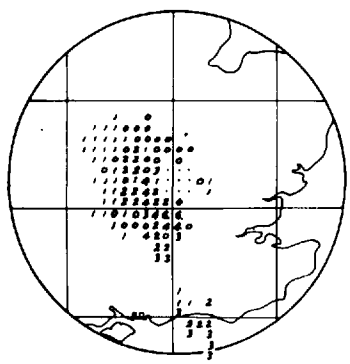

1255

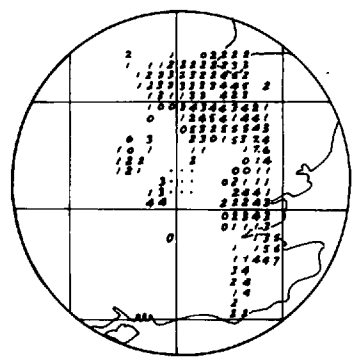

1423

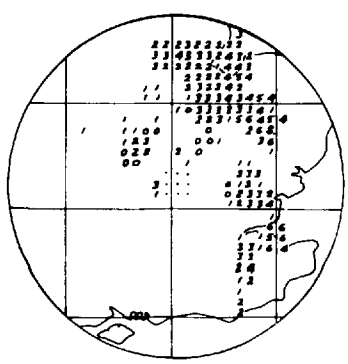

1440

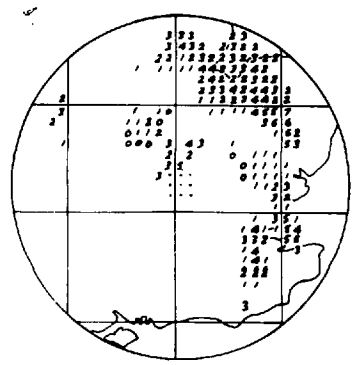

1452

fig. 2.3.1 (Contd.)

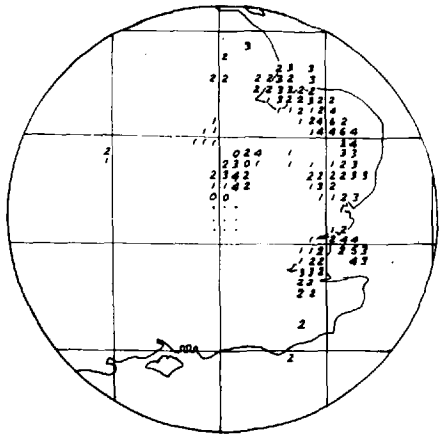

1510

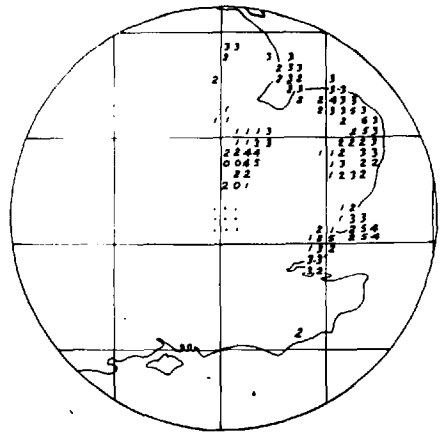

1528

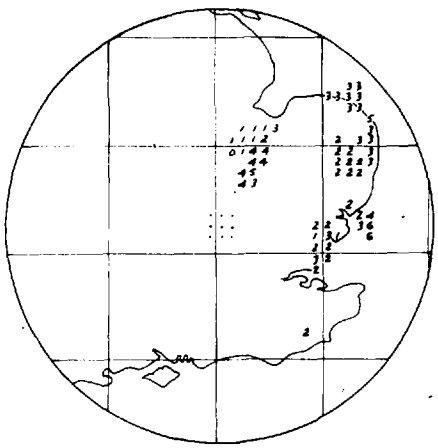

1540

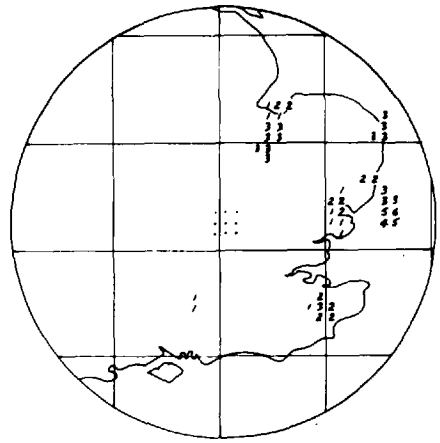

1559

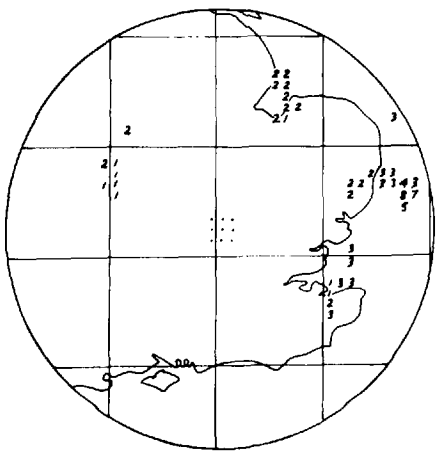

1623

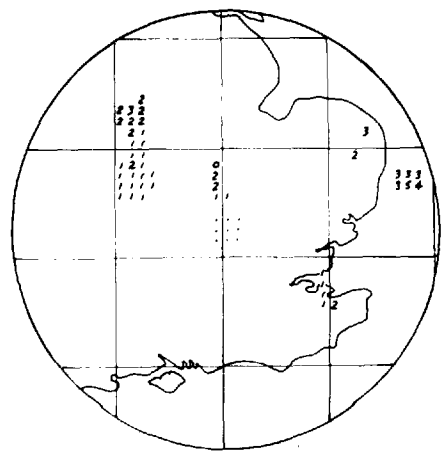

1646

Fig. 2.3.1 (cont'd)

Those values followed by a dot in Fig. 2.3.2 may be underestimated since they correspond to occasions when it was impossible to reduce gain sufficiently to remove the echo from the 10cm PPI display.

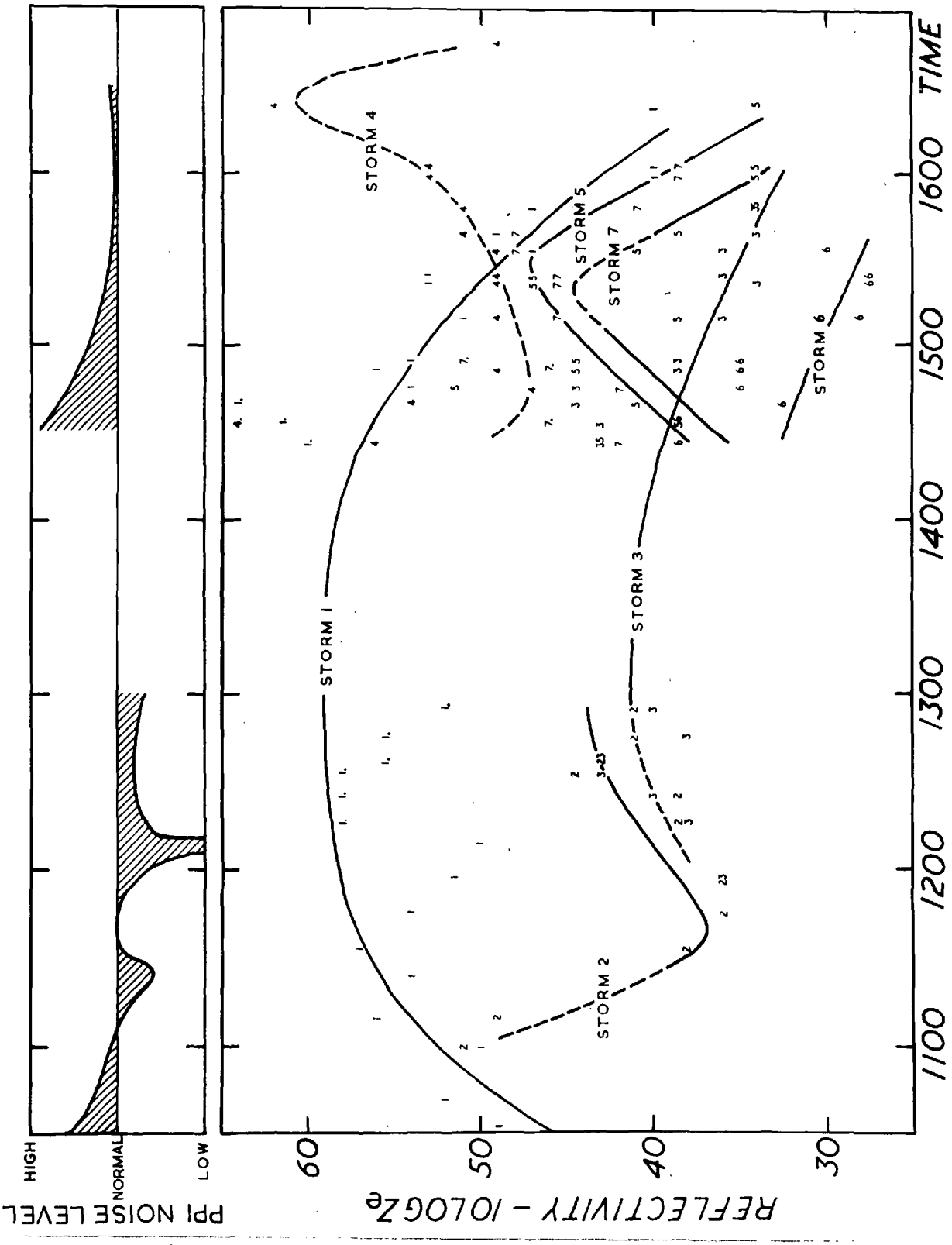

Fig. 2.3.2
The maximum intensity within each of the 7 storm areas as a function of time. The individual measurements have smoothed curves drawn through them, which are dashed during periods when the storms were over the sea.

Appendix 2.3a: Corrections for beam-width

The RH1 sets have beams which are broader in the horizontal, being filled in the vertical at all working ranges. Intensity measurements have been adjusted for horizontal beam-widths on the assumption that the intense echoes had a width of 2 miles at right angles to the beam axis, and that where the beam-width was greater the excess contained negligible echo. Accordingly, the apparent intensities are increased as a function of range by the amounts given in table 2.3a.1.

The 10 cm PPI set has a beam which is broad in the vertical. One correction to observed intensities is necessary because a part of the beam lay below the radar horizon: another was made on the assumption that strong echo occurred only from the ground up to 30,000 ft, with negligible echo outside these limits. The resulting corrections are given in table 2.3a.1.

Table 2.3a.1: Beam-width adjustments to apparent echo-intensities

Range	Increment of 10 log Z_e			
(mi)	3.3 cm	4.7 cm	10 cm RHI	10 cm PPI
26-30	0	-	2½	2
31-35	0	-	2½	2
36-45	0	1½	4	2
46-55	0	2½	5	2
56-65	0	3	6	2
66-75	0	-	6½	3
76-85	-	-	7	4
86-95	-	-	7½	5
96-105	-	-	8	6
106-115	-	-	8½	7

4. The distribution of hail and rain at the surface

From the ground observations, mostly from the network of about 1500 volunteers, it appears that only storm 1 produced significant hail inland. Storm 2 also traversed the area which experienced hail, but in view of its comparatively low intensity it is unlikely to have discharged any hail: The isopleths of maximum hail size at the ground (Figs. 2.4.1 (i & ii)), which indicate size according the code in Table 1.2.2, can therefore be associated with the passage of the main storm (1). Some of the longest falls of large hail occurred near the town of Wokingham (Berkshire), after which this storm has been named. Figs. 2.4.1 (i & ii) include the path of the right-hand edge of the 10 cm PPI full-gain echo of this storm; it has a number of bulges owing to the intermittent formation of new echoes on this flank. The large hail occurred in a rather narrow strip near this path (within 3-8 miles), and both the path and the strip are very nearly straight over the whole distance of about 200 miles between the south and east coasts. To the south of East Hill their orientation was approximately from 220°, whereas the upper winds at nearby Larkhill were from 190° and 200°, and from between 200° and 210° at Crawley on the other side of the path (Figs. 2.1.2 (v & vi)). Thus the path of the most intense part of the storm was orientated 20°to the right of the upper winds. Near the east coast the storm was weakening, and the hailswath (along 230° - 050°) was more nearly parallel to the upper winds (from 210° to 220° at Hemsby), but the deviation still amounts to more than 10°. This behaviour is typical of severe storms (Newton, 1960).

Fig. 2.4.2 shows the smoothed pattern of the total rainfall, in the 24 hours beginning at 1000 on 9 July[1]. Possibly because the heavy rain was usually accompanied by strong winds, some at least of the individual rainfall observations appear to be unrepresentative: nevertheless it is clear that rain from the Wokingham storm reached the ground over a 60 mile wide swath and that most places in the path of its intense core received between ¼ and ¾ inch of rain[2]. (Storm 2 made an unknown but probably unimportant contribution to this total).

The next most intense storm (4) produced totals of around ¼ inch over a 10 mile wide swath as it crossed Sussex and Kent prior to its brief intensification. On the other hand, storms 3 and 5 respectively produced totals which rarely exceeded 0.05 and 0.1 inch.

For each 10 km square in a small area of central southern England has been evaluated the sum of the products of the intensity values (as plotted in Fig. 2.3.1) and the time to which each value pertained. This enabled the construction of Fig. 2.4.3 showing smoothed isopleths of a quantity I, where

---

[1]The 7 storms discussed in this study were the only ones during this period.

[2]This is only about one quarter of the fall in the similar but more severe Horsham storm in S.E. England on 5 September, 1958 (Ludlam and Macklin, 1959); on that occasion the speed of travel was less (about 25 mi. hr^{-1} compared with 40 mi. hr^{-1}), and the direction of motion veered by as much as 30 - 40° from the observed winds.

$$I = \sum \left[\frac{t}{25} (\log Z_e - 2.3) \right] \qquad 2.4.1$$

and t is the time (in minutes) during which the greatest echo intensity present over at least 4 km^2 within each 10 km square was given by $Z_e (mm^6\ m^{-3})$. The resulting pattern resembles that of the rainfall distribution in Fig. 2.4.2: that the two are quantitatively consistent is now shown.

According to Jones (1956), for thunderstorm rainfall

$$Z_e = 486\ R^{1.37} \qquad 2.4.2$$

where R is in $mm\ hr^{-1}$. Substituting for Z_e in 2.4.1, and taking $\bar{R}$ to be the mean rainfall rate throughout the storm of duration T minutes, gives

$$I = \frac{T}{25} (0.39 + 1.37 \log \bar{R}) \qquad 2.4.3$$

Taking T = 30 minutes gives total falls, $\bar{R}T$, of 0.04, 0.17, and 0.68 in corresponding to I = 1,2, and 3 respectively. (Because Jones' relation breaks down in the presence of hail and because maximum instead of mean intensities have been considered, it might seem surprising that the rainfall rate deduced for the comparitively small region containing both the hail and the large intensity gradients has not been exaggerated. That it has not may be attributed to the smaller value of T in this region).

Although relevant to this section, the importance of Fig. 2.4.3 lies mainly outside this context as it exemplifies a technique for obtaining rainfall distribution without the delay and labour involved in utilizing observations from numerous outstations.

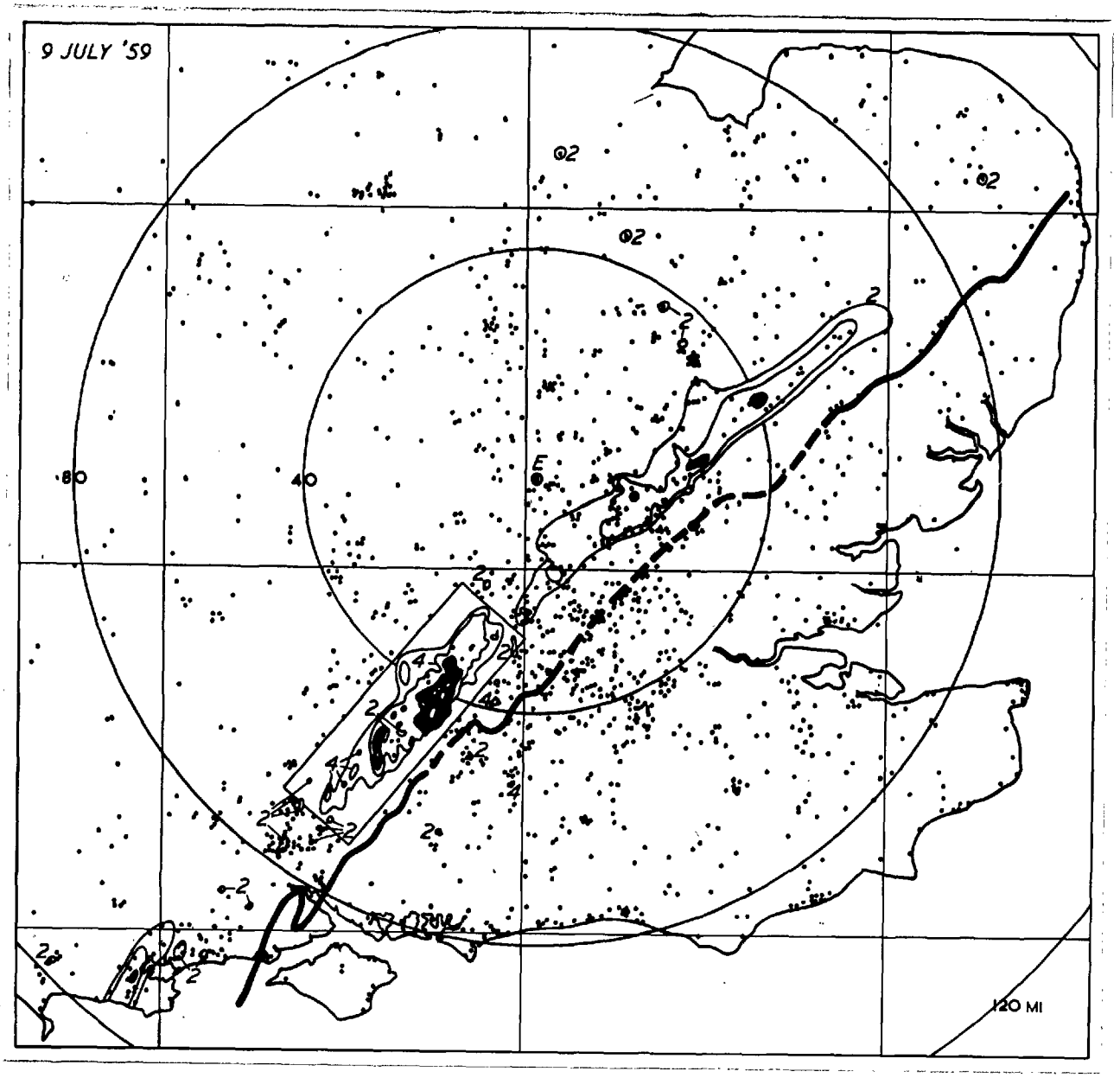

Fig. 2.4.1 (i)

Distribution of maximum hailstone size for 9 July 1959. The isopleths are for stones of sizes 2, 4, 6 and 8 (for scale see Table 2, p. 6).

The area between the size 6 and 8 isopleths is shown in black. Altogether there are 1935 observations whose positions are indicated. 442 of these lie within the rectangle surrounding the most severely affected area; their positions are indicated in the enlarged diagram in Fig. 6(b). The thick line is the path of the right flank of the main storm determined from the 10 cm PPI radar (continuous line) or the 4.7 cm PPI radar (dashed line); the rings are range markers drawn at distances of 40, 80, and 120 miles from East Hill radar station (E).

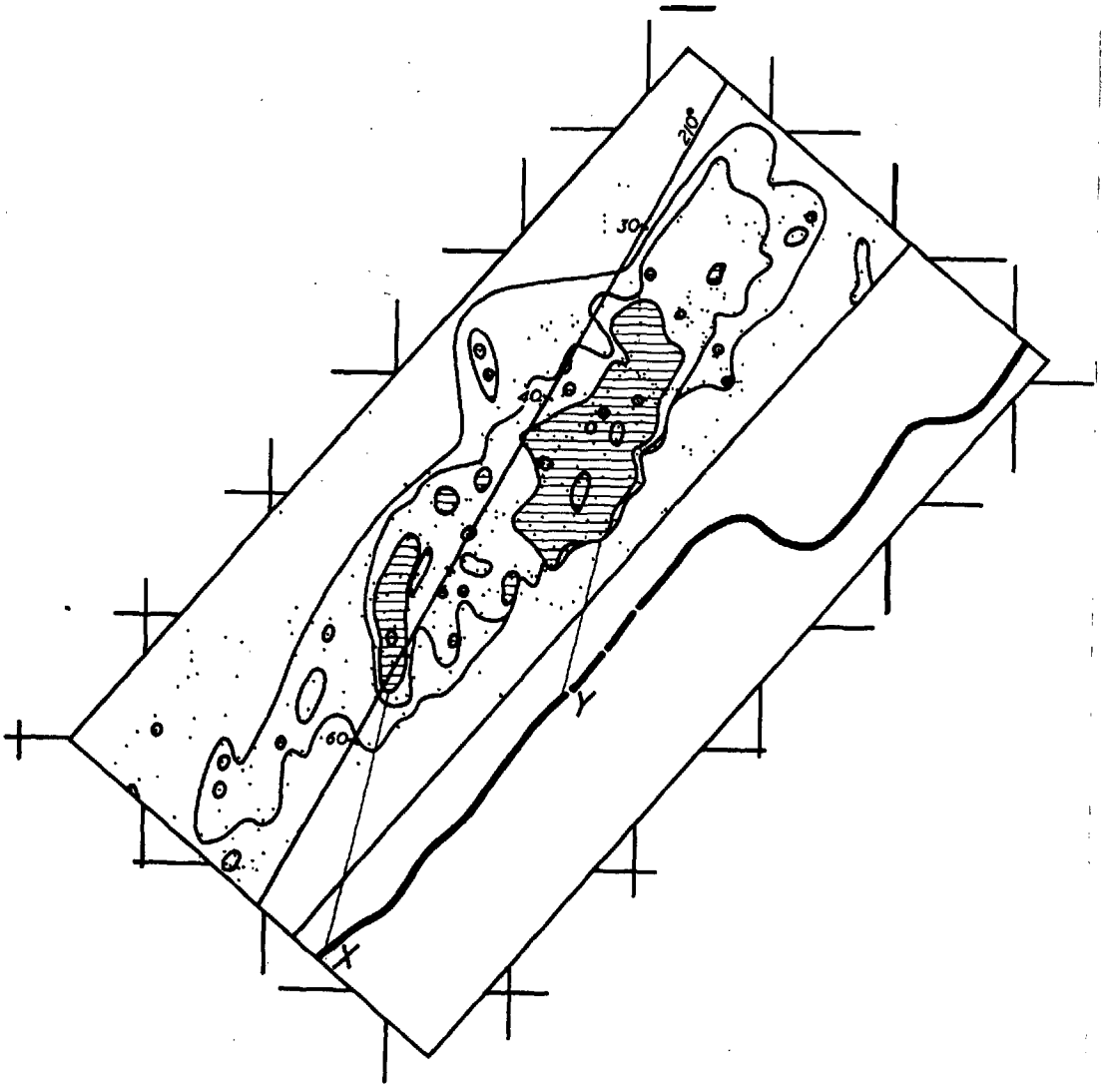

Fig. 2.4.1 (ii)

Distribution of maximum hailstone size for 9 July 1959 within the rectangle shown in Fig. 2.4.1(i) containing the most severely affected area. The isopleths are for stones of sizes 2, 4, 6 and 8 (for scale see Table 2, p. 6).

The areas experiencing sizes greater or equal to 6 are shaded. The positions of the 442 observations within the rectangle are also indicated.

In addition, to the right of this rectangle is included the path of the right flank of the main storm determined from the 10 cm PPI radar. Two lines are drawn along a direction 195° indicating the likely displacements of those size 6 stones which fell nearest to the right flank at 2 different times. The lines leading from X and Y are shown in the text to imply periods of 760 and 1200 sec respectively for the growth of hail from a size which is just detectable to size 6.

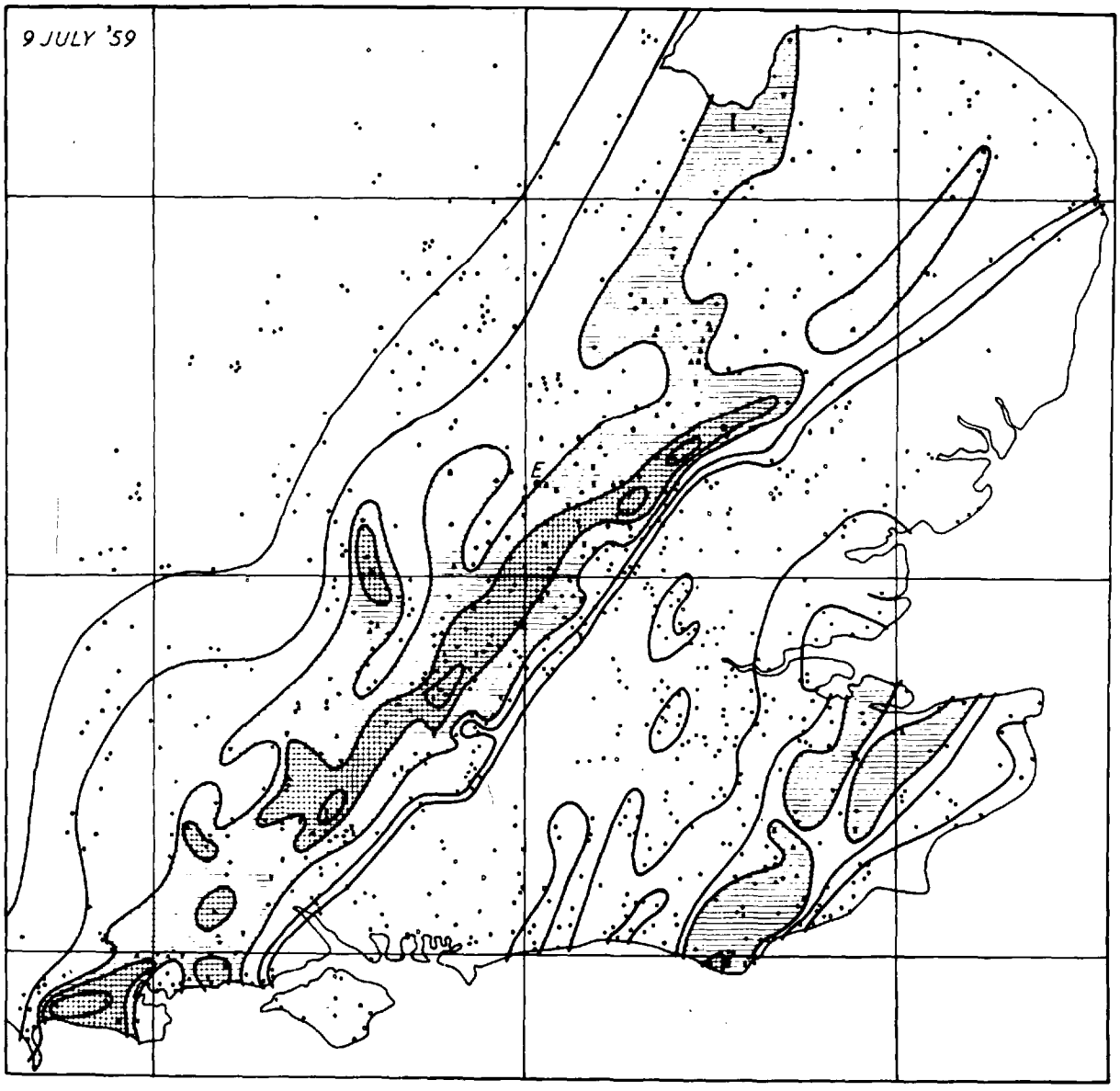

Fig. 2.4.2
Distribution of rainfall in Southern England, 9 July 1959. Smoothed contours are shown for totals of 0.05, 0.10, 0.25, 0.50 and 0.75 in, areas experiencing more than 0.25 and 0.50 in respectively being represented by horizontal and vertical hatching. The positions of the 910 observations are indicated as black dots or open circles according to whether or not measurable rainfall was reported.
E denotes the location of the East Hill radar station.

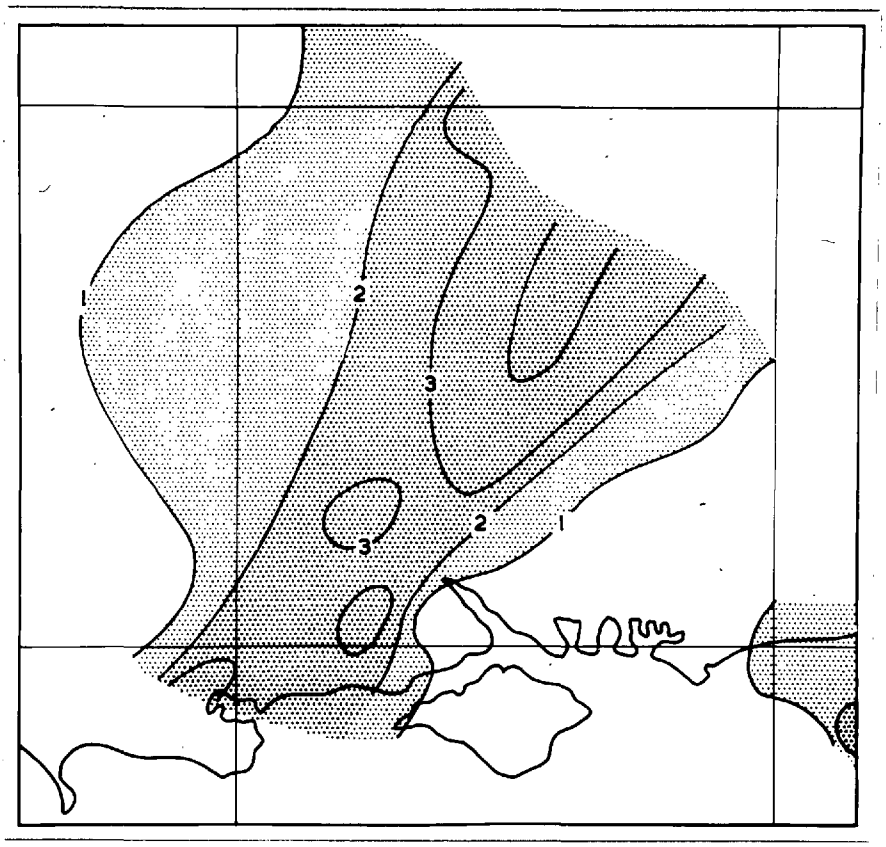

Fig. 2.4.3
Distribution of rainfall over a part of the path of the Wokingham storm as determined from a time integration of the radar intensity distribution. Contours are of a quantity I, explained on p.41.

5. The motion of the storm cells

The echo-masses of the 7 storms already discussed each comprised a number of distinguishable, but not necessarily completely detached, regions of higher intensity which are referred to as cells. The velocity of travel of each echo-mass was determined not only by the motion of these constituent cells but also by their positions of formation and dissipation. In this respect there is found to be a notable difference between the behaviour of the two intense storms (echo-masses 1 and 4) and that of each of the others.

Storm 3 was the weakest of the seven: it developed off the Sussex coast around mid-day as a cluster of small weak cells. Fig. 2.5.1 shows that these formed and dissipated in an unsystematic manner, the majority persisting for short periods only. The motion of the weaker cells (from about 195°) was along the wind direction in the medium levels (Fig. 2.1.2 (v)): the more intense cells moved up to about 10° to the right of this.

The cells comprising storm 2 showed more organization (Fig. 2.5.2). When the storm first came within range of the East Hill radars it was over the English Channel and consisted of a single intense cell moving at 40 mi. hr^{-1} from 209°: as it approached the south coast it weakened but further cells formed on both sides, aligned approximately at right angles to their motion (from about 195°). The most intense cells occurred near the right-hand end of the line, but none had an intensity within an order of magnitude of that of the first one.

The intense storms 1 and 4 were even more highly organised, maintaining a similar structure over long periods, (over four hours in the case of the Wokingham storm (1)). With both storms the principal new development invariably occurred on the right flank in the form of cells[1] which became elongated along their direction of motion. This process is illustrated schematically in Fig. 2.5.3 which emphasises the resulting propagation of the echo-mass as a whole to the right of the winds[2]. Each individual cell eventually decayed on the left flank, its persistence determining the overall size of the echo-mass.

Fig. 2.5.4 portrays a series of full-gain 10 cm PPI photographs showing the changing form of the echo-mass of the Wokingham storm (1) during its passage across S.E. England. A painstaking analysis of similar photographs taken at 3-minute intervals together with frequent gain reduction series has enabled the preparation of Fig. 2.5.5. This shows the paths of the constituent cells of the Wokingham storm (1) and also of storm 4.

---

[1] No satisfactory explanation has been found to account for the discrete nature of this propagation.

[2] A similar process can be inferred where this deviation is evident, even though the resolution of the radar is inadequate to distinguish the freshly-formed parts of the echo, as in the instance of the most intense cells in storms 2 and 3.

The orientation of every path lies within 5° of 210-030°. This is in good agreement with the wind direction of 214 ± 6° at all heights between 3,000 and 30,000 ft at Hemsby at 1200 (Fig. 2.1.2 (vii)), but is veered a little from the wind direction at all medium levels at both Crawley and Larkhill at this time (Figs. 2.1.2 (v & vi)). However this need not necessarily imply a discrepancy between cell motion and the predominant direction of the large-scale geostrophic wind, as the sounding at Crawley and more particularly that at Larkhill were made fairly close to (and therefore may have been modified by) the Wokingham storm (1) during its most intense phase. The Crawley sounding shows the wind veering with height throughout the medium levels; this suggests that the motion (from 195°) of the weaker cells comprising storms 2 and 3 was influenced by the winds at lower levels than were the cells within storms 1 and 4.

During the most intense phase of the Wokingham storm (1) an amalgamation of four intense cells[1] (labelled A,B,C, and D in Fig. 2.5.5) within it could be traced as a resolvable entity for three hours before decreasing in intensity to that of the diffuse decaying echo in which it was embedded. All the time the echo-mass of the Wokingham storm (1) was progressively increasing in size as it continued to propagate towards the right owing to the formation of fresh cells at intervals of about 20 minutes. In contrast with the growth of new cells during the intense phase, the cells developing after

---

[1]Later referred to as a 'supercell', (see appendix 2.2a).

about 1445 formed quite detached from the main body of the Wokingham storm (1) echo-mass, even at full-gain (see Fig. 2.5.4). Thereafter the rate of formation of new cells increased in inverse proportion to their intensity, size, and persistence until the storm reached the North Sea when regeneration ceased altogether.

Some of the cells comprising storm 4 persisted for two hours but the average duration of cells, as well as the rate of propagation, was such that this echo-mass remained appreciably smaller than that of the Wokingham storm.

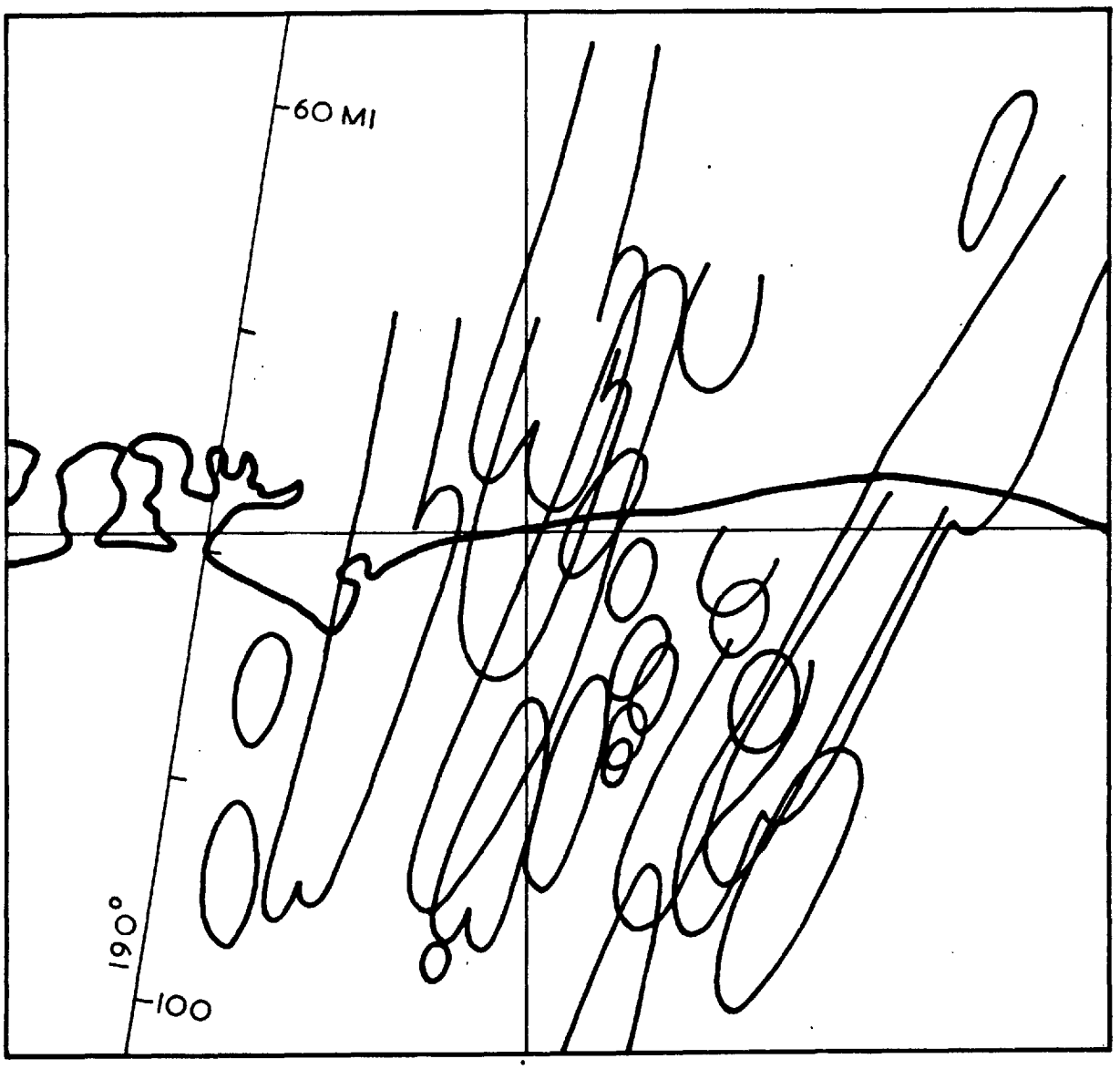

Fig. 2.5.1.
Paths of cells comprising the group classified as storm 3 during the period 1150 to 1300 as they crossed the Sussex shoreline. Notice their short duration and lack of organization.

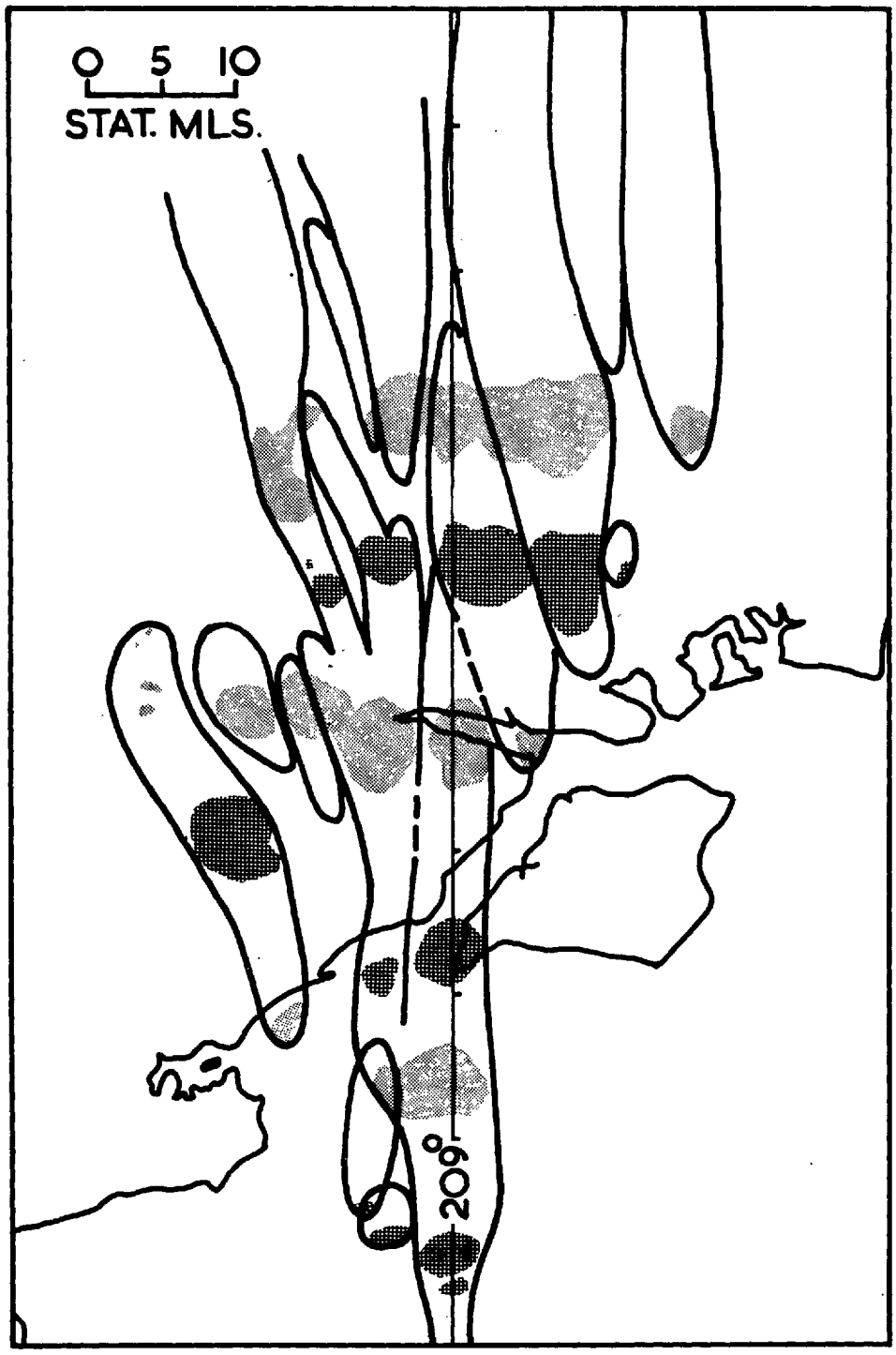

Fig. 2.5.2 Paths of echo-masses comprising storm 2. Their positions are indicated at times 1051, 1109, 1124, 1145, 1203 and 1218.

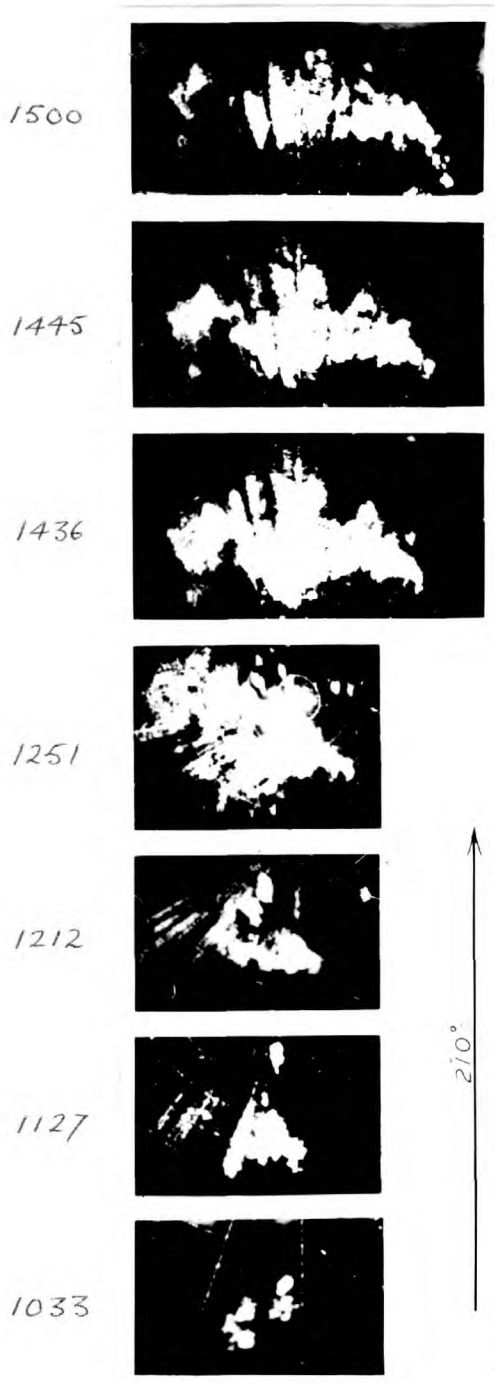

Fig. 2.5.3

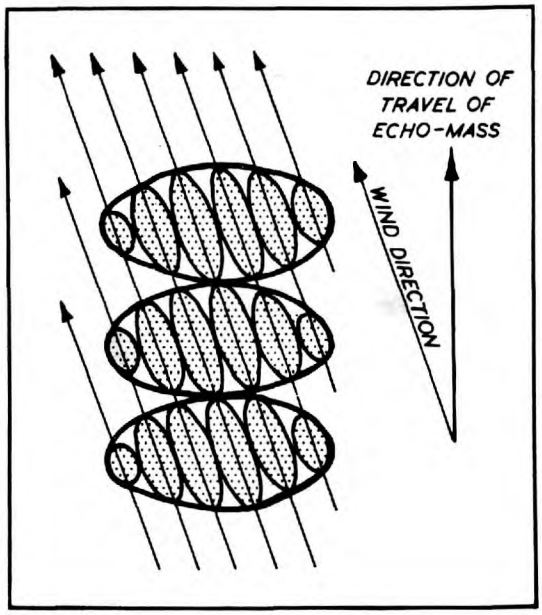

Schematic diagram illustrating how the formation of new echoes at the right flank of the storm and their eventual decay on the left flank causes the movement of the echo-mass as a whole to the right of the winds.

Fig. 2.5.4
Series of full-gain 10 cm photographs showing the changing form of the echo-mass of the Wokingham storm (1) as it travelled across S.E. England. The scale is such that the larger photographs represent areas 115 mi wide. Care has had to be exercised in the interpretation of these pictures because certain breaks in the left-hand part of the echo-mass are due to the blocking effect of obstacles close to the radars.

Fig. 2.5.5
Paths of cells comprising storms 1 and 4, as determined largely from the 10 cm PPI records. Boundaries between adjacent cells are terminated as soon as it becomes impossible to resolve them on all reduced-gain photographs. (The two heavily shaded paths are of the compact CLUSTERS of cells which can be seen in the 1033 photograph in Fig. 2.5.4).
Note especially the longevity of many of the cells and their systematic formation on the right flank of each echo-mass.

6. The behaviour of the Wokingham storm (1) before its intense phase

Fig. 2.4.1 (i) shows that 1-inch hail (size 6) occurred just inland of the south coast. It appears that this fell at about 1035 from a cell at the rear of the left-hand cluster of cells shown in Fig. 2.5.4; its maximum echo height was 40,000 ft and the maximum intensity was [63][1]. Afterwards this particular cell decayed remarkably quickly: during a period of 10 minutes its leading edge remained stationary, while the rear continued to advance until the echo disappeared. Almost certainly the cloud producing this echo had previously discharged hail over the sea, since hail of size 5 was reported only 1 mile from the coast (at the habitation nearest to the coast in this vicinity).

While this cell was decaying others within a second cluster but a few miles east were moving inland. By 1124 two further cells (A and B) had formed on their right flank and at 1133 a third (C) was appearing. These cells are represented schematically in Fig. 2.6.1 and their paths are shown in Fig. 2.5.5. They greatly intensified as they moved inland, and soon after they had come within range of the 3.3 cm radars they had merged to form a large and very intense 'supercell', the nature of which is the subject of later sections. All of

---

[1]Echo intensity is written as 10 log Z_e, where Z_e is the equivalent radar reflectivity in $mm^6 m^{-3}$; the figures are given alone, in ordinary brackets, or in square brackets, according as they are obtained from the 3.3 cm, 4.7 cm on 10 cm radar, respectively.

these cells were elongated along their direction of motion having been built from rows of yet smaller cells. This is demonstrated in the case of cell A by Fig. 2.6.3, which shows the range of its rear and leading edges as a function of time, determined from the full gain 10 cm PPI photographs taken at 3-minute intervals. It indicates that the cell was developed by the appearance of 8 small echoes successively during a 25-minute period within a strip 5 miles long, strongly suggesting the triggering of convection (in the medium levels[1]) by a ground feature some 10 to 20 miles upwind, in this case probably the coast-line. Accordingly most of the new echoes appeared at the rear of the row. The first three were short-lived, but others persisted to produce a cell which was 13 miles long by 1130.

At this time the axis of the cells lay along the beams of the RHI radars, so that they displayed sections along the whole length of the cells. It is interesting to compare that given by the 10 cm RHI set at 1130 (Fig. 2.6.2) with the 10 cm PPI picture for 1133 (Fig. 2.6.1), which shows that this particular cell had been extended rearwards more than its neighbours by the formation of new columns. Thus, even though the beam of the RHI set is very broad horizontally at this range, one can be confident that the succession of columns which it shows at the rear of the echo-mass, with tops lowering rear-

---

[1]Since the stability of the lowest layers precluded the formation of large clouds by convection from the ground.

ward, are actually those inferred to have existed in this cell from the PPI records (Fig. 2.6.3). During the ensuing 10 minutes (1130 to 1140) the rear edge of cell A advanced steadily at 50 mi hr^{-1}, indicating that no new columns formed at the rear during this period. The history of this cell is continued in Fig. 2.6.4, a series of 3.3 cm RHI photographs. Two particular column tops, marked T_1 and T_2, can be followed throughout this series, and can be seen to move through the cell, demonstrating that it consisted of columns which grew at the rear, reached a peak development in the middle, and eventually emerged at the front as decaying, tilted columns of particles falling freely (since they were evidently no longer in an updraught).

The 3.3 cm radar beam was carefully centred on the top T_2 for several minutes. From the pictures taken it is possible to make reasonable estimates of its rate of rise and horizontal speed, with the results which are shown in Fig. 2.6.5. At first the rising speed was nearly 20 m sec^{-1} and the forward horizontal speed was less than 30 mi hr^{-1}, at a level where the representative wind in the environment had a speed of about 70 mi hr^{-1} (Fig. 2.6.6); a little previously when the top rose through the level of strongest winds at about 35,000 ft the difference in speeds must have exceeded 50 mi hr^{-1}. As the top rose above the tropopause level (37,000 ft) the rapid diminution of its rate of rise was accompanied by a forward acceleration of about 40 mi hr^{-1} within 3 minutes. As the tower was sinking back again its forward speed appeared to be several mi hr^{-1} greater than that of the wind in the environment. It seems possible that this was due to a

divergent outflow from the column T_3 (Fig. 2.6.4) which was rising about 3 mi to the rear (see appendix 2.6a). The high forward speed persisted in the echo at lower levels, but this may simply be because the particles were falling from the spreading tops at about 35,000 ft, so that this was their effective 'generating level'.

While cell A was developing, another (B) was forming with its centre 3 miles to the right of that of cell A. Because of the narrow beams of the 3.3cm RHl radars it was possible to resolve its constituent columns from those within the adjacent cell. These may be seen in Fig. 2.6.7 together with the tops of the columns in cell A, which lay in the edge of the beam: the lower parts of these columns do not appear, their particles having been carried sideways out of the beam by a cross-wind (see section 2.13). Fig. 2.6.8 shows similar RHl sections of the next cell (C), which formed 3 miles to the right of row B; again the highest tops faintly shown in the pictures are the more strongly developed columns of the previous row (B) which lay in the edge of the beam.

Owing to appreciable attenuation by intervening precipitation, the rearmost columns comprising each row are not reliably displayed in any of the above 3.3cm RHl photographs (Figs. 2.6.4, 2.6.7 & 2.6.8). Their vertical structure can be studied using 10 cm RHl data for which attenuation may be neglected. However except in the case of cell A at the time corresponding to Fig. 2.6.2 (when there were no stronger columns on either side), the wide beam of this particular radar precluded the possibility of resolving them.

Fig. 2.6.2

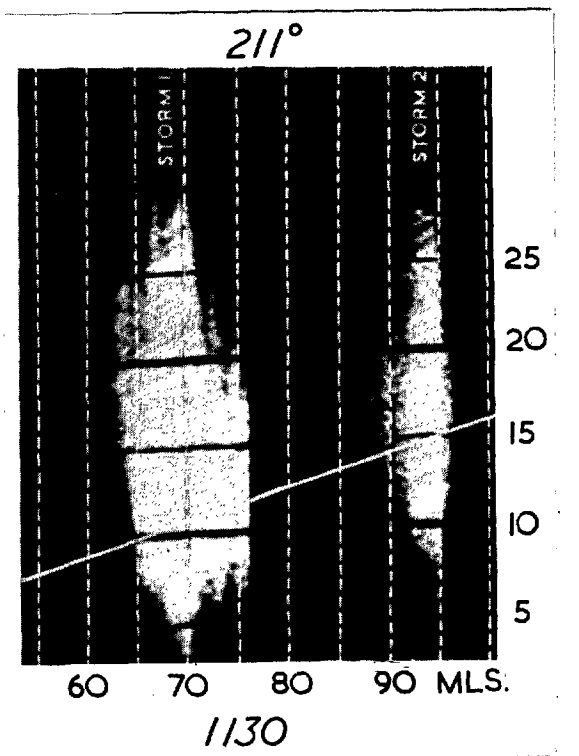

10 cm RHI photograph along the axis of cell A at 1130. Storm 2 can be seen some 15 miles behind the main storm (1). Height markers are shown at intervals of 5,000 ft and range markers at intervals of 5 miles. Notice the great height of the radar horizon at these ranges.

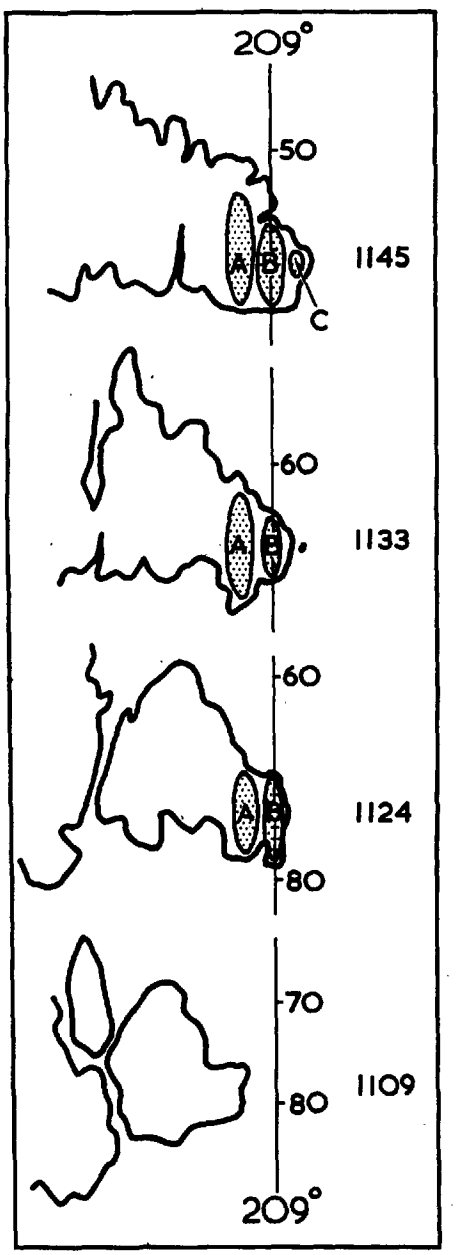

Fig. 2.6.1

Cell structure within the core of the main storm (1) before it reached its peak intensity. For clarity only one intensity contour is shown; this corresponds to [38] at 60 miles range and [42] at 80 miles range. The echo to the left of cell A was an amalgamation of a cluster of echoes which earlier had crossed the south coast; it possessed no discernible row structure.

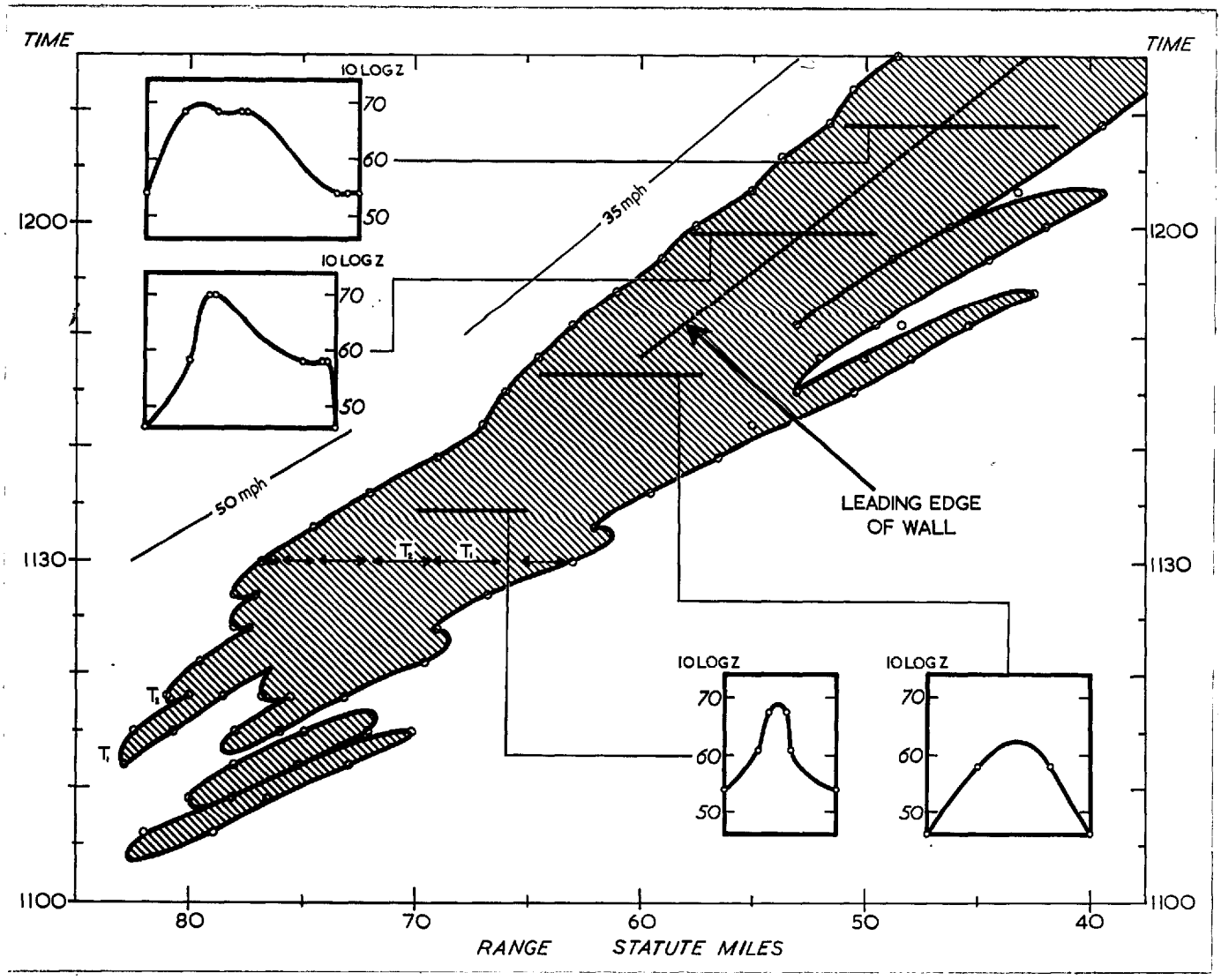

Fig. 2.6.3.
Range of the rear and leading edges of the echo of cell A as a function of time, determined from the full-gain 10 cm PP1 photographs taken at 3-min intervals. Also indicated is the position of the wall, which was obtained from the 3.3 cm RH1 photographs. Profiles of intensity are shown for times 1134, 1147, 1159 and 1209; these were deduced from series of reduced gain 10 cm PP1 photographs.
The approximate positions of the columns visible in the 10 cm RH1 photograph of cell A at 1130 (Fig. 2.6.2) are shown, and the two towers T_1 and T_2 (which can be traced throughout the series of photographs in Fig. 2.6.4) are identified.
At around 1147 cell A merged with its neighbours to form a supercell; thereafter Fig. 2.6.3 has been derived by considering that section of the echo-mass which corresponded to the continuation of cell A.

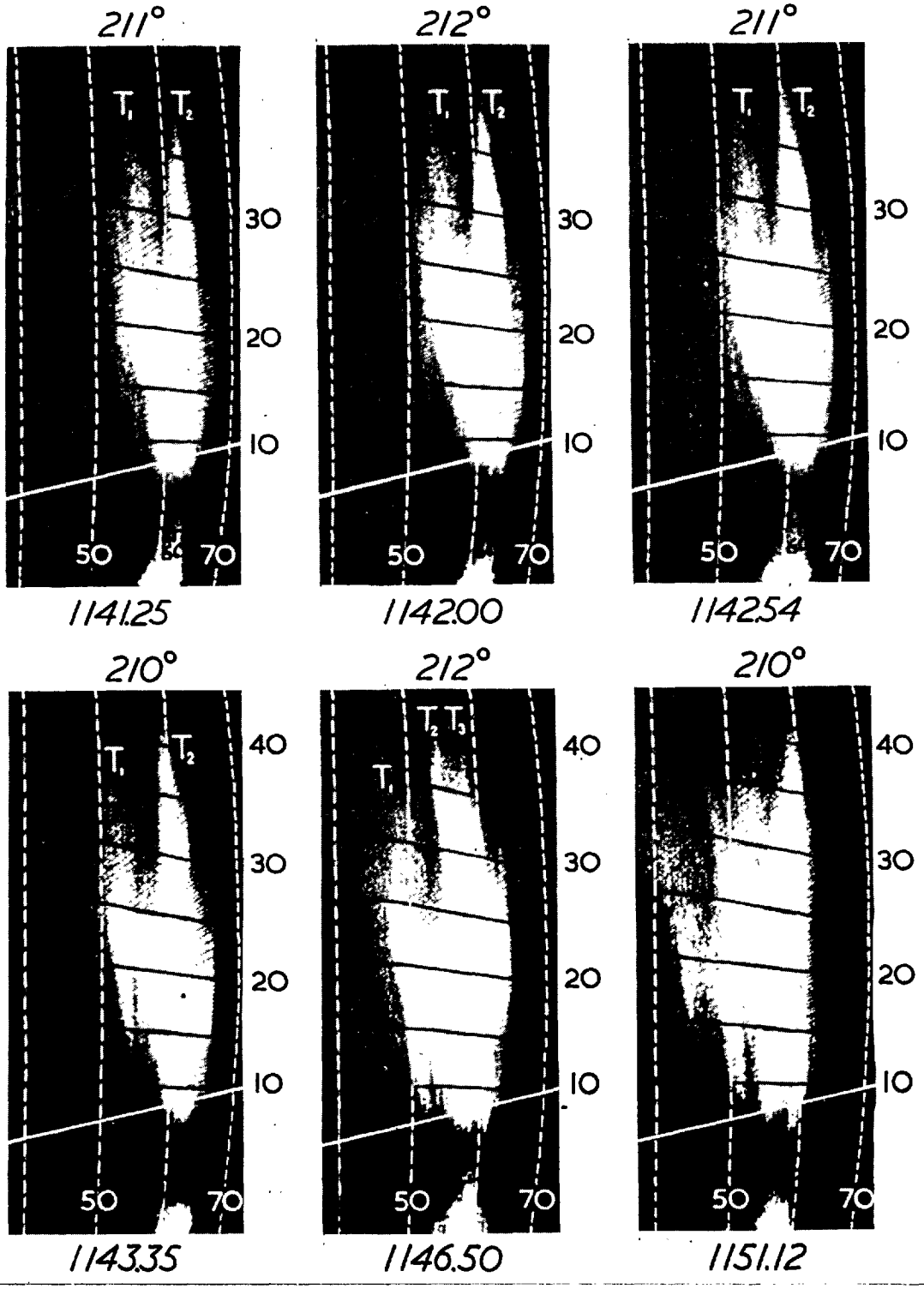

Fig. 2.6.4

Full gain 3.3 cm RHI photographs along the axis of cell A. Two towers, T_1 and T_2, can be followed throughout the series as the storm approached the radar.

Height markers are at intervals of 5,000 ft and range markers at intervals of 10 miles. The radar horizon ($1\frac{1}{4}^0$) is indicated in each photograph.

Fig. 2.6.5

Horizontal and vertical velocity of the top T_2 as a function of time: a part of the history of this top is shown in Fig. 2.6.4

Fig. 2.6.6

Comparison of the horizontal velocity of top T_2 with that of the environment. Notice that the top reached a speed which was 5 mi/hr greater than the maximum speed of the environmental wind.

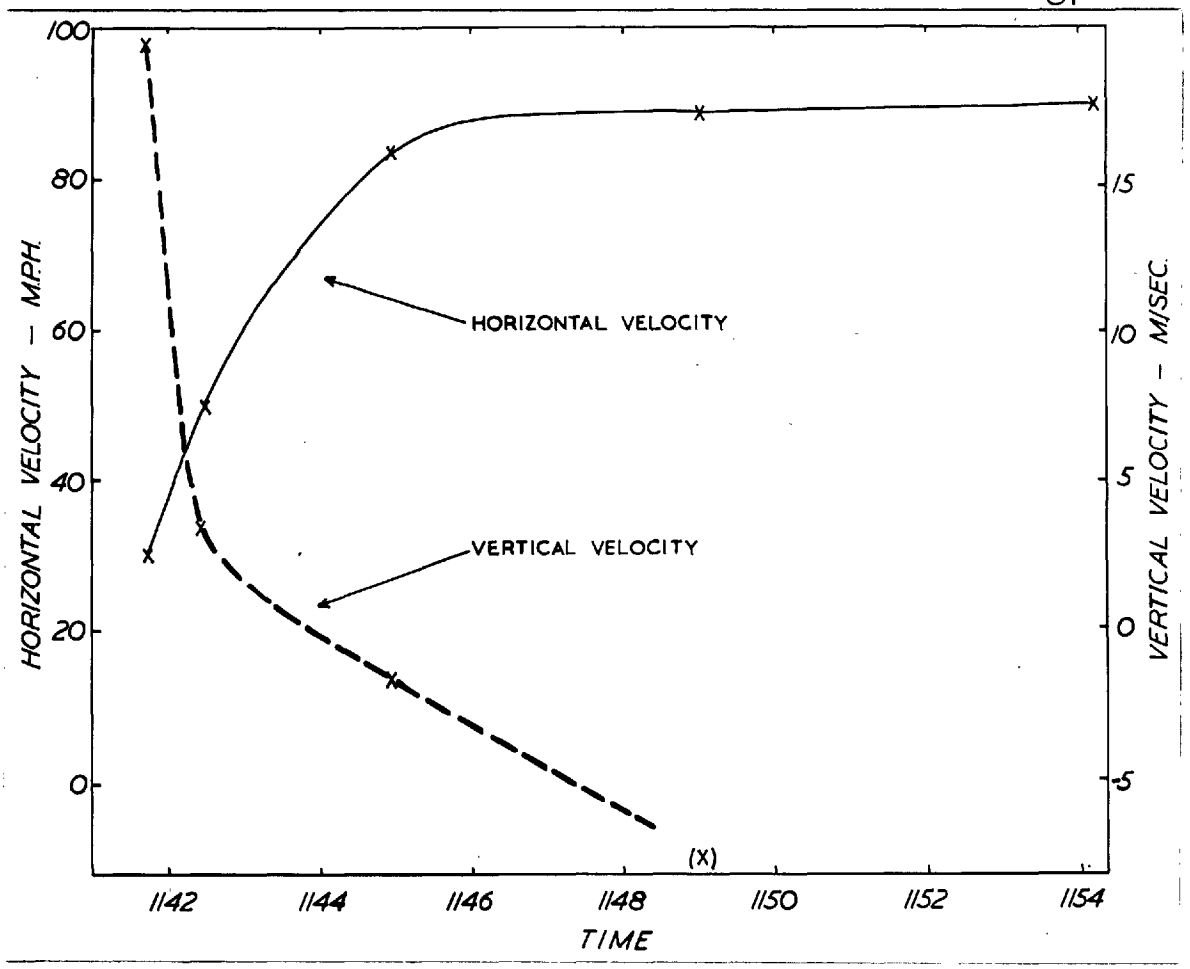

Fig. 2.6.5

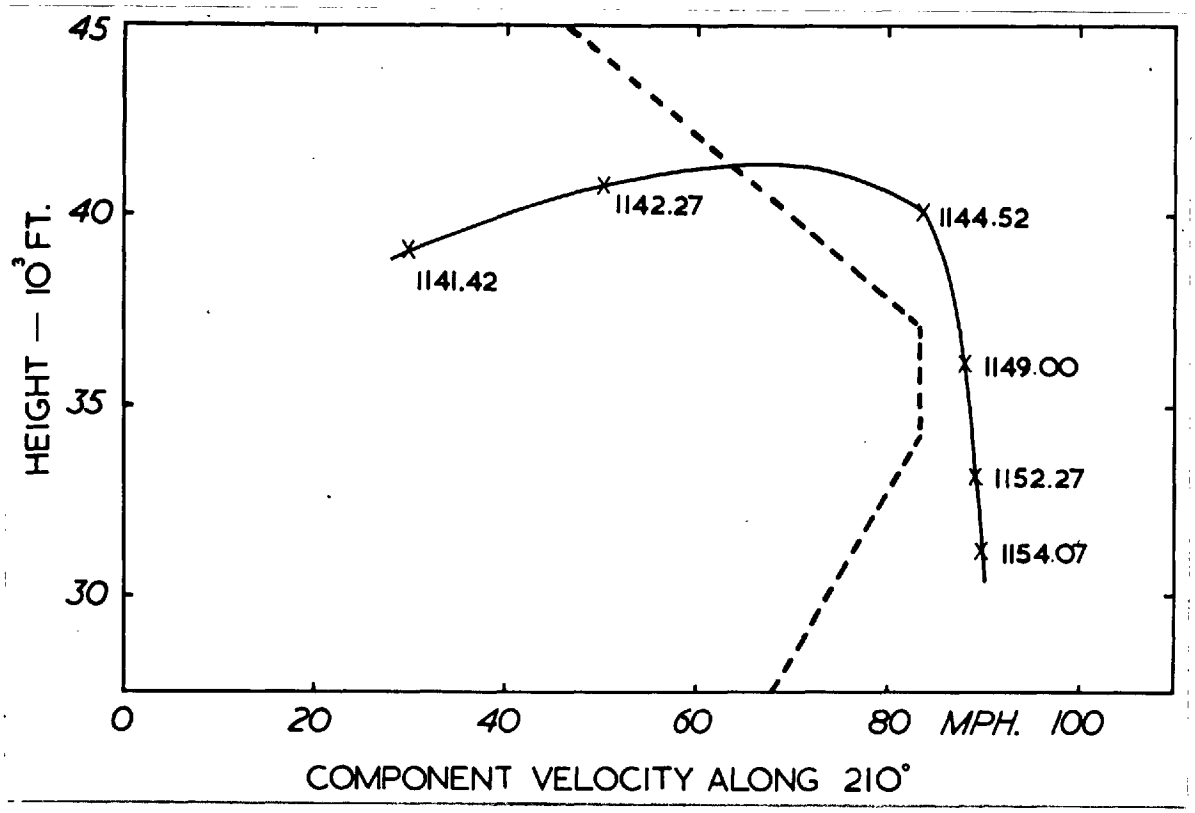

Fig. 2.6.6

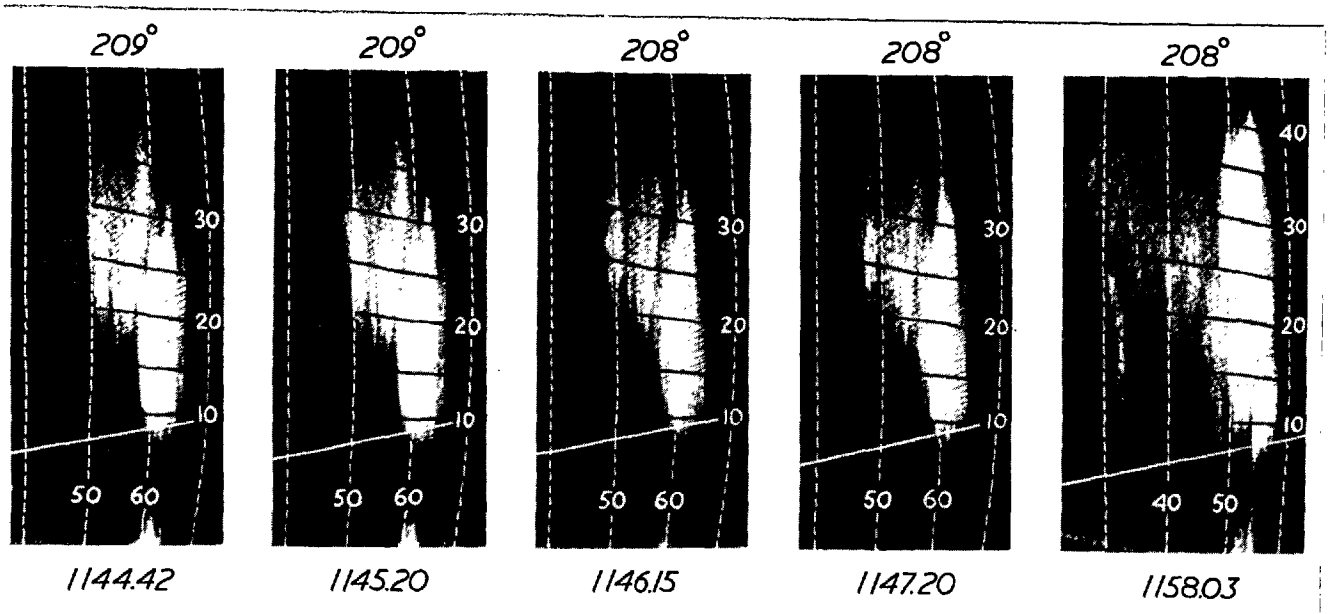

Fig. 2.6.7

Full-gain 3.3 cm RHI photographs along the axis of row B. The first 4 photographs in this series include the tops of the columns in cell A which lay in the edge of the beam. The fifth photograph, taken some time later, is typical of the most intense phase and shows the characteristic forward overhang, echo-free vault and wall with the highest top vertically above it.

Height markers are at intervals of 5,000 ft, and range markers at intervals of 10 miles. The radar horizon (at 1½°) is indicated in each photograph.

Fig 2.6.8

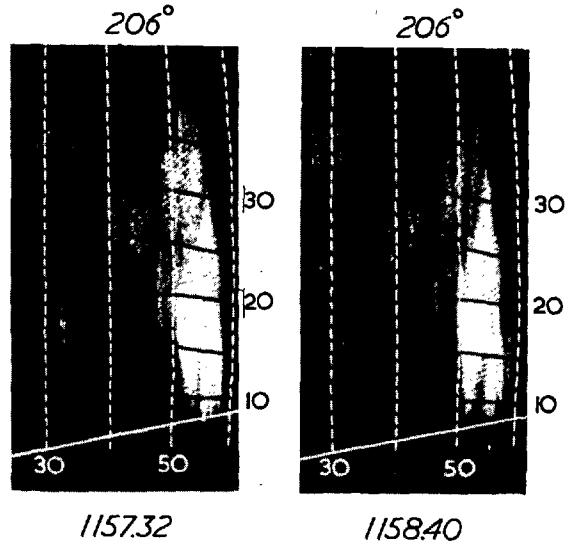

Full-gain 3.3 cm RHI photographs along the axis of row C. Also visible are the (higher) tops of the columns in cell B, which lay in the edge of the beam.

Height markers are at intervals of 5,000 ft, and range markers at intervals of 10 miles. The radar horizon (1½°) is indicated in both photographs.

Appendix 2.6a: The divergent outflow around a rising column

If the divergence was produced by the reduction of average rising speed from 20 m sec^{-1} to zero within a circular cylinder of diameter 2 miles between the levels 32,000 and 40,000 ft, the average speed of outflow 3 miles from the axis of the updraught would have been 5 mi hr^{-1}. Divergence of this magnitude is also implied by the rate of increase of echo width at a particular level as an echo column rose through it, since the echoing particles at the edges of the column near its top can be regarded as moving with only small speeds relative to the air. Typically, the columns at the 30,000 ft level had a width of about 2 miles when the tops were at 36,000 ft. If the rate of rise of the column top were 20 m sec^{-1} (4,000 ft min^{-1}) and the column had a circular cross-section, then an echo at the 30,000 ft level had a radius which increased at the rate $\frac{2}{3}$ mi min^{-1} while the column was rising. The resulting divergence is such that 3 miles from the column axis the outward velocity would again have been about 5 mi hr^{-1}.

7. The intensification of the Wokingham storm (1)

Already at 1130 cell A had become the most intense part of the Wokingham storm (1): subsequently cells B and C developed so as to share this status, by which time all three cells had become indistinguishable (within the resolution of the radars). This intensification is illustrated by Figs. 2.7.1 and 2.7.2, which contain radar data mainly from the 3.3 cm sets. These were operated manually, one to locate and follow the tops of individual echo columns (with the aim of measuring their rates of rise), and the other to locate and measure the maximum echo intensities by reducing gain until the echoes almost faded from the display. Fig. 2.7.1 shows the trends in the intensity[1] and height of the strongest echoes, in the maximum echo height, and in the maximum hailstone size as the storm was approaching the radar site.

The possibility exists that the height of the radar echo tops during the intense phase was determined by a side-lobe from a region of higher intensity some way below, thereby giving rise to an exaggerated estimate of the height of the actual cloud tops. Fortunately this possibility may be rejected since agreement to within 1,000 ft was obtained between the height of the highest 3.3cm echo tops and that of the actual cloud tops during their steady rise between 1140 and 1200 as ascertained by reconnaissance aircraft from Manby.

---

[1] Comparison of the maximum intensity of the Wokingham storm as measured by the 10 cm RH1 radar (Fig.2.7.1) with that measured by the 10 cm PP1 radar (Fig. 2.3.2) reveals a persistent discrepancy of about 10db. Although the absolute intensity values rendered by the latter are liable to some error it is unlikely that this could account for the whole difference. It is possible that the explanation of this difference may be found in the different planes of polarization of the two radars and the eccentricity of the echoing particles.

Fig. 2.7.2 illustrates in relation to the hail region where intensities exceeding 65 and 70 were found, and where column tops were observed above 40,000 and 43,000 ft. Because the 3.3cm sets were not operated systematically the monitoring of the storm was not perfect; nevertheless the diagram shows that the supercell reached its greatest intensity, with tops above 43,000 ft over a front 8 miles across at ranges between 55 and 40 miles, where the largest hailstones fell. At the same time Fig. 2.7.1 shows that the height and magnitude of the maximum radar intensity were reaching values comparable with those of echoes accompanied by tornadoes in the U.S.A. (Donaldson, Chmela and Shackford, 1960). In spite of this no definite evidence has been obtained to establish the association of a tornado with this storm, although five eye-witnesses reported 'whirlwinds', and some characteristic damage (trunk — snapping and twisting) to individual trees was found.

Around 1200 — near the height of the intense phase — a series of 13 full-gain 3.3 cm RHI sections of the Wokingham storm was obtained: this has enabled the three-dimensional description of the whole echo-mass of the storm, in the context of which the subsequent detailed analysis of the supercell is to be viewed, (see Fig. 2.7.3: because of the importance of attenuation at 3 cm wavelength only contours of the lower surface of the echo-mass are shown). It is clear from this figure that hail reached the ground over an area (deduced from surface observation) which was only a small fraction of that covered by the entire echo-mass. Much of the echo came from cumulonimbus anvil 'cloud', and was not seen on the 10 cm PPI display at short ranges, since there it lay above the beam. (The particles comprising an anvil cloud decrease

in size towards its tip and upper surface, but at moderate ranges are mostly sufficiently large to produce a detectable radar echo).

Although the storm temporarily weakened (with a consequent diminution of maximum hail size) as it approached within 30 miles of the radar site, Fig. 2.7.2 shows that it reintensified when it was some 15 miles to the east of the site. A three-dimensional picture of this storm (and also of storms 3 and 4) during this phase has been constructed from 17 full-gain 10 cm RHI photographs taken at 10° intervals between 1353 and 1357. This is shown in Fig. 2.7.4 which contains contours of the upper surface of the echo: these are not unduly affected by attenuation but are smoothed azimuthally owing to the wide beam of this radar. An interesting feature of this diagram is the presence of a region of echo extending above 30,000 ft to the left of the intense core of the main storm. This region comprised the amalgamation of the cells which earlier had given rise to the first intense phase. Although these had formed up to 2½ hours previously the firmness of their tops indicates that convection was still active within them — a point which is developed in the next section.

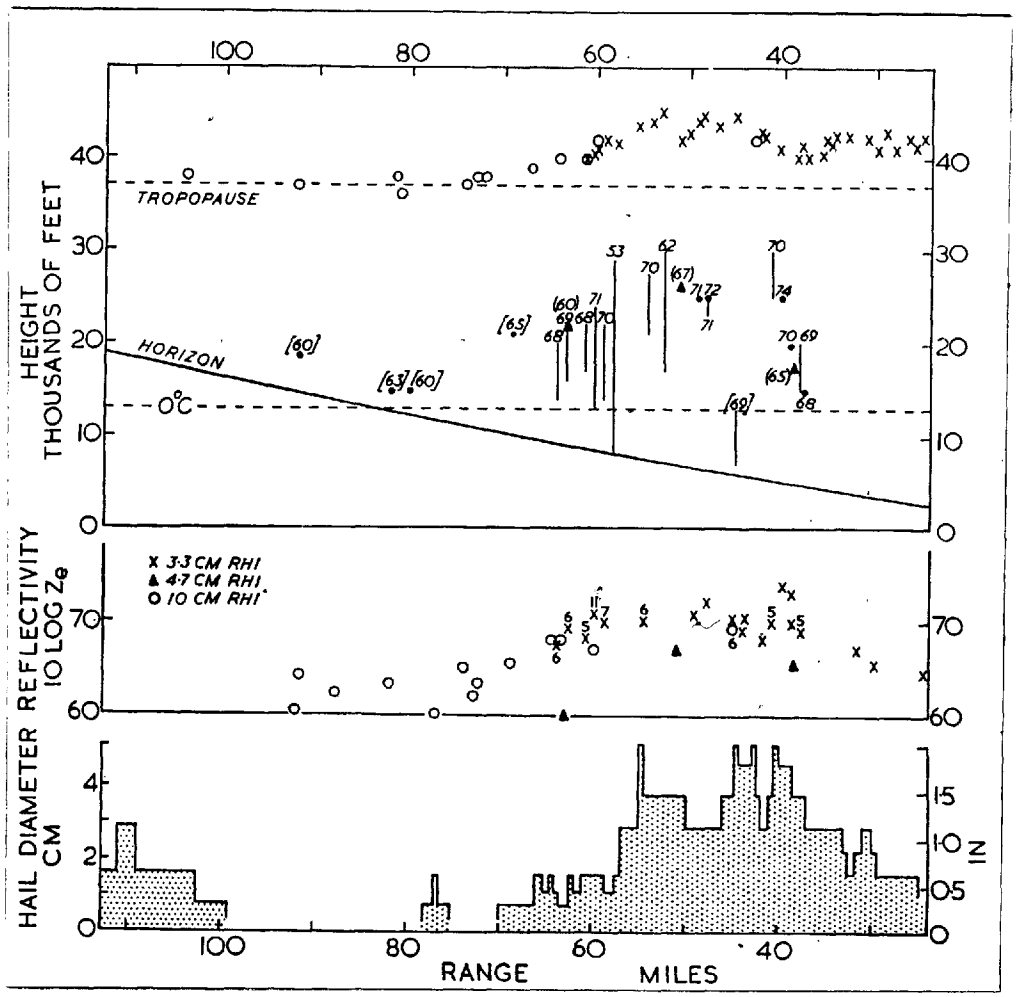

Fig. 2.7.1 Maximum hail size at the ground (bottom), and observations at 3 wavelengths of radar echoes (above), in the Wokingham storm. In the uppermost diagram the position of the radar horizon, peak echo heights, and the vertical extent of strong echoes are shown (figures beside the last indicate intensity as 10 log Z_e, alone or in square or ordinary brackets according to whether the wavelength is 3·3, 10 or 4·7 cm respectively). The middle diagram again shows the intensity of the strongest echoes. Figures beside the crosses indicate the vertical extent, in thousands of feet, of the strongest 3·3 cm echoes.

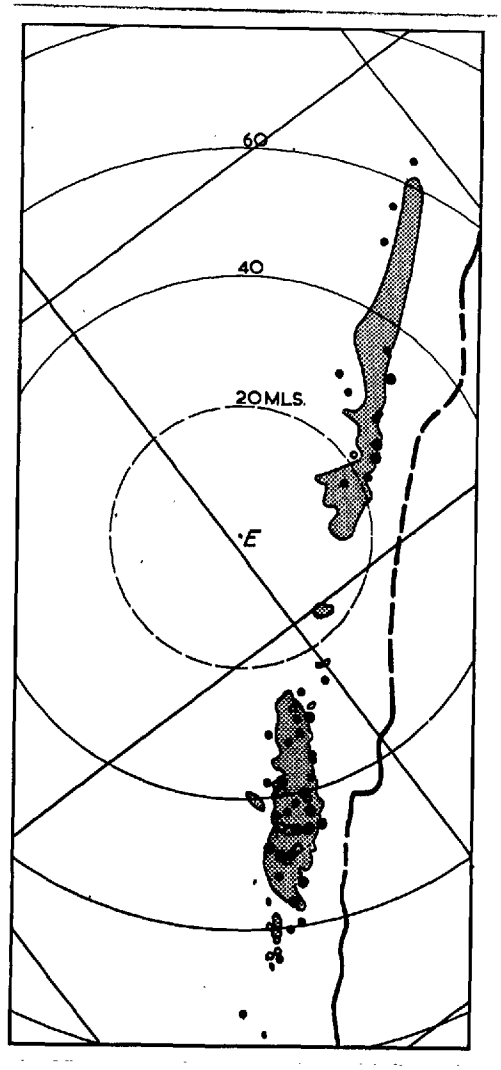

Fig. 2.7.2 The positions of highest echo tops and greatest echo intensities, as obtained by the 3.3 cm RHI radars, superimposed upon the region where the maximum hail size exceeded size 4 ($\geq \frac{1}{2}$ inch).

The small and large open circles denote observations of intensities which are equal to or exceed 65 and 70 respectively: the small and large filled circles denote the positions at which tops were observed at or higher than 40,000 ft and 43,000 ft respectively. (When a top exceeding 40,000 ft was followed for some time, only the position at which it reached its peak height is plotted.)

E denotes the position of the East Hill radar station. The thick line represents the path of the right flank of the main storm. Notice that tops above 43,000 ft occurred over an 8-mile-wide front at a range of 45 miles.

It was impossible to survey the tops within 20 miles because they were above the tops of the radar beams.

Fig. 2.7.3

General structure of the main storm (1) at 1200 as shown by contours of the height of the full gain echo base obtained from a series of 13 3.3 cm RHI sections along the azimuths indicated. The contours are drawn dashed at long ranges where they are rendered inaccurate owing to attenuation, and at short ranges where the base of the anvil 'cloud' lay above the top of the radar beam. The right-hand edge of the anvil at 30,000 ft was obtained from the MPS-4 data, and the approximate extent of the hail region was inferred from ground observations. E denotes the location of the East Hill radar station.

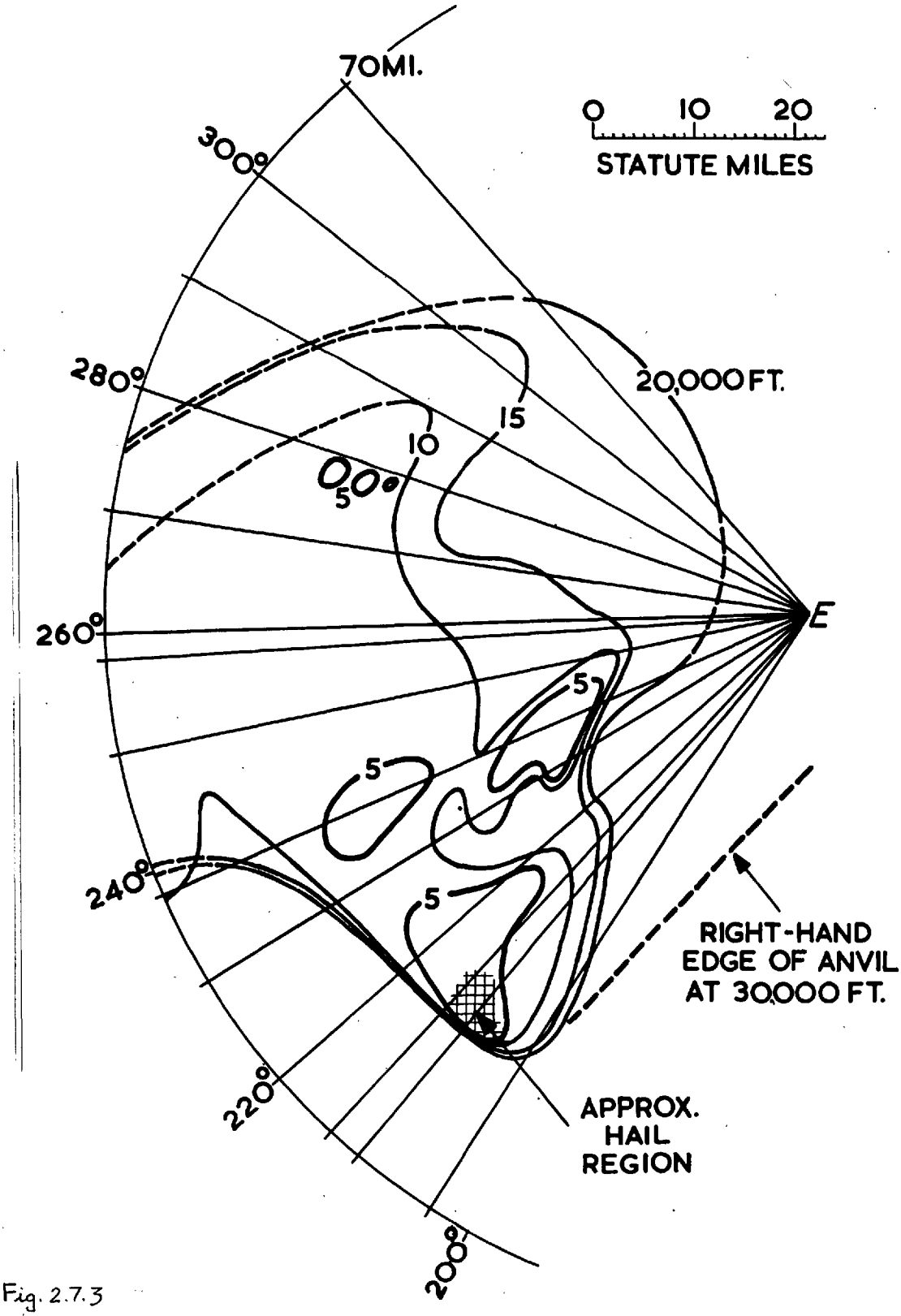
70MI.
300°
280°
260°
240°
220°
200°
0 10 20
STATUTE MILES
20,000FT.
15
10
5
0
5
E
5
5
RIGHT-HAND
EDGE OF ANVIL
AT 30,000 FT.
APPROX.
HAIL
REGION

Fig. 2.7.3

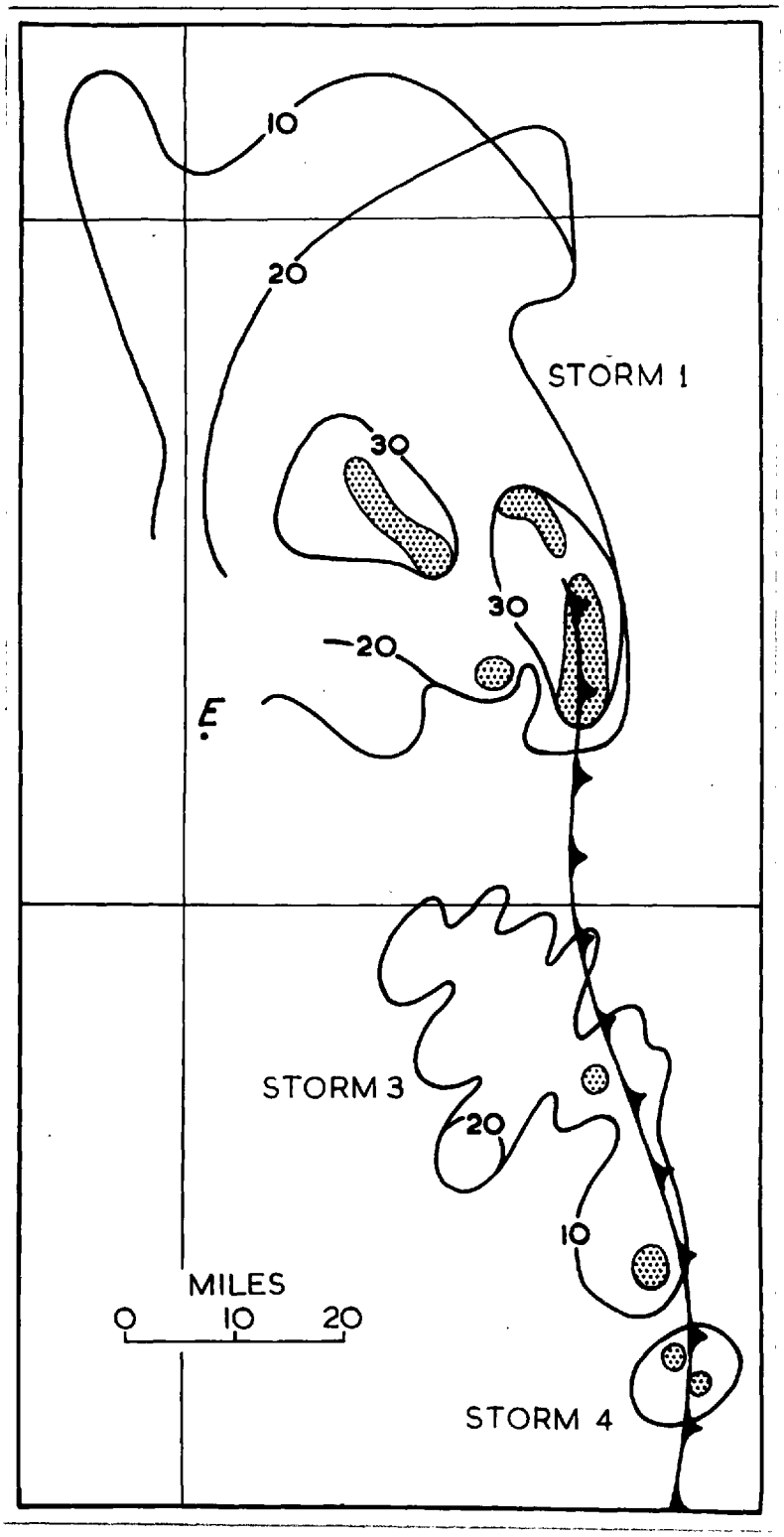

Fig. 2.7.4
Contours of maximum echo height (labelled in units of 10,000 ft) deduced from a series of 10 cm RHI photographs taken at 10° — intervals between 1353 and 1357. The approximate extent of regions of sharply-defined (i.e. rising) echo tops is denoted by stippling. Also indicated is the position of the surface gust front, as determined from surface wind observations at 1400.

8. Some characteristics of severe storms in general

(1) The duration of storms

It has been demonstrated in section 2.2 that the Wokingham storm persisted more than 8 hours, and that for most of this time it was travelling rapidly (at 40 mi hr^{-1} increasing to 45 mi hr^{-1} as it weakened after 1400), depositing hail over a long, narrow, and nearly straight swath. It was already established in the last century that this is typical of the behaviour of severe thunderstorms in middle latitudes. For example, Gibson wrote in 1863 that "in Europe hailstorms usually travel in straight bands of great length but small breadth..... A hailstorm which fell on 13 July 1788 began in the morning in the south-west of France and reached Holland in a few hours destroying a narrow line of country in its path". Marriott (1892), who studied British thunderstorms with the help of about 200 voluntary observers, cited two examples in which storms "were tracked across England in a direct line from south to north for over 400 miles, the rate of progression being 50 miles an hour", (Fig. 2.8.1). Prohaska (1907), who investigated storms with a network of several hundred observers in Austria, also showed that hailstorms affected bands of country some hundreds of km long but less than 20 km across, usually moving at a speed of about 30 mi hr^{-1} from some westerly or south-westerly point, often against a cool surface wind. In more recent studies travelling storms have been observed to produce hail over long tracks in New England: these have been called 'hail repeaters' by Donaldson. Well-developed downdraughts in these storms are implied by the finding that damaging

winds are associated only with hail repeaters and not with local storms (Donaldson, Chmela and Shackford, 1960).

According to Newton (1960) intense storms typically travel to the right of the winds, and the analysis in section 2.5 suggests that this be attributed to their composition from cells of shorter duration which intermittently form on the right flank. Thus although severe storms comprise convective cells persistently over long periods — so that one can talk of a persistent convective process on a large scale — the individual convective cells have a shorter life. Occasionally a cell disappears within 10 minutes of its initial appearance, the precipitation evidently all reaching the ground or evaporating, but more commonly the cell quickly enlarges and intensifies; afterwards it can often be followed for an hour or two without great change (or even longer, as in the case of the amalgamation discussed at the end of the previous section), and this is much longer than the period required for air in a moderate convective updraught to move through the cloud or for the precipitation particles formed in it to reach the ground. Clearly there must then be a persistent updraught within such a cell, and a continual renewal of precipitation by a process whose details generally seem to be beyond the capability of radars of conventional resolution to detect.

(2) The speed of travel of storm cells

Prohaska recognised that the severe storms typically occurred in the border regions between warm and cool air masses (cold front zones) where there is a marked variation of wind with height, and that they

move with the velocity of a middle level current, frequently opposed to the surface wind (in accord with the popular belief that thunderstorms "come up against the wind"). In recent years it has been confirmed that the travelling speed of convective cells is that of the wind at some level in the middle troposphere (Ligda and Mayhew 1954; Newton and Katz, 1958): moreover, on occasions of severe storms there is often a strong wind shear in the lower troposphere, high wind speeds occurring in the middle and upper troposphere (see e.g., Ramaswamy, 1956, referring to Indian storms, Dessens, 1960, and Newton, 1960).

(3) The air circulation in storm cells

A consequence of the preceding section is that convective cells must in general contain a circulation in which the potentially warm low-level air enters their forward (down-shear) side. In the typical circumstance that the wind shear is almost uniform with height and the wind in the high troposphere has the same direction and a greater speed than the storm velocity, it is observed that the anvil cloud stretches in front of the storm, often for great distances. This implies that the potentially warm air also leaves the storm (in the high troposphere) on the forward side. Furthermore, since the potentially cold air present in the upper troposphere overtakes the storm from the rear, and can often be identified at the ground in the rain area and behind the storm (Normand, 1946), it follows that the circulation also contains a downdraught derived from high levels and is organised as shown schematically in the vertical section in Fig. 2.8.2 (i).

At the ground behind a storm the low wet-bulb potential tempera-

tures often observed imply not only the descent of upper-level air but also the evaporation into it of a large amount of water. This can be derived only from that condensed within the updraught, so that the circulation is likely to be of the form shown in Fig. 2.8.2 (ii): here the updraught is partly inclined over the downdraught, so that one can envisage the precipitation of condensed water into the downdraught. As Normand pointed out (1946), this enables a storm to benefit from energy available in descending currents instead of having to supply energy to them as in the case of dry descent. The invigoration of convective clouds often noticed after the onset of precipitation (e.g. Thorkelsson, 1946; Craddock, 1949; Ludlam and Saunders, 1956; Howell, 1960) is probably associated with the establishment of such a downdraught. Whereas in cumulus convection buoyant air ascends intermittently in thermals of restricted volume which are released following a convective overturning within a superadiabatic layer at the ground which is only a few hundred feet deep, the cold downdraught produced by the precipitation in cumulonimbus gives rise to strong horizontal temperature differences throughout the lower troposphere with the result that overturning occurs within a layer which can be some two orders of magnitude deeper. In the presence of a wind shear and the ground, which causes a spreading of the downdraught, the overturning becomes organized in such a manner that the cloud is fed by a much larger updraught in which conditions are closer to adiabatic.

In Fig. 2.8.2(ii) the updraught is drawn separated from the downdraught by a sloping surface which near the ground can be identi-

fied with the familiar squall front which heralds the approach of the storm. The model now resembles those often drawn to represent an ordinary cold front: it differs from previous storm models mainly in that it implies that in the presence of some wind shear the up-and downdraughts can be maintained continuously, without serious interference, from opposite sides of the storm. It represents a disturbance which is essentially an open system, working in an extensive environment which is inverted with a conversion of potential into kinetic energy.

Many storms have a duration which suggests that for a considerable part of their existence they contained this circulation in a virtually steady state. An unpublished preliminary theoretical treatment by Pearce suggests that such a steady circulation can be maintained by a distribution of heat sources and sinks plausibly representing the effects of vapour condensation in the updraught and precipitation evaporation in the downdraught. However, some important aspect of the behaviour of real storms have become apparent which cannot be represented in only the two dimensions of the model drawn above (see section 2.12). Unfortunately the development of a theory accepting the storm as a three-dimensional disturbance, and eventually also embracing its development into a virtually steady state, is a formidable task. Nevertheless even the simple two-dimensional model may explain some familiar properties of storms such as (1), the preference of the severest to occur where there is marked wind shear and a low wet-bulb potential temperature in the middle troposphere, and (2), the organized storm's

independence of surface heating, the lifting near the squall front being sufficient to realise latent instability. It may also account for some properties of other disturbances in which precipitation develops in the presence of wind shear, such as in 'stable' air at warm and cold fronts, and in cirrus clouds.

In the ensuing sections the respective intensive analyses of the radar data and surface weather associated with the intense phase of the Wokingham storm of 9 July 1959 are utilized to deduce the existence of a virtually steady air flow of the kind adumbrated above. It is shown in the next section that this was made possible because the persistent strength and extent of the updraught within part of this storm enabled certain characteristic feature of the echo distribution to be resolved by the radar.

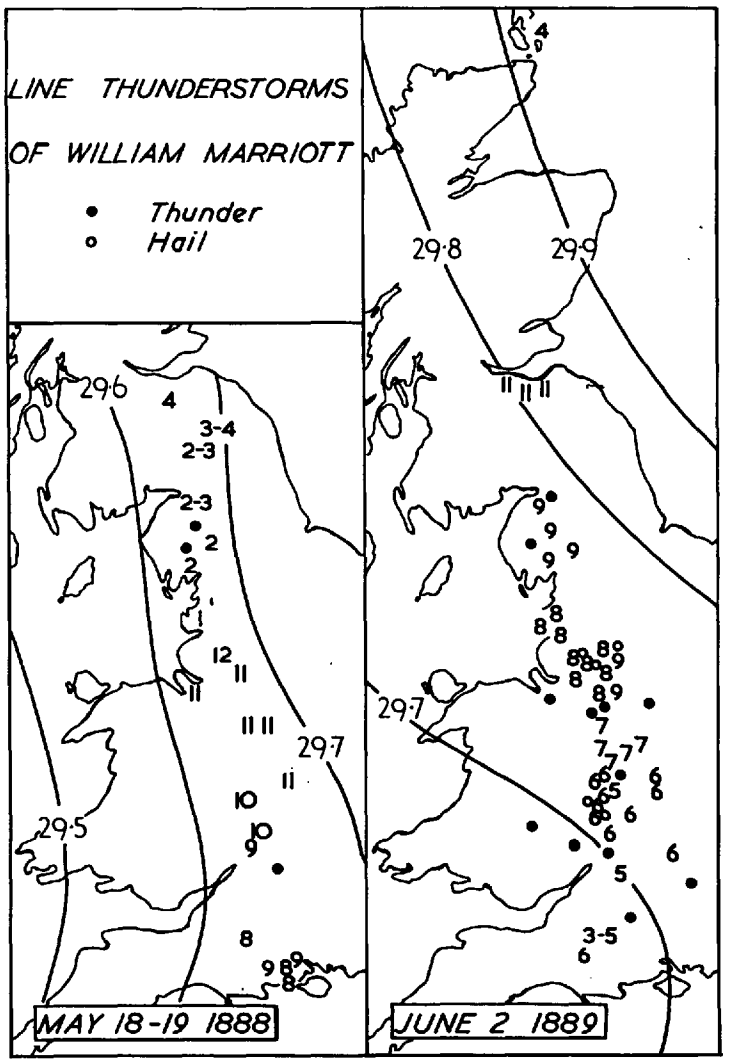

Fig. 2.8.1 Examples of the "line thunderstorms" of Marriott; the lines are sea-level isobars and the numbers show the last figure of the clock hour nearest to the time of the thunderstorm, according to the reports of voluntary observers.

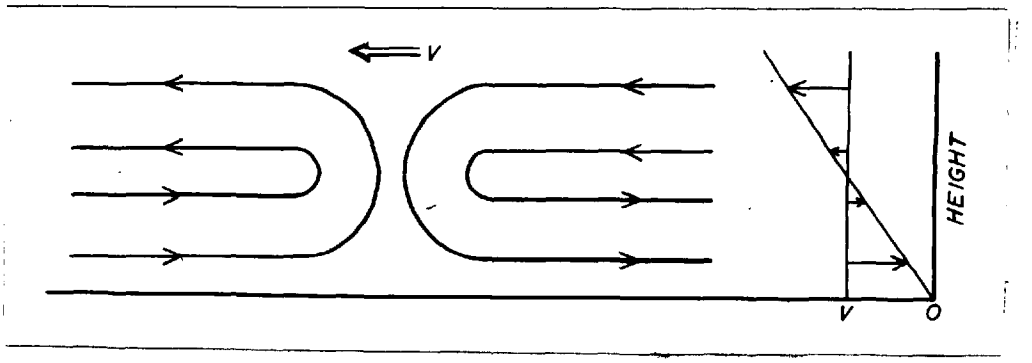

Fig. 2.8.2 (i)
Large and persistent convective disturbances travel at the speed of the wind at some mid-tropospheric level. This figure shows schematically the kind of circulation which this implies in a vertical section along the direction of travel when the wind speed increases practically linearly with height at all levels.

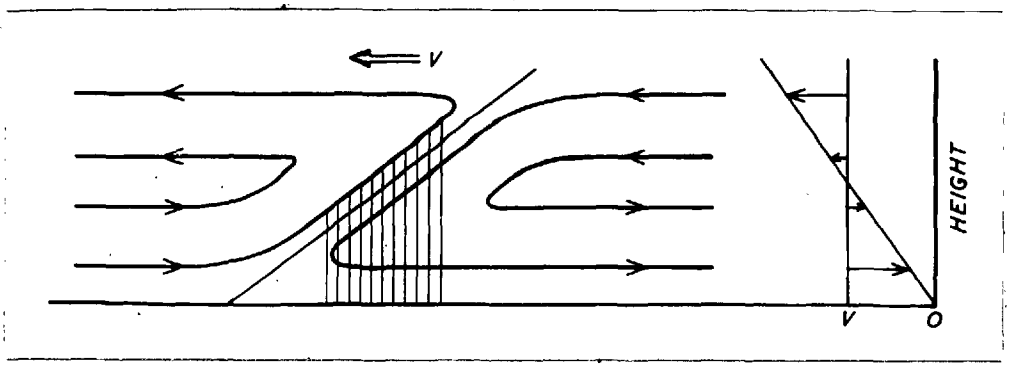

Fig. 2.8.2 (ii) shows the air-flow in Fig. 2.8.2 (i) modified so that condensed water may be precipitated from the updraught and evaporated in the downdraught.

9 The characteristic features of the supercell

It was shown in section 2.6.7 that the part of the Wokingham storm which produced the widespread large hail was formed by the amalgamation of 4 cells (A,B,C and D) to give what is called a supercell (see appendix 2.2a). These had appeared on the right flank of the intense echo-mass which earlier had deposited a little large hail near the Dorsetshire coast. At this time, before the intense phase, and also later, after the intense phase (Fig. 2.9.1 (ii)), the composition of each cell from smaller units was apparent in RHI displays which showed a succession of individual columnar echoes rising at their rear, each of which became the highest echo before subsiding and decaying at the forward side (Fig. 2.6.4).

The motion of the columns within cell A was displayed in Fig. 2.6.3: each of them travelled at between 50 and 60 mi hr^{-1}. After 1130 no new individual columns developed at the rear and so the rear edge of the cell advanced steadily at 50 mi hr^{-1}. However, with the development of the supercell this diminished to less than 40 mi hr^{-1}, although it still advanced steadily. At the same time it became impossible to discern any individual rising columns on the RHI display, even though the overall height of the echo-mass rose steadily to reach a peak of 45,000 ft, 8,000 ft above the tropopause level. This change in behaviour is attributed to the transition from a discontinuous to a continuous updraught, an explanation amply supported by further observations discussed later in this section. (A similar absence of distinct individual turrets at the storm top led Cunningham to the same

conclusion in a paper (1960) in which he describes a similar 'self-propogating' storm with the aid of some fine photographs from the air). Although the supercell weakened as the storm later approached the radar site another one developed during a second intense phase when the storm was to the east of the radars. This is demonstrated by Fig. 2.9.1 (i), which should be contrasted with Fig. 2.9.1 (ii), showing the structure 21 minutes later after the reversion to an intermittent updraught.

Throughout the first intense phase (1150 to 1220) the supercell travelled at a uniform velocity and without any marked variation in its character. Consequently it has been possible to construct representative vertical sections from the records of the 4.7 cm radar, which was used in a scanning cycle of period 12 minutes to explore the echo-mass quantitatively. Sections through the supercell along its direction of travel (210^{o}) are shown in Figs. 2.9.2 (i,ii & iii): they refer to 3 successive intervals corresponding to just before, during, and just prior to the end of, the period 1150 to 1220. The sections comprising Fig. 2.9.2 (ii) resemble in the essential features the instantaneous 3.3 cm RHI displays at about the same time (Fig. 2.9.5). Figs. 2.9.3 (i,ii & iii) contain vertical sections across 210^{o} and illustrate the tendency for the precipitation carried ahead of the storm to fall towards its left flank (right of the diagram): the discussion of this aspect is postponed to section 2.13.

Throughout the period 1150 to 1220 the vertical sections exhibited features which will be called the 'wall', the 'forward overhang' and the 'echo-free vault'.

The wall

In the central and right-hand parts of the echo-mass the leading precipitation which approached the ground formed a 'wall' with a sharply-defined upright front face orientated perpendicularly to the direction of movement of the storm. It was first observed at a range of nearly 61 miles (RH1 section for 1146.50 in Fig. 2.6.4), close to where the hail swath at the ground suddenly doubled in width (Fig. 2.4.1 (ii)). By 1158 the wall had become so much as 7 miles across and rose above 13,000 ft over much of its extent (Figs. 2.9.2 (ii) and 2.9.3 (ii)).

The steadiness of the echo structure of the supercell during the intense phase is again demonstrated by Fig. 2.9.6, which shows that the wall advanced uniformly at 40 mi hr^{-1} with its range always within 1½ miles of that of the highest echo top. (Before the wall formed at about 1147 an individual top — such as T_1, T_2 or T_3 in Fig. 2.6.4 — could be identified as the highest for 10 minutes before it was succeeded by another up to 5 miles behind; consequently in the lower part of Fig. 2.9.6 there is a greater spread in the ranges of the highest tops).

The forward overhang

This is the name given to echo which reached down to about 12,000 ft along the length of the wall and 1 to 3 or more miles ahead of it (see Figs. 2.9.2 (ii & III), 2.9.3 (ii & iii), and 2.9.5).

The echo-free vault

Nearer to the wall the base of the forward overhang rose to form

the 'echo-free vault', whose ceiling reached upwards to almost 15,000 ft close to the wall. (The conventional laterally — compressed RHI display gives a poor impression of the horizontal extent of such a feature). It too extended for several miles across the storm: on the PPI presentation of the shallow-beam 4.7 cm radar which intersects the storm between 12,000 and 15,000 ft the echo-free vault appears as an echo-free wedge or notch (Fig. 2.9.4 (i): the finger of echo ahead of the wedge represents the intersection with the tip of the forward overhang).

The existence of the forward overhang for over half an hour confirms the presence of a persistent updraught which prevented the descent of its particles. The great width of the updraught is shown by the width of the overhang, by the width at the ground of the swath of large hail (whose high fall-speed prevented significant lateral displacement after fall from the updraught), and by the lateral extent of that echo which rose above tropopause level: the 3.3 cm radars showed that at the peak of the intense phase echo reached 43,000 ft over an 8 mile front (Fig. 2.7.2).

Some irregularity in the hail distribution at the ground, the occasional brief protrusion of columnar echo tops from the summits of the echo-mass and the somewhat discontinuous nature of the curtain of precipitation falling ahead of the updraught (Figs. 2.9.4 (ii) and 2.13.1) indicate that at least in its upper parts the updraught was not quite steady, but it is evident that a persistently strong and remarkably broad updraught entered the forward right quadrant of the supercell throughout at least the half hour during which the wall and forward overhang were observed.

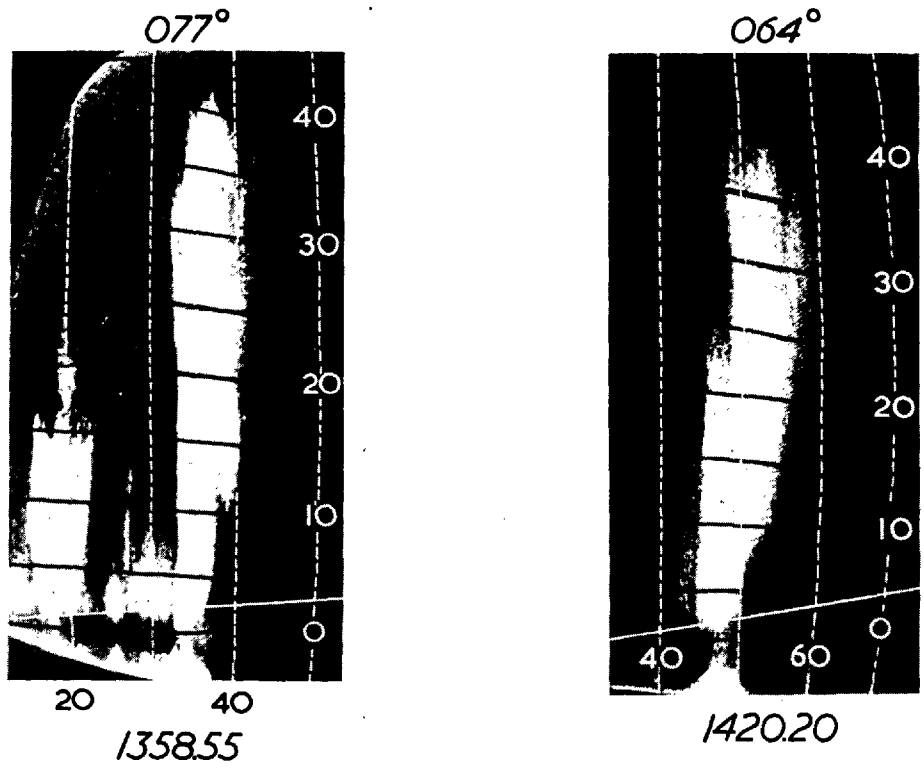

Fig. 2.9.1

Full-gain 3.3 cm RHI photographs showing (a) the characteristic forward overhang, echo-free vault, and wall with the highest top vertically above it, after the re-organisation of the storm; (b) the different appearance, with separate rising tops at the rear, during the final decline of the storm.

Fig. 2.9.2

RHI sections at 2^0 intervals through the main storm approximately along its direction of movement for the 3 periods:

(a) 1137 - 1149 (during the development of the new organisation)
(b) 1156 - 1208
(c) 1213 - 1225

These have been derived from 4.7 cm PPI photographs taken at a series of gain steps at successive elevations. These photographs have been displaced assuming that the storm as a whole moved uniformly along 210^0 at 40 mi/hr to make the ranges indicated in Figs. (a), (b) & (c) applicable to the times 1142, 1202, and 1220 respectively. The times at which the photographs at the indicated elevations were obtained are shown to the right of each figure.

The radar horizon is shown as a thick line where it intersects each RHI section.

The contours refer to different gain steps, the intensities corresponding to which are listed below:

Range to which intensity is strictly applicable (mi)	Fig. (a) 60	Fig. (b) 50	Fig. (c) 40
Coarse stipple	(17)-(30)	-	-
Medium stipple	(30)-(39)	(29)-(38)	(27)-(36)
	(39)-(51)	(38)-(49)	(36)-(48)
Fine stipple	(51)-(56)	(49)-(58)	(48)-(56)
	> (56)	> (58)	(56)-(62)
	-	-	> (62)

Because of the large horizontal extent of intense echo, the small corrections for beam-width have not been applied to these values.

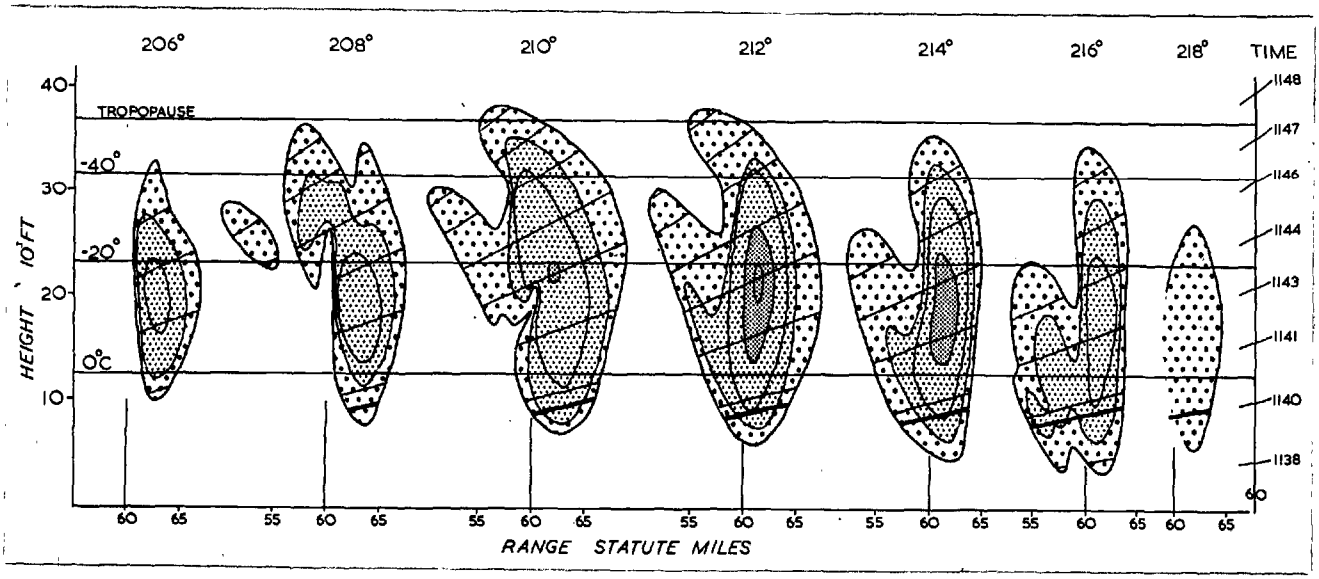

Fig. 2.9.2 (i)

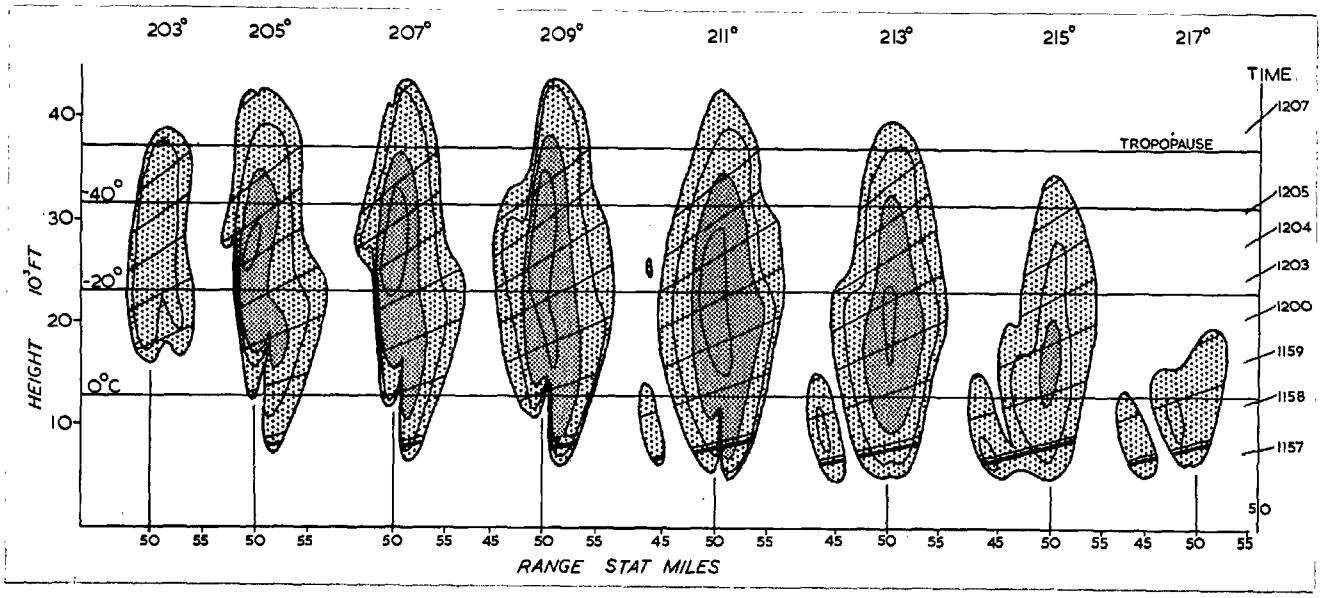

Fig. 2.9.2 (ii)

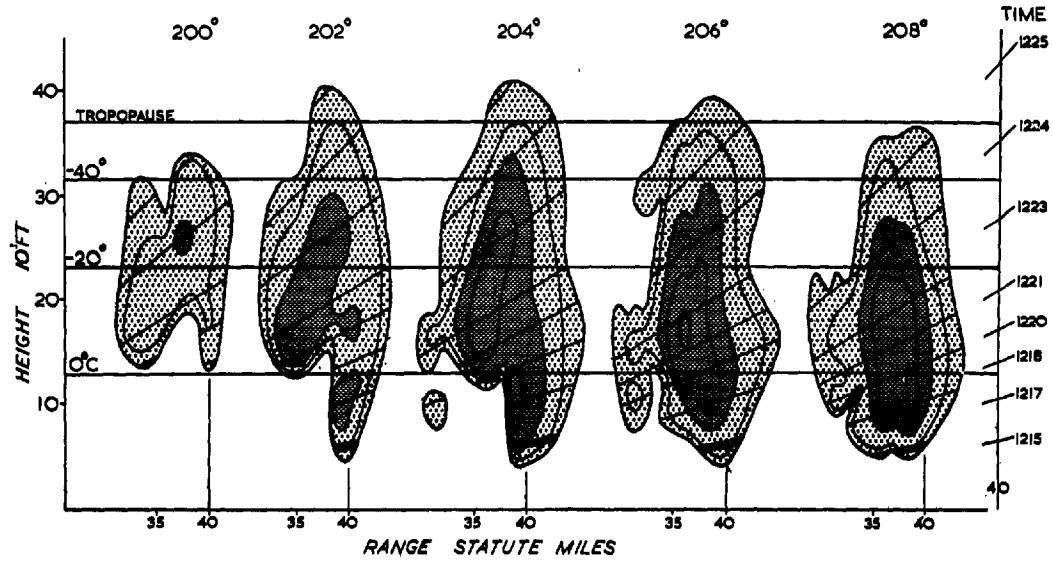
200°
202°
204°
206°
208°
TIME
1225
1224
1223
1221
1220
1218
1217
1215
40
TROPOPAUSE
-40°
-20°
0°C
HEIGHT 10³FT
40
30
20
10
35
40
RANGE STATUTE MILES

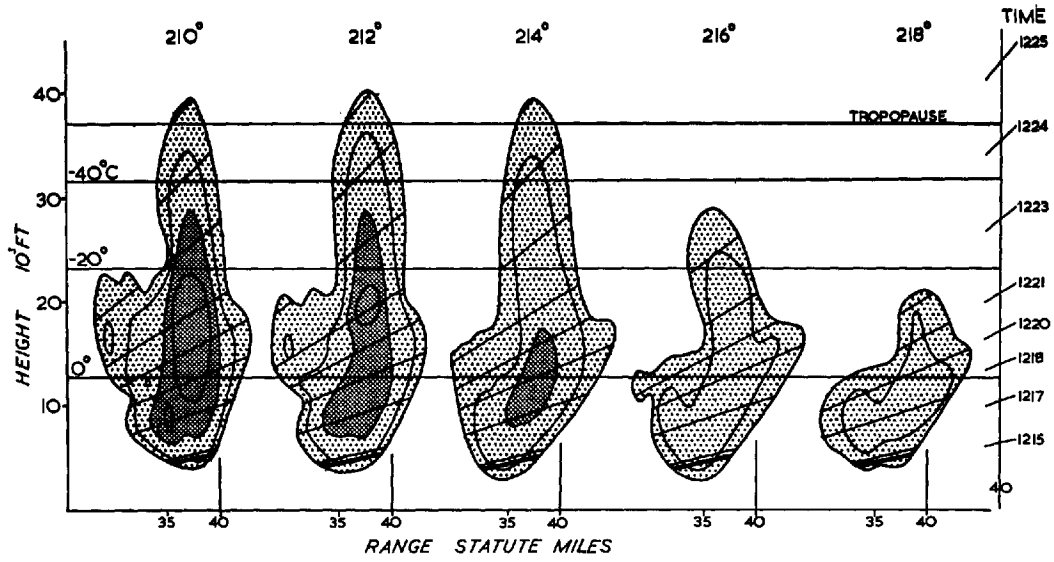
210°
212°
214°
216°
218°
TIME
1225
1224
1223
1221
1220
1218
1217
1215
40
TROPOPAUSE
-40°C
-20°
0°
HEIGHT 10³FT
40
30
20
10
35
40
RANGE STATUTE MILES

Fig. 2.9.2 (iii)

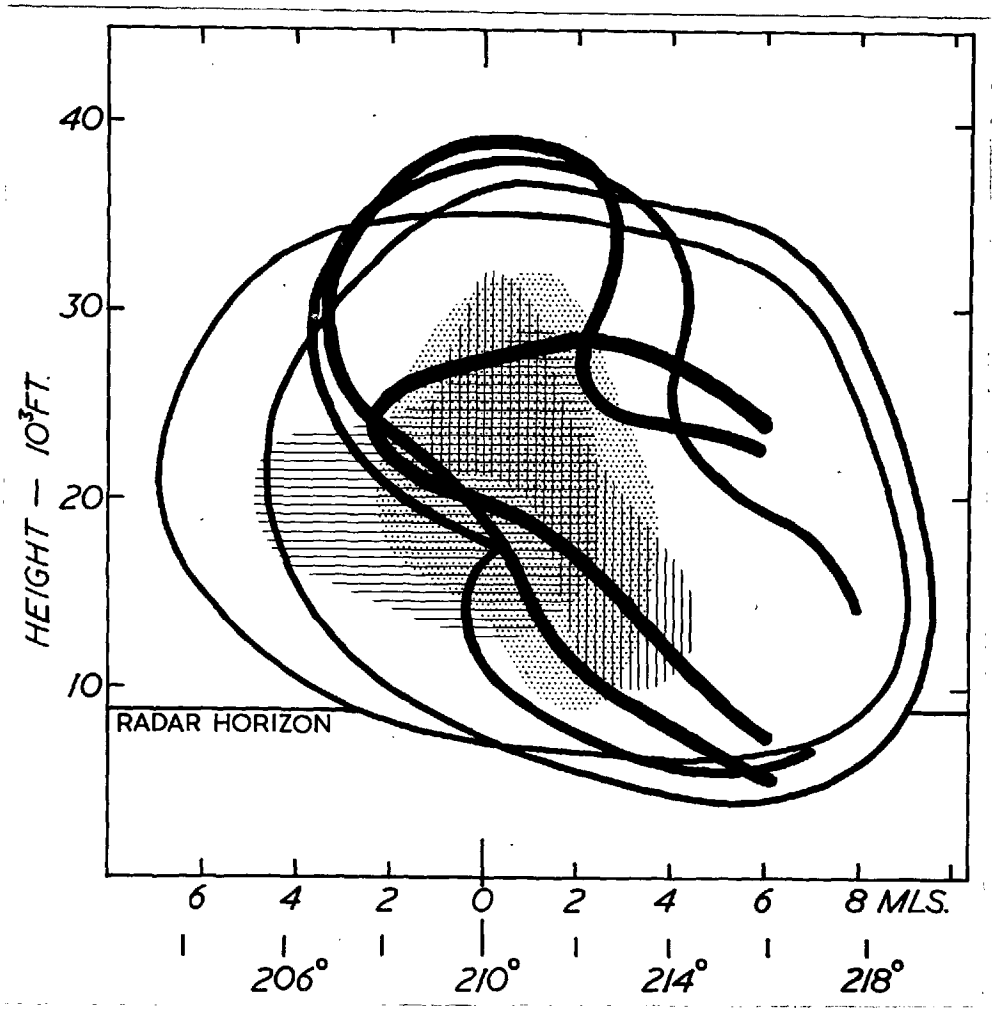

Fig. 2.9.3 (i)

Distance-height sections through the main storm at right angles to its direction of movement, applicable to the period 1137-1149 during the development of the new organisation. These are derived from Fig. 2.9.2(i). The contours represent the extent of intensity (17) at distances of 6 (thickest line), 4, 2, 0 and -2 (thinnest line) miles ahead of the wall. The vertical hatching, stippling, and horizontal hatching indicate the extent of intensity (39) at distances ahead of the wall of 2, 0, and -2 miles respectively. Sections at greater distances behind the wall are not shown because attenuation makes their interpretation difficult.

Fig. 2.9.3 (ii)

Distance-height sections through the main storm at right angles to its direction of movement, applicable to the period 1156-1208. These are derived from Fig.27(b). The contours represent the extent of intensity (29) at distances of 4½ (thickest contour), 2½, ½, and -1½ (thinnest contour) miles ahead of the wall. The vertical hatching, stippling, and horizontal hatching indicate the extent of intensity (49) at distances ahead of the wall of 2½, ½ and -1½ miles respectively. Sections at greater distances behind the wall are not shown because they are distorted by attenuation.

This diagram clearly shows the considerable horizontal extent of the forward overhang; it also shows that on the left front of the storm (right of diagram) precipitation was falling below the radar horizon (and presumably reaching the ground) more than 4 miles ahead of the wall.

Fig. 2.9.3 (iii)

Distance-height sections through the main storm at right angles to its direction of movement, applicable to the period 1213-1225. These are derived from Fig. 27(c). The contours represent the extent of intensity (26) at distances of 8 (thickest contour), 5, 2, and -1 (thinnest contour) miles ahead of the wall. The vertical hatching, stippling, and horizontal hatching indicate the extent of intensity (46) at distances ahead of the wall of 5, 2, and -1 miles respectively. Sections at greater distances behind the wall are not shown because they are distorted by the effect of attenuation.

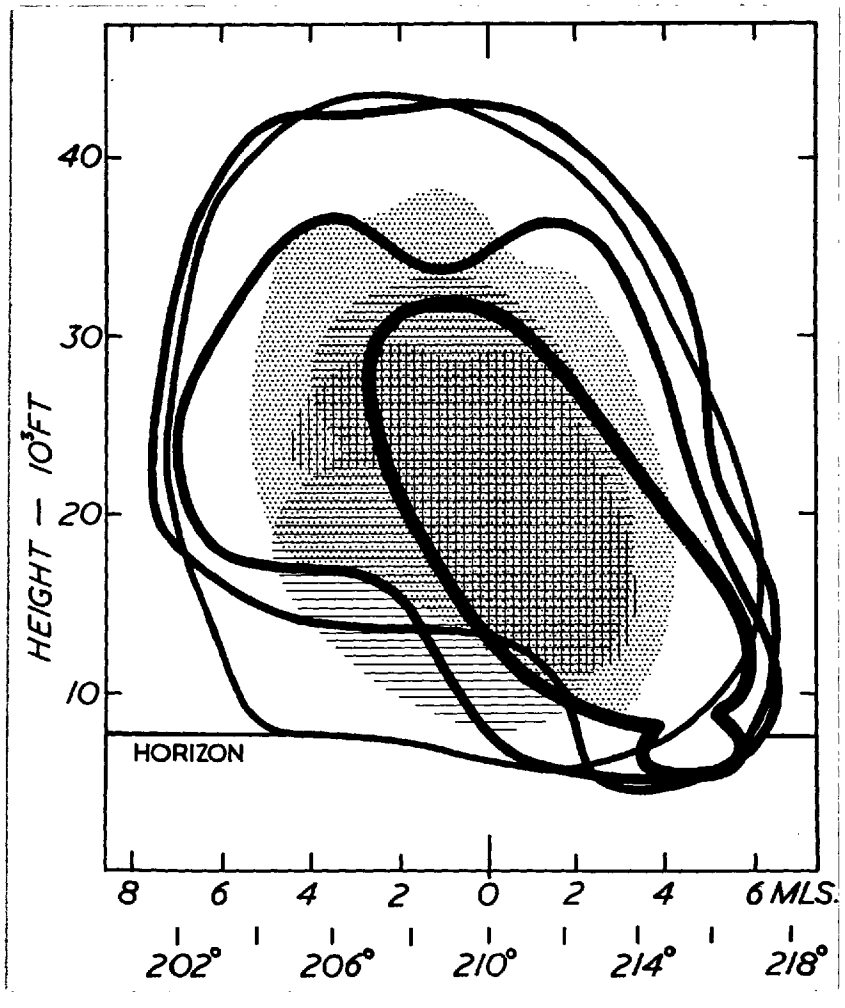

Fig. 2.9.3 (ii)

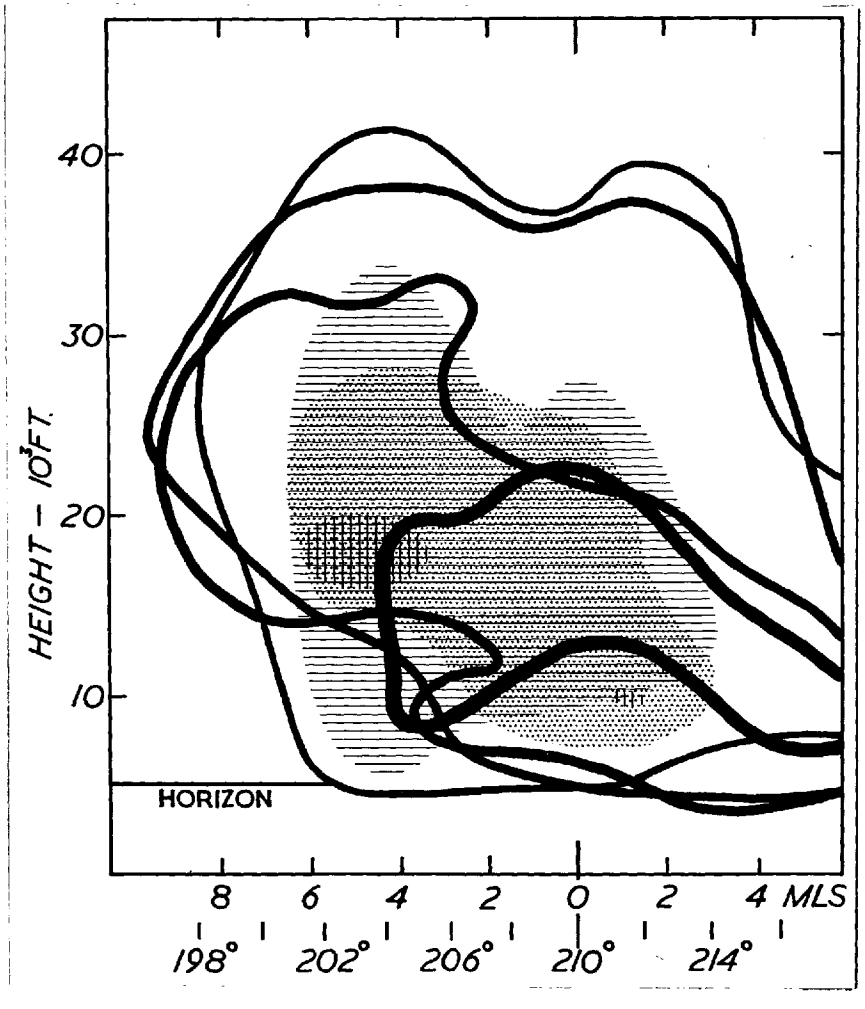

Fig. 2.9.3 (iii)

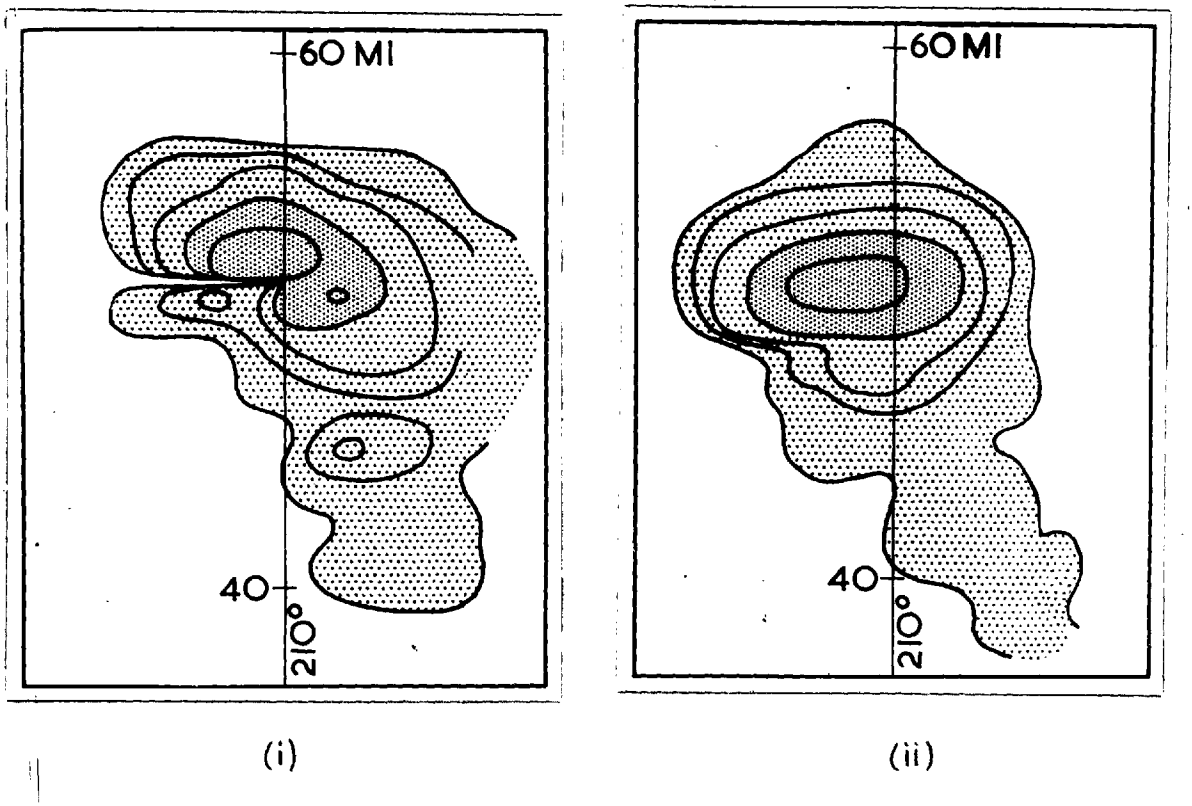

Fig. 2.9.4 (i and ii).
Intensity contours at 1202 in nearly horizontal sections through the Wokingham storm at 13,500 ft (Fig. 2.9.4 (i)) and at 32,000 ft (Fig. 2.9.4 (ii)) (heights refer strictly to 50 mi range), derived from the 4.7 cm data. Contours are for intensities (16), (29), (38), (49) and (58) (again strictly only at 50 mi range). No correction for beam-width effects has been applied.
Fig. 2.9.4 (i) illustrates the extent of the wall and the echo-free vault (which here appears as an echo-free notch). The echo just ahead of the echo-free vault lies in the lower part of the forward overhang. Fig. 2.9.4 (ii) shows that the curtain of precipitation carried ahead (down-shear) of the storm is displaced by a wind possessing an appreciable component towards the left flank at high levels (from left to right in the figure).

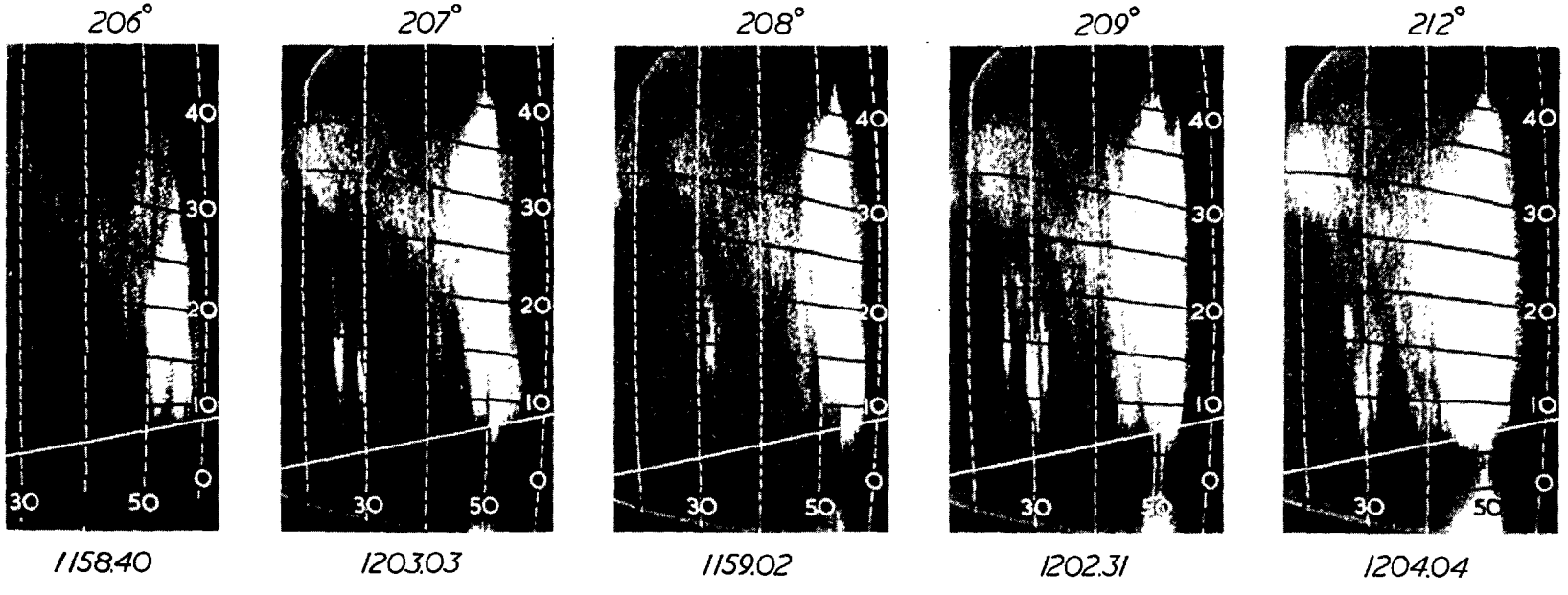

FIG. 2.9.5 Full-gain 3.3 cm RHI photographs of different sections through the main storm during the period to which Figs. 2.9.2 (ii) & 2.9.3 (ii) are applicable. Note the presence of the characteristic features of the new organisation - the forward overhang, and the wall with the highest top practically vertically above it (in the first 4 photographs), the echo-free vault (in the first two photographs), and the broader extent of the low-level echo on the left flank where precipitation reached the ground ahead of the wall (last photograph). The top in the centre photograph is practically at 45,000 ft and was the highest observed during the day.

Height markers are at intervals of 5,000 ft, and range markers at intervals of 10 miles. The radar horizon ($1\frac{1}{4}^0$) is indicated in each photograph.

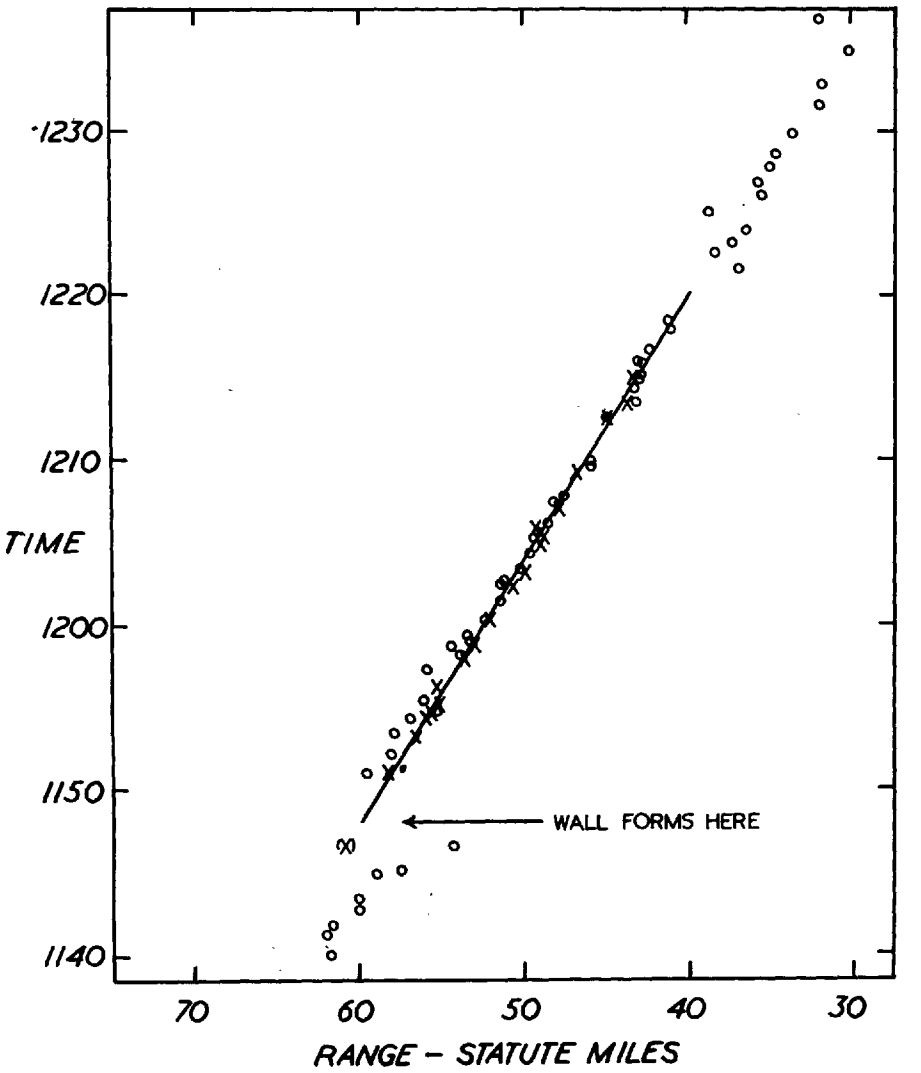

Fig. 2.9.6

The crosses (through which the straight line is drawn) represent the range of the wall as observed by the 3.3 cm radars. The circles represent the range of the highest top on each 3.3 cm photograph of the main storm. Notice that the highest tops were found vertically above the wall (within 1½ miles), but that before the formation of the wall and after its collapse their range was more variable.

10 The surface weather associated with the Wokingham storm

Accurately timed observations of the surface weather accompanying this storm were obtained from a number of voluntary observers and from the few official stations which lay near its path. A summary of those which lay in the path of the supercell is given in table 2.10.1, a simplified representation of 5 of the more comprehensive ground observations of which is shown in Fig. 2.10.1. The position of these observations and of hail exceeding size 2 ($\geqslant$ ¼ in) with respect to the radar echo from the supercell are shown in Fig. 2.10.2.

Using observations from a wider area made at about 1250 (somewhat after the most intense phase but when observations were more plentiful) and supplementing these by the study of autographic records, it has been possible to relate the surface weather in the vicinity of the main storm to position with respect to the radar echo, with the result shown in Fig. 2.10.3 The density of synoptic reporting stations is indicated in the figure and is adequate to permit it to be drawn with some confidence, though it is by no means sufficient, even in combination with conventional autographic records, to reveal as much detail as could be desired.

A prominent feature is the well-known gust front which heralded the approach of the severe part of the storm, and where on this occasion the surface wind direction was suddenly almost reversed. Behind the front the surface wind generally increased while veering from SW'ly to NW'ly, and reached a maximum mean speed of 30 to 35 mi hr^{-1} near the region of heaviest precipitation. During the intense phase there

were probably gusts exceeding 60 mi hr^{-1} — as at White Waltham — but even so it seems that the mean SW'ly component behind the gust front was substantially less than the speed of the storm.

As occasionally remarked before (Prohaska, 1905), the largest hail fell towards the right flank of the swath. Here the first precipitation experienced was large hail practically without any rain. The timed observations in this region, which are plotted in Fig. 2.10.4, show that it began within 3 minutes of the arrival of the wall at 8,000 ft (determined from the records of the radars, which at these ranges could not see below this level). Figs. 2.9.2 (ii & iii) show that an echo intensity of (50) was attained practically at the edge of the wall, and this is confirmed by the 3.3 cm intensity contours shown later in Fig. 2.11.1. Further evidence of the high intensity attained near the wall is supplied by the full-gain 3.3 cm RHI pictures in Fig. 2.9.5, which illustrate the echo extending farthest below the radar horizon near this position. This is because echo displayed at elevations between 0° and the radar horizon at $1¼^{\circ}$, is a side-lobe effect: the first side-lobe of the 3.3 cm radar lies 1.1° from the beam axis, so that the distance which the echo extends below the radar horizon is a measure of the echo intensity just above the horizon. The intense echo behind the wall is to be associated with the region of large hail. This mostly fell for rather more than 5 minutes, to be succeeded by heavy rain for a similar period. Evidently this sequence of events was familiar to Shelley who, before 1820 in his anthropomorphic description of "The Cloud", had written:

"I wield the flail of the lashing hail,
And whiten the green plains under,
And then again I dissolve it in rain,
And laugh as I pass in thunder".

Fig. 2.10.5 (i) shows that all the giant hail fell near the position where the forward overhang and wall ceased to exist. To the left of this position precipitation falling ahead of the updraught arrived at the ground ahead of the wall as rain and small hail so that the overall duration of hailfall on this side exceeded that on the right, as shown by Fig. 2.10.5 (ii), although its predominant size was smaller.

At the rear of the storm the rain diminished gradually, and before it ceased completely the sun shone, indicating the absence of the medium-level clouds which had spread over the sky well in advance of the storm. A few timed observations show that the rain stopped a few miles behind the rear of the 10 cm echo (which suffers negligibly from attenuation), showing that in falling from above the radar horizon it had been displaced by the low-level (relative) winds, which were by then reverting to light NE'ly[1].

Behind the gust front the screen-level temperature and wet-bulb potential temperature θ_w fell, both reaching a minimum of about 14°C in and behind the region of heaviest rainfall. The soundings made at Crawley, Hamsby, and Shoeburyness show that in the environment of the storm values of θ_w as low as 14 to 15°C occurred only at heights above

---

[1]Actually Fig. 2.10.3 shows that the winds only reverted to NE'ly some considerable distance behind the Wokingham storm. This is because the drawing of the streamlines has been influenced by the presence of storm 2, which has (for simplicity) been omitted from this figure.

10,000 ft; because of the strong horizontal gradient of temperature and possibly also of θ_w in the frontal zone it is not possible to be quite sure that in the path of the storm such values could not be found at rather lower levels, but the form of the isopleths of θ_w in the diagram and the strong divergence of the surface wind in and behind the rain area are consistent with the view that in the precipitation area the air near the ground had descended from above 10,000 ft in a downdraught. Nearer the gust front θ_w was not as low and can be associated with air drawn through the precipitation area extending to the northwest of the storm, either from near the ground or from levels just below 10,000 ft.

There was some tendency for the NNE'ly surface current ahead of the storm to be deflected southward near the gust front, but the near-discontinuity in the flow indicates that the current was lifted over the front. The main updraught was presumably derived from the potentially warm air initially at heights below 8,000 ft; its position at the level of the cloud base was marked by a dark arch-cloud lying approximately above the position of the front at the ground. In a vertical section drawn along the direction of travel of the supercell (210°), the updraught thus entered the storm near the ground several miles ahead of the region where the fall of large hail and the highest echo-tops indicated its presence in the high troposphere. Considering also that potentially cold air overtook the storm from the rear at heights above 13,000 ft and entered a downdraught in the precipitation area before flowing out of the rear of the storm near the ground, it

follows that all the observations are consistent with a flow in this direction which is like that drawn in Fig. 2.8.2 (ii). Study of some of the characteristics of the radar echo allows the drawing of the updraught to be refined, as explained in the following section.

TABLE 2.10.1 Summary of timed observations in path of storm 1 during its most intense phase.

Times followed by 1 exclamation mark are reported as reliable to the nearest 3 minutes.
Times followed by 2 exclamation marks are reported as reliable to the nearest 1 minute.
When the code letter is enclosed in brackets there was definitely no rain prior to the onset of the hail

	Position Grid Ref. E	N	Max. size	Hail Duration From	To	Rain Duration From	To
A	763	819	0	-	-	1230	1255
B[1]	851	778	6	1234!!	1240!!	1230!!	1250!!
C	722	722	2	1224!!	1228	1216!!	1230!!
(D)	794	697	6	1223!!	1227!!	1227	
(D)[2]	795	697	6	1223½!!	1227½!!	1227½!! (1232½)!!	1232½!! (1241½)!!
(E)	798	680	7	1220!!			
(E)	802	683	6 4	1225 1231!	1231 1234!	1234!	1255!
(E)[3]	805	675	7	x	x + 15 min	x + 14 min	
F	732	683	6	1220!	1230!		
(G)	757	667	7	1210		1225	
(H)[4]	795	645	7 6 decreasing	y + 8 y + 9	y + 9 y + 13	y + 13!!	y + 23!!
(J)	792	632	4	1220	1224	1224	
(K)[3]	752	564	7 decreasing	x	x + 4 min	x + 4 min	
L[5]	612	621	2	1207! 1214!!	1208! 1217!!	1205	1221!
M[6]	622	551	2	1205!	1215	1205	1215
N	619	532	2	1205!!	1210!!	1200!	1215!
N	620	522	4	1202!!	1210!!	1140!	1230!
N	637	528	4	1201!!	1204!!		
O	~~615~~ 638	~~517~~ 521	6	1158!!	1210!!		
P	583	525	4	1155	1215		
Q	682	437	0	-	-	5 mins	

Supplementary information:
1. First hail size 4, then size 6, then sizes 2 - 6 inclusive. Highest recorded gusts at 42ft above ground: 21 mi/hr at 1229; 23 mi/hr at 1229½; 33 mi/hr at 1232; 40 mi/hr at 1232½; 43 mi/hr at 1233
2. Bracketed times refer to light rain; wind violent and gusty before and during hail.
3. x = time of onset of hail
4. y = time of arrival of main gust front; wind subsequently 30 mi/hr dropping to 5 mi/hr in hail
5. Total rainfall due to storm 1 at this position = 0.6"
6. Main gust front passed at 1145.

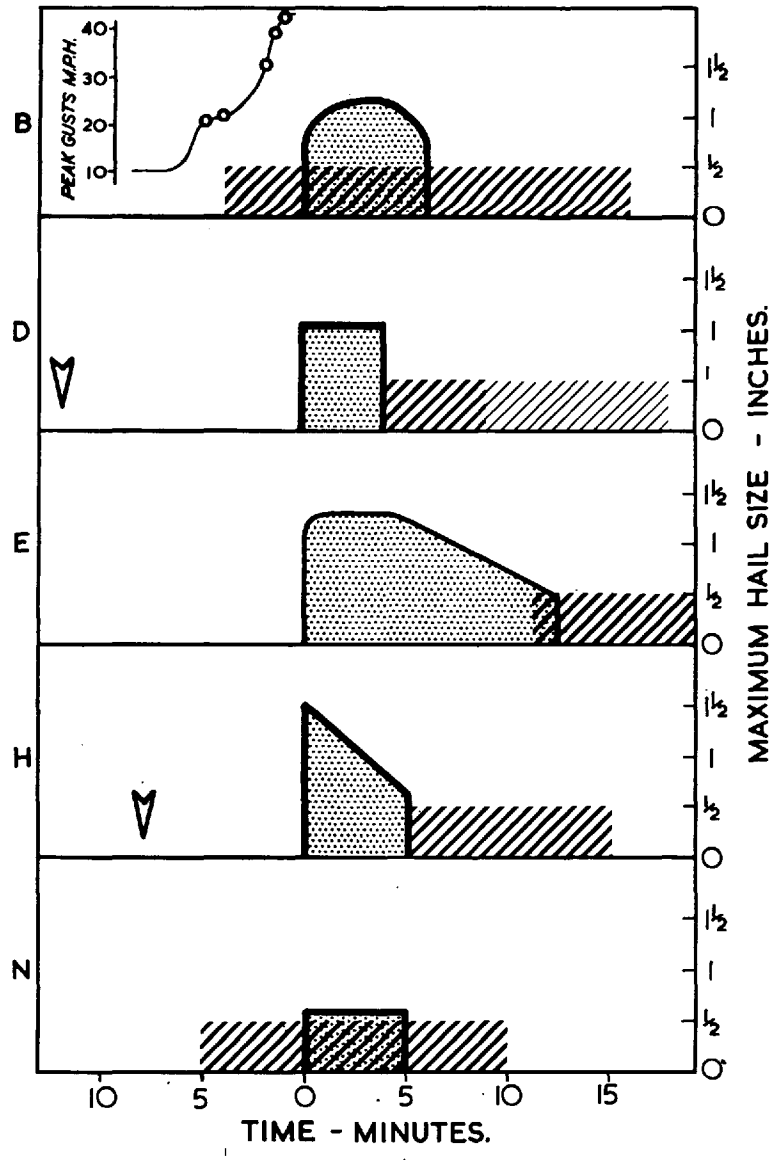

Simplified representation of five of the more comprehensive ground observations, showing rainfall (diagonal hatching) maximum hail size (stippled shading) and (where reported) the passage of the nose of the gust front as a function of time from the onset of the hail.

Fig. 2.10.1

Fig. 2.10.2

The position of the ground observations (represented by letters and listed in Appendix 5) and of hail exceeding size 2 ($\geq \frac{1}{4}$ in) (denoted by stippled shading) with respect to the radar echo.

Three intensity contours of the 4.7 cm PPI radar echo at about the 14,000 ft level are shown for each of the three times 1141, 1158 and 1218

1. At 1141 contours indicate intensities of (17), (52) and (56) respectively (strictly only at 62 miles range)
2. At 1158 contours indicate intensities of (16), (50) and (55) respectively (strictly only at 55 miles range)
3. At 1218 contours indicate intensities of (27), (48) and (56) respectively (strictly only at 40 miles range)

Corrections for beam-width have not been applied to these values.

The straight line along the direction 225^0 - 045^0 represents the locus of the position to the left of which the tip of the (28) intensity contour of the forward overhang had dropped below 10,000ft, and can be regarded as the line followed by the left-hand end of the wall.

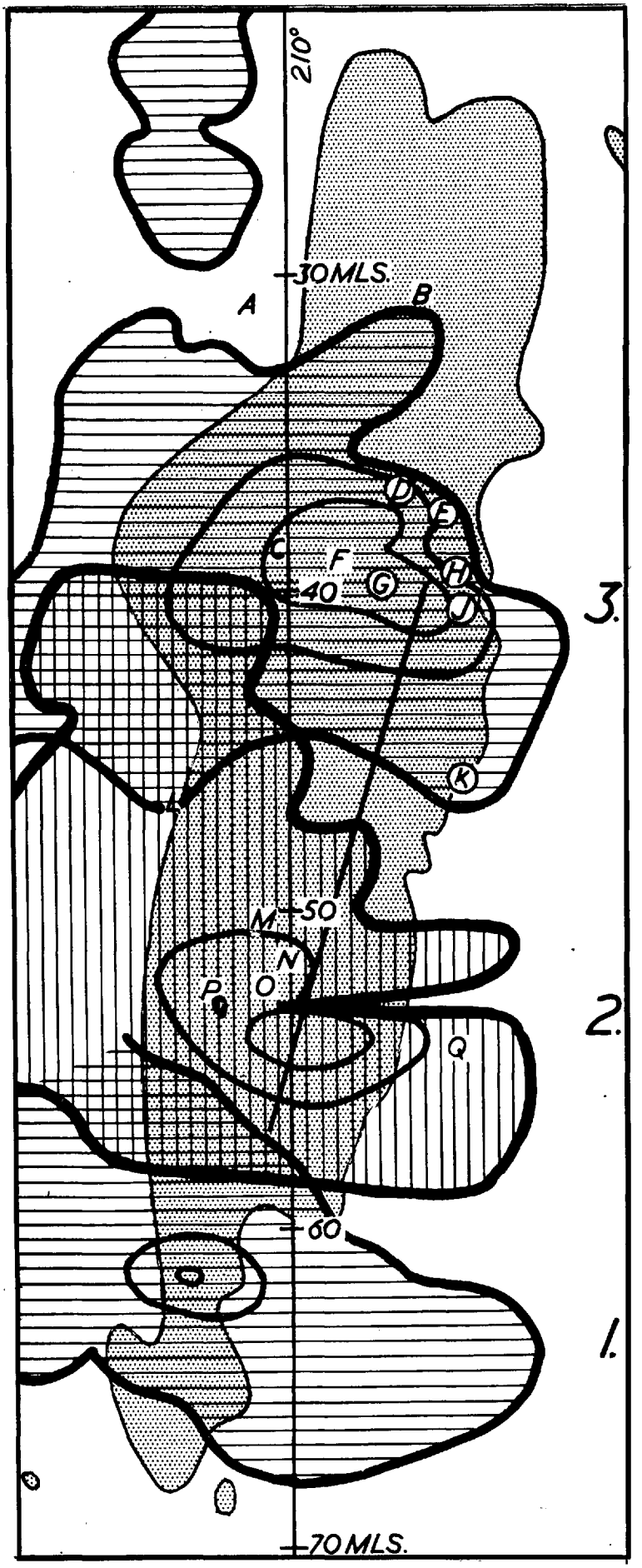

Fig. 2.10.2

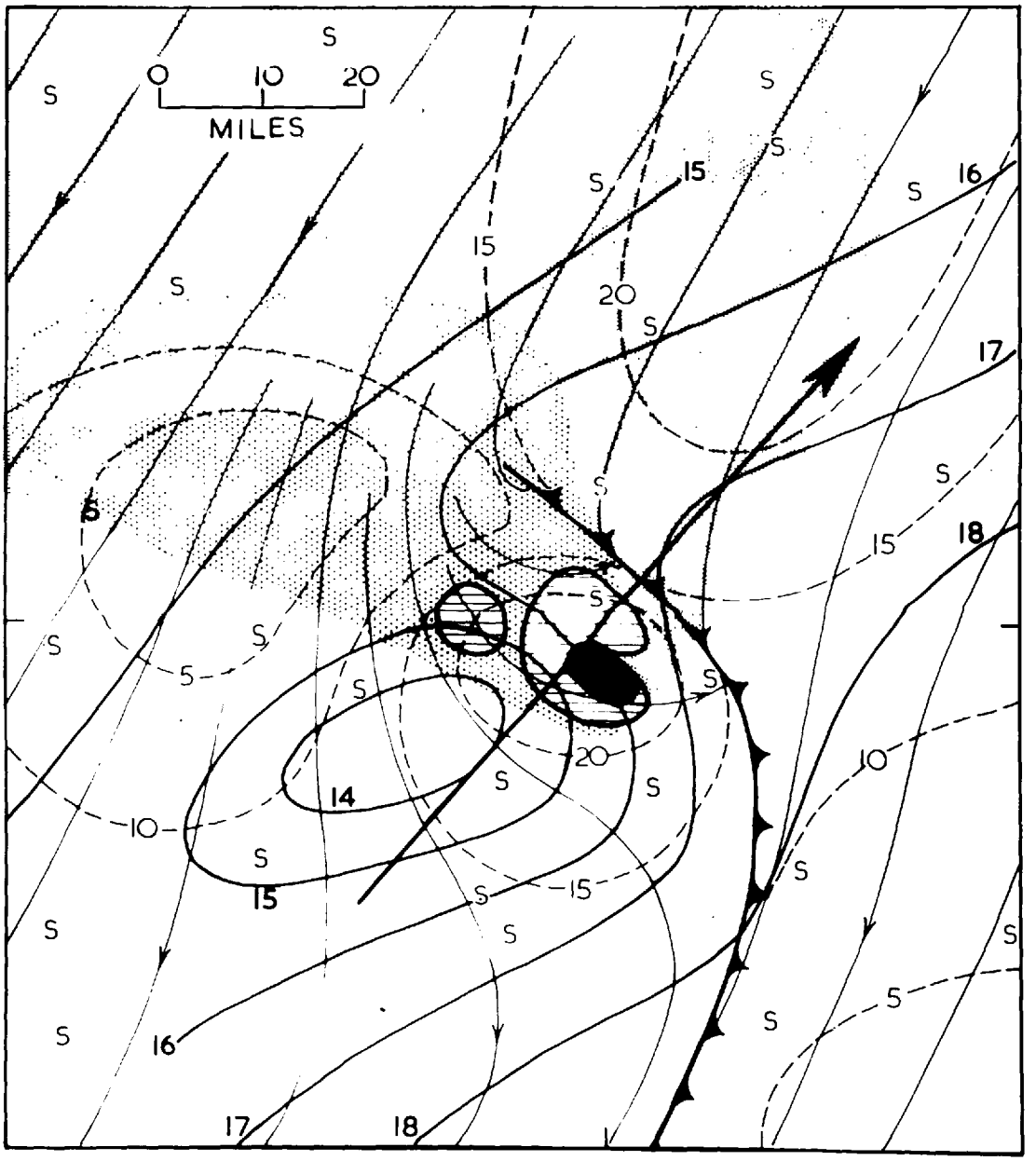

Fig. 2.10.3 Surface weather associated with the Wokingham Storm.

This diagram has been constructed mainly from observations made at about 1250, after the intense phase of the storm but when they were more plentiful: their distribution is shown by the letter 'S'. The air flow near the surface is represented by thin lines (streamlines) and pecked lines (isotachs, labelled in knots). The gust-front is marked as a cold front. The thick lines are isopleths of screen-level wet-bulb potential temperature, θ_w, labelled in degrees Celsius. The area overshadowed by the radar anvil 'cloud' is represented by a fine stipple and that over which at least light rain reached the ground by a coarse stipple. Over the hatched areas the echo intensity exceeded Z_e 10^4 and the surface rain was probably intense; in the small heavily shaded area hail reached the ground. The arrow shows the direction of movement of the storm.

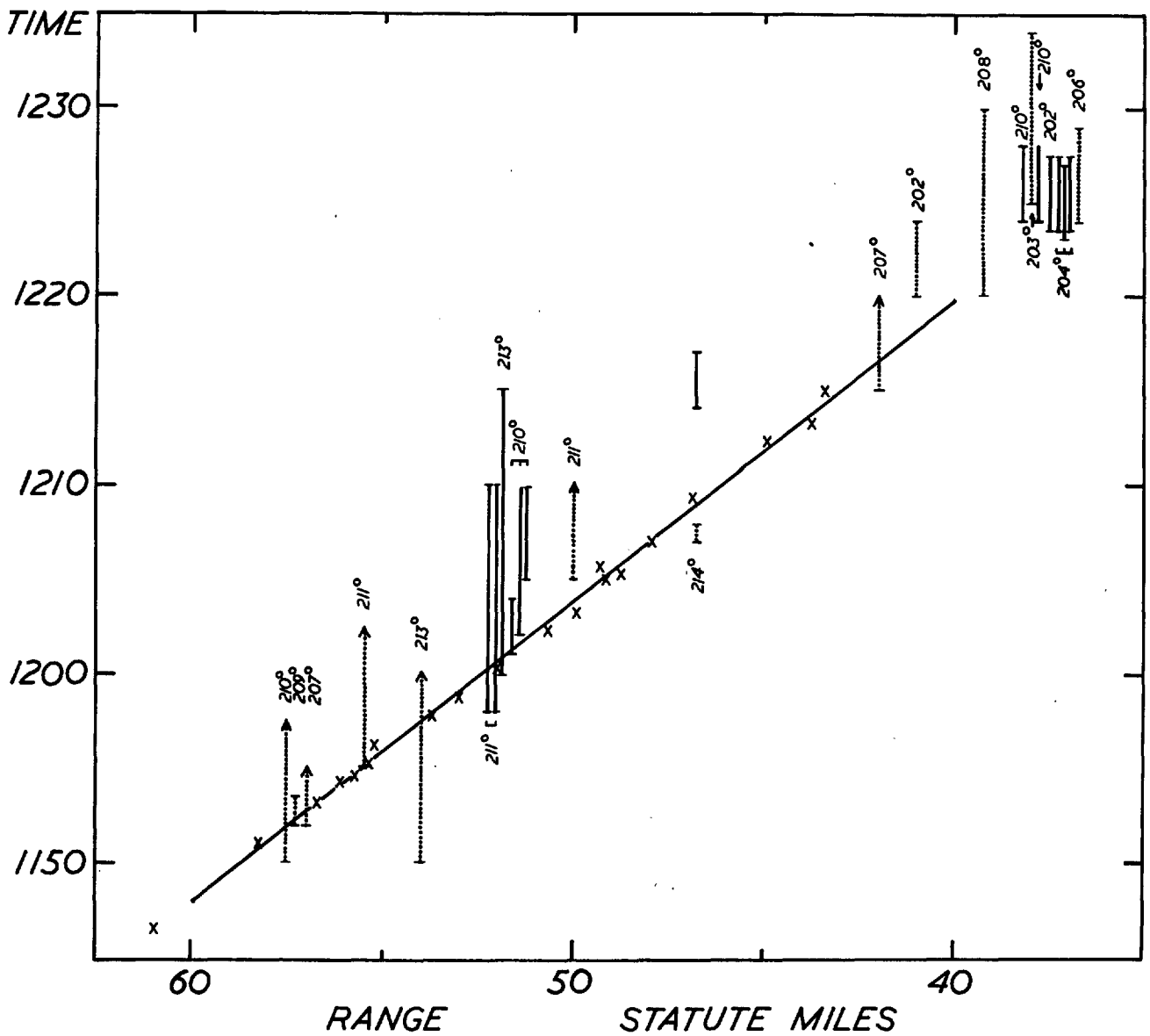

FIG. 2.10.4 Times of occurrence of hail and arrival of the wall. Crosses denote the position of the wall as ascertained from 3.3 cm RHI photographs. Vertical lines represent the period during which hail fell at the azimuths indicated: continuous or dotted lines are drawn according to whether the observations are accurate to within 1 min or 3 min. It can be seen that, except on the left flank of the storm (towards higher azimuths), the onset of the hail coincides within 2 or 3 min with the arrival of the wall.

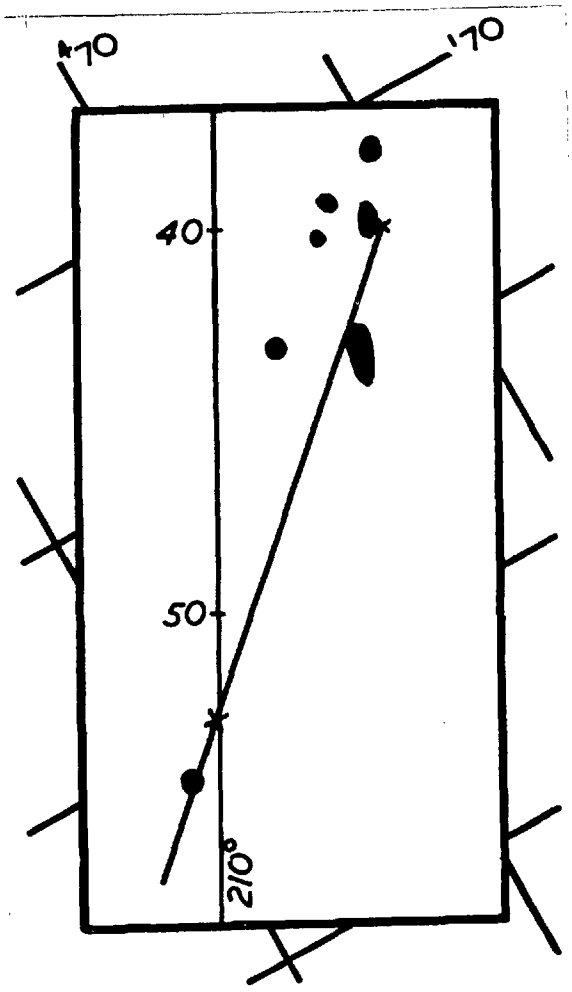

(i)

Areas experiencing giant hail. These are all within 2 miles of the position to the left of which the top of the echo-free vault was below 10,000ft.

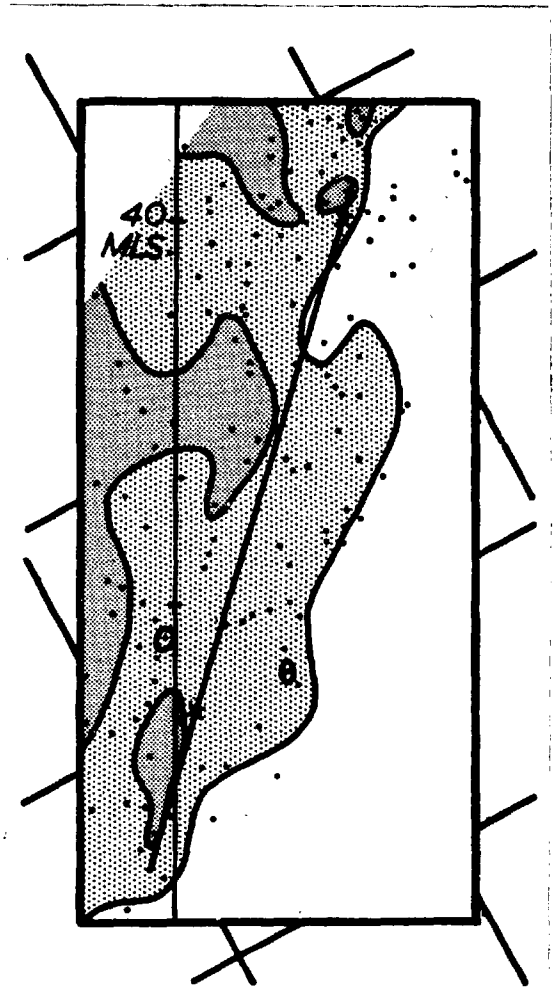

(ii)

Duration of hail in the main storm during its intense phase. Areas shaded lightly had 5 min or more of hail; areas shaded heavily had 15 min or more of hail. The positions of the individual observations are also indicated. The straight line along the direction 225° - 045° represents the locus of the position to the left of which the (28) intensity contour within the forward overhang had dropped below 10,000 ft, and can be regarded as the path of the left-hand end of the wall.

Fig. 2.10.5

11. The interpretation of the echo intensity distribution within the supercell

(1) The region of maximum intensity

Fig. 2.11.1 is a vertical section through the heart of the supercell along its direction of motion (210°) at about 1203: it shows the structure representative of the intense phase as seen by the 3.3 and 4.7 cm radars.

During this phase the intensity at 4.7 cm beneath the position of the highest top decreased rapidly with height above 35,000 ft (see Fig. 2.9.2 (ii)). The -40°C level occurred at a height of 32,000 ft, and so it is certain that the surface of the hailstones above this level would have been dry. Now the reflectivity of large dry hail at a wavelength of 4.7 cm increases (somewhat erratically) with its size (Fig. 2.11.2), so that the decrease above 35,000 ft is likely to be associated predominantly with a decrease in the size of the largest stones found at each level. This in turn implies that the vertical updraught velocity had already started to decrease at 35,000 ft.

The strongest echo occurred at a height of about 23,000 ft in a position (marked X in Fig. 2.11.1) about one mile ahead of the wall. Applying small corrections for the effects of beamwidth and attenuation to the maximum intensities obtained at 3 wavelengths at 1143 and 1203 (Fig. 2.7.1), Atlas and Ludlam (1961) have obtained the values of 10 log Z_e shown in Table 2.11.1:

Table 2.11.1

Wavelength	3.3 cm	4.7 cm	10 cm
1143 BST	71	(62)	[67]
1203 BST	75½	(70½)	[70]

Fig. 2.11.2 indicates that the comparatively low reflectivity at 10cm can be accounted for in terms of spherical hailstones with an almost uniform diameter of about 5 cm and with a dry surface. Hailstones of this size occasionally reached the ground but over areas only about ½ mile across. This, and the embarrassingly high echo intensity (after correction for attenuation) which would otherwise be implied, shows that the region aloft containing such large hail must have been small. Now 52 out of 92 measured hailstones were markedly spheroidal with longest and shortest axes in a ratio exceeding 4 to 3. Moreover preliminary (unpublished) experimental results obtained by Harper indicate that the signal received by vertically polarized radars from freely falling spheroidal hailstones is greater than that from spherical stones with diameters equal to the longest axis of the spheroidal stones. Thus the reflectivity at X may be interpreted in terms of correspondingly smaller spheroidal stones. Since the fall-speeds of such stones depends upon their shortest axis (see eq§. 4.5.5), the greatest fall-speed at X implied by any of the collected stones was little greater than 30 m sec^{-1}. Although those collected do not necessarily correspond to the largest which reached the ground, it seems that this is a more realistic fall-speed than the 42 m sec^{-1} that would have been implied by the 5 cm spherical stones. Typically the largest hailstones fell at the wall and therefore appear to be those which had come via X after having been released from near the summit of the updraught. It is later shown in Fig. 2.12.1 that such a trajectory is compatible with the model of the air-flow deduced in section

2.12 if the fall-speed of the stones at X was nearly 30 m sec^{-1}. It is not possible to explain on the basis of this model how 40 m sec^{-1} stones at X could avoid descending ahead of the wall.

Owing to the low signal which is received at 3.3cm wavelength from large hailstones when they are wet (Fig. 2.11.2), it is unlikely that the presence of spheroidal stones could invalidate the conclusion that the stones at X must have been dry. Now Atlas et al (1960) have shown that a water coat of only 0.01 cm thickness has a major effect upon the reflectivity at 3.3 cm wavelength, so that it is reasonable to assume that the hailstones at X were not only electromagnetically dry but were also 'physically' dry. Reference to Fig. 4.1.1 shows that, for stones of fallspeed 30 m sec^{-1} to be dry at 23,000 ft (7.0 km), the effective water content must not exceed 2 g m^{-3}. Such a low value was probably only experienced near the edge of the updraught at this level, implying that the position X must have been either outside or on the edge of the updraught.

(2) <u>The intensity distribution within the forward overhang</u>

Although the basis of Atlas and Ludlam's argument in favour of a monodisperse spectrum of large stones at X is weakened by the eccentricity of the hailstones, it is probably still necessary that the large stones should comprise the major portion of the total concentration if the absolute magnitude of the signal is to be accounted for in terms of just a few g m^{-3}. However there is every reason to believe that a broad spectrum of particles fell forward from the

upper part of the updraught: the approximately monodisperse size spectrum at X (and presumably elsewhere ahead of the updraught) arose by wind-sorting owing to the release of hailstones from a relatively small region near the top of the updraught into an airflow moving faster than the storm as a whole.

Within the updraught a wide size-range of stones was present, and most of these will have been growing wet, especially at lower levels. Now Fig. 2.11.2 shows that the signal received from water spheres considerably exceeds that from ice spheres of comparable size at 10 cm wavelength, so that quite high signals might have been expected within the updraught. The fact that a signal of [70], after correction for beamwidth effects, was never reached on the 10 cm RH1 set (nor even approached on the 10 cm PP1 set) indicates that even wet hailstones were behaving electromagnetically dry at this wavelength (c.f. section 4.6). As a result the 10 cm RH1 display showed a region of maximum intensity which extended with very little change below the melting level.

The 3.3 and 4.7 cm echo intensities on the other hand steadily decreased below X. Although this decrease commenced above the melting level (13,000 ft) it is nevertheless attributed to the diminution in reflectivity of the large hail as it became wet (Fig. 2.11.2), the wetting being caused by the re-entry of the hail into the updraught. This hail formed part of a wide size-range of stones which descended ahead of the updraught after being released from its summit (as the updraught air lost its rising speed and took up the horizontal speed

of the environmental winds at high levels). Particles with fallspeeds less than 1 m sec^{-1} were carried far ahead into the spreading anvil cloud and mainly evaporated before reaching the ground: the progressively larger hailstones encountered nearer the updraught re-entered it at lower levels where it was strongly inclined. These were then carried rearwards within the updraught to fall behind the wall. Because the horizontal component of the air-flow relative to the storm within this lower part of the updraught was in the opposite sense to that through which the hail had fallen at high levels, these stones were subjected to wind-sorting in the opposite sense as they traversed the width of the updraught, causing them to be reconcentrated. Together with the increase at shorter wavelengths in the reflectivity of small hail (Fig. 2.11.2), this produced the secondary intensity maximum which can be seen behind the wall in some RHI photographs (e.g. Figs. 2.9.2 (iii) and 2.11.1). This echo maximum had an intensity of 60 at 3.3 cm. It is best explained in terms of hail of diameter 1 cm, of which only 1 g m^{-3} would have been required, in contrast with 4 and 10 g m^{-3} respectively of 2 and 4 cm hail.

In Figs. 2.9.2 (ii) and 2.11.1 the intensity contours (29) and (49) in the forward overhang between 10,000 and 15,000 ft turn upwards towards the wall, corresponding to where the updraught was sweeping up the particles and carrying them once more towards the heart of the storm. At the tip of the contours the updraught speed must have been at least equal to the fall-speed of the largest particles which were present, and this can be estimated in the following

way.

First, neglecting the size sorting during the fall of the particles from high levels into the base of the overhang, it may be assumed that they had a size distribution similar to that found by Jones (1960) for the ice particles in the dense anvil clouds of the tropics: i.e.

$$N_D = 10^3/D^3 \qquad 2.11.1$$

where $N_D \delta D$ is the concentration (m^{-3}) of particles with diameters between D and δ D mm. Assuming that they behaved like dry spheres of ice, that D/λ was small and therefore that the scattering was in the Rayleigh regime,

$$\begin{aligned} Z_e &= 0.21 \sum ND^6 \\ &= 0.21 \int_{D_o}^{D_1} 10^3 D^3 dD \\ &\approx 50\ D_1^4 \qquad 2.11.2. \end{aligned}$$

where D_1 is the diameter of the largest particle present. Accordingly this diameter is 2.0 and 6.3 mm where 10 log Z_e is (29) and (49) respectively. Assuming a drag-coefficient of 0.6 (Macklin and Ludlam, 1961) and a mean density of 0.8 g cm^{-3}, the corresponding fall-speeds at the base of the overhang (about 12,000 ft) were 6.5 and 11.5 m sec^{-1}.

Because the dominant contribution to the echo was made by the largest particles, the estimate of their size is not much affected by the particular form assumed for the spectrum; for example, if it is alternatively assumed that the echo of intensity (49) was produced by particles of uniform size present in a concentration of 1 gm^{-3}, their

diameter is again found to be about 6 mm.

However on entering the updraught near the 0°C level and presumably renewing their growth, it is likely that particles of about this size quickly became so wetted that their radar cross-sections increased to the values appropriate to water spheres (Atlas et al, 1960). The diameter of the largest particles where the intensity reached (49) then decreased to about 4 mm, but the fall-speed (assuming now a mean density of 0.9 g cm^{-3}), is reduced only to about 10 m sec^{-1}.

Consequently it may be inferred that in the neighbourhood of the base of the overhang, at about 12,000 ft, particles of diameter up to 6 mm re-entered the updraught, and that here it had already an upward speed of at least 10 m sec^{-1}. The general configuration of the updraught streamlines (Fig. 2.12.1) implies that here the horizontal component of motion towards the rear of the storm must have had an equal or perhaps greater value and was therefore capable of appreciably tilting the trajectories of the largest hailstones which descended immediately behind the wall. Now even the largest hailstones possessed fall-speeds of only 30 m sec^{-1} near the ground (and if they had been within the updraught the speed relative to the ground would have been less), so that the observed uprightness (within $^{1}/_{5}$ mi over a height interval of at least 1 mi) indicates that in its vicinity the air could not have had a relative horizontal speed in the direction of motion of the storm of more than 6 m sec^{-1}. This means that the lower boundary of the updraught could not have intersected the wall far below its upper extremity, which was at around 13,000 ft at 1200.

(3) The nature of the trailing edge of the precipitation

During the most intense phase as the supercell was approaching the radar station the rear edge of the echo at 3.3 and 4.7 cm (see Figs. 2.9.2 and 2.9.5) was distorted by attenuation from intervening hydrometeors, so that it gave no reliable indication of the rearward extent of the precipitation. The 10 cm RHl photographs during this period (e.g. Fig. 2.11.3) show that the rear edge of the supercell was practically vertical at all heights between the horizon and 33,000 ft, but because of the wide horizontal beam of this radar this might again be misleading. However 3.3 cm RHl photographs of the storm were taken as it receded to NE of the radar at a time of renewed vigour (during which the features characteristic of a supercell had redeveloped). These show the rear edge of the echo-mass with no intervening echo to produce attenuation (see Fig. 2.9.1 (i)). It is seen to be vertical within $\pm$ $^{1}/_{3}$ mi up to about 32,000 ft: furthermore it is considered to be reasonable to assume that this was so throughout the intense phase. In view of this it becomes possible to determine the range of the edge during the most intense phase using the 10 cm PPl data plotted in Fig. 2.6.3 in spite of the fact that the beam extended vertically to a height of around 26,000 ft at the relevant ranges. Also plotted in this figure is the range of the wall: although determined from the 3.3 cm RHl data, this is not affected by attenuation as there was no intervening echo between the wall and the radar during the existence of the forward overhang. It is therefore clear from Fig. 2.6.3 that

the horizontal distance between the wall and the rear edge remained remarkably constant between 5 and 6 mi throughout the 33 minutes during which the wall was identified. That the relative positions of these features remained so nearly constant is regarded as indicating that the particles which defined these two faces were produced within the same updraught.

(4) The disposition of the draughts within the supercell in relation to the radar echo

Evidently it is possible to construct for this particular cell a more accurate outline of the form of the updraught in a vertical section than that sketched in Fig. 2.8.2 (ii) not only by ensuring that it passes through the cloud base level near the position of the surface gust front and through the region of the highest tops, but also that it skirts the position of maximum echo intensity, X, and extends as far as the rear edge of the echo-mass. Further than this, when the distribution of updraught speed (or of speed along the streamlines of the updraught) is specified, it should be kinematically consistent and lead to calculated hailstone trajectories which accord with the presence of large hailstones in the position of maximum echo intensity, X, and at the wall, and of smaller hailstones in the echo ahead of the updraught at high levels and to the rear of the wall at low levels (see section 2.12). The resulting closer approximation to the form of the updraught is portrayed in Fig. 2.11.4, which shows a few schematic hailstone trajectories and the surface weather in relation to the main draughts.

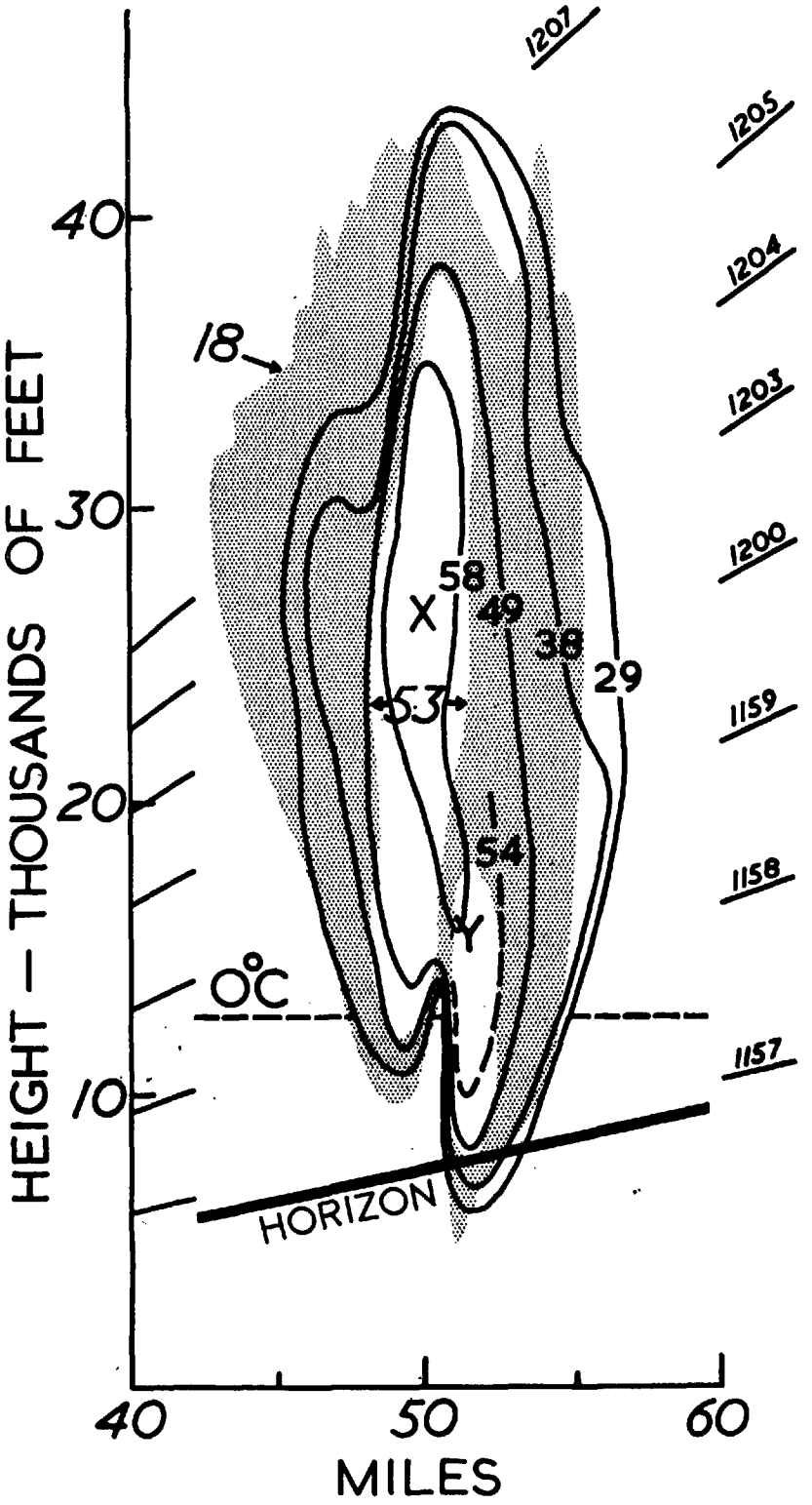

FIG. 2.11.1. Range-height sections through the main storm along azimuth 209°. The stippled area denotes the region occupied by full-gain 3.3 cm echo at 1202.31: in the unshaded regions in its interior the intensity exceeds 53, according to a photograph on reduced gain at 1203.40. The contours represent the intensity distribution in the corresponding vertical section derived from the 4.7 cm data for the period 1156-1208. Corrections for beam-width have not been applied to these values. (All three sections have been displaced in range at 40 mi/hr along 210° to make them applicable to the time 1203).

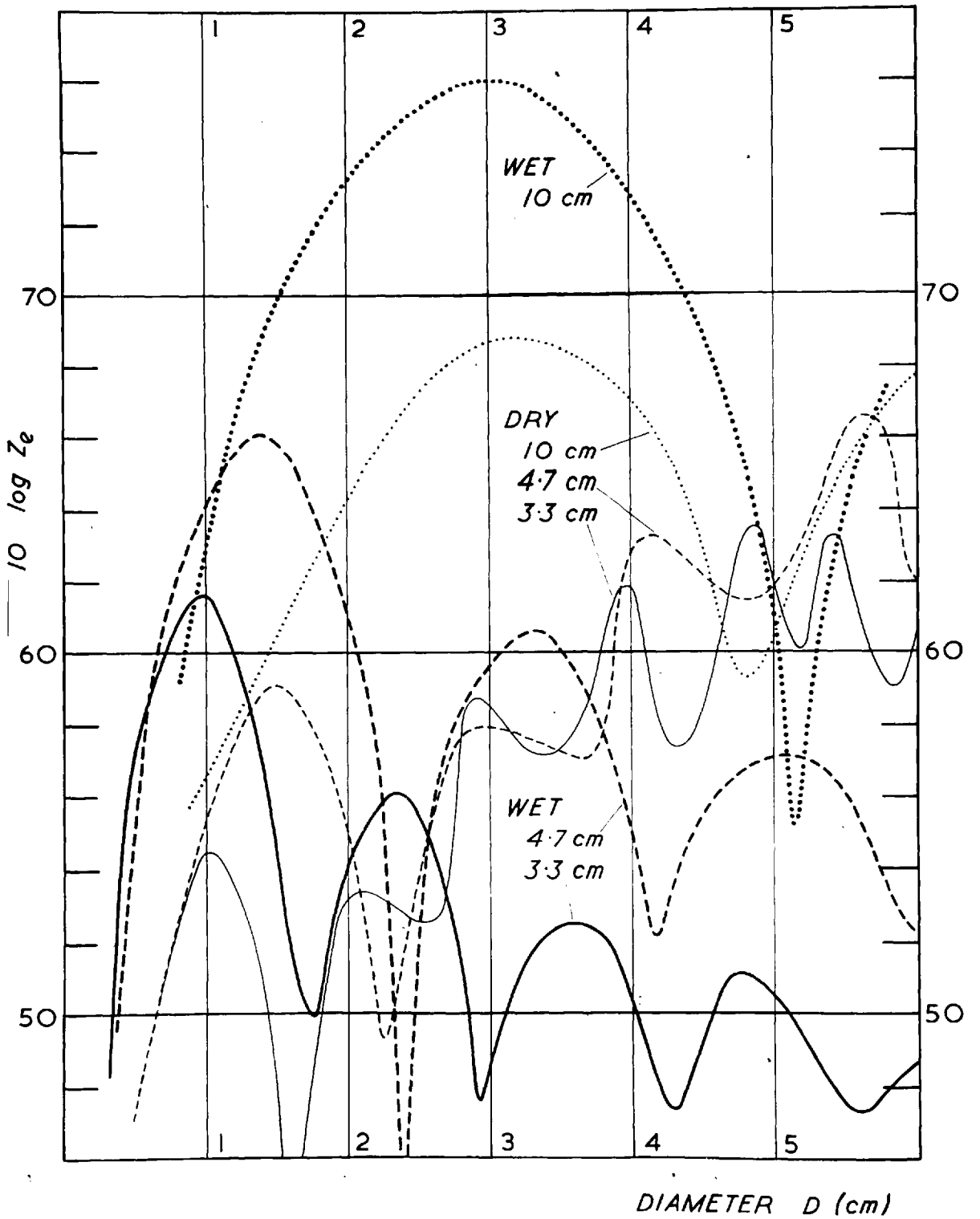

Fig. 2.11.2
Equivalent reflectivity corresponding to 1 g m^{-3} of electromagnetically wet and dry hailstones of uniform diameter D at three wavelengths. (Amended from Atlas and Ludlam, 1961).

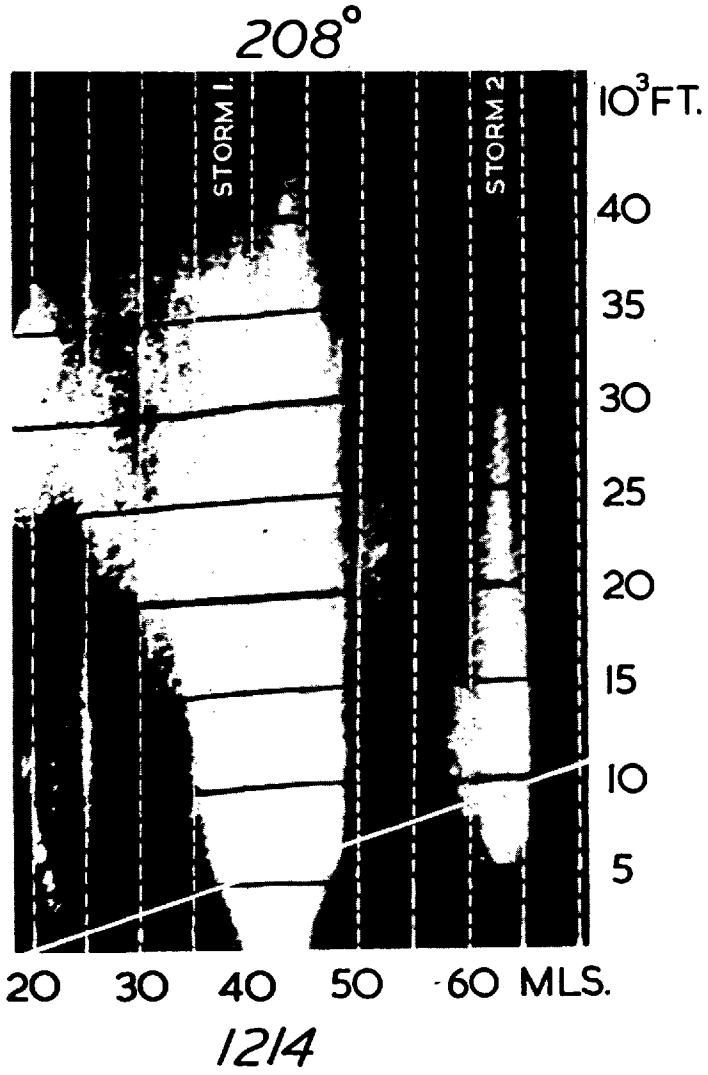

Fig. 2.11.3 10 cm RHI photograph showing the uprightness of the rear of the main storm. Storm 2 can be seen behind the main storm; it is comparatively small.

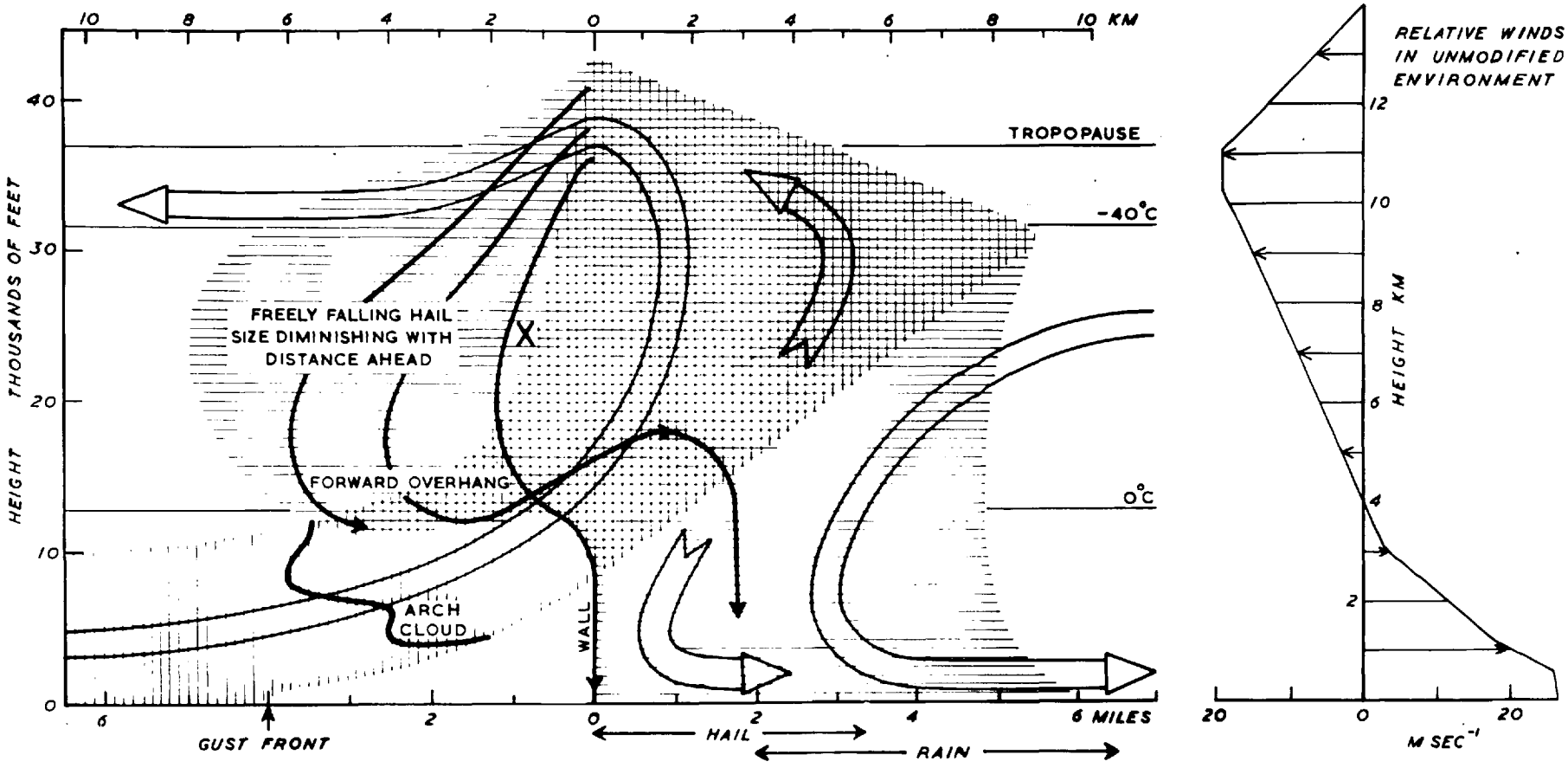

Fig. 2.11.4
Vertical section through the centre of the Wokingham supercell along its direction of motion (from right to left of the diagram). The extent of the updraught is shown by vertical hatching and that of echo whose intensity Z_e exceeds 10^3 mm^6 m^{-3} is denoted by horizontal hatching. A number of hailstone trajectories are also indicated.

12 The air-flow within the supercell

(1) A two-dimensional model and its inadequacy

Owing to the small change in wind direction with height it seemed reasonable as a first approximation to attempt to describe the airflow two-dimensionally: this has been done quantitatively assuming that (in view of their size and persistence) the same mass-flux was maintained within the draughts throughout their extent within a vertical section along the direction of motion of the supercell.

The updraught Fig. 2.1.5 shows that, neglecting latent heat of fusion released and negative buoyancy owing to condensed water (effects which counteract each other), only air from below about 8,000 ft was potentially warm enough to develop buoyancy upon being lifted adiabatically, the greatest temperature excess (no more than $1.5^{\circ}C$) occurring between 12,000 and 16,000 ft. Now the component along the direction of motion of the supercell of the wind in its environment is indicated in Fig. 2.1.3 (i): it was such that in the absence of significant convergence, the horizontal flux of ~~mass~~ air entering the storm (per unit distance across 210°) within the unstable layer was 4.5×10^{5} g cm^{3} sec^{-1}. Even had the updraught tapped air from levels above 8,000 ft, this value would not have been significantly increased, owing to the small speed of inflow above this level. Further, in accordance with the experience of glider pilots (Wichmann, 1948) it has been assumed that the flow within the draughts was practically laminar, so that streamlines of the air-flow could be constructed. Their form had to be consistent with the boundary conditions already

enunciated in the preceding section and had to accord with the horizontal and vertical windcomponents partly specified by considerations discussed in the following paragraphs.

The most unstable layer occurred at a height of 4,000 ft, so that the streamline originating from this level was taken as defining the axis of the updraught. Now the analysis of the structure of the largest hailstones (section 4.4) indicates that the vertical velocity along this axis in the interval 12,000 Z 28,000 ft was given by

$$U_m \approx 5(Z-1) \qquad 2.12.1$$

where U_m is in m sec^{-1} and Z is the height in km. Moreover this same analysis has shown that the growth of the largest hailstones can only be accounted for provided they crossed the core[1] of the updraught at a mean horizontal velocity of less than 8 m sec^{-1} whilst between the 19,000 and 28,000 ft levels (section 4.9), thereby setting an upper limit to the permissible inclination of the streamlines in this region.

A model of the updraught which is consistent with these considerations is presented in Fig. 2.12.1. In order to account for a portion of the updraught penetrating to the rear of the echo in terms of a constant flux within this section it has been necessary to assume that a part 'mushroomed' rearwards below the tropopause. Evidence in support of the presence of at least some 'rearward outflow' of this kind is provided by the behaviour of a small tower (T^1) which was seen protruding 3,000 ft above the main echo-mass some 3 mi behind

---

[1] In this context the core is that part of the updraught where the updraught velocity exceeded ¾ U_m at the same level.

the highest top (Fig. 2.12.2): during the two minutes for which it was observed its vertical velocity was practically zero and it possessed a rearward velocity of 25 mi hr^{-1} relative to the storm in spite of environmental relative velocities around 35 mi hr^{-1} in the opposite direction.

The above two-dimensional model applies to the period for which Figs. 2.9.2 (ii), 2.9.3 (ii) and 2.9.5 are valid, when the wall extended to around 13,000 ft. However Fig. 2.12.3 shows that it subsequently increased its vertical extent to reach 20,000 ft at around 1215 (presumably because the depth of the dome of cold downdraught air was increasing). In order to redraw Fig. 2.12.1 to apply to this time so that the updraught does not cross the wall and so that it also extends right to the tip of the rearward outflow, it would be necessary to assume high horizontal velocities within the region above 20,000 ft where much of the hail growth occurred. This would have the effect of transporting the stones across the growth region far too quickly to permit them becoming large. This difficulty may be overcome by assuming that the updraught air within what has been called the rearward outflow was derived predominantly from outside the section.

The model in Fig. 2.12.1 has been constructed with the maximum possible flux commensurate with two-dimensional flow: nevertheless the width of that part of the updraught where the vertical velocity exceeds 20 m sec^{-1} is nowhere greater than 4,000 ft. As is clear from the two limiting hail trajectories shown in the figure, this precludes the fall of large stones for longer than three minutes

whereas it is necessary to account for durations typically twice as long as this. This difficulty too may be surmounted by assuming that the mass-flux in the updraught within such a section was augmented from outside.

The downdraught If the air-flow within the downdraught had been strictly two-dimensional and continuous with the (unmodified) environmental flow, air could have entered it only from the rear and within the height interval $13{,}000 < Z < 30{,}000$ ft, in which case it would have comprised a ~~mass~~-flux of only 3×10^5 $cm^3\ g\ sec^{-1}$ (per unit distance across 210^o). However even this is likely to be an overestimate: this is because it is based upon relative forward velocities across the rear edge of the echo reaching 30 mi hr^{-1} at 30,000 ft, which would have made this edge obviously non-vertical had it been defined by particles of a size capable of being grown within the updraught in the two-dimensional model. Now the light winds experienced in the area of heavy rain and the restoration of a light NE'ly wind at the ground behind it imply that the downdraught air left the storm rearwards with a relative speed of fully 40 mi hr^{-1}: even if this outflow had been limited to a shallow layer some 2,000 ft deep it would have accounted for all of the 3×10^5 $cm^3\ g\ sec^{-1}$ of flux. However in order to get continuity with the environmental airflow, some outflow would have occurred at all levels up to around 13,000 ft (Fig. 2.1.3 (i)) to give a flux exceeding 5×10^5 $cm^3\ g\ sec^{-1}$. It is therefore necessary to augment the downdraught flux, as well as that of the updraught, by air from outside the section of the model.

(2) A three-dimensional model

The streamlines of the wind near the ground (Fig. 2.10.3) show that the downdraught spread out towards the right flank of the storm. Immediately behind the gust front the surface wind also had a mean relative component of velocity away from the front. This was probably due to surface friction, the cold air a little distance above the ground keeping pace with the front. The air near the ground just behind the front was replaced not only by the descent of this air but also by a flow from the left flank. The cause of the sweep of the low-level downdraught air towards the right flank is not understood: it cannot be attributed to the effect of Coriolis acceleration owing to the short time for which the air remained within the storm.

On the left flank of the supercell precipitation fell into low-level air approaching the front of the storm. This air could acquire buoyancy if lifted sufficiently but could also be regarded as potentially cold if precipitated into, since it was unsaturated. The downdraught could therefore be fed on the left flank not only by middle-level air which overtook the storm but also by air below 13,000 ft which entered at the front. Probably the downdraught flux was also augumented by a convergence in the middle troposphere associated with increased wind component from the left flank.

It seems significant that the low-level potentially warm air approached the gust front with a components from the right which was observed to increase near the front (see, for example, the Silwood sounding in Fig. 2.1.2 (iii)). The disposition of the echo from

precipitation falling ahead of the updraught shows that the updraught air also left the storm with a substantial component in the same direction (see Fig. 2.13.5). The updraught must therefore be envisaged as inclined upwards from the right as well as from the forward flank: moreover the great rearward extent of the echo at high levels (previously explained solely in terms of a strong rearward outflow) can also be largely attributed to the entry into the section of updraught which rose near the gust front outside the section, farther to the right of the storm and behind the position of the front at the surface in the section. It therefore appears that the total mass flux in the updraught was substantially increased over that given by the relative speed of approach of the potentially warm air in the undisturbed environment by a low-level convergence associated with increased wind components from the right. Accordingly there was an organized circulation in vertical sections across, as well as along, 210°: however whereas the latter circulation was of the type shown in Fig. 2.8.2 (ii) the former was of a kind shown schematically in Fig. 2.12.5.

The gust front weakened and presumably the cold air behind it became shallower with increasing distance behind the storm (see appendix 2.12a). Along its length the smooth arch cloud in front of the supercell, where the updraught was strong and persistent, was probably replaced by a line of cumuliform clouds where the weaker updraught broke into a succession of thermals. Such a line of cumulus on the right rear flank with tops becoming successively

higher nearer the storm has been described by Fujita and Byers (1960) in connection with the cumulonimbus photographed by Cunningham (1960): (on this occasion the wind field in the environment was remarkably similar to that around the storm under discussion). During the intense phase the storm echo extended towards the right practically continuously, but before and after this phase it was observed that the new cells formed intermittently to the south-east of the right flank of the main echo-mass, at first separated by a mile or two from it but then expanding and after some minutes becoming fused with it. This behaviour is interpreted as being due to the formation of precipitation in the largest of the cumuliform clouds above the gust front near the right flank, followed by their invigoration and development into cumulonimbus which amalgamated with the main storm cloud. A belt of cumuliform clouds extending along the gust front to the rear of a large cumulonimbus may be made more striking by the virtual absence of convective cloud over a large neighbouring area where the cold air behind the front is deeper. Consequently an instantaneous view of the whole cloud system may give a false impression that the updraught approaches the storm from the rear.

A three-dimensional model of the air flow in and around the main storm is shown in Fig. 2.12.4. At a certain distance away on the right flank air ascended over the gust front and produced cumuliform cloud but failed to rise above the level at which the wind velocity was equal to that of the storm (13,000 ft on this occasion).

It is interesting to note that the trailing part of the gust

front, even though it only demarcated a very shallow pool of cold air (see appendix 2.12a), nevertheless was a preferred position for the formation of new storms. This is demonstrated by Fig. 2.7.4 which shows that storms 3 and 4 lay on the gust front which trailed behind the Wokingham storm.

As the Wokingham storm approached, an observer at East Hill noted that the arch cloud extended from horizon to horizon and thus some distance to the left of the position at which the gust front ceased to exist at the surface (Fig. 2.10.3). Since the arch cloud is symptomatic of an updraught at cloud base level it seems that overturning of the kind depicted in Fig. 2.8.2 (ii) was also proceeding to the left of the supercell, even though the surface wind direction did not change much during the passage of the storm. Indeed such organized overturning is known to have persisted within cells in this position because of their longevity (Fig. 2.5.5). Consequently the microstructure of the gust front within a vertical section is visualized as changing from that shown in Fig. 2.12.6 (i) on the right flank of the supercell through that shown in Fig. 2.12.6 (ii) to that in Fig. 2.12.6 (iii) away to the left of the supercell, the region near the nose of the front and within the cold air being one in which the winds blew predominantly from left to right across these sections.

Fig. 2.12.1
Quantitative two-dimensional model of the air-flow within the updraught in a vertical section through the centre of the supercell along its direction of motion (from right to left of the diagram).

Streamlines of the air flow are shown as thin dashed curves, isopleths of vertical and horizontal velocity respectively as thick continuous and thick dashed curves, and some hailstone trajectories as dotted curves.

Velocities are labelled in m sec^{-1}: they are shown alone when they refer to component air velocities and are encircled when they refer to hailstone fall-speeds.

Most of the hailstone trajectories within the updraught were derived in a step-by-step manner assuming growth with an effective water concentration of 3 g m^{-3}; however the trajectories (from H′) of stones α and β (during the growth of which U-V was always small) are based upon the analysis in section 4.8 (see also p.142).

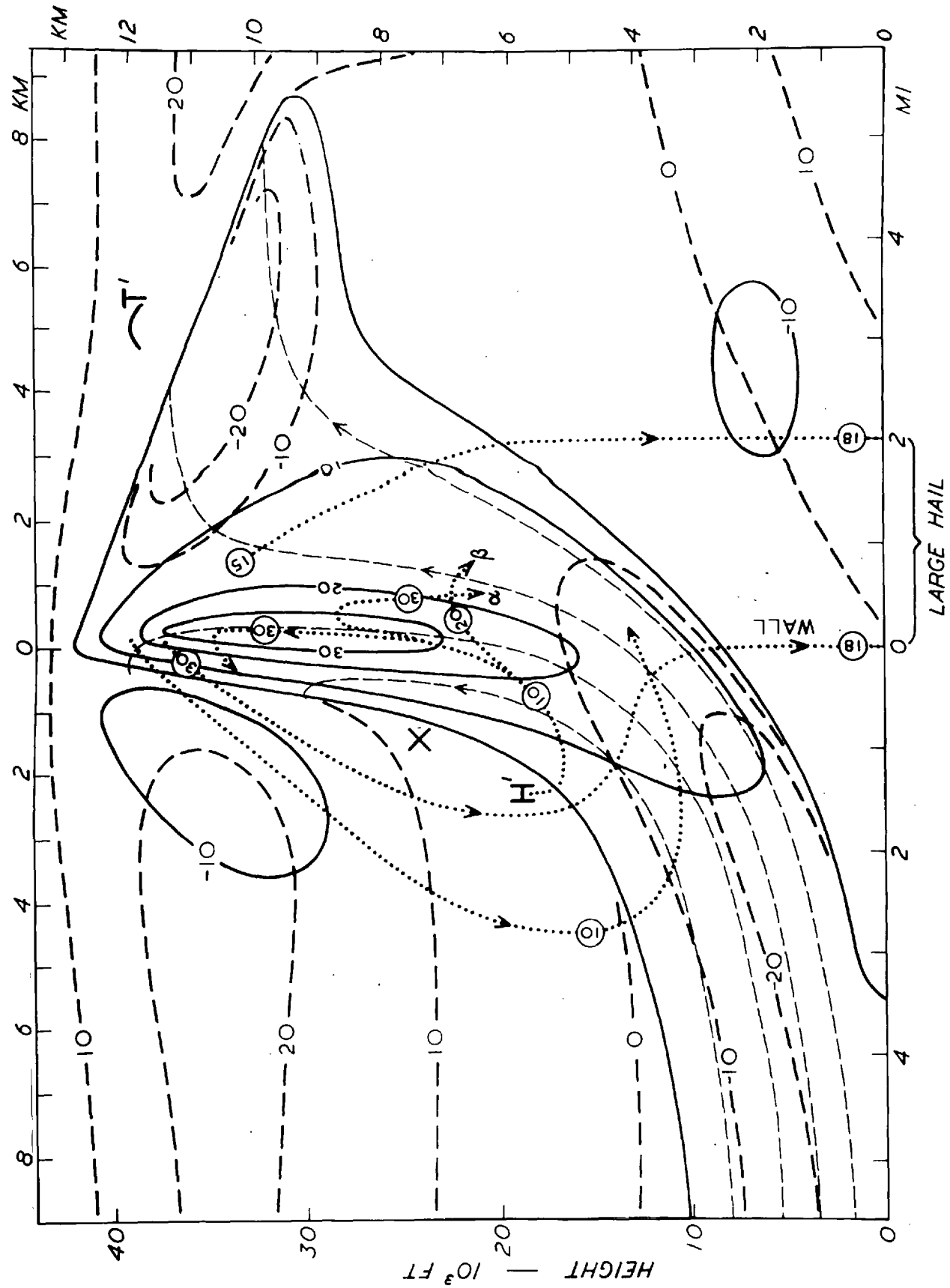
KM
12
10
8
6
4
2
0
MI
8 KM
6
4
2
0
2
4
6
8
T'
-20
-10
0
10
20
30
(15)
(30)
(20)
(10)
(18)
WALL
LARGE HAIL
X
H
40
30
20
10
0
HEIGHT — 10³ FT

Fig. 2.12.1

Fig. 2.12.2

Full-gain 3.3 cm RHI photographs along 209° at 1200.34 and 1202.31 to show a top at range 55 miles moving with a component velocity along this azimuth of only 15 mi/hr.

Fig. 2.12.3

Full-gain 3.3 cm RHI photographs showing the Wokingham supercell at a time when the wall was attaining its greatest observed vertical extent. This phase was associated with the fall of large hail at Wokingham; (see observation E in Figs. 2.10.1 and 2.10.2 and Table 2.10.1).
Comparison of these photographs with the 10 cm records indicates that the rear edge of the echo suffers from extreme attenuation.

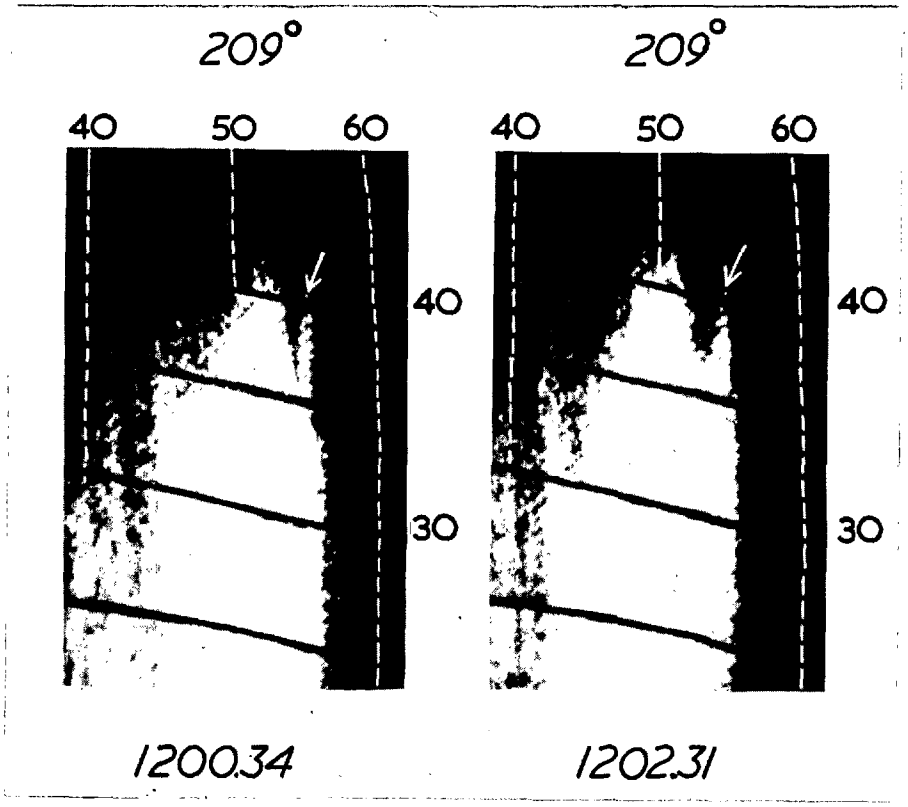

Fig. 2.12.2

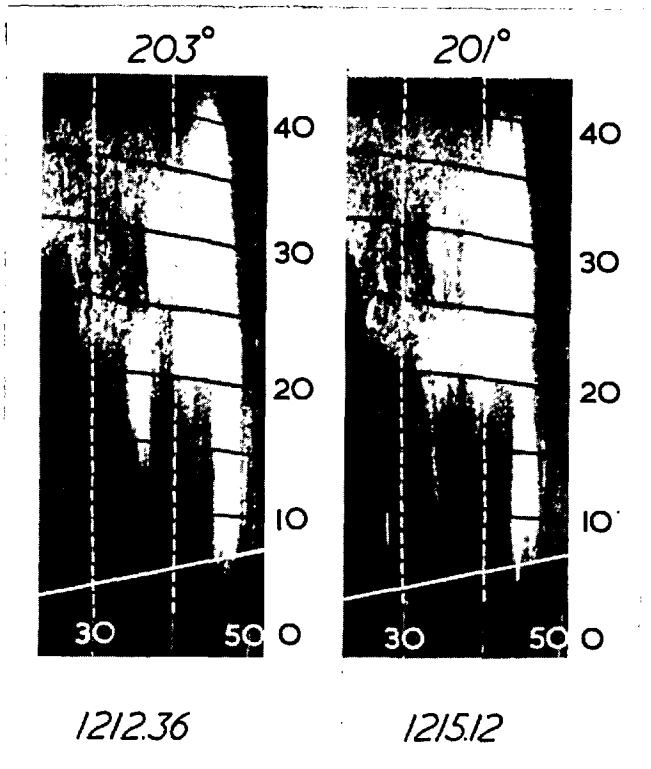

Fig. 2.12.3

Fig. 2.12.4 THREE DIMENSIONAL MODEL OF THE AIR FLOW WITHIN THE WOKINGHAM STORM

Streamtubes of air in which condensation has occurred are shaded. The extent of hail and of light rain at the surface are represented by dark and stippled shading respectively. The gust-front is marked as a cold-front and the belt of cumulus above it on the right flank of the storm is indicated schematically. Precipitation forms in the larger of these cumulus in air which enters the storm from a position near H; some of it is carried at levels above 13,000 ft forward and across relative to the storm, and falls to re-enter the strong updraught and form the forward overhang, near H′. A small proportion of the particles rise to great heights and grow into large hailstones before again falling forward of the strong updraught near the position X, (cf. Fig. 2.12.1). Here their surfaces become dry and they produce a very intense 3.3 cm radar echo. Subsequently they traverse the updraught again before reaching the groumd. The path HH′X can therefore be regarded as the trajectory of a particle which becomes a large hailstone.

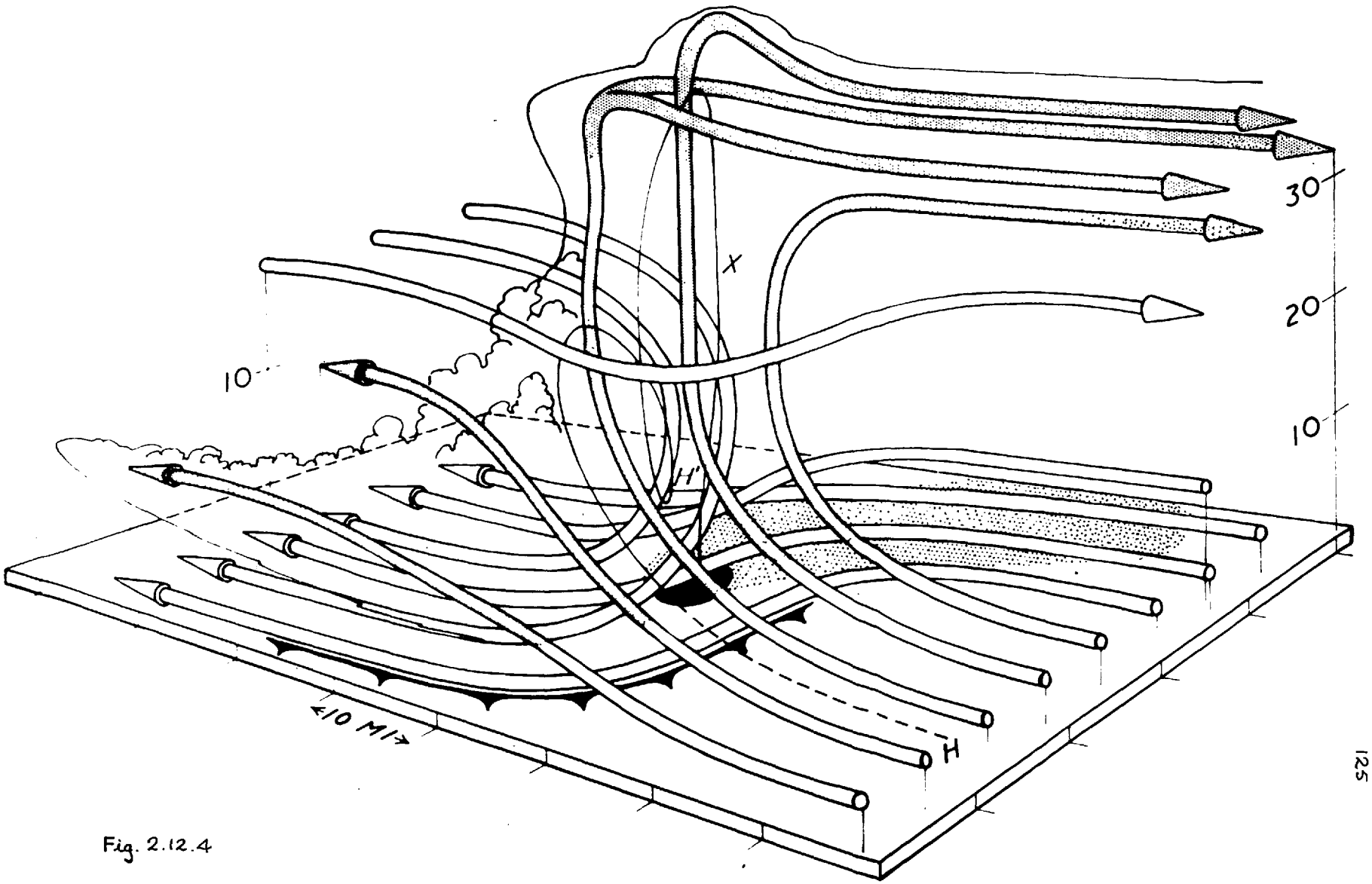

Fig. 2.12.4

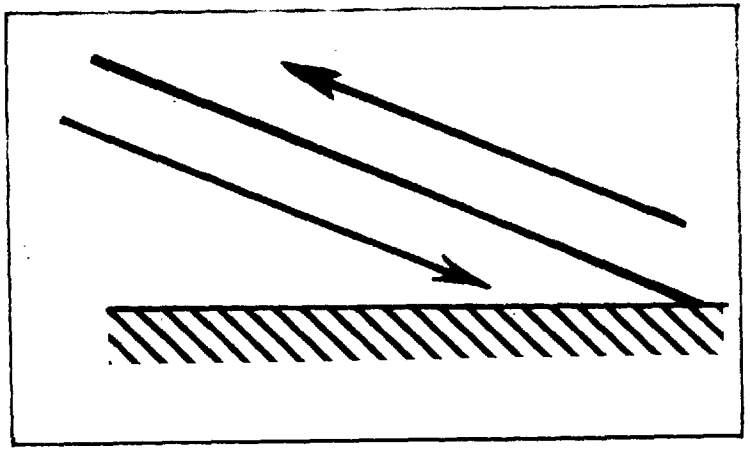

Fig. 2.12.5

Schematic representation of the circulation within the Wokingham supercell in a vertical section normal to its direction of motion.

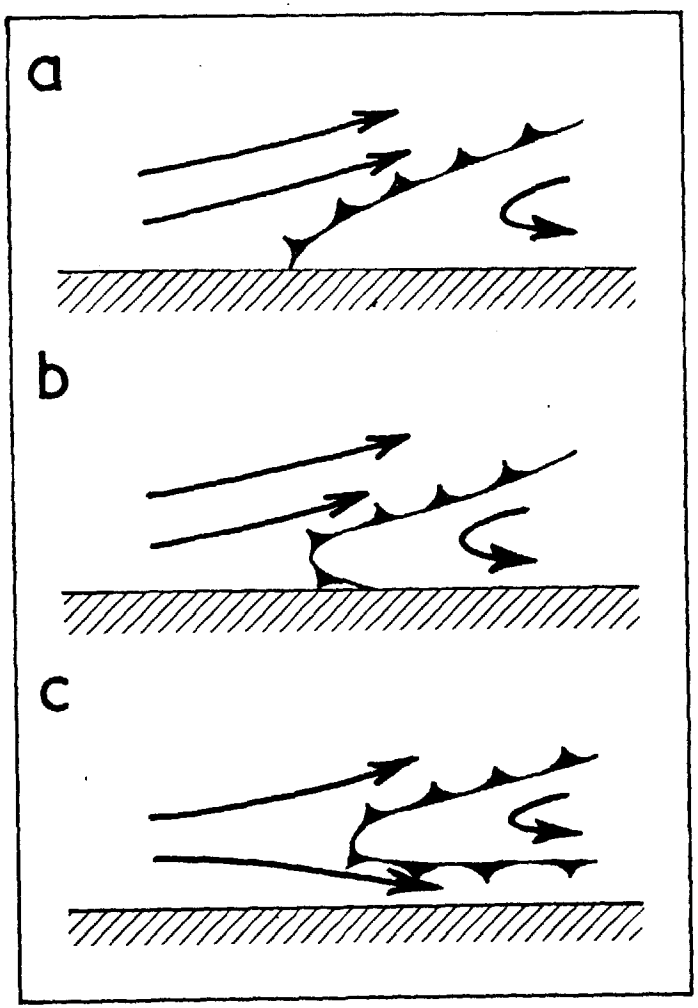

Fig. 2.12.6 (i, ii, & iii)

Schematic representation of the air-flow in the vicinity of the gust-front within vertical sections along the direction of motion of the supercell which pass through its right flank, centre and left flank respectively.

Appendix 2.12a. Anomalous propagation of radio waves after the passage of storms.

According to Booker (1951) super-refraction (or duct propagation) of centimetric radio waves is usually associated with the rapid decrease with height of refractive index which accompanies an inversion of temperature exceeding about $5^{\circ}F$ per 100 ft and/or a lapse rate of humidity exceeding about ½ gm kg^{-1} per 100 ft: such a gradient must be maintained over an interval of height of order 100 ft at a level not more than a few thousand feet above the earth's surface.

Although this situation does not occur generally during the unstable conditions favouring the development of convective storms, it may be associated with the shallow pools of cool moist downdraught air left behind by cumulonimbus. Consequently the extent and duration of anomolous reception of ground echoes at centrimetric wavelengths could enable the extent of these areas to be estimated (see e.g. Mathur and Kulshrestha, 1961). The absence of this phenomenon on 9 July 1959 may be due to the moderate surface winds causing the refractive index gradient to be diminished by eddy diffusion: alternatively it may be a result of the rather poor horizon at the East Hill radar site (typically 1°).

13 The airflow in the near environment ahead of the updraught

In this section the ratio of the x and y[1]-components of wind velocity just ahead of the supercell is determined from the disposition of the precipitation which was carried ahead of it by the relative horizontal airflow. This analysis is based upon the assumption that the air-flow within and around the supercell had been in a quasi-steady state throughout the period during which the observed precipitation was being released from near the summit of the updraught.

The raw material for the analysis is presented in Fig. 2.13.1, which shows a series of low gain 4.7 cm PPI reflectivity contours for the times to which Figs. 2.9.2 (ii) and 2.9.3 (ii) are applicable. These sections are approximately in the x-y plane and they show the directions in which the precipitation falling ahead of the supercell extended at different levels. Because of the finite extent of the region where particles were released from the updraught, the region of precipitation blown ahead had a substantial width in the x-y plane. However the analysis is carried out by considering the approximate axes of the echo-extensions produced in the x-y planes by these particles: these are drawn as continuous lines in each PPI section in Fig. 2.13.1. The region of precipitation ahead of the supercell is then treated as though it formed a curved surface, or

---

[1] Natural coordinates are defined (as shown in Fig. 2.13.2) with the origin at the ground practically vertically beneath the highest top and the positive x-direction along the direction of travel of the supercell. Throughout this section distances are in km and velocities in m sec^{-1}.

curtain, passing through these lines and originating from a point source[1], Q, of particles at the centre of the actual region of release. The relation of this curtain and the source Q to the supercell, and its direction of motion, is shown schematically in Fig. 2.13.2. It was shown in section 2.11 (i) that, at the time to which Figs. 2.13.1, 2.9.2 (ii) and 2.9.3 (ii) apply, the largest stones were released at a height of nearly 11 km, whereas the maximum top occurred 2 km higher on 208°. Consequently Q is taken to be at Z = 12 km on 208°: any error in this will only affect the accuracy of the determination of the winds near Q, and this is already poor as will be seen later.

Before proceding further, a correction is applied to the orientation of the curtain to compensate for the propogation of the core of the supercell to the right as it grew in extent during the intense phase. Thus the paths of the region of maximum radar reflectivity and highest tops, as well as the hailswath, were orientated along 220°. Presumably Q also moved in this direction, implying a component of -3.5 m sec^{-1} in the y direction. This caused the y-component of the orientation of the curtain to be exaggerated, and so the dashed lines in Fig. 2.13.1 have been constructed so as to represent the intersections of the curtain with the x-y planes as they would have appeared had the source been moving along the x-axis (210°). The manner in which this amendment has been deduced is now discussed.

---

[1]The fact that there was a single curtain of particles is further evidence for the existence of a single large updraught within the supercell.

Consider a particle released at Q which subsequently fell through a vertical distance of n km to a height z_o in a time ΔT whilst travelling through Δx km in the x-direction

$$\Delta x = \sum_n \left(\frac{\bar{u}_x}{-dz/dt} \right) \qquad 2.13.1$$

and

$$\Delta T = n / \overline{\overline{-dz/dt}} \qquad 2.13.2$$

where $\overline{\quad}$ denotes an average taken over a 1 km interval,

and $\overline{\overline{\quad}}$ denotes an average taken over the height interval (12km, z_o km)

where $z_o = (12-n)$ km. Dividing eq. 2.13.1 by eq. 2.13,2 gives

$$\overline{\overline{u}}_x = \frac{1}{n} \overline{\overline{\frac{dz}{dt}}} \sum_n \left(\frac{\bar{u}_x}{dz/dt} \right) \qquad 2.13.3$$

Now

$$-\frac{dz}{dt}(z) = k(z) V_o - u_z(x,y,z) \qquad 2.13.4$$

where V_o is the fall-speed of the particle at the ground, $-u_z(x,y,z)$ is the vertical downdraught velocity and $k(z)$ is the correction factor which takes into account the variation in fall-speed owing to the decrease in air density with height (see equation 2.13.13).

Little is known concerning the magnitude of the downdraught in the near environment, but it is shown in appendix 2.13a that for any reasonable value it may be neglected in the context of this analysis. This enables $\overline{\overline{u}}_x$ to be expressed independently of V_o (i.e. of particle size), so that even though the particles comprising the curtain became progressively smaller with increasing horizontal distance from Q, $\overline{\overline{u}}_x$ is nevertheless independent of x(and y) at any given level. Thus, substituting in eq. 2.13.3 in terms of eq. 2.13.4, with $u_z(x,y,z)=0$

gives,

$$\overline{\overline{u}}_x(z_o) = \frac{\overline{\overline{k}}(z_o)}{n} \sum_n \left(\frac{\bar{u}_x(z_o)}{\bar{k}(z_o)} \right) \qquad 2.13.5$$

The form of the curtain merely specifies the relative magnitude of the x- and y- components of wind velocity; the absolute values can only be determined if one or the other be assumed. As a first approximation, therefore, $u_x(z)$ is taken as that obtained for the far environment (Fig. 2.1.3 (i)): the validity of the analysis should therefore increase with distance ahead of Q. Substituting this profile in eq. 2.13.5 has enabled $\overline{\overline{u}}_x$ to be plotted as a function of z_o (Fig. 2.13.3).

Now Q moves with a constant component velocity of -3.5 m sec^{-1} in the y-direction so that the correction to the y-coordinate of the curtain required to eliminate the effect of propogation is given by

$$\Delta y(z_o) = - \frac{3.5\, x(z_o)}{\overline{\overline{u}}_x(z_o)} \qquad 2.13.6$$

The corrected orientations of the curtain where it intersects the x-y planes in Fig. 2.13.1 are now used to determine the vertical profile of the y-component of the wind-field, $u_y(z)$, in the near-environment at distances ahead of Q of 3.5, 7.0 and 14.0 km, at which ranges the intersection of the curtain with the respective y-z plane is as shown in Fig. 2.13.4

$\overline{u_y}(z)$ is evaluated over 1 km height intervals by considering particles which arrive at the lower limit, z_o, of the interval at the required distances, $x(z_o) = 3.5$, 7.0 or 14.0 km, from Q. Thus

$$\overline{u}_y(z_{o+1} > z > z_o) = \frac{\delta y(z_{o+1} > z > z_o)}{\delta t(z_{o+1} > z > z_o)} . \qquad 2.13.7$$

where $\delta y(z_{o+1} > z > z_o)$ is the increment of y accrued by the particles in the interval $(z_{o+1} > z > z_o)$, during which $x(z_{o+1}) < x < x(z_o)$ and

$$\delta t(z_{o+1} > z > z_o) = \frac{1}{-dz/dt\,(z_{o+1} > z > z_o)} = \frac{1}{\bar{k}(z_{o+1} > z > z_o)\,V_o} \qquad 2.13.8$$

if the downdraught velocity is neglected. However a formula is required which is independent of the size of the particle; V_o is therefore expressed in terms of $\bar{\bar{u}}_x(12 > z > z_o)$ in the following way:

$$\Delta t(z(0) > z > z_o) = \frac{(12 - z_o)}{-dz/dt\,(12 > z > z_o)} = \frac{(12 - z_o)}{\bar{\bar{k}}\,(12 > z > z_o)\,V_o} \qquad 2.13.9$$

Also $$\Delta t(z(0) > z > z_o) = \frac{x(z_o)}{\bar{\bar{u}}_x\,(12 > z > z_o)} \qquad 2.13.10$$

Therefore eqs. 2.13.9 and 2.13.10 give

$$V_o = \frac{\bar{\bar{u}}_x(12 > z > z_o)}{\bar{\bar{k}}\,(12 > z > z_o)} \cdot \frac{(12 - z_o)}{x(z_o)} \qquad 2.13.11.$$

Substituting in eq. 2.13.7 from eqs. 2.13.8 and 2.13.11 gives

$$\bar{u}_y(z_{o+1} > z > z_o) = \delta y(z_{o+1} > z > z_o)\,\bar{\bar{u}}_x(12 > z > z_o)\left(\frac{12 - z_o}{x(z_o)}\right)\left(\frac{\bar{k}(z_{o+1} > z > z_o)}{\bar{\bar{k}}\,(12 > z > z_o)}\right) \qquad 2.13.12$$

But eq. 4.1.10 gives $$k(z) = \left(\frac{8g\bar{\delta}}{3C_D\rho(z)}\right)^{\frac{1}{2}} \qquad 2.13.13$$

where C_D are $\bar{\delta}$ are the drag coefficient and mean density of the precipitation particles and $\rho(z)$ is the air density, so that equation 2.13.12 becomes

$$\bar{u}_y(z_{o+1} > z > z_o) = \delta y(z_{o+1} > z > z_o)\,\bar{\bar{u}}_x(12 > z > z_o)\left(\frac{12 - z_o}{x(z_o)}\right)\left(\frac{\bar{\bar{\rho}}(12 > z > z_o)}{\bar{\rho}(z_{o+1} > z > z_o)}\right)^{\frac{1}{2}} \qquad 2.13.14$$

The chief difficulty in evaluating this arises from the fact that $\delta y(z_o+1 > z > z_o)$ may not be determined directly, because of the non-zero x-component of motion. Consequently the following procedure is adopted.

$$\delta x(z_o+1 > z > z_o) = \frac{\bar{u}_x(z_o+1 > z > z_o)}{\bar{u}_y(z_o+1 > z > z_o)} \delta y(z_o+1 > z > z_o) \qquad 2.13.15$$

Substituting in eq. 2.13.15 from eq. 2.13.14 gives

$$\delta x(z_o+1 > z > z_o) = \frac{\bar{u}_x(z_o+1 > z > z_o)}{\bar{u}_x(12 > z > z_o)} \left(\frac{x(z_o)}{12-z_o}\right) \left\{\frac{\bar{\rho}(z_o+1 > z > z_o)}{\bar{\rho}(12 > z > z_o)}\right\}^{\frac{1}{2}} \qquad 2.13.16$$

But $$x(z_o+1) = x(z_o) - \delta x(z_o+1 > z > z_o) \qquad 2.13.17$$

so that $x(z_o+1)$ may be calculated from eqs. 2.13.16 and 2.13.17 for $x(z_o) = 3.5$, 7.0, and 14 km and for various values of z_o. Thereupon $y(z_o)$ and $y(z_o+1)$ may be estimated by interpolation from the various sections in Fig. 2.13.1, enabling $\delta y(z_o+1 > z > z_o)$ to be calculated for each value of z_o from

$$\delta y(z_o+1 > z > z_o) = y(z_o) - y(z_o+1) \qquad 2.13.18$$

Fig. 2.13.5 shows $\bar{u}_y(z_o+1 > z > z_o)$ plotted as a function of $(z_o+\frac{1}{2})$ for $x(z_o) = 3.5$, 7.0 and 14.0 km. $\bar{u}_y$ is thus meaned over 1 km height intervals and over intervals of $\delta x(z_o+1 > z > z_o)$ in the x-direction, where δx increases with height according to eq. 2.13.16. To a degree of approximation which is adequate in view of the assumptions involved in their derivation, these curves may be regarded simply as plots of $u_y(z)$ AT x = 3.5, 7.0 and 14.0 km, (with the proviso

that u_y is likely to be slightly in error where δx extends towards values of x for which u_y is significantly different). These curves are only valid in so far as the x-component of the near environment is equal to that observed in the far environment. Although this is plausible for x >7 km, it is most unlikely at x=3.5 km. Indeed such an assumption implies cross-winds there of order 35 m sec^{-1} in the mid-troposphere. As this seems excessive, and because it is nevertheless of interest to compare the form of the profiles at this range with that at others, the ad hoc assumption has been made that

$$u_x(z)\,(x = 3.5\ \text{km}) = \alpha\, u_x(z)\,(x \to \infty) \qquad 2.13.19$$

where $\alpha = ½$, and curve I in Fig. 2.13.5 has been drawn accordingly. Since it is unlikely that α would have been independent of z, this curve is best regarded as adumbrating only the relative magnitudes of the x and y components.

The importance of Fig. 2.13.5 arises from the comparison of the more reliable curves II and III with the curve for the far environment. These show interesting differences, for, although the mean y-component of velocity averaged over the entire troposphere may not vary significantly with distance ahead of the supercell (except perhaps very close to it), this is certainly not true of the vertical distribution of this component. Whereas there is a small positive component throughout most of the far environmental troposphere, this component is enhanced just ahead of the supercell in the upper troposphere but diminished in the lower troposphere, where it even reverses

in direction. This suggests that the storm was embedded within a circulation of the kind portrayed in Fig. 2.12.5.

The enhancement of the cross-component in the medium and upper troposphere had the effect of increasing the extent of the updraught near the right flank which could rise above the condensation level without being precipitated into and consequently cooled. However, because of the low-level reversal in this component, most particles (except the very smallest) were not carried far enough to the left to cause constituent cells of the echo-mass to become undistinguishable except when they were particularly close. As a result the constituent cells of the Wokingham storm could be resolved and tracked along 210° long after new ones had formed on their right flanks (Fig. 2.5.5).

Fig. 2.13.1

Series of low-gain 4.7 cm PPI intensity contours for the period to which Figs. 2.9.2(ii) and 2.9.3(ii) apply. The contours represent an intensity (16) at 80 km range after taking into account beamwidth effects according to appendix 2.3a.
The continuous lines in each section represent the axis of the finger of echo extending ahead of the core: the pecked lines denote the orientation which would have occurred in the absence of propogation of the particle source, Q. The marks along these lines correspond to distances ahead of Q of x = 3.5, 7.0 and 14.0 km: the heights of these positions are tabulated below.

Height of PPI sections as a function of range

Distance ahead of Q. : x (km)		3.5	7.0	14.0
Distance from radar	(km)	80.0	76.5	69.5
Z(km)	A	2.7	2.5	2.2
	B	4.2	3.9	3.5
	C	5.7	5.3	4.9
	D	7.2	6.7	6.1
	E	8.6	8.0	7.2
	F	9.7	9.1	8.2
	G	10.9	10.4	9.2
	H	13.7	13.0	11.8

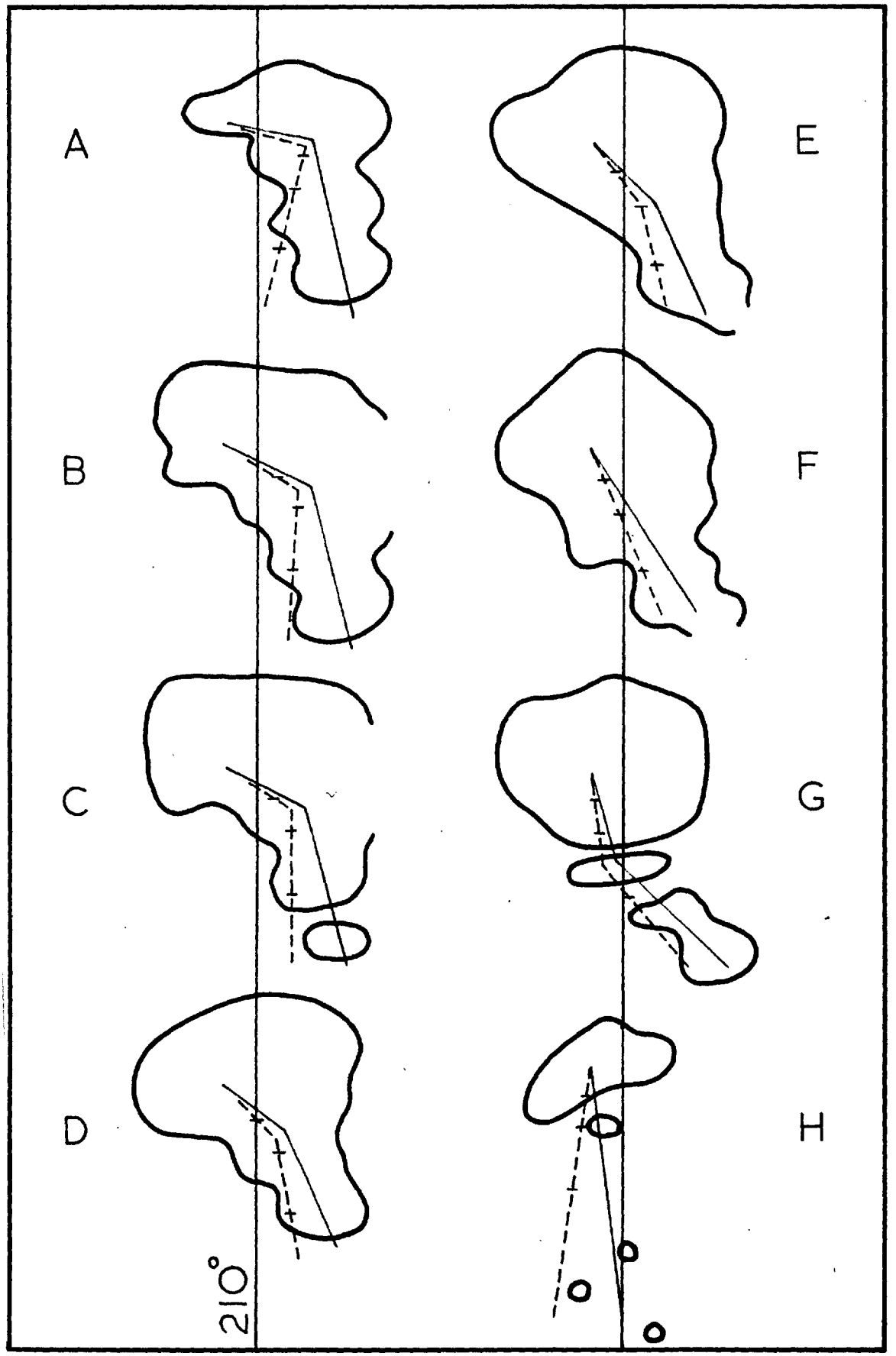

Fig. 2.13.1

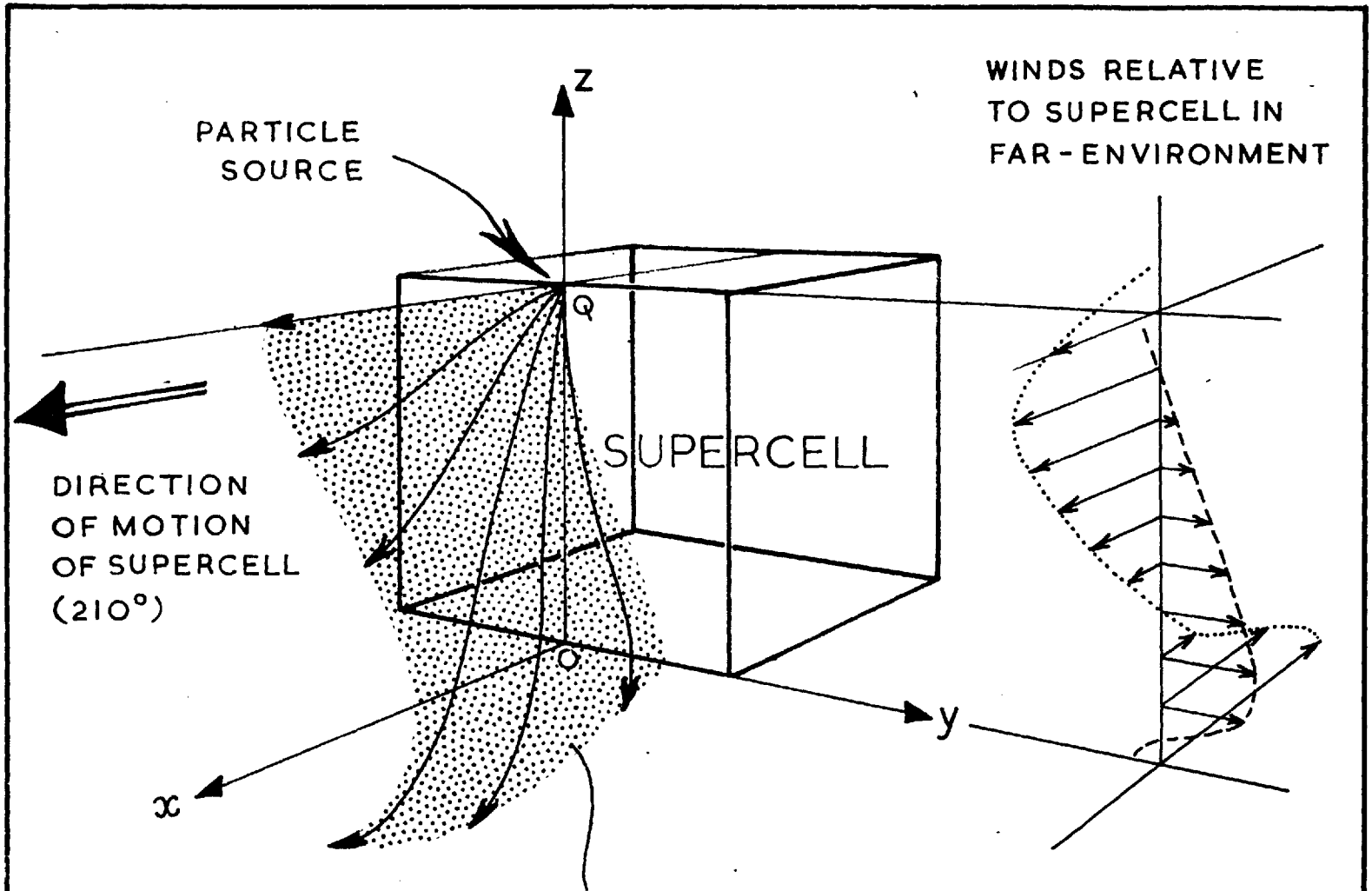
PARTICLE SOURCE
z
WINDS RELATIVE TO SUPERCELL IN FAR-ENVIRONMENT
Q
SUPERCELL
DIRECTION OF MOTION OF SUPERCELL (210°)
O
y
x
CURTAIN AHEAD OF SUPERCELL SHOWING TRAJECTORIES OF PARTICLES COMPRISING IT

FIG. 2.13.2

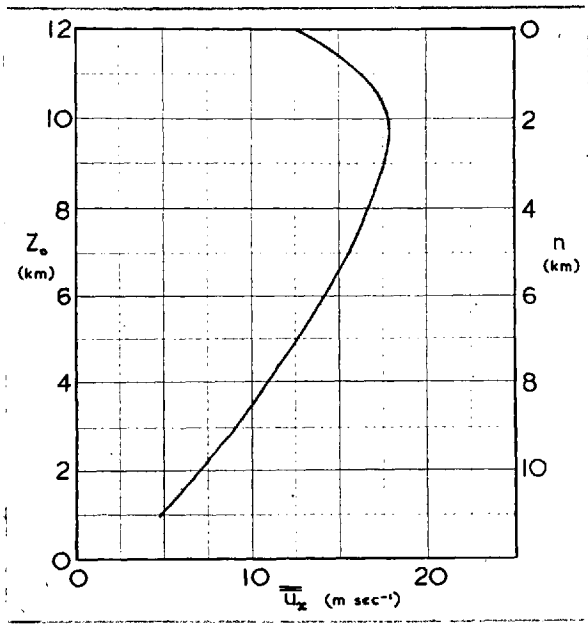

Fig. 2.13.3
Mean x-component of the relative horizontal environmental wind velocity for particles falling in the interval $12 > z > z_o$ plotted as a function of z_o(=(12-n)).

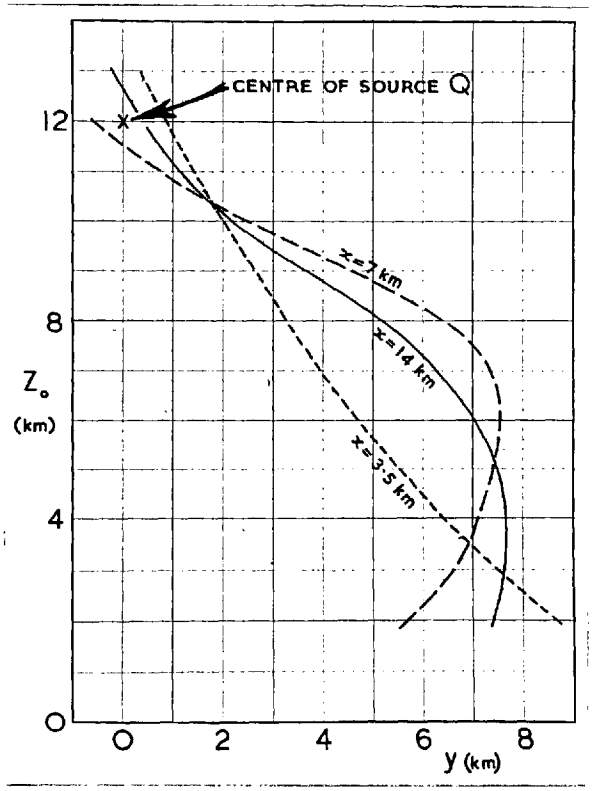

Fig. 2.13.4
Intersection of the curtain with the y-z plane at 3 particular distances ahead of the particle source, Q.

Fig. 2.13.5

$U_y(z)$ in the vicinity of the curtain at distances ahead of the particle source, Q, of 3.5, 7.0, 14.0 km and at infinity.
Whereas U_y has a small positive value throughout most of the far environment, it is enhanced just ahead of the supercell in the upper troposphere but diminished in the lower troposphere.
(U_y is meaned over intervals of x given from eq. 2.13.15 and curve I is very approximate, being based upon eq. 2.13.19).

Fig. 2.13.5

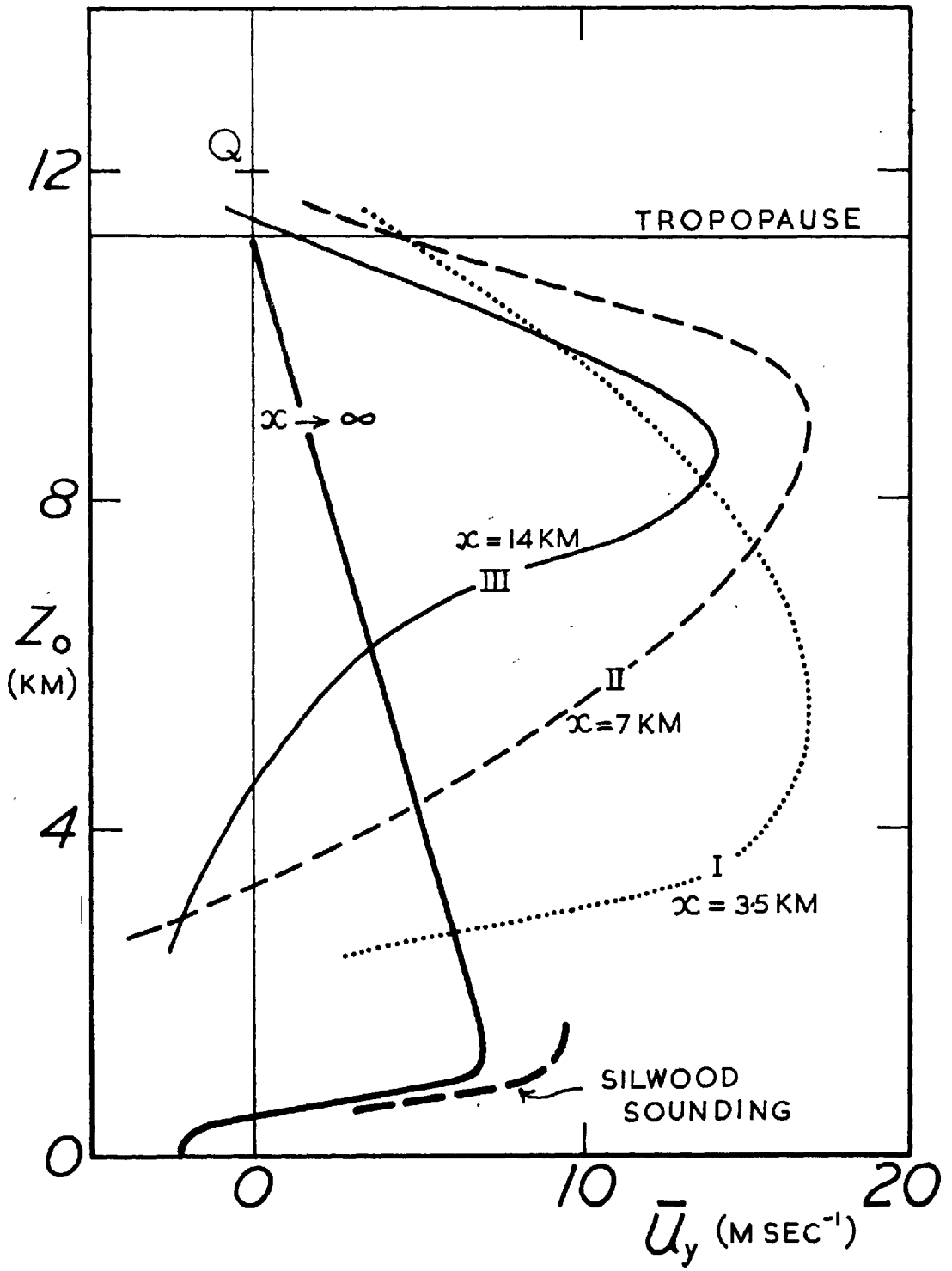
Q
12
TROPOPAUSE
$\varkappa \to \infty$
8
$\varkappa$ = 14 KM
III
Z_0
(KM)
II
$\varkappa$ = 7 KM
4
I
$\varkappa$ = 3·5 KM
SILWOOD
SOUNDING
0
0
10
20
$\bar{u}_y$ (M SEC^{-1})

Appendix 2.13a: The validity of the assumption, $U_z(x,y,z) = 0$

Assuming that $u_z(x,y,z) = 0$, then the mean fall-speed since their release from Q of particles at (x,z_o) is given by

$$\overline{\overline{V(x,z_o)}} = \frac{n}{x}\,\overline{\overline{u_x(z_o)}} \qquad 2.13a.1.$$

This equation has enabled the construction of Fig. 2.13a.1, using values of $\overline{\overline{u_x(z_o)}}$ given from Fig. 2.13.3. It shows $\overline{\overline{V}}$ as a function of z_o at three particular distances ahead of the particle source, Q, in the absence of any downdraught.

The assumption breaks down when $\overline{\overline{u_z}}$ becomes comparable with $\overline{\overline{V}}$. According to eq. 2.13.4 this occurs when $\overline{\overline{u_z}}$ at any given position is half the value of $\overline{\overline{V}}$ indicated in Fig. 2.13a.1. Thus it is clear that the restriction upon the downdraught velocity is least stringent near Q (where the greatest values are to be expected). Moreover, although $\overline{\overline{V}}$ drops as low as 4-6 m sec^{-1} 14 km ahead of Q, this is still likely to be more than twice as great as the actual downdraught velocity so far ahead.

The maximum possible error that this assumption could involve occurs when $u_z \gg V$, in which case the ratio $\overline{\overline{k(z_o)}} \Big/ \sum_n \overline{k(z_o)}$ in eq. 2.13.5 must be replaced by unity. However except that this be so over a majority of the depth of the troposphere the resulting error is negligible, so that the neglect of the downdraught velocity is quite justified in this context.

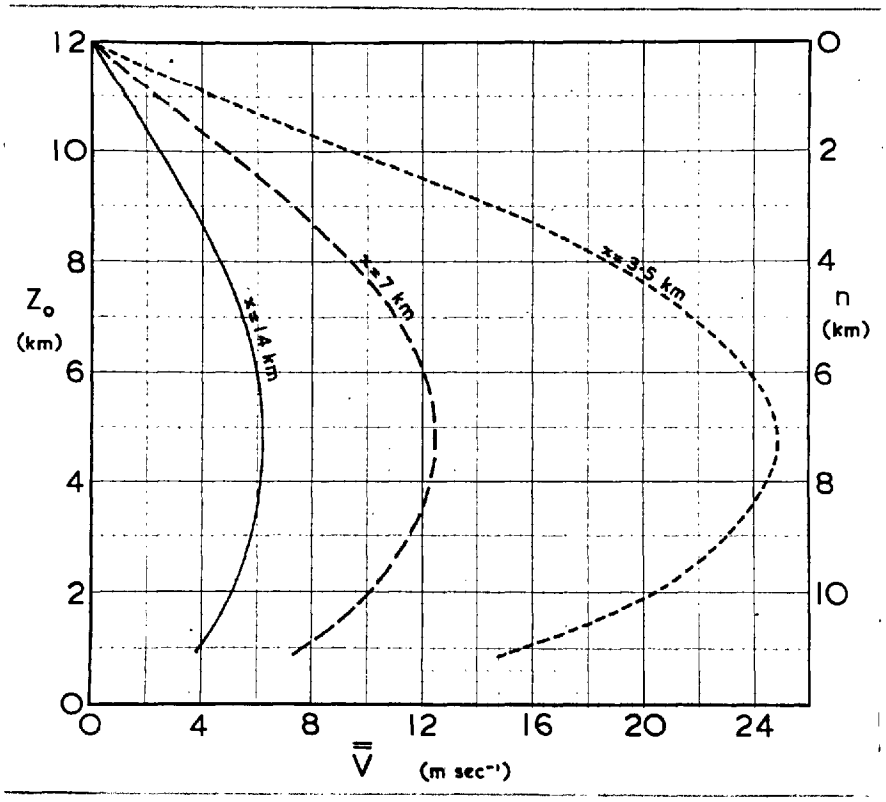

Fig. 2.13a.1.
The mean fall-speed after their release from Q of particles as a function of height at three particular distance ahead of Q.

14 The growth of hail within the supercell

Ludlam (1958) has shown that in a model cloud in which supercooled water occurs between the 0°C and -40°C levels there is time for only a very restricted growth of cloud particles to occur when the updraught between these levels has speeds comparable with the fall-speeds of large hailstones. He therefore concludes that when large stones grow some unsteadiness of the updraught prolongs the period spent by the stones in the region of supercooling: for example, stones might fall from one thermal and enter another near the 0°C level. The tilted quasi-steady updraught of the new model (Fig. 2.11.4) is a more efficient means to the same end, permitting embryo stones to descend from the cloud tops and to re-enter the updraught near the 0°C level.

The analysis in section 4.8 of the largest hailstones collected during the Wokingham storm has enabled the determination of the vertical velocity of the updraught in which they were growing as well as the height as a function of their size whilst $R > 2$ mm. This has permitted the construction of their trajectories within the quantitative two-dimensional model (Fig. 2.12.1), and these have been extended backwards for short distances in a step-by-step manner for $R < 2$mm (assuming a change from the square - law ih eq. 4.1.10 to the linear fall-speed relationship, $V = 10^4 R$, at $R = 1$mm). Although the pattern of air-flow depicted in Fig. 2.12.1 has been derived neglecting the large increment of flux owing to air entering the section, it has been inferred that this mostly entered at medium

and high levels, so that the form of the updraught near the forward overhang is probably still a fair approximation. Consequently at least the lower part of the hail trajectory is reasonably valid. It therefore follows that the largest stones grew from embryos of fall-speed nearly 10 m sec^{-1} which entered the updraught just above the 0°C level some 2 km ahead of the wall (position H' in Fig. 2.12.1).

Owing to the y-component of the air-flow ahead of the updraught (section 2.13) particles of this fall-speed released from the summit of the updraught within the section of Fig. 2.12.1 reached the ground ahead of H' and on the left flank: the 10 m sec^{-1} particles reaching the position H' came from the lower tops of vigorous cumulus growing on the right flank of the supercell. A three-dimensional trajectory of one of these is illustrated schematically in Fig. 2.12.4: it formed in air which started to rise at H and was carried forward and across relative to the storm after having risen above 13,000 ft within the cumulus; subsequently it fell into the main updraught within the forward overhang at H'. As shown in Fig. 2.12.1, it then rose slowly close to the updraught axis until, depending upon its precise position, it either crossed the axis (like stone β and probably α also) to descend to the ground some way behind the wall, or rose above the -40°C level to fall ahead of the updraught. Those stones in the latter category descended via the position X (where they became dry and produced a very intense 3.3 cm radar echo) before re-entering and crossing the updraught en route to the ground near the wall.

Embryos which on the first entry into the main updraught at H' had fall-speeds too small to ensure that they attained the largest size on traversing the updraught were lifted more swiftly through the updraught and released ahead of it. Owing to their smaller fall-speed they then descended farther ahead of the updraught to re-enter it at some lower level where it was not sufficiently strong to prevent them falling through it rather quickly with very little further growth. Whenever an embryo entered the updraught with too great a fall-speed it grew too rapidly to be lifted into the updraught maximum and was borne towards the rear of the storm to fall out of the updraught well behind the wall without attaining the largest possible size. It does not seem important whether or not the embryos in their early history were small hailstones (graupel) or small raindrops: moreover the supply of embryos from the cloud tops was probably abundant and not sensitively related to the properties or concentrations of freezing nuclei present in the updraught.

In addition to small particles seeding the updraught at H' in the manner already described, large numbers of embryos of a suitable size were probably produced in situ within the updraught near H' in the form of drops shed by hailstones growing wet at these levels (see section 5.2). However this mechanism for supplying embryos does not differ in principle from the one discussed previously since it still requires that the updraught near H' be seeded by particles descending ahead of the updraught at higher levels.

There is some tendency for the isopleths of maximum hail size at the ground within the broad hailswath to be orientated along about 195°; this is particularly evident in a region at ranges between about 50 and 60 miles in Fig. 2.4.1 (ii) where the first large hail occurred. This could be a symptom of the cross wind component within the updraught; in order to account for the orientation its mean value would need to have been 11 mi hr^{-1}. In Fig. 2.4.1 (ii) a line has been drawn along 195° from the edge of the first swath of large hail to meet the path of the edge of the 10 cm echo (at X). Now at range 50 to 60 miles the minimum detectable intensity on the 10 cm PPI radar was about 24 (plus a small correction owing to the radar drifting off tune). According to eq. 2.11.2 it can therefore be supposed that particles of radius slightly exceeding 1 mm were present at the right hand edge of this echo-mass. Consequently the length of the line to X implies a period of 1200 sec for the growth of hail from a radius of 1 mm to 13 mm and its subsequent descent to the surface. A shorter period of about 760 sec found at a later stage is about the minimum period which can be inferred (see line leading to Y in Fig. 2.4.1 (ii). In both localities hail of radius exceeding 21 mm occurred about 2½ miles farther along the hail path implying an additional period of about 200 sec. Bearing in mind that the reported hail sizes were biased towards their largest diameter these times are consistent with those estimated in section 4.8, where it is established that, for the largest stones collected, the minimum possible time taken to fall to the surface after growing from a radius of 2mm was 670 sec (+ 160 sec for the descent below the 0°C level).

CHAPTER III

OTHER CONVECTIVE STORMS

1. The convective storms of 18 July, 1959

In the daily aerological record for this day issued by the meteorological office it is stated that "the general resemblance to the pattern of 9 July is rather striking. The European high had its centre of gravity further northeast, however, with not quite such hot air being drawn up over France, and the cold trough which came into the British Isles progressed more readily across England." In particular the vertical wind fields over S.E. England on these two occasions were very similar (see Fig. 3.1.1), the main difference being the smaller shear in the lowest levels on the 18th.

During this day the only significant showers occurred over East Anglia in the Norwich area. There were two main storm areas, each of which comprised a seemingly random cluster of cells which appeared to the lee of some low hills: the first cluster developed soon after 1600 and the second soon after 1800. The paths of the individual cells as they travelled NNEwards are shown in Fig. 3.1.3; the positions of the cells in the first cluster at three times are shown in Fig. 3.1.4 in order to illustrate their lack of organization.

Except whilst decaying all cells were observed to travel at between 25 and 35 mi hr^{-1}. That this is only about three quarters of the speed of travel of the cells on the 9th is probably partly a consequence of the shallower layer possessing potential instability.

Together with the smaller wind shear in the lowest levels this lower speed of travel implies that (in the absence of a convergent inflow in either case) the updraught could only have comprised a third of the flux which could have occurred on the 9th.

Unfortunately temperature soundings were made only at midday and midnight (Fig. 3.1.2), so that the thermodynamic state of the troposphere in the vicinity of the storms can be estimated only approximately by interpolation. Now the value of the wet-bulb potential temperature at screen level reached at 1700 was only 19.2°C, so that in view of the shallowness of the potentially warm layer near the surface it is likely that there could have been no more (and probably was less) latent instability than on the 9th, even with the most favourable composite sounding which can be derived from those shown in Fig. 3.1.2. As a result the echo tops seldom rose within 10,000 ft of the tropopause (at 39,000 ft). Nevertheless the most intense cells in each group persisted for more than two hours (producing at their peak falls of up to 0.4 in of rain and also isolated pea-sized hail). In order to emphasize this persistence Fig. 3.1.5 has been prepared; this shows the trend in the height of the top and in the maximum intensity of the two cells, A and B, (each of which was the most persistent member of its own cluster).

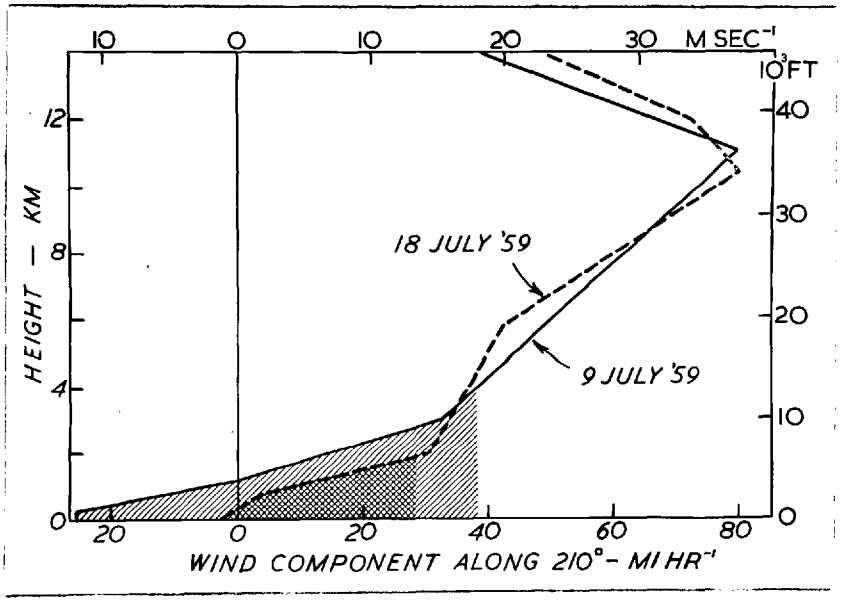

Fig 3.1.1

Wind profiles for the environments of the Wokingham storm of 9 July 1959 and the storms of 18 July 1959.
The hatched areas illustrate that, because of the smaller shear in the lowest levels and the slower speed of travel of the cells on the 18th, the updraught flux per unit distance across their direction of travel would only have been about one third of that on the 9th (in the absence of any convergent inflow in either case).

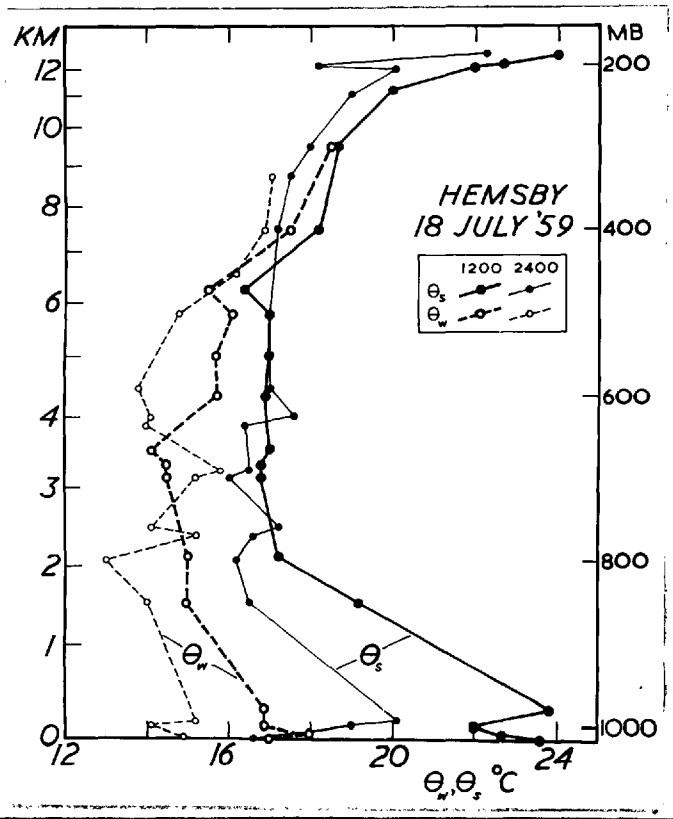

Fig 3.1.2

Distribution with height of θ_w, the wet-bulb potential temperature, and θ_s, the wet-bulb potential temperature if the air were saturated.
(Explanation of θ_s in legend to Fig. 2.1.5).

Fig. 3.1.3.
Paths of the centres of the major storm cells as they travelled NNEwards over East Anglia on 18 July 1959. The paths of cells comprising the earlier group are shown as continuous lines and those within the later group as dashed lines. The positions of rainfall observations are indicated by circles which are open where no precipitation was detected: the approximate extents of measurable precipitation and of that in excess of ¼ in respectively are depicted by the regions of horizontal and cross-hatching. Land over 200 ft is stippled.

Fig. 3.1.4
Positions of the major cells comprising the earlier cluster at 1650, 1735 and 1808 on 18 July 1959 illustrating their lack of organization.

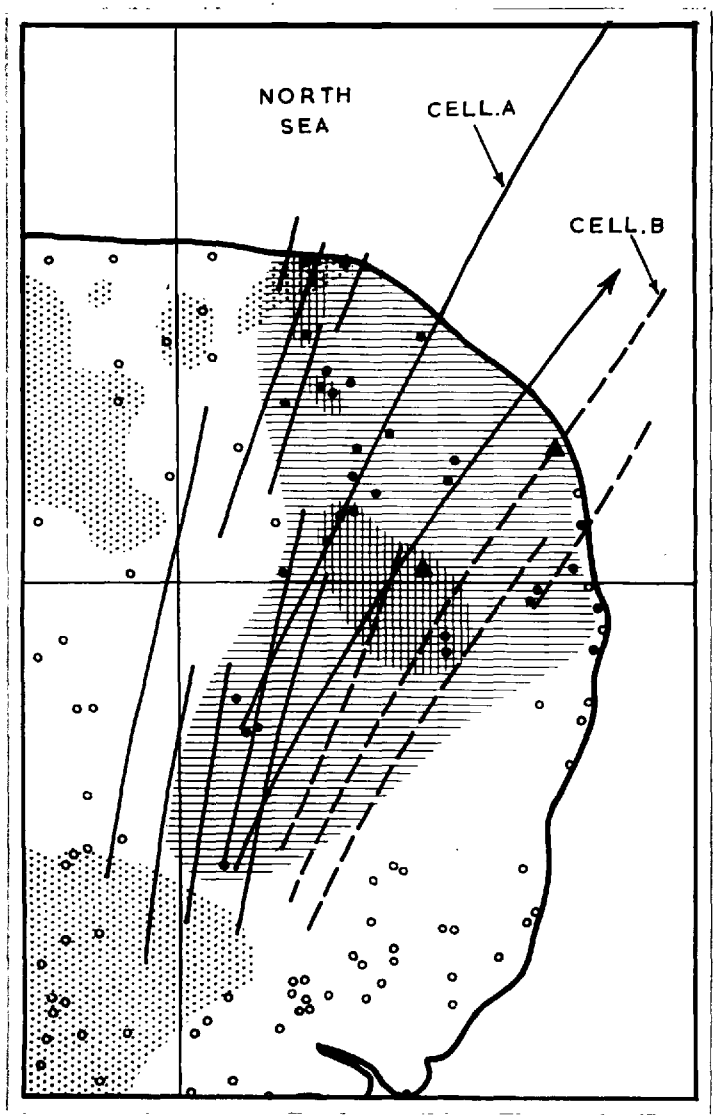

Fig. 3.1.3

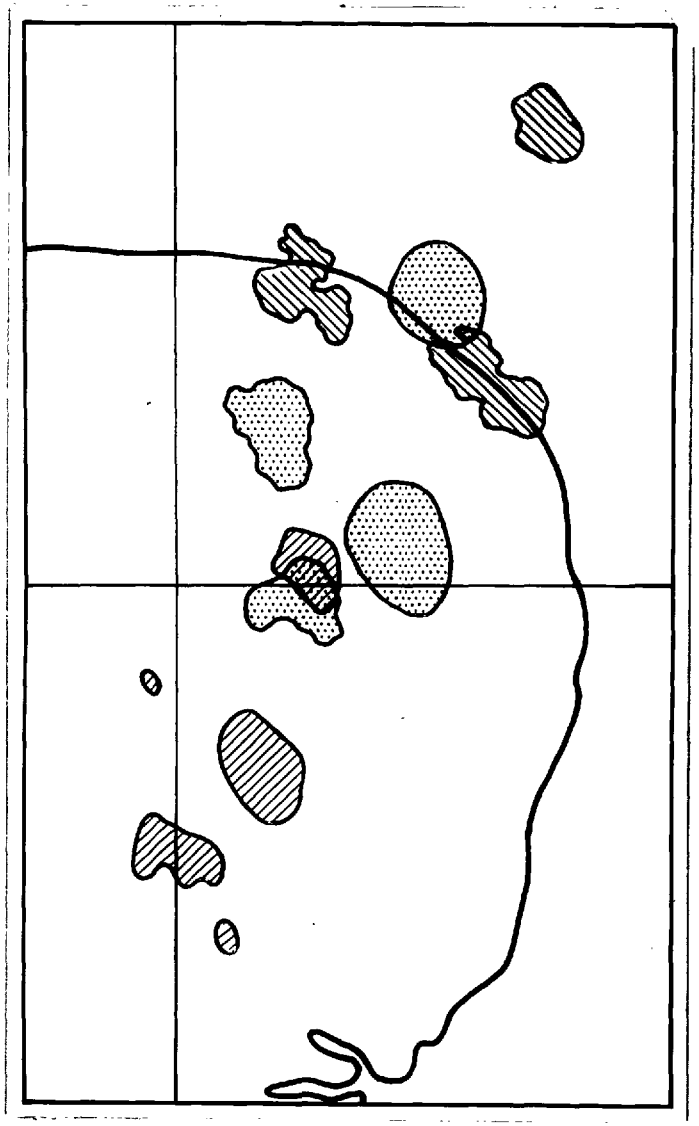

Fig. 3.1.4

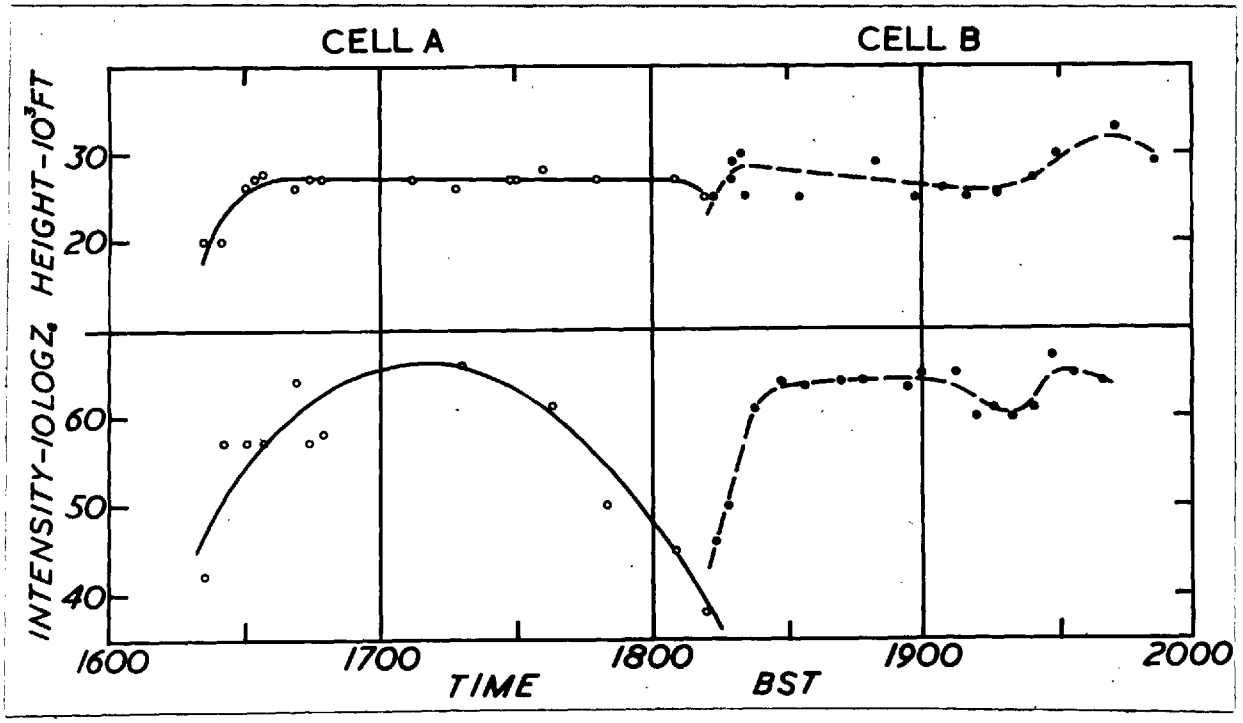

Fig. 3.1.5.
The variation with time of the height of the echo tops and the value of the maximum intensity of the two cells, A and B (each of which was the most persistent member of its own cluster). The observations were made with the 10 cm RH1 set and beamwidth corrections have been applied in accordance with appendix 2.3a.

2. The convective storms of 18 June 1957

This day was characterised in southern England by considerable latent instability but little wind shear in the vertical. Widespread showers developed over land during the afternoon reaching a peak of activity between 1600 and 1800.

The Crawley temperature sounding for 1200 is plotted in Fig. 3.2.1: this shows that already at noon substantial latent instability was present throughout the lowest 2 km and that adiabatic ascent of this air would have led to temperature excesses of up to 2°C and more occurring over a large height interval. Indeed it is clear that there was far greater latent instability on this day than on the occasion of the severe storm of 9 July 1959 when widespread large hail was produced. However, although large rainfall totals occurred on the 18th (see Fig. 3.2.3), hail was neither widespread nor anywhere large (see Fig. 3.2.4). It is therefore important to ascertain the nature and cause of this difference in behaviour of the storms on these two occasions.

The vertical wind profile at Crawley at 1800 is represented in hodograph form in Fig. 3.2.2: it shows that the wind increased with height from an easterly direction reaching a maximum of 18 mi hr^{-1} at heights between 2 and 3 km. However, unlike the profiles associated with the July 1959 storms the sign of the vertical shear reversed above this level. Now the motion of individual cells varied appreciably from one cell to the next but most of the larger ones travelled at about 17 mi hr^{-1} from the east (Table 3.2.1). Therefore considering flow

TABLE 3.2.1

CELL	TIME WHEN FIRST DETECTED BY 10CM PPI (BST)	DURATION OF 10CM PPI ECHO (MIN)	HIGHEST OBSERVED TOP (10^3FT)	MEAN SPEED OF TRAVEL (MI HR^{-1})	MEAN DIR^N OF TRAVEL ($^\circ$ TRUE)
A_1	1527	60	37	14	090
A_2	1545	43	27	17	099
A_3	1603	28	37	20	080
B	1621	66	38½	17	077
C_1	1609	78	41	17	080
C_2	1609	78	38	15	078
C_3	1639	48	34	18	076
C′	1645	60	38	18	075
D_1	1700	37	-	15	085
D_2	1709	68	41	13	093
D_3	1710	36	-	14	091
D′	1733	33	41½	17	083

in a vertical section along the direction of motion of these cells, the updraught must have been disposed as shown in Fig. 3.2.5 (c.f. Fig. 2.8.2). This same form may be associated with the convective storms which affect Equatorial West Africa; these too produce copious rain but generally little hail. The rarity of hail may be partly due to the air flow within the updraught preventing the hail from being recycled in the manner described in section 2.14. A further reason may be that an updraught of the form depicted in Fig. 3.2.5 does not

permit a persistent downdraught to coexist with it without interference, so that either or both of the draughts have to be intermittent. It is therefore not surprising that, throughout 18 June 1957, the individual cells had a short duration. That this was so is evident from the shortness of their paths in Fig. 3.2.6. Twelve of the cells (which were studied in more detail on account of their greater height or persistence) are labelled in Fig. 3.2.6: their duration, speed and direction of travel, as well as the greatest observed height of their tops, are listed in Table 3.2.1. Most of these cells (those in groups A,C and B) amalgamated to form larger echo-masses but even so the typical duration of these cells was only an hour.

Fig. 3.2.7 shows that at any instant cells lay along two lines; one was parallel to the south coast and moved slowly inland; the other was orientated from SW to NE and moved steadily westward. However, whereas with the severe storms of 9 July 1959 the downdraught acted so as to trigger the formation of new cells always on the right flank of the intense cell, on this occasion there was no obviously preferred position of formation of new cells along the line, as is clear from the seemingly random distribution of the places of origin of cells (see Fig. 3.2.6). Rather it appears that these cells were triggered largely by topographical features, especially in view of the presence of cumulonimbus over north France during the afternoon with unbroken blue sky over the intervening Channel.

At 1642 a 10 cm RHI photograph was taken looking along the main

line of cells as indicated in Fig. 3.2.7: a sketch of this photograph is shown in Fig. 3.2.8 and shows a strong inclination of the northernmost column within echo-mass C. In view of the small wind shear in the undisturbed environment this tilt is presumably symptomatic of a convergent inflow towards the echo-mass at lower levels. Regardless of the actual disposition of the up-and down-draughts, neither could have been sustained without this convergence.

Comparison of the behaviour of the severe storm of 9 July 1959 with the storms of 18 June 1957 indicates the importance of the Richardson number[1] in determining the nature of the overturning process: when applied to the whole troposphere this parameter represents the ratio of the potential energy present as latent instability to the kinetic energy available by virtue of the integrated vertical wind shear. If the Richardson number is small then convective storms may occur with persistent and extensive draughts in which conditions are nearly adiabatic, whereas if it is large the convective overturning will occur intermittently and less nearly adiabatically. Of course in either case a prerequisite of any convection is the availability of some mechanism for initiating the release of the latent instability (such as precipitation from medium-level cloud or a suitable topographical feature).

---

[1]The storms studied in The Thunderstorm Project had large Richardsons numbers (c.f. Section 1.1).

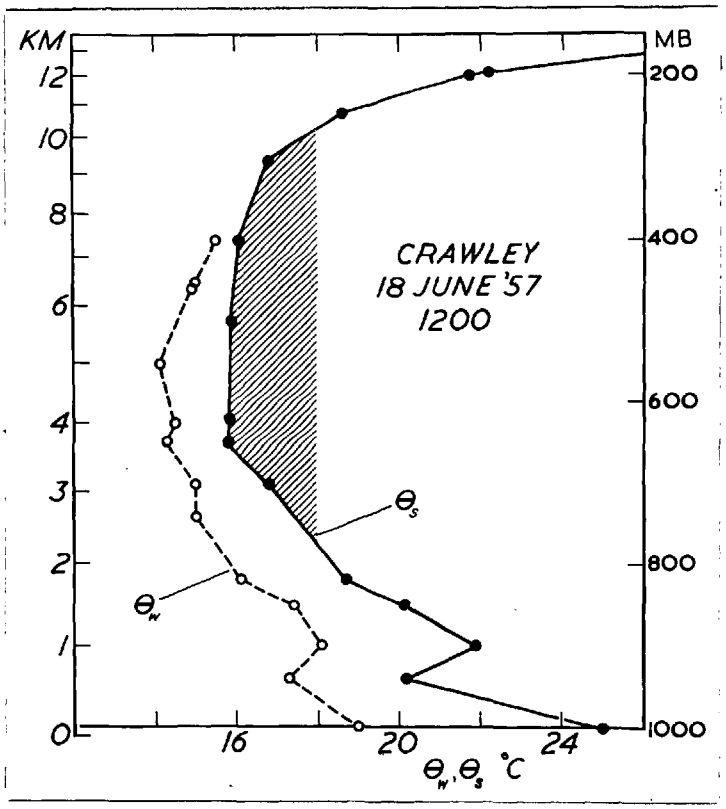

Fig. 3.2.1.
Distribution with height of θ_w, the wet-bulb potential temperature, and θ_s, the wet-bulb potential temperature if the air were saturated. (Explanation of θ_s in legend to Fig. 2.1.5). The adiabatic ascent of unmodified low-level air leads to temperature excesses as much as 2°C in the interval $3 < z < 10$ km (hatched area).

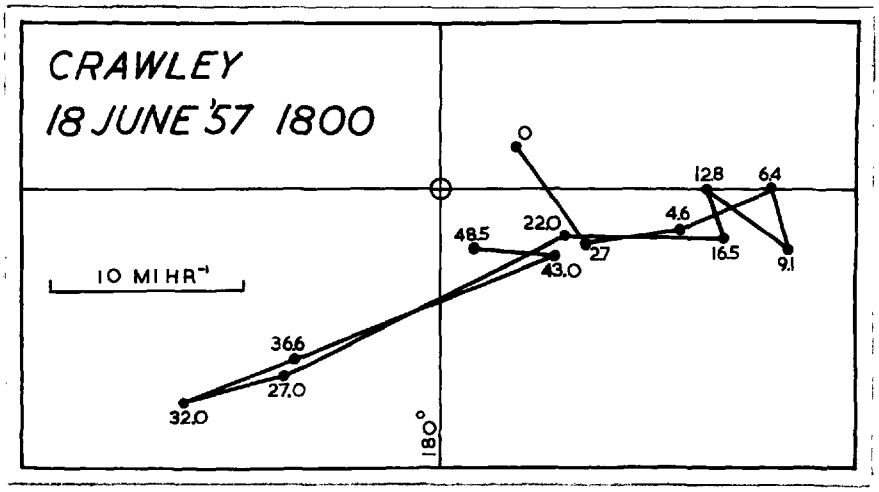

Fig. 3.2.2
Wind hodograph: the numbers denote height in thousands of feet.

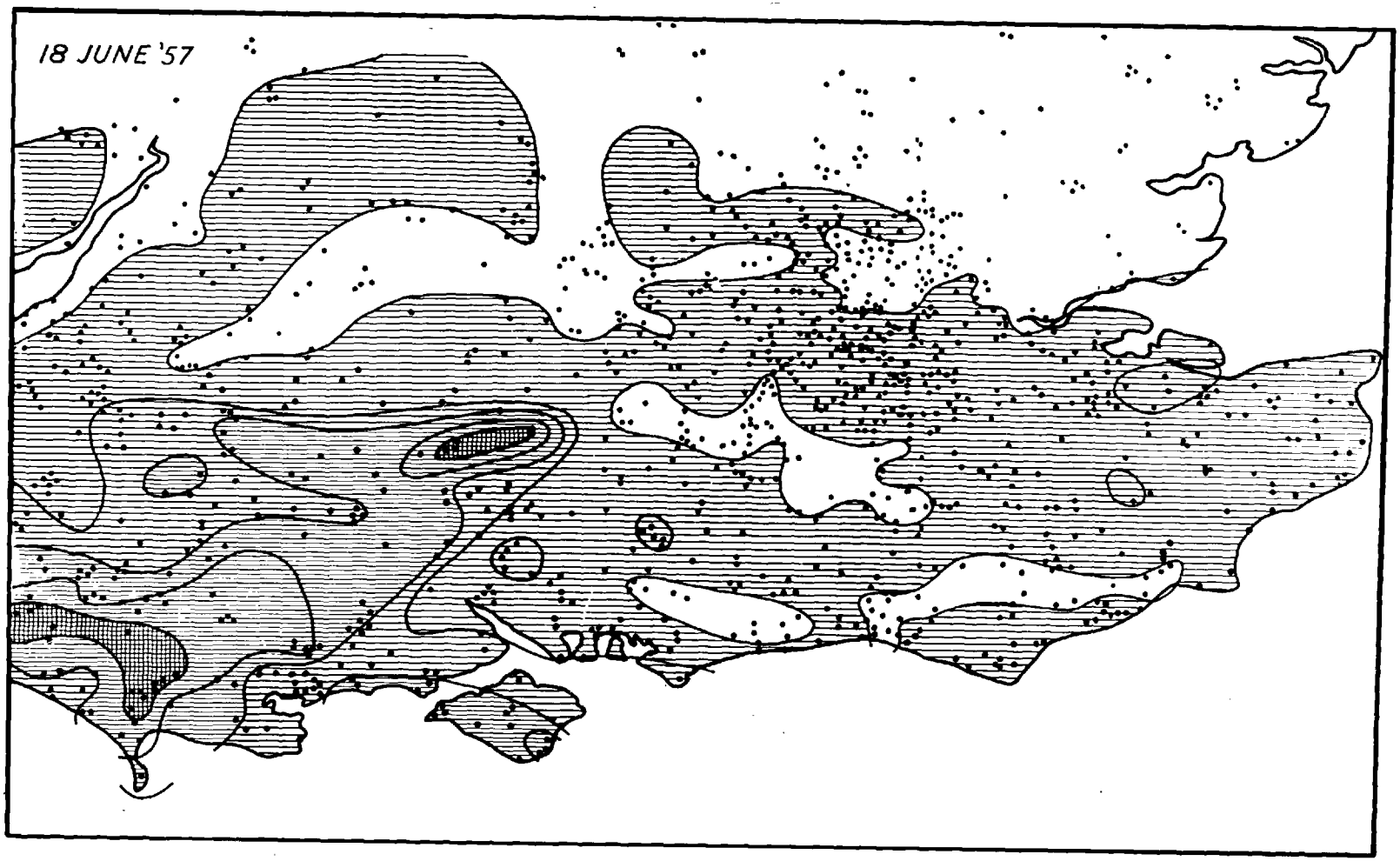

Fig. 3.2.3
Rainfall distribution in southern England on 18 June 1957: the positions of individual observation are indicated and isopleths are drawn for tr, ¼, ½, 1 and 1½in. (The high totals in the Isle of White and near the Dorsetshire coast are due to further thunderstorms which broke out overnight in the English Channel).

Fig. 3.2.4
Observations of maximum hailstone size in southern England on 18 June 1957: they are plotted according to the scale in table 1.2.2, reports of hail of unknown size being entered as black dots. The principal hail regions are hatched.

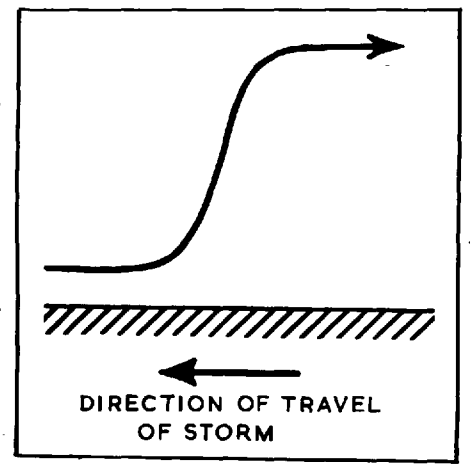

Fig. 3.2.5
Form of the updraught within storms on 18 June 1957. This same form may be associated with the convective storms which affect Equatorial West Africa and perhaps S.W. India.

Fig. 3.2.6
Tracks of storm cells in southern England during the afternoon of 18 June 1957: positions of origin and disappearance of these as seen by the 10 cm PPI radar are represented as black dots and open circles respectively.

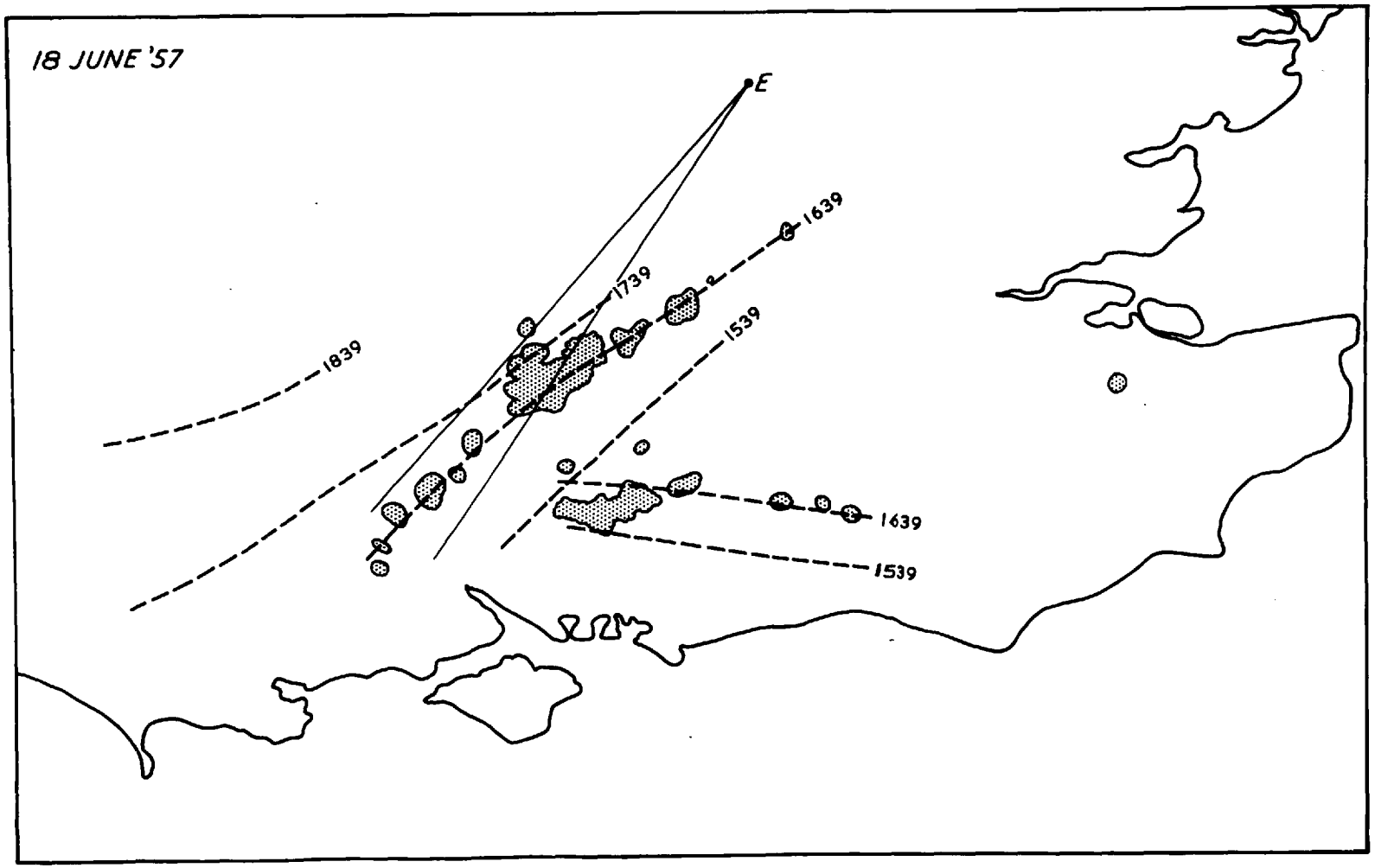

Fig. 3.2.7
Positions of storm cells in southern England at 1639 on 18 June 1957. They lay along 2 lines whose position at times 1539, 1639, 1739 and 1839 are indicated by the pecked lines.
The 7½° sector centred at East Hill (E) represents the area covered by the 10 cm RH1 beam at 1642: cf. Fig. 3.2.8

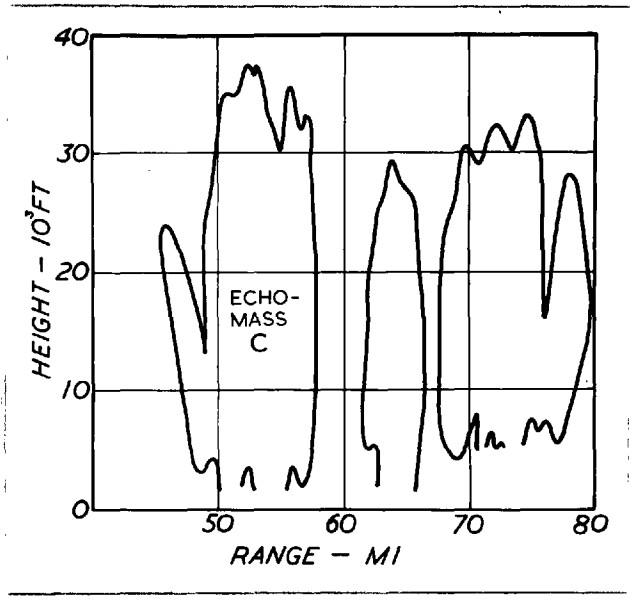

Fig. 3.2.8
Sketch of full-gain 10 cm RHI photograph along 217° at 1642 on 18 June 1957.

CHAPTER IV

The Growth of Hail Within A Quasi-Steady Updraught

1. The heat economy of a growing hailstone

It is generally accepted that hailstones grow predominantly by the accretion of supercooled water droplets (Mason 1957, p.262).

Provided that all the accreted water is retained the rate of growth of a hailstone is given by

$$\frac{dR}{dt} = \frac{(EW)\ V(z)}{4\bar{\rho}} \qquad 4.1.1$$

where $\bar{\rho}$ is the mean density of accreted material,

V(z) is the fall-speed of the hailstone (assumed large compared with that of the accreted droplets),

E is the collection efficiency of the hailstone,

and W is the water content in the environment.

In most conditions the value of E is close to unity but because W also is not accurately known consideration of E is avoided by referring to the effective water concentration (EW).

During the growth of a hailstone its surface temperature, T_s, is raised above that of the environment, T, until the rate of release of latent heat by the freezing droplets is balanced by the rate at which heat may be transferred to the environment. If the size of the stone and the conditions in the cloud are such that all the accreted water can be frozen, then it grows with its surface dry and $T_s \leq 0^{\circ}C$; on the other hand, if the rate of accretion of supercooled droplets is

sufficiently high the surface of the stone will be covered by a film of water with $T_s = 0^{\circ}C$. Accordingly Ludlam calls these respectively "dry" and "wet" growth, and from a consideration of the heat balance of a growing hailstone (1950, 1958), he has derived the conditions for the transition between these two growth regimes. The rate of transfer of heat from the surface of a growing hailstone to the environment is given by

$$\frac{dQ}{dt} = 4\pi R \left[b D L_v \Delta\rho_v + a K (T_s - T) \right] \qquad 4.1.2$$

where K is the coefficient of thermal conductivity of air,

D is the coefficient of diffusion of water vapour in air,

L_v is the latent heat of vaporisation of water,

$\Delta\rho_v = \{\rho_v(T_s) - \rho_v(T)\}$, the difference between the vapour density at the surface and that in the undisturbed airstream, and a and b are coefficients whose values vary with the Reynolds number (Re) according to the empirical formula of Kramers (1946)

$$a = 1.6 + 0.295\ (Re)^{1/2} \qquad 4.1.3$$

and according to the empirical formula of Frössling (1938)

$$b = 1 + 0.229\ (Re)^{1/2} \qquad 4.1.4$$

These expressions are valid only provided the airstream is free of turbulence on the scale of the hailstone. (Such turbulence would increase both coefficients). Both formulae are valid for $(Re) < 10^5$, which embraces practically the complete range of possible hailstone

sizes. Further since we are generally concerned with stones for which $(Re) > 10^3$ when falling at their terminal velocity, and since the experimentally determined expressions can be regarded as only approximate when applied to this problem, Ludlam (1958) takes,

$$a = b = 0.3\ (Re)^{1/2} \qquad 4.1.5$$

Now if all the accreted water freezes, the rate of liberation of latent heat of fusion is given by

$$\frac{dQ_L}{dt} = \pi R^2 V\ (EW)\ \ (L_f + T - T_s) \qquad 4.1.6$$

where L_f is the latent heat of fusion of water and T and T_s are the ambient and surface temperatures respectively. At equilibrium, when $\frac{dQ_L}{dt} = \frac{dQ}{dt}$, eq. 4.1.2 and eq. 4.1.6 give

$$4\pi R a \left[D L_v \Delta\rho_v + K (T_s - T) \right] = \pi R^2 V\ (EW)\ (L_f + T - T_s) \qquad 4.1.7$$

When T_s just reaches 0^oC eq. 4.1.7 becomes

$$4\pi R^* a \left[D L_v \Delta\rho_v - KT \right] = \pi R^{*2} V^* W_c\ (L_f + T) \qquad 4.1.8$$

where W_c is the critical effective water content for the transition between wet and dry growth regimes — hereafter referred to as the W/D transition, and the index (*) denotes growth at this transition.

The drag force exerted upon a freely falling hailstone is given by

$$C_D(\tfrac{1}{2}\rho\ V^2)A = Mg \qquad 4.1.9$$

where C_D = the drag coefficient,

ρ = the air density,

$A = \pi R^2$,

and $M = \frac{4}{3}\pi R^3 \bar{\delta}$, where $\bar{\delta}$ is the mean density of the hailstone

Therefore

$$V^2 = \left(\frac{8g\bar{\delta}}{3C_D\rho}\right)R \qquad 4.1.10$$

Moreover $(Re) = 2RV\rho/\eta$ 4.1.11.

where η is the coefficient of viscosity of air.

Substituting in eq. 4.1.8 from eqs. 4.1.5, 4.1.10 and 4.1.11 gives

$$W_c^2 V^{*3} = (7.7g\bar{\delta}/C_D\eta)\left\{(DL_v\Delta\rho_v - KT)/(L_f + T)\right\}^2 = f_1(z) \qquad 4.1.12$$

from which isopleths of W_c have been computed in the z-V plane for $10 < V < 46$ m sec^{-1}, assuming that $\bar{\delta} = 0.9$ (Macklin et al, 1960), $C_D = 0.6$ (Macklin and Ludlam 1961), and that T(z) (for the Wokingham storm) is that corresponding to a wet-bulb potential temperature, θ_w, of 19°C. The isopleths of W_c are shown in Fig. 4.1.1 along with isopleths of $\frac{dt}{dR}$ deduced from eq.4.1.1 and also isopleths of R computed from eq. 4.1.10 assuming that $\rho(z)$ (for the Wokingham storm) decreased from 0.82×10^{-3} g cm^{-3} at the 0°C level through 0.68, 0.59 and 0.51×10^{-3} g cm^{-3} at the -10, -20, and -30°C levels to 0.44×10^{-3} g cm^{-3} at the -40°C level. Any stone lying to the right of the relevant W/D line grows with its surface wet and at 0°C: any stone to the left grows with its surface dry and below 0°C. Some isopleths in the z-V plane have also been derived from eq. 4.1.7 for T_s = -1, -2, -3 and -4°C, and these are indicated in Fig. 4.1.2: they are needed for the later

discussions. Evidently for any given value of (EW) it is possible for a stone to ascend at such a speed that the effect of the increased rate of accretion as it grows is just balanced by the effect of the lower ambient temperature, so that it may continue to grow with an unchanging surface temperature. It is this fact, coupled with the dependence of the hailstone structure upon the surface temperature, that is used in subsequent sections to account for the layer structure of hailstones in terms of a steady updraught.

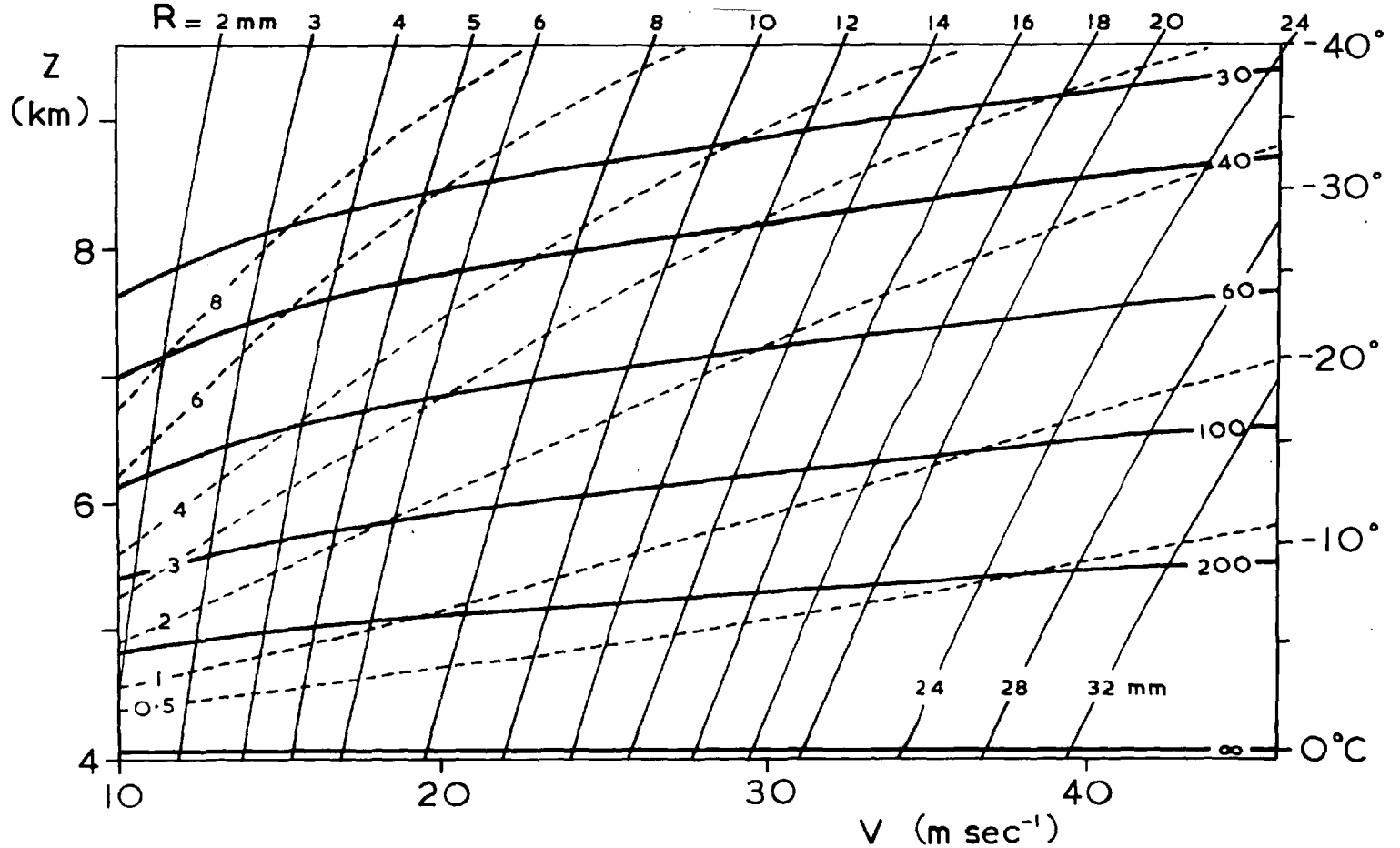

Fig. 4.1.1

Isopleths in the z-V plane of hailstone radius R (thin solid curves labelled in mm) and of the critical water content W_c (pecked curves labelled in g m^{-3}), derived as indicated on p. 164. Also shown are isopleths of dt/dR for (EW) = W_c (thin solid curves labelled in sec mm^{-1}).
When (EW) < W_c a hailstone grows with its surface dry and $T_s \leq 0°C$: when (EW) > W_c it grows with its surface wet and at 0°C. The condition (EW) = $W_c(z,V)$ defines what is called the W/D transition.

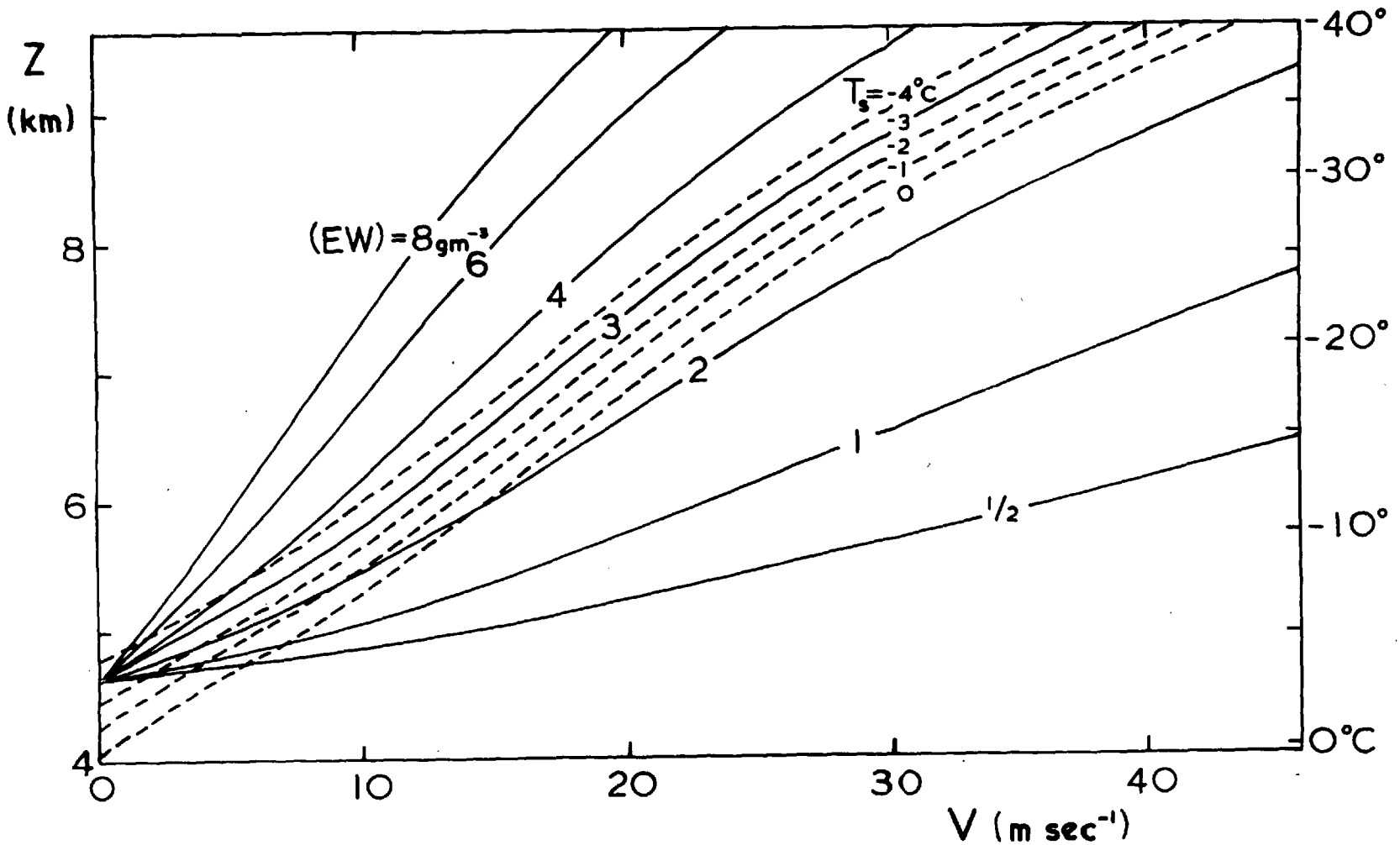

Fig. 4.1.2.
Isopleths of $T_s = -3^{\circ}C$ for various values of (EW) (solid curves) and isopleths of $T_s = -4, -2, -1$ and (just) $0^{\circ}C$ for (EW) = 3 g m^{-3} (pecked curves).

2. The structure of the Wokingham hailstones

Macklin has made thin sections of 60 hailstones which fell during the Wokingham storm of 9 July 1959. He obtained sections through their centres with an approximately uniform thickness of 0.3 mm by melting the stones between parallel metal plates. They were carefully dried in filter paper to minimise effects produced by the re-freezing of melt-water (see section 4.7) and then photographed in colour between crossed polaroids and also by using transmitted unpolarized light. The former photographs enabled the constituent crystallites of the hailstones to be distinguished, since the varying orientation of their optical axes caused the plane of polarisation to be rotated differently for each crystallite thereby rendering each in a different colour.

The crystallites occur in two size ranges. The larger ones vary in volume between 10^{-4} and 10^{-1} cm^3. Since it is later shown that these are probably associated with wet growth, it seems necessary for their size to be accounted for by assuming that each ice crystal incorporated from the airstream led to the growth of a fresh crystallite with a randomly orientated optical axis.

Also observed are regions of very small crystallites (volume $\leqslant 10^{-5}$ cm^3). These invariably occur with numerous minute bubbles, the distribution of which is best seen in the photographs obtained using transmitted unpolarised light (see, for example, Figs. 4.8.1 and 4.8.2): they give the ice a milky appearance. Bubbles are less numerous (but usually larger) and sometimes entirely absent in the regions comprising the larger crystallites, giving rise to transparent or clear ice.

The transition between large and small crystallites is discontinuous and is invariably accompanied by a pronounced change in bubble concentrations. It is unlikely that such a discontinuity could be due to a parallel change in the ice crystal concentration in the airstream, since a change of concentration of several orders of magnitude within a small fraction of a minute would often be implied. Now in wind tunnel experiments in which supercooled droplets were accreted by rotating cylinders, Macklin (1960), has shown that the milky ice (associated with copious bubbles and very small crystallites) formed when the surface temperature, T_s, was below about $-3^{\circ}C$. At higher temperatures he observed fewer but larger bubbles and, for wet growth with $T_s = 0^{\circ}C$, no bubbles at all, (the dissolved air evidently having escaped by diffusion and by the migration of bubbles to the surface). Consequently the growth transitions in hailstone are attributed to changes in T_s in the manner summarized in Table 4.2.1.

TABLE 4.2.1

The dependence of the hailstone structure upon its surface temperature

SURFACE TEMPERATURE OF HAILSTONE T_s	NATURE OF SURFACE OF GROWING HAILSTONE	CRYSTALLITE SIZE	NATURE OF BUBBLES	APPEARANCE OF DEPOSIT	T_s
$-3^{\circ}C$	DRY	VERY SMALL ($10^{-5}cm^3$)	COPIOUS MINUTE BUBBLES	MILKY	$-3^{\circ}C$
$0^{\circ}C$		LARGE ($10^{-1}cm^3$)	FEW LARGE BUBBLES	TRANSPARENT	$0^{\circ}C$
	WET*		NONE	CLEAR	

*Alternatively spongy growth could occur in the presence of high ice crystal concentrations.

The dependence of the hailstone structure upon the surface temperature may be explained in the following way. When $T_s < -3^{\circ}C$ incident droplets are nucleated by contact with its dry surface thereby forming crystallites whose optical axes are aligned with the underlying surface. However the riming surface is irregular, so that if an incident droplet hits a small projection it may be nucleated and subsequently slide a little farther under the influence of its remaining momentum with a consequent reorientation of its optical axis and the production of a distinguishable small crystallite. (The size of the very small crystallites in the Wokingham hailstones implies mean droplet radii of the order of 100 μ if each droplet produced a distinguishable crystallite — such a size is credible in view of section 5.2). The measurement of hail densities indicates that the concentration of bubbles within milky ice may be explained wholly in terms of air coming out of solution which is unable to escape owing to the rapid freezing of the accreted droplets. For hailstones growing with surface temperatures above $-3^{\circ}C$ it appears that the slower rate of freezing of the accreted droplets permits them to coalesce with the formation of bigger crystallites and bubbles.

During wet growth the bubbles are able to escape from the surface so that clear ice forms. The impossibility of surface nucleation suggests that fresh crystallites might only then be nucleated by ice crystals accreted from the airstream. It is hypothesized that

there exists a one-to-one correlation between the number of crystallites and the number of ice crystals accreted from the airstream, implying concentrations of no more than 1 per litre up to the -20°C level (section 4.8). Spongy growth, in which any unfrozen water is retained within a tenuous ice-structure (List, 1961), may occur in lieu of wet growth in the presence of sufficiently high ice crystal concentrations: consideration of this possibility is deferred to section 4.6.

3. An interpretation of the layer structure of hailstones in terms of growth within a steady updraught.

Transitions between the three modes of growth discussed in the previous section produce the familiar layer or onion-like structure, from which it is possible to identify transitions as a function of the hailstone radius. It is now shown how the growth of a stone comprising any number of such layers can be accounted for in terms of a steady updraught.

$V = V(\rho, R)$ so that

$$\frac{dV}{dz} = \left(\frac{\partial V}{\partial R}\right)_\rho \cdot \frac{dR}{dt} \cdot \frac{dt}{dz} + \left(\frac{\partial V}{\partial \rho}\right)_R \cdot \frac{d\rho}{dz} \qquad 4.3.1$$

Now $$\frac{dz}{dt} = U_z - V \qquad 4.3.2$$

where U_z is the vertical updraught velocity.

and eq. 4.1.10 gives $$\left(\frac{\partial V}{\partial R}\right)_\rho = \left(\frac{8q\bar{\delta}}{3C_D\rho}\right) \cdot \frac{1}{2V} \qquad 4.3.3$$

and $$\left(\frac{\partial V}{\partial \rho}\right)_R = -\frac{V}{2\rho} \qquad 4.3.4$$

Substituting in eq. 4.3.1 from eqs. 4.3.2, 4.3.3, 4.3.4 and 4.1.1 and rearranging gives

$$U_z - V = \frac{f(z)\,(EW)}{\frac{dV}{dz} + V\left(\frac{1}{2\rho} \cdot \frac{d\rho}{dz}\right)} \qquad 4.3.5$$

where $$f(z) = g \Big/ 3C_D\rho(z)$$

Now consider a hypothetical stone growing permanently along one

of the W/D transition lines in Fig. 4.1.1[1]. For growth to occur at the W/D transition at a particular height it must have a fall-speed V* which is fixed by the value of (EW) (Fig. 4.1.1). For growth to continue along the W/D line the vertical updraught velocity, U_z^*, must be given by

$$U_z^* - V^* = \left(\frac{dz}{dt}\right)^* = \frac{f(z)\ \ (EW)}{\frac{dv^*}{dz} - V^*\left(-\frac{1}{2\rho}\ \frac{d\rho}{dz}\right)} \qquad 4.3.6$$

$\left(-\frac{1}{2\rho}\cdot\frac{d\rho}{dz}\right) = 0.54 \pm \leqslant 7\%\ km^{-1}$ for $4 < Z < 10$ km in the Wokingham storm, and $\frac{dv^*}{dz}$ has been determined from Fig. 4.1.1 as a function of V* for various constant values of (EW), enabling the construction of Fig. 4.3.1 which shows $\left(\frac{dz^*}{dt}\right)$ as a function of V for various (EW), and for the values of C_D and $\rho(z)$ quoted in section 4.1.

From Figs. 4.1.1 and 4.3.1 has been derived Fig. 4.3.2, which illustrates the variation with height of U_z^* for hailstones of different sizes and for various (EW). It is evident from this figure that there exists for any given value (or monotonic variation with height) of (EW) a steady updraught increasing monotonically with height which will permit a stone to grow up to a certain radius with its surface temperature always just 0°C, or any other chosen value. In the event of the requisite mean updraught profile occurring within any height interval, fluctuations in either $U_z(z)$ or (EW) can cause actual growth transitions.

---

[1] A parallel treatment could be carried out for growth with $T_s = -3°C$ near the transition from transparent to milky ice.

It is instructive to consider the relative perturbations of each of these parameters required to promote a growth transition at various radii. To illustrate this, the change of surface temperature of a growing hailstone, ΔT_s, resulting from a 10% change in the above parameters is computed for (EW) = 3 gm^{-3}. The effect of varying (EW) is readily ascertained from Fig. 4.1.2: the effect of varying $U_z(z)$ is obtained with more difficulty in the following manner.

Rearranging eq. 4.3.5 gives

$$\frac{dV}{dz} = \frac{(EW)\ f(z)}{U_z - V} + V\left(-\frac{1}{2\rho}\frac{d\rho}{dz}\right) \qquad 4.3.7$$

This is valid only if all the accreted material is retained. When (EW) > $W_c(z,V)$, where the critical water content, $W_c(z,V)$, is given according to eq. 4.1.12, the stone will grow with its surface wet and, if all the unfrozen water is shed, eq. 4.3.7 becomes

$$\frac{dV}{dz} = \frac{W_c\ (z,V)\ f(z)}{U_z - V} + V\left(-\frac{1}{2\rho}\frac{d\rho}{dz}\right) \qquad 4.3.8$$

From eqs. 4.3.7 and 4.3.8 growth curves have been computed by the method of isoclinals, being shown in Figs. 4.3.3 (i,ii,iii, and iv) and 4.3.4 (i,ii,iii, and iv). Both series of growth curves are for linear updraught profiles corresponding to $U_z(z)$= ½, ¾, 1 and $^5/_4$ U_m, where U_m is given from eq. 4.4.1 and is shown in section 4.4 to represent the profile along the axis of the updraught during the intense phase of the Wokingham supercell. Only the curves in Fig. 4.3.3 will be used in the present section. They have been derived for (EW) = 3 gm^{-3}, and for each one $\frac{dT_s}{dR}$ has been determined as a function of R both along W/D line and along

the isopleth for $T_s = -3^{\circ}C$ corresponding to this effective water content. The resulting variations in $\frac{dT_s}{dR}$ are shown in Fig. 4.3.5, from which it appears that $\frac{dT_s}{dR}$ does not depend critically upon T_s. Fig. 4.3.5 enabled the determination of the change of surface temperature which results during the accretion of a 0.5 mm layer when the updraught differs by 10% from that required to maintain T_s constant at either of the two transition temperatures. This and the change resulting from a 10% change in (EW) from its critical value are plotted in Fig. 4.3.6, showing that changes in surface temperature arising from fluctuations in updraught velocity are comparatively small. It therefore follows that growth transitions, both at $0^{\circ}C$ and $-3^{\circ}C$, are most likely to result from fluctuations in the effective water content, but to enable such fluctuations to effect a transition it is ofcourse necessary for the mean updraught to be such that $\frac{dT_s}{dR} = 0$ (see Fig. 4.3.5).

The collision efficiency of the larger cloud droplets with hailstones is unlikely to depart much from unity except conceivably as the result of electrical forces, and so it is probably more profitable to look for variations in the water content to account for the growth transitions. Now the model of the airflow within the Wokingham supercell illustrated in Fig. 2.12.1 involves a steady laminar flow, so that variations in the water content are likely to be encountered by a hailstone as its trajectory crosses the streamlines of airflow within the updraught owing to variations in the mixing ratio with height within the potentially unstable layer from which the updraught is derived.

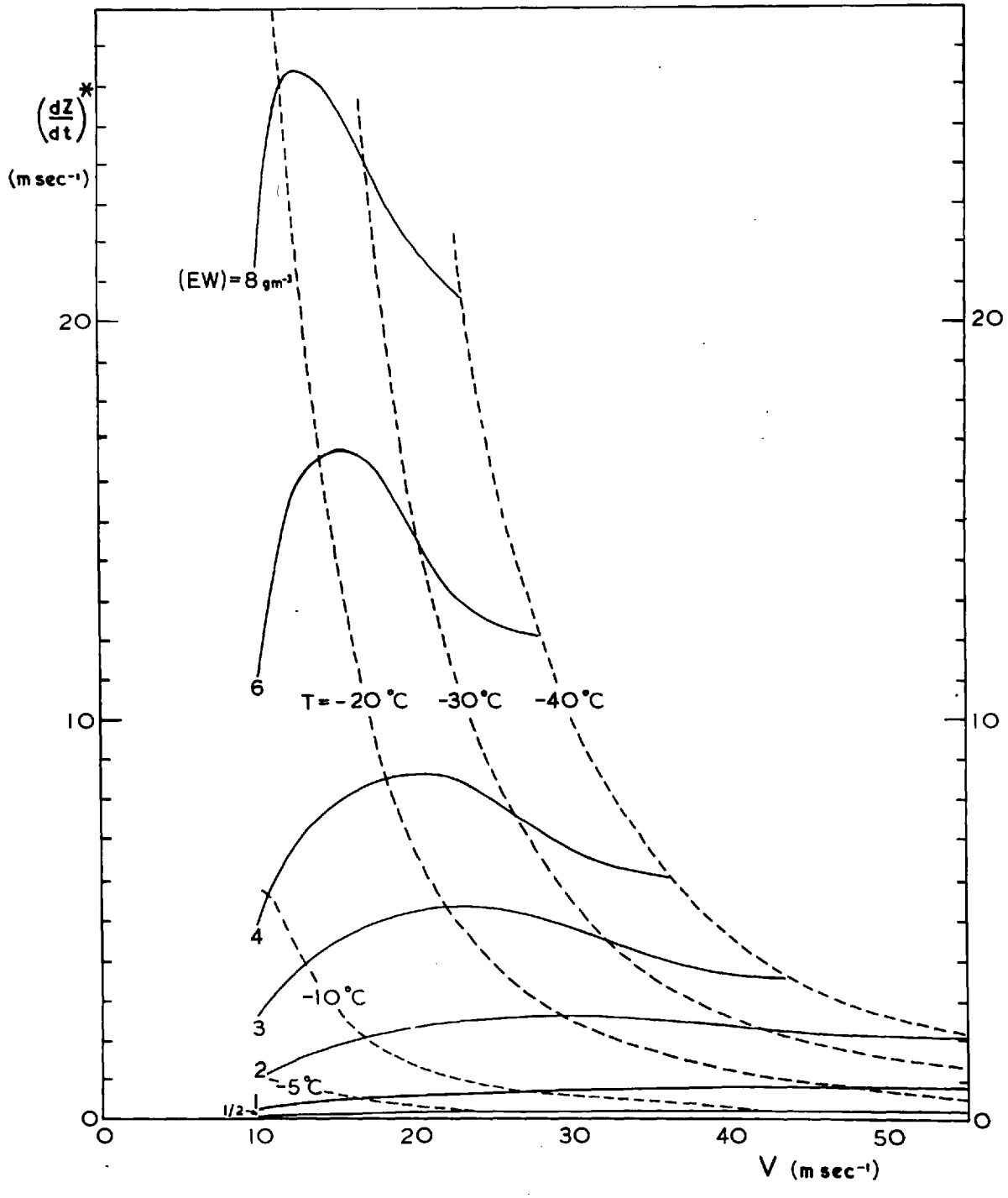

Fig. 4.3.1.
The rate of ascent $\left(\frac{dz}{dt}\right)^*$ which permits a hailstone of fall-speed V to grow along the W/D line as a function of height at various effective water contents.

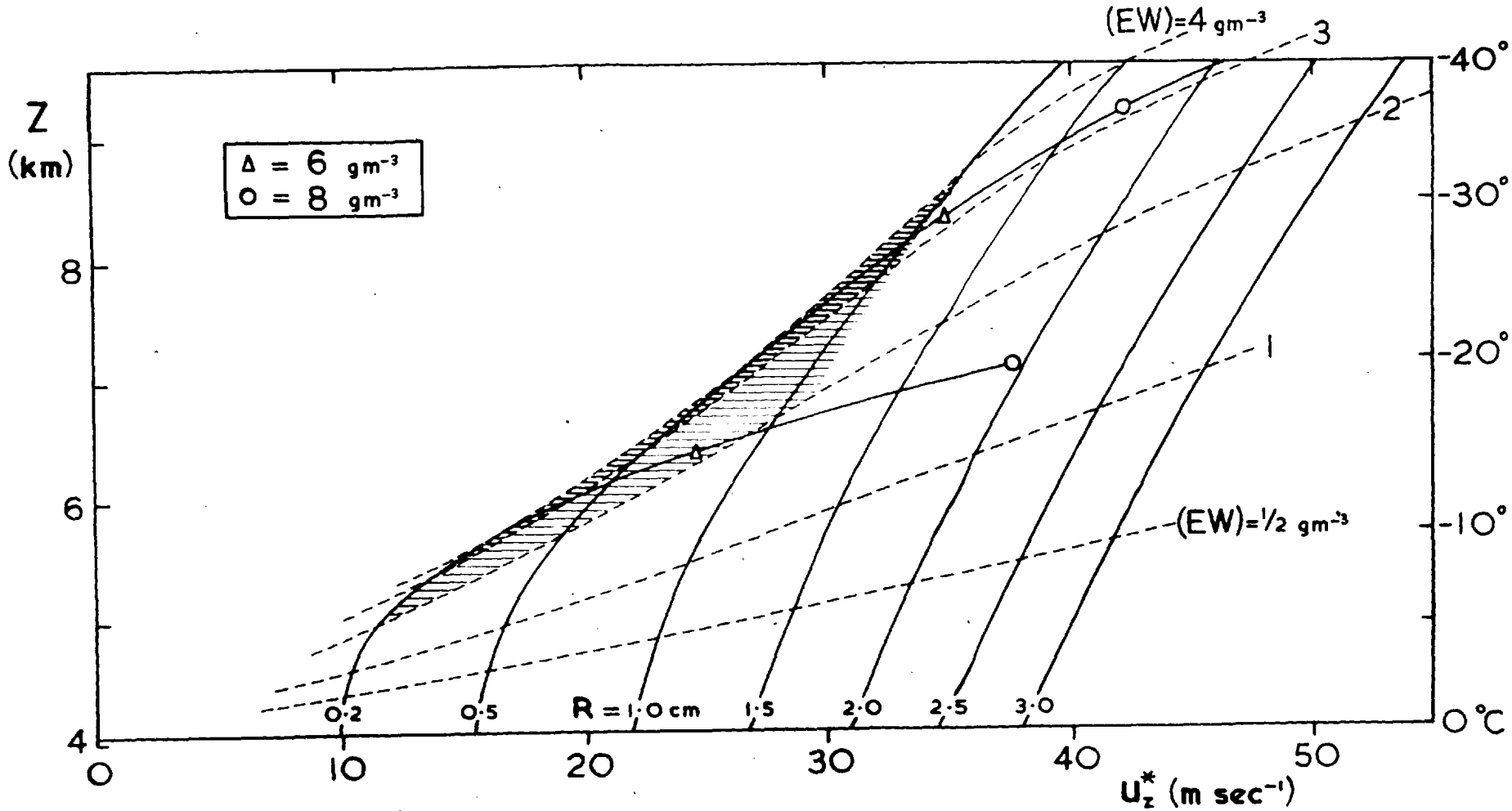

Fig. 4.3.2. The variation with height of the updraught velocity U_z^* which is required to maintain growth along the W/D line for hailstones of various radii and for different effective water contents. Isopleths of radius are shown as solid lines and isopleths of (EW) as pecked lines for (EW) = ½, 1, 2, 3 and 4 g m^{-3}. (Isopleths for 6 and 8 g m^{-3} should pass through the triangles and circles respectively, but are omitted to avoid confusion).

Fig. 4.3.3 (i-iv).
Growth curves for (EW) = 3 g m^{-3} when all the accreted material is retained: Figs. (i),(ii),(iii) and (iv) respectively are for profiles of vertical updraught velocity corresponding to $U_z(z)$ = ½, ¾, 1 and 5/4 U_m.

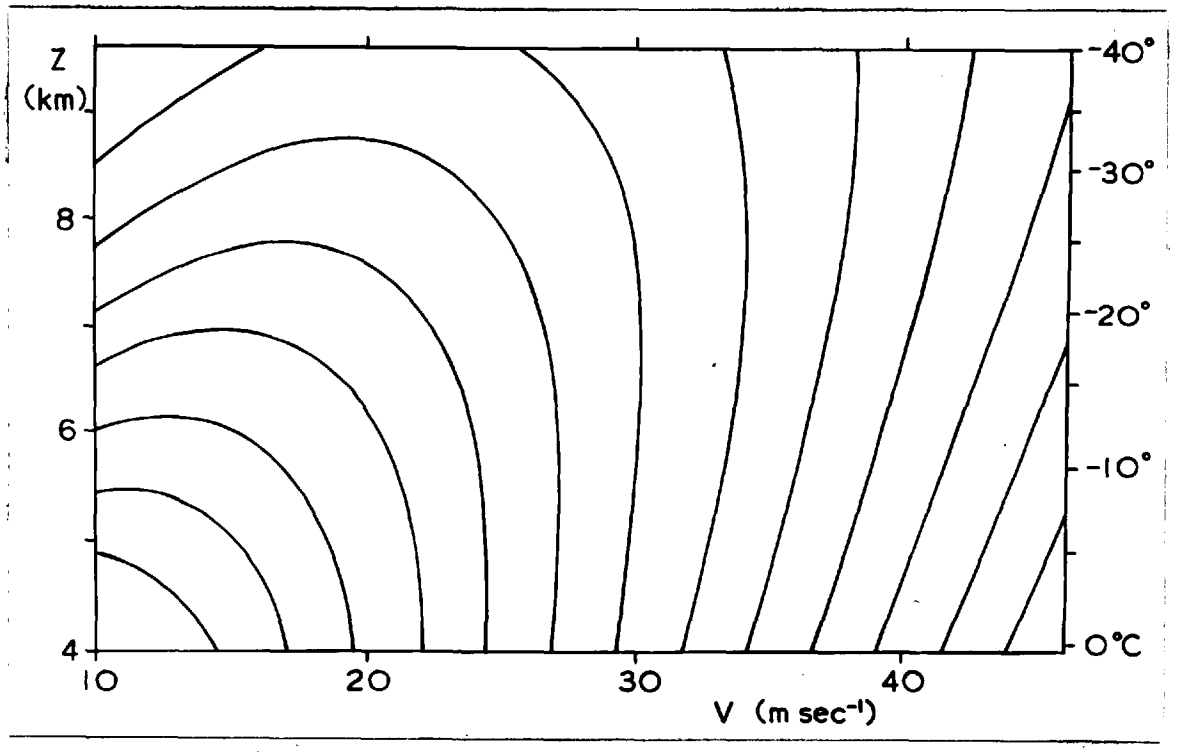

Fig. 4.3.3 (i)

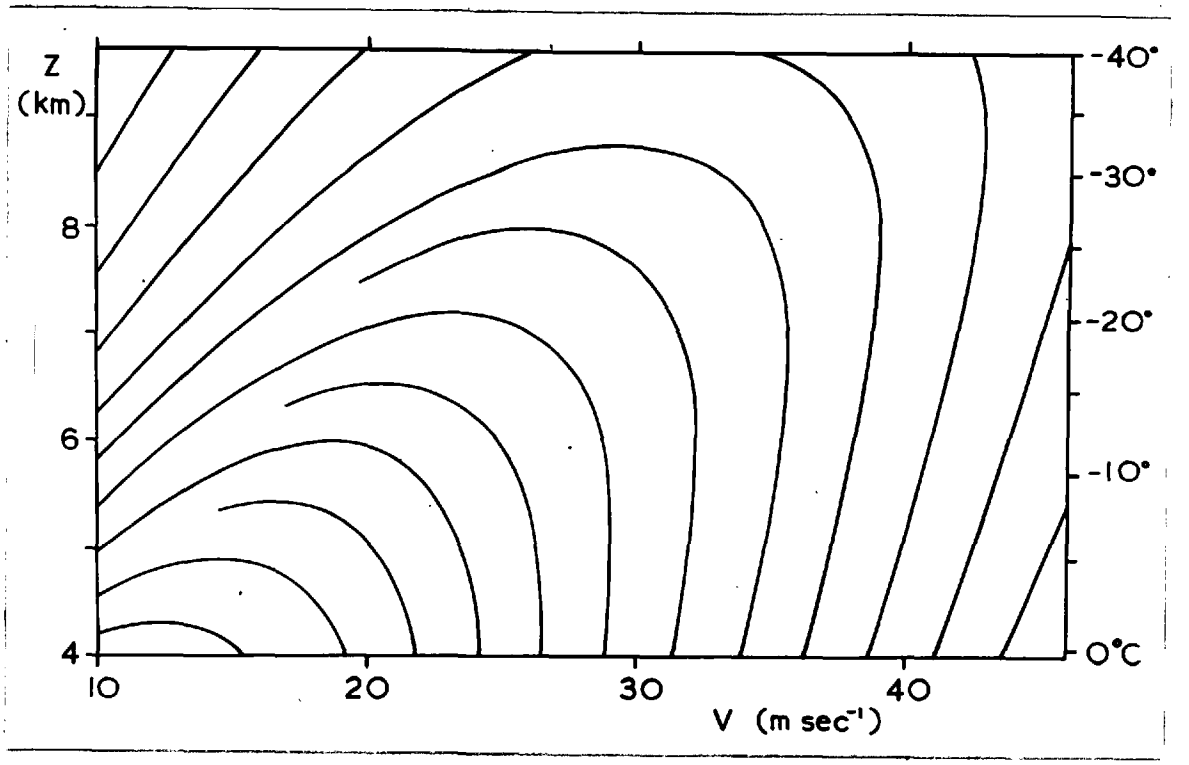

Fig 4.3.3 (ii)

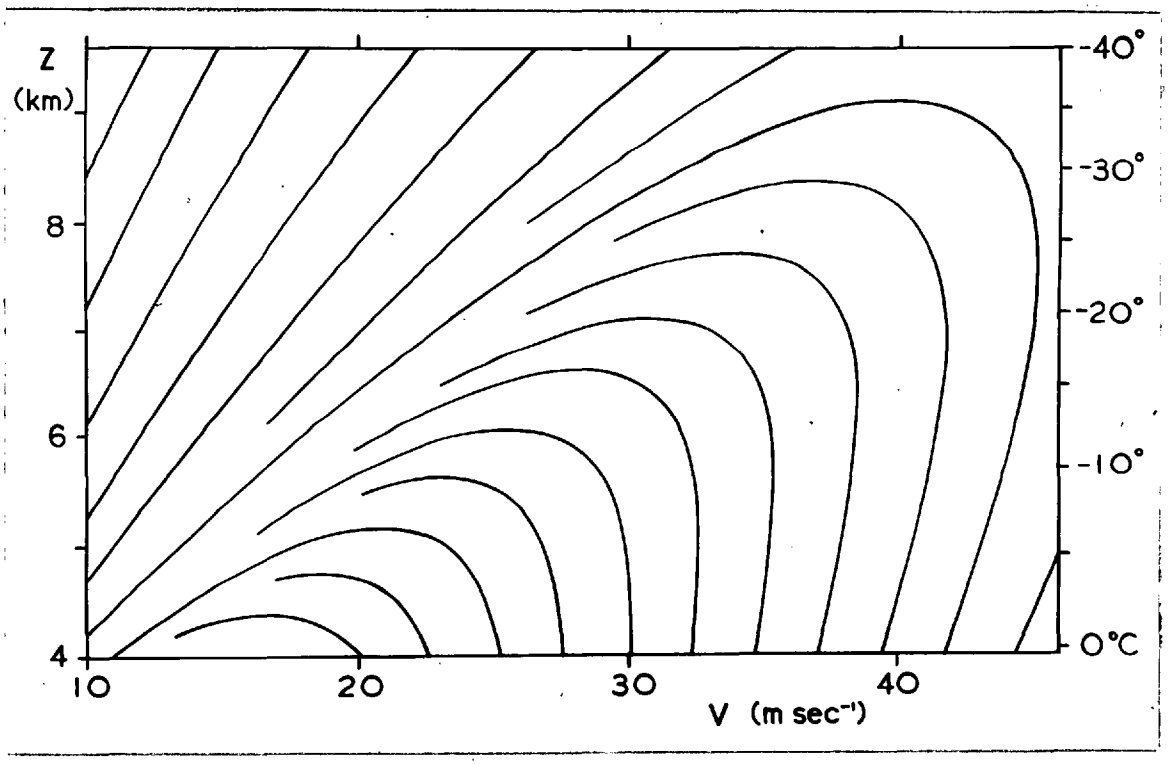

Fig. 4.3.3 (iii)

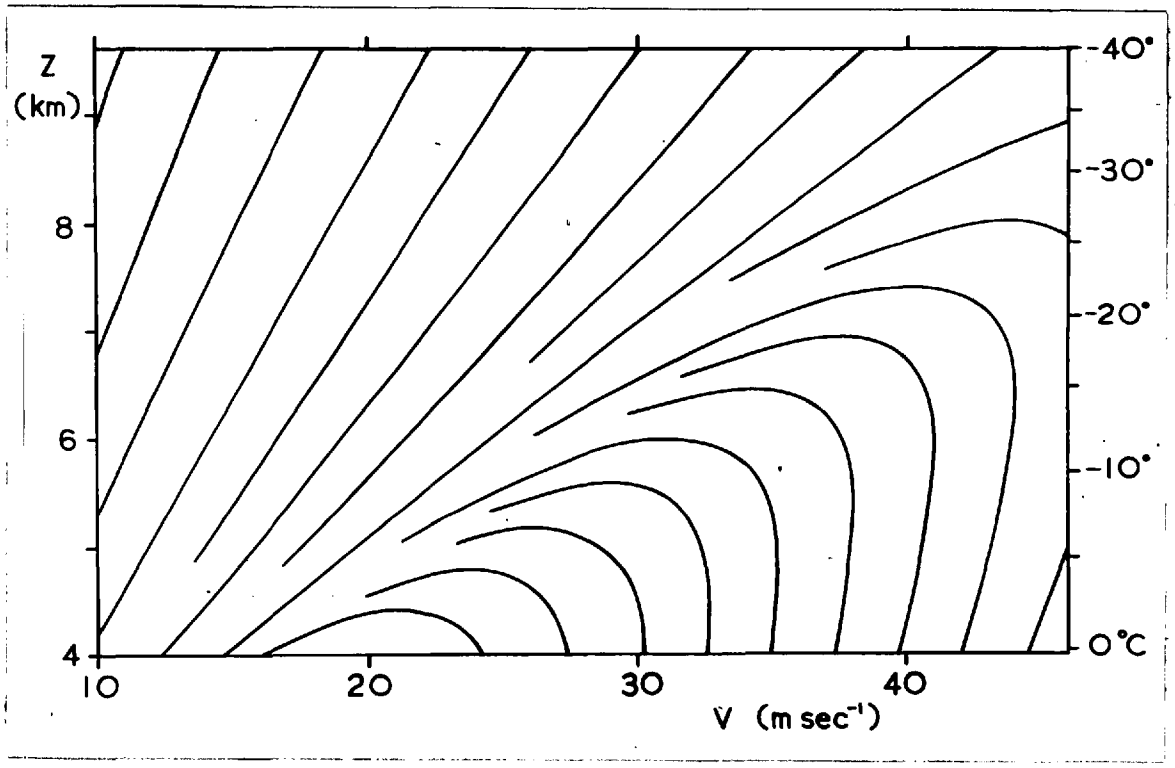

Fig. 4.3.3 (iv)

Fig. 4.3.4 (i-iv)
Growth curves based on the retention of the critical water content $W_c(z,V)$: Figs. (i),(ii),(iii) and (iv) respectively are for profiles of vertical updraught velocity corresponding to $U_z(z)$ = ½,¾,1 and 5/4 U_m. Irrespective of the actual value of (EW), these curves apply to any stone whose internal structure indicates growth along or on the wet side of the W/D line.

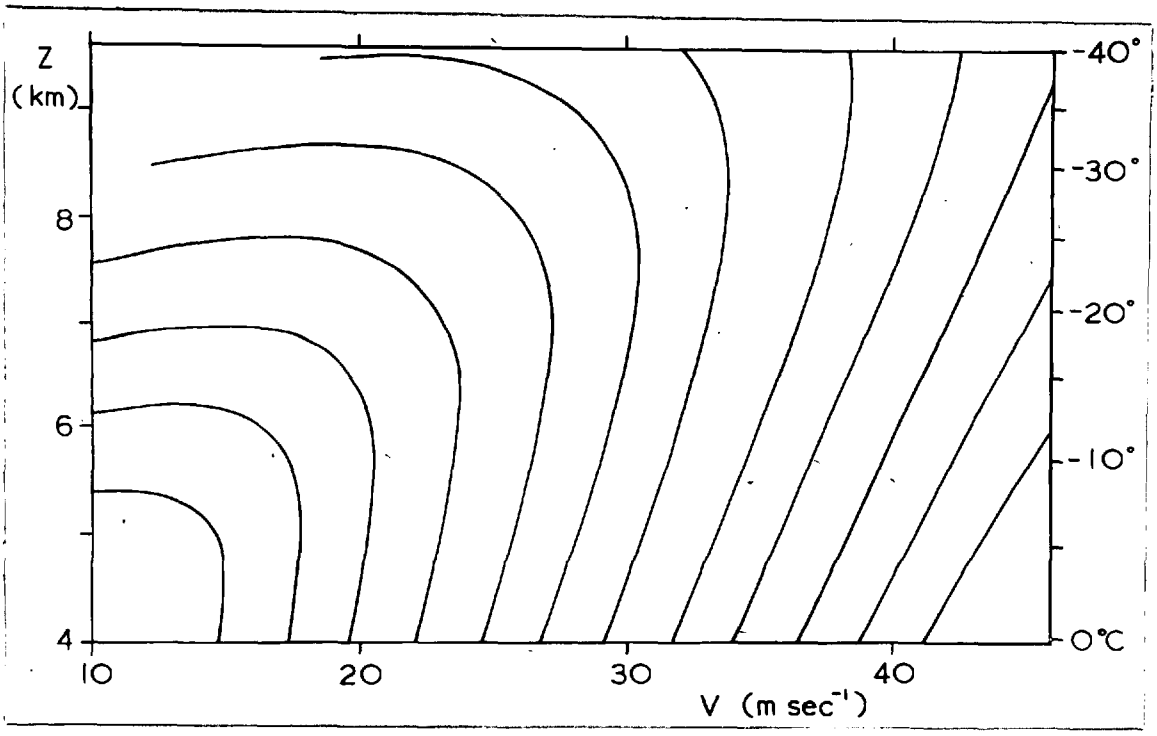

Fig. 4.3.4 (i)

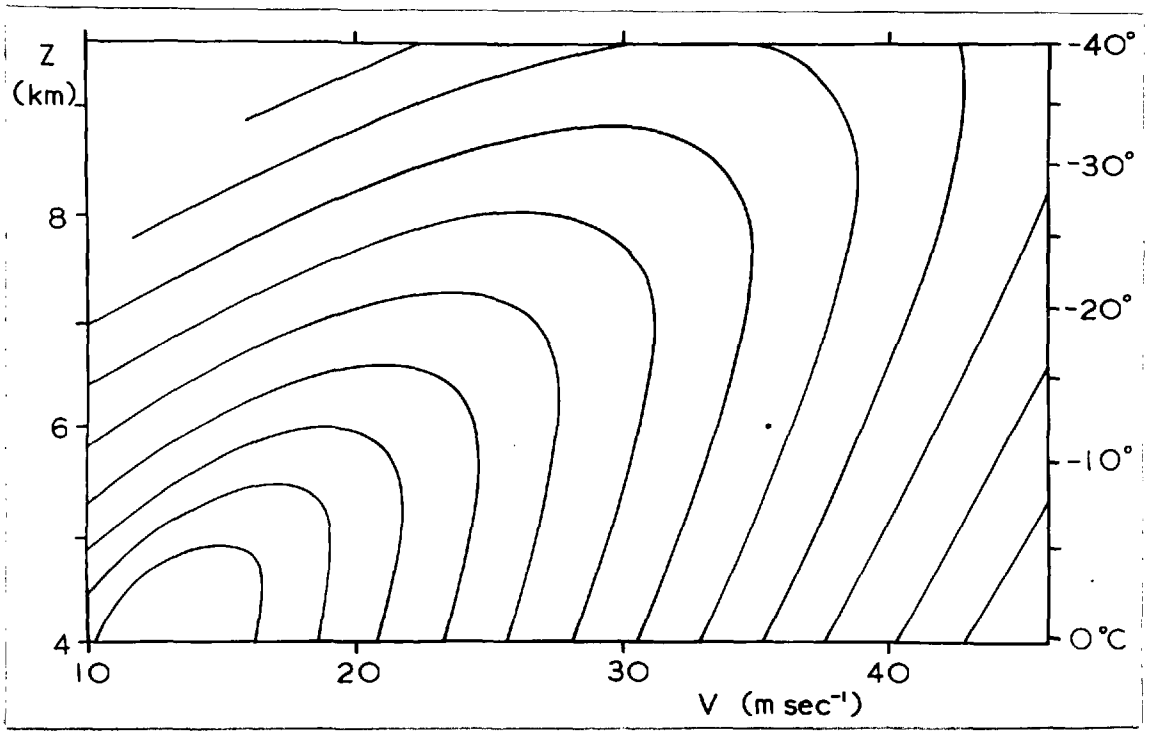

Fig. 4.3.4 (ii)

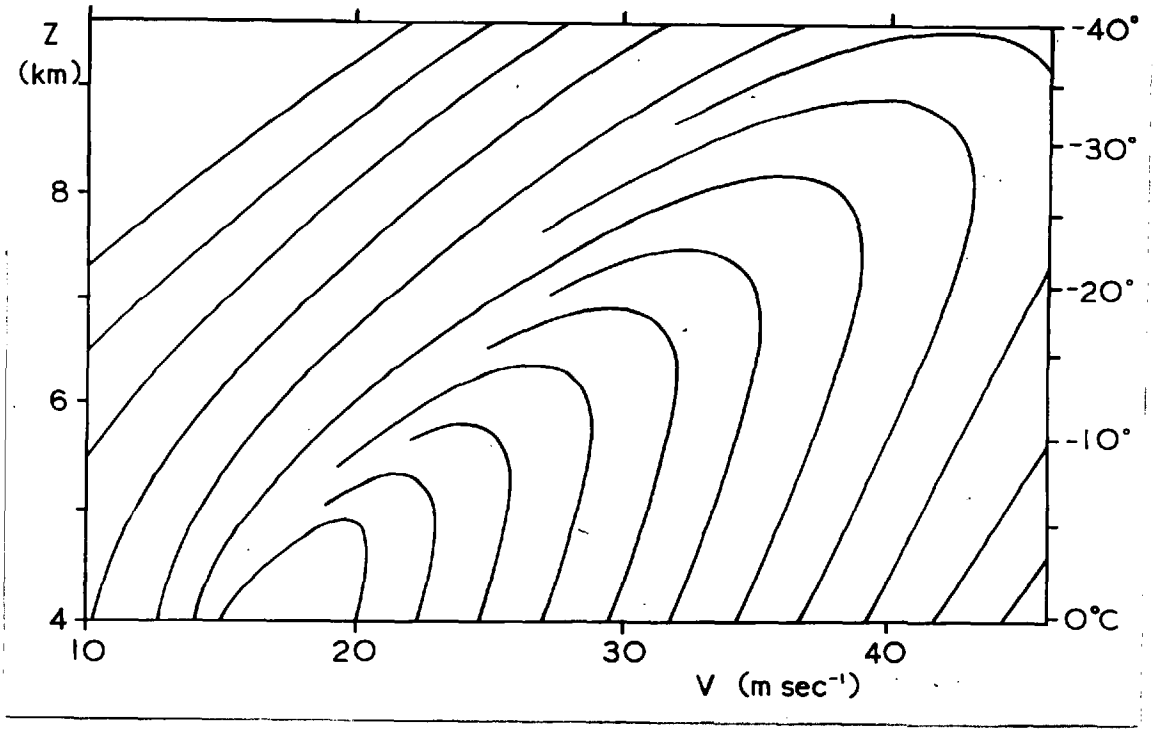

Fig. 4.3.4 (iii)

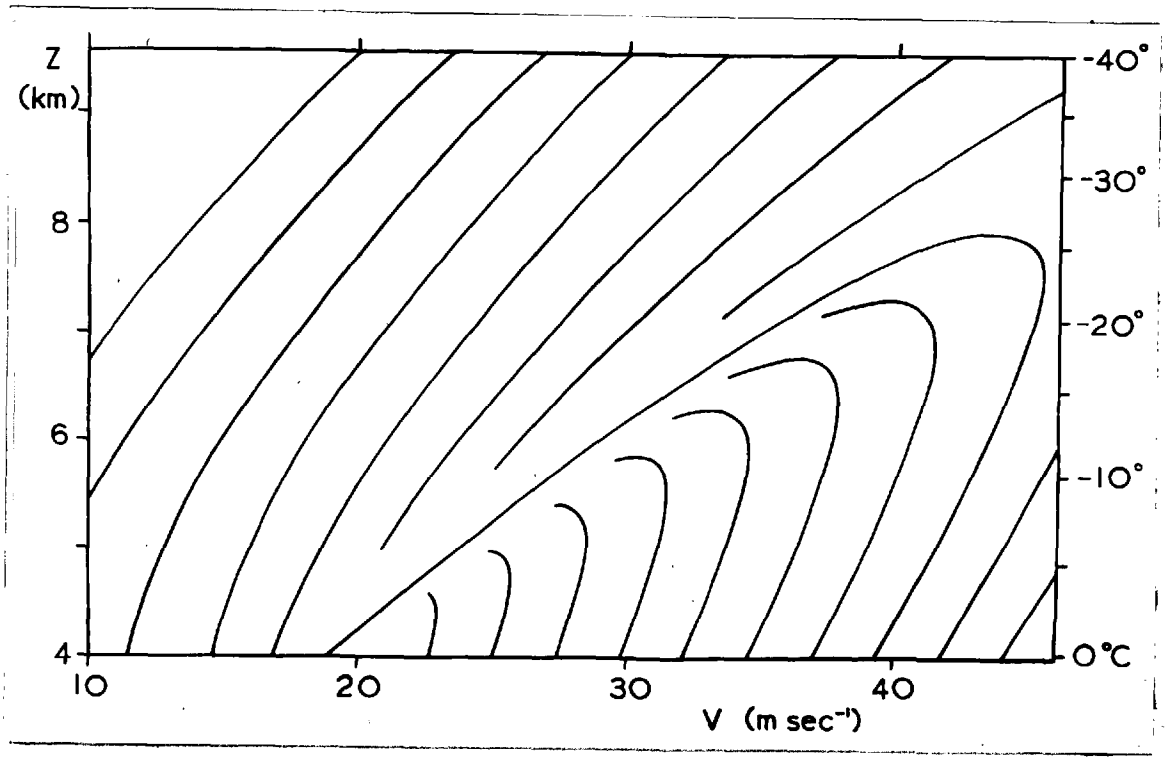

Fig. 4.3.4. (iv)

Fig. 4.3.5
The variation of dT_s/dR with R along the W/D line (solid curves) and along the $T_s = -3^{\circ}C$ isopleth (pecked curves) for hailstones growing within various updraught profiles with (EW) = 3 g m^{-3}. These curves have been computed graphically from Figs. 4.1.1, 4.1.2 and 4.3.3 with an estimated probable error in dT_s/dR of $\pm$ 0.2°C mm^{-1}.

Fig. 4.3.6
The deviation of the surface temperature from the transition values which would result from a 10% change

(1) in (EW)

and (2) in U_z, during the accretion of a 0.5 mm increment of radius.

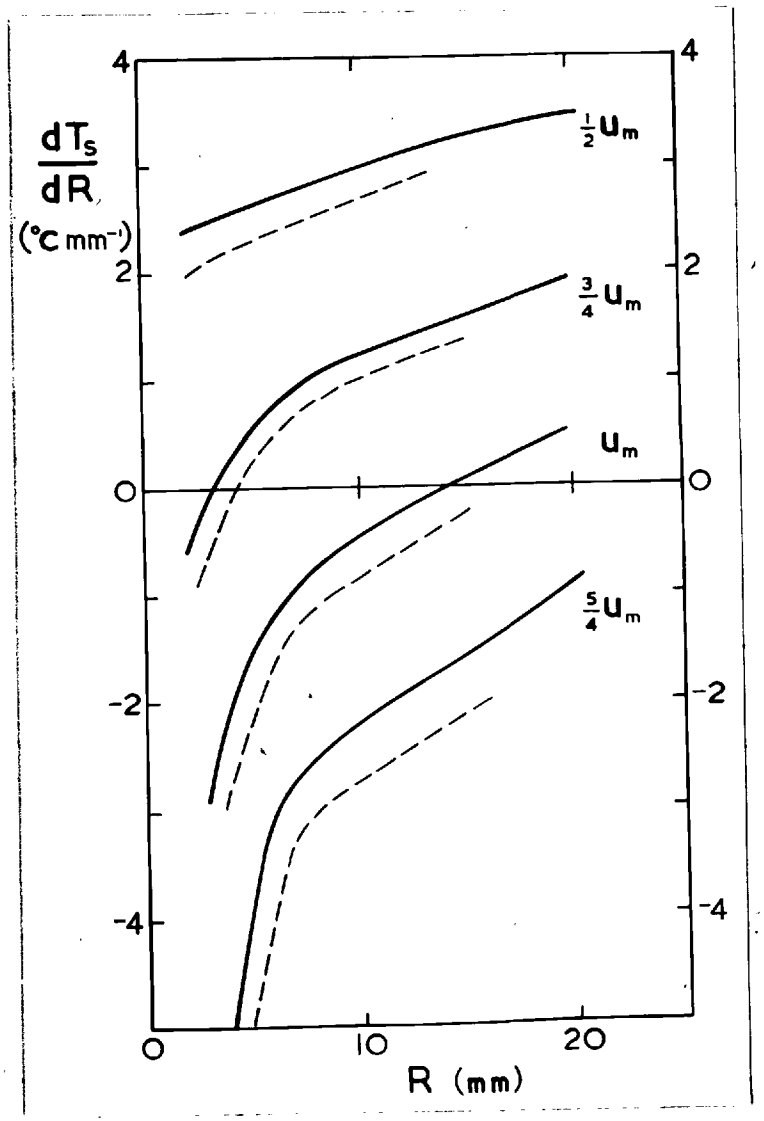

Fig. 4.3.5.

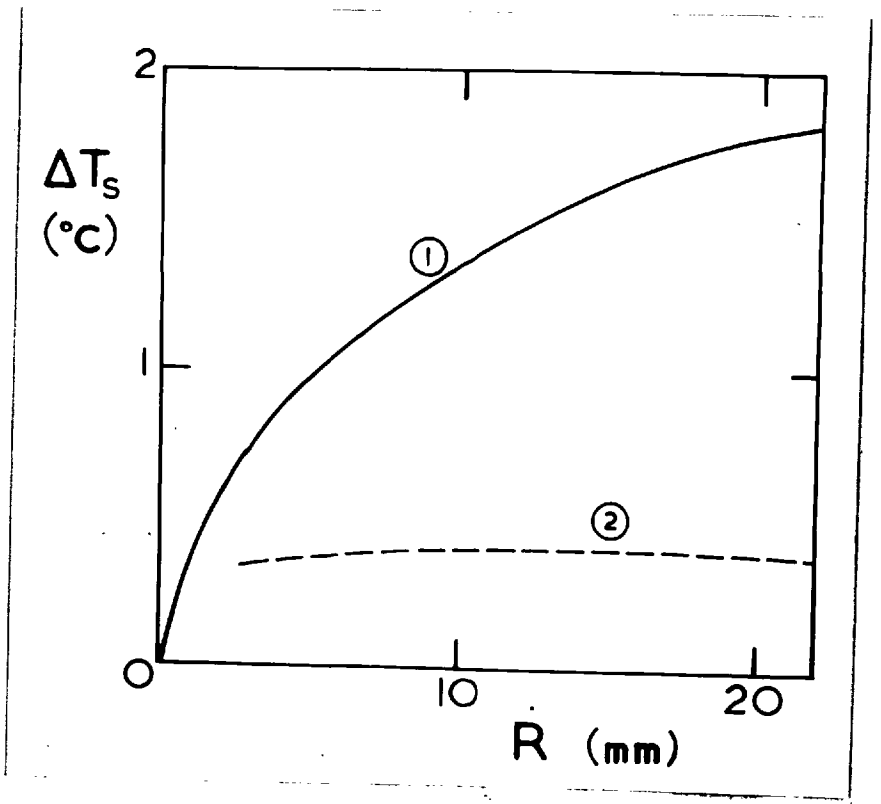

Fig. 4.3.6

4 An estimation of the profile of vertical velocity along the updraught within the Wokingham supercell

It is shown in section 4.8 that the largest hailstone collected during the Wokingham storm (hailstone α) grew persistently near the W/D line whilst $0.2 < R_3 < 1.06$ cm, where $2R_3$ is the length of the shortest axis of the stone (and is shown in section 4.5 to be the relevant dimension in this context when a stone is spheroidal rather than spherical). During this phase of growth the smoothed vertical updraught velocity experienced by the stone must have been that given by U_z^* in Fig. 4.3.2. Now the updraught profile implied by growth along the W/D line within this radius interval is seen to be insensitive to the effective water content provided $2 < (EW) < 8$ g m^{-3} resulting in a profile falling within the ~~stippled~~ hatched region of Fig. 4.3.2: the most likely profile is shown heavily ~~stippled~~ hatched, being that corresponding to $3 < (EW) < 4$ g m^{-3}. However this profile applies only to the local environment of the hailstone concerned and, for the general case of an inclined updraught, it will not be proportional to the vertical velocity profile along the axis of the updraught. This is because the component of horizontal velocity within an inclined updraught causes the hailstone trajectories to intersect the streamlines of air motion, so that, assuming that the updraught velocity decreases smoothly on either side of the updraught axis, each hailstone will grow on the axis of the updraught at only one stage in its history. Nevertheless it is possible to infer the profile along the axis in the following manner.

Since stone α was the largest stone collected it is likely that

its trajectory would have crossed or approached the axis of the updraught at some high level so as to take advantage of the region of greatest vertical updraught velocity within the growth region (below the -40°C level). Because of the backward tilt of the updraught in the Wokingham supercell, it would have been growing forward of the axis at lower levels, so it follows from Fig. 4.3.2 that a reasonable axis-profile is given by

$$U_m = 5(z-1) \qquad 4.4.1$$

where U_m is in m sec^{-1} and z is in km.

However the choice of this profile was also influenced by other considerations, which will now be mentioned. First, the persistence of the forward overhang can only be explained in terms of a vertical velocity which already exceeded 10 m sec^{-1} in the vicinity of its lowest point (at 4 km). Second, the profile must be such that, together with the condition of continuity of mass-flux and with the restriction upon the width of the updraught set by the positions of the maximum radar intensity (X) and the wall (see Fig. 2.12.1), it is possible to construct reasonable streamlines of air-flow which accord with section 4.9 and which permit trajectories of the largest observed hailstones, coming from the position X, to terminate at the wall.

5 The growth of oblate spheroidal hailstones

In sections 4.1, and 4.3 only the growth of spherical hailstones has been considered. However, few real stones have axes equal to within 10%. Some have a degree of eccentricity (both in their final shape and, judging by the shape of the growth transitions, at earlier stages in their growth) which demonstrates that they had grown notably eccentrically: indeed the ratio of the longest to the shortest axes sometimes exceeds 2.

In the Wokingham storm — and probably in most storms in which the hailstones fail to attain "giant" dimensions (see Table 1.2.2) — the shape of the majority of stones approximated to that of oblate spheroids, so that before proceding with the detailed analysis of the growth of individual stones it is necessary to investigate the applicability of the growth curves in such circumstances.

Under conditions of dry growth the accreted material freezes rapidly and may not be moulded by the airstream, so that a spherical stone (free to turn about any axis) will accrete evenly over its entire surface so as to remain substantially spherical. Once its surface beoomes wet, and especially if it accretes sufficient ice crystals to permit the retention of much of the deposit as a spongy growth, the newly accreted material may be moulded by the airstream. Thus because of the nature of the airflow in the wake of the hailstone comparatively little material collects on the downstream side, so that eccentricity develops. Once a stone has acquired significant eccentricity its preferred attitude of fall will prevent a reversion to a

spherical shape.

Since freely falling objects fall so as to maximize their form drag, ellipsoids fall with their shortest axis (length, $2R_3$) normal to the airflow. In the Wokingham hailstones the other two axes (lengths $2R_1$ and $2R_2$) differed by less than 10%, so that they are treated as oblate spheroids with major axes given by $2R = R_1 + R_2$. Their growth is now considered under the assumption that it obeys one of two laws;

(1) $R/R_3 = X$, where X = constant,

(2) R_3 = constant.

The latter is used only to describe the transition from a spherical to a spheroidal shape.

(1) Growth with $R/R_3 = X$

The mass of an oblate spheroidal hailstone is given by

$$M = \frac{4}{3}\pi R^2 R_3 \bar{\delta} = \frac{4}{3}\pi X^2 R_3^3 \bar{\delta}$$

Therefore $$\frac{dM}{dt} = 4\pi X^2 R_3^2 \frac{dR_3}{dt}\bar{\delta} = 4\pi R^2 \frac{dR_3}{dt}\bar{\delta} \qquad 4.5.1$$

The surface area normal to the airflow, $A = \pi R^2$, so that for growth at the dry growth rate

$$\frac{dM}{dt} = (EW)V(z)\pi R^2 \qquad 4.5.2$$

Eqs. 4.5.1 and 4.5.2 give

$$\frac{dR_3}{dt} = \frac{(EW)V(z)}{4\bar{\delta}} \qquad 4.5.3$$

Now the drag experienced by a spheroidal hailstone is given by

$$C_D' \, (\tfrac{1}{2}\rho V^2) A = Mg \qquad 4.5.4$$

where C_D' is the drag coefficient for a spheroidal hailstone, so that

$$V^2 = \left(\frac{8g\bar{s}}{3C_D'\rho}\right) R_3 \qquad 4.5.5$$

But $\left(\frac{\partial V}{\partial t}\right)_z = \frac{dR_3}{dt}\left(\frac{\partial V}{\partial R_3}\right)_z$, so that eq. 4.5.3 and eq. 4.5.5 give

$$\left(\frac{\partial V}{\partial t}\right)_z = \frac{(EW)g}{3C_D'\rho} \qquad 4.5.6$$

Thus, if primed terms are used to distinguish spheroidal growth from spherical growth

$$\left(\frac{\partial V}{\partial t}\right)_z' = \left(\frac{C_D}{C_D'}\right)\left(\frac{\partial V}{\partial t}\right)_z \qquad 4.5.7$$

Moreover eq. 4.3.4 shows that $\left(\frac{\partial V}{\partial z}\right)_t = V\left(-\frac{1}{2\rho}\frac{d\rho}{dz}\right)$, and $\left(-\frac{1}{2\rho}\frac{d\rho}{dz}\right)$ is a function of the environment only, so that for a stone of a given fall-speed at a height, Z,

$$\left(\frac{\partial V}{\partial z}\right)_t' = \left(\frac{\partial V}{\partial z}\right)_t \qquad 4.5.8$$

Substituting in eq. 4.3.67 then gives

$$\left(\frac{dV}{dz}\right)' = \left(\frac{C_D}{C_D'}\right)\left(\frac{\partial V}{\partial t}\right)_z \Big/ (u_z - V) + \left(\frac{\partial V}{\partial z}\right)_t \qquad 4.5.9$$

Now the growth curves in Figs. 4.3.3 and 4.3.4 have been derived for spherical stones upon the assumption that $C_D = 0.6$, whereas Macklin and Ludlam (1961) find that $C_D' \approx 0.7$ for distinctly spheroidal hailstones. Nevertheless $\left(\frac{dV}{dz}\right)'$ is not seriously overestimated if it is

assumed that $\left(\frac{dV}{dz}\right)' \approx \left(\frac{dV}{dz}\right)$, and so the dry-growth curves in Fig. 4.3.3 will be used for spheroidal hailstones. However the isopleths of R and $\frac{dt}{dR}$ shown in Fig. 4.1.1 must be reinterpreted. Comparison of eq. 4.1.10 with eq. 4.5.5 shows that isopleths of R must be reinterpreted as isopleths of $\left(\frac{6}{7} R_3\right)$, and comparison of eq. 4.1.1 with eq. 4.5.3 shows that isopleths of $\frac{dt}{dR}$ must be reinterpreted as isopleths of $\frac{dt}{dR_3}$.

The above applies equally to the wet-growth solutions provided that $W_c'(z,V) = W_c(z,V)$. The approximate validity of this identity will now be established.

When a hailstone grows distinctly oblately it does not grow very rapidly on its downstream side. Consequently it is assumed that the effective surface area from which heat may be lost to the environment depends on the equivalent radius R_e, where $R_e \equiv \sqrt[3]{R_1 R_2 R_3}$. (This assumption is exactly valid in the limit for a spherical hailstone which, being free to turn about any axis, permits growth to proceed evenly over the entire surface. As X increases however, $(4\pi R_e^2)$ becomes increasingly less than the actual surface area of a spheroid, thereby taking some account of the non-uniform accretion). Using the same notation as in section 4.1 the rate of flow of heat to the environment from an oblate hailstone is therefore given by

$$\frac{dQ'}{dt} = 4\pi R_e a' \left[D L_v \Delta\rho_v + K(T_s - T) \right] \qquad 4.5.10$$

where

$$a' = 0.3 (Re)'^{1/2} \qquad 4.5.11.$$

and (Re)' depends on the characteristic dimension perpendicular to the airflow (i.e. 2R). so that

$$(Re)' = \frac{2RV\rho}{\eta} \qquad 4.5.12$$

The rate of liberation of latent heat of fusion at the surface of the hailstone is given by

$$\frac{dQ_L'}{dt} = \frac{dM}{dt}(L_f + T - T_s) = \pi R^2 V (EW)(L_f + T - T_s). \qquad 4.5.13.$$

At equilibrium and when all the accreted water is just frozen,

$$\frac{dQ'}{dt} = \frac{dQ_L'}{dt}, \quad T_s = 0^\circ C, \quad \text{and} \quad (EW) = W_c'(z,V).$$

Equating eq. 4.5.10 and eq. 4.5.13 therefore gives

$$W_c'(z,V) = \frac{a' R_e}{R^2 V} f'(z) \qquad 4.5.14$$

where $$f'(z) = 4\left[DL_v \Delta\rho_v - KT\right]/(L_f + T)$$

Substituting for a' from eq. 4.5.11 and eq. 4.5.12 and for V from eq. 4.5.5 gives

$$W_c'(z,V) = (R_3^{\frac{1}{12}}/R^{\frac{5}{6}})\, F'(z) \qquad 4.5.15$$

where $$F'(z) = 0.3\left(\frac{3\rho^3 C_D'}{2\eta^2 q \bar{\delta}}\right) f'(z)$$

In the limit for a sphere, $R \to R_3$, and $W_c' \to W_c$, so that

$$F'(z) = R^{\frac{3}{4}} W_c(z,V) \qquad 4.5.16$$

Therefore eq. 4.5.15 and 4.5.16 give

$$W_c'(z,V) = X^{-\frac{1}{12}} W_c(z,V) \qquad 4.5.17$$

Now X seldom exceeds 2, so that $\frac{W_c - W_c'}{W_c} < 6\%$ and $W_c'(z,V) \approx W_c(z,V)$ to a good approximation. (Q.E.D.).

In the above it has been assumed that the rate of loss of heat to the environment depends on R_e. However this might yield a slight underestimate at large X when little accretion occurs on either the top or bottom surfaces. Consider therefore the limiting case when all the freshly accreted material is deposited on the sides of a cylindrical hailstone of circular cross-section. In this case the effective surface area from which heat is lost is ($2\pi R . 2R_e$), so that the heat loss, $\frac{dQ'}{dt}$, is proportional to $\sqrt{RR_e}$ which gives

$$W_c'(z,V) = X^{\frac{1}{12}} W_c(z,V) \qquad 4.5.18$$

This corresponds to a 6% fractional difference in the opposite sense when $X = 2$, so that again $W_c'(z,V) \approx W_c(z,V)$ to a good approximation.

(2) Growth with R_3 = constant, R_x.

It sometimes happens that a hailstone section, the periphery of which is markedly elliptical, possesses a circular growth transition at some smaller radius, R_x say, indicating that the stone at this earlier stage in its growth was probably spherical, and that only subsequently did it become spheroidal. In order to determine the growth time of such a stone its growth will be considered in three phases:

(i) $R \leq R_x$ ——— spherical growth

(ii) $R_x < R \leq XR_x$ ——— spheroidal growth with R_3 = constant, R_x.

(iii) $R > XR_x$ ——— spheroidal growth with R/R_3 = constant, X,

where X is determined by the value of R/R_3 at the outside of the stone. Phase (iii) may be considered using the spherical growth curves in the manner already discussed: phase (ii) must be considered separately in a manner which will now be described.

The mass of an oblate spheroidal hailstone is given by $M = \frac{4}{3}\pi R_3 R^2 \bar{\delta}$

But $R_3 = R_x$(constant), so that

$$\frac{dM}{dt} = \frac{8}{3}\pi R_x R \frac{dR}{dt}\bar{\delta} \qquad 4.5.19$$

Equating eq. 4.5.19 with eq. 4.5.2 (dry growth rate) gives

$$\frac{dR}{dt} = \left[\frac{3(EW)V(z)}{8\bar{\delta}R_x}\right]R \qquad 4.5.20$$

Normally this phase of growth lasts for less than a minute, during which period z varies little. Consequently V may be taken as remaining constant, so that eq. 4.5.20 gives for the total time taken for this phase

$$t = \frac{8\bar{\delta}R_x \log_e X}{3(EW)V} \qquad 4.5.21$$

6. Spongy hailstone growth

The wet growth curves illustrated in Fig. 4.3.4 refer to situations in which the effective water content, (EW), exceeds the critical water content, W_c, so that the heat economy of the growing hailstone prevents the freezing of all the accreted water: they further involve the assumption that all the unfrozen water is shed, so that a severe restriction is placed on the growth rates of large stones, especially at low levels. However in wind tunnel experiments on the growth of artificial hail, List (1961) has found that over a wide range of conditions no water is shed and that a spongy (or mushy) ice-water mixture is formed. By centrifuging hailstones comprising such a layer he has found ice/water ratios of less than 0.1 in which the water was retained within a tenuous ice structure.

Hallet (1960) considers that if an ice crystal alights with arbitrary orientation on a water surface which is supercooled, crystal growth in the form of branching dendrites occurs both along the surface and into the water. In the case of a hailstone growing with its surface wet crystallization at the surface might be favoured, since there the temperature will be lowest. When the number of nucleating centres in the form of accreted ice particles is sufficiently large, an intervowen mesh of dendritic ice might therefore form within the water film to produce the kind of spongy deposit which List observed. Macklin (1960) lends credance to this interpretation by emphasizing the difficulty in avoiding the production of ice crystals owing to incidental splintering from rimed auxiliary equip-

ment within a wind tunnel.

It therefore appears that spongy growth might occur under conditions of natural growth, and that it is most likely upon large stones which can grow wet at high levels where the ice crystal concentration is highest. However, it was demonstrated in section 2.11(2) that hailstones within the updraught behaved predominantly dry at 10cm wavelength and this is unlikely to be compatible with the existence of large numbers of hailstones possessing thick spongy layers. Nevertheless spongy growth might still have played a minor role, so that it would need to have been taken into consideration in the analysis of the Wokingham hailstones in section 4.7 were it not for the fact that its importance can be discounted (in this particular storm) in the following way.

For the purpose of the present discussion it is useful to classify the Wokingham hailstones into two broad groups. One group comprises stones which, because of their layer structure, evidently grew either predominantly dry or fluctuated between the wet and dry conditions. These latter may have grown spongily for quite short periods, but in the absence of large short-period fluctuations (EW) can never have significantly exceeded W_c, so that the dry growth rate accompanying spongy growth will never have greatly exceeded the wet growth rate. The second group comprises stones which, judging by the predominantly clear ice and large crystallites, grew with T_s at $0^{\circ}C$: some of these may well have grown with (EW) much greater than W_c and it is for these that spongy growth might have been of considerable

importance. Now no observers reported seeing any spongy hailstones at the ground during the Wokingham storm: indeed most spoke vividly of hailstones bouncing 2 or 3 m in the air after hitting the ground. Consequently if spongy growth played any part in their growth the spongy layer must have been consolidated at least near the surface as a result of the stone leaving the growing region for a significant period whilst above the 0°C level. This it can do either by ascending above the -40°C level or by falling out of the updraught well above the 0°C level. The former occurrence is unlikely since there is commonly no evidence of the dry growth which would have occurred in the presence of a reasonable effective water concentration at high levels before the stone reached the -40°C level. In the event of the latter occurrence the stones could only have fallen out of the lower edge of the inclined updraught (see Fig. 2.12.1): in order to consolidate a sufficiently thick shell for it to melt only incompletely during the 4 km fall below the melting level the stone would need to have left the updraught more than 4 km above this level. Fig. 2.12.1 shows that this condition can only marginally be satisfied, so that if some stones did grow a spongy layer they would probably have disintegrated before or upon reaching the ground.

The question then arises as to whether all the ice formed during a phase of spongy growth would have been in the form of a dendrite lattice (and therefore subsequently lost) or whether the radius of the totally frozen core, R_f, beneath the layer of spongy ice would

have continued to increase. Clearly the former possibility must be ruled out if a substantial layer of clear ice is to be accounted for but the question still remains as to what value is to be taken for $\frac{dR_f}{dt}$ during the period of spongy growth. An upper limit to this growth rate is obtained by assuming that the ice/water ratio in the spongy layer is small so that the rate of freezing of the core is governed largely by the rate at which its own latent heat can be liberated from the outer surface. Thus the only effect of the spongy layer would be to reduce the efficiency of heat loss to the air-stream by ~~increasing the outside radius (see eq. 4.1.2)~~ the addition of a layer through which heat could only be transferred by conduction, thereby retarding the growth rate of the totally frozen core. Consequently any spongy growth that might have occurred would have increased rather than decreased the minimum possible growth times deduced for the Wokingham hailstones.

7. Recrystallization within the hailstone sections

A striking feature of the (coloured) photographs of each large stone taken using transmitted polarized light is the occurrence of very large elongated crystals whose optical axes are orientated in the plane of the section so that they appear practically black. Because of the great disparity of size between these and the neighbouring crystallites and because they are totally unaffected by intervening transitions of growth regime, which gave changes in bubble concentrations at small radii in stones α and α' for instance (see Figs. 4.8.1 and 4.8.2), these crystals are regarded as having arisen as a result of recrystallization. This might easily have occurred subsequent to melting incurred during the sectioning procedure. In stones α and α' the large crystals terminate at transitions to extensive regions of very small crystallites, whereas in stone β (Fig. 4.8.3), which contains no very small crystallites, the large crystal extends across the whole width of the section. It is therefore suggested that the presence of very small crystallites renders recrystallization less likely since these are associated with high concentrations of minute air bubbles which lower the thermal conductivity and decrease the probability of melting.

The occurrence of recrystallization has the effect of partially obscuring transitions in crystallite size, so that where this occurs the bubble structure (which does not appear to be changed significantly by the recrystallization) must be utilized alone when ascertaining the positions of growth transitions.

8 Growth-times of Wokingham hailstones

In this section the internal structure of 3 of the largest hailstones collected during the Wokingham storm is analysed to determine their height and growth rate throughout their growth and also the magnitude of the local updraught. Since the horizontal extent of the updraught has been estimated from the radar records, it is therefore possible to deduce an upper limit to the mean horizontal velocity with which these stones could have traversed the core of the updraught.

Two of the stones (α and α') grew persistently near the growth transitions: the third β grew predominantly with its surface wet.

(1) Analysis of stones α and α'.

These two stones fell together (at National Grid Ref. 754 608): each weighed about 16 g with R = 1.8 cm, and it is evident from their internal structure that they possessed rather similar growth histories. Sections of each were obtained in the plane of their longest axes and photographs of these are reproduced in Figs. 4.8.1 and 4.8.2. Neither was unduly eccentric: the axis/diameter ratio of stone α, $X(\alpha)$, was 1.22, and that of α', $X(\alpha')$, was 1.38. It is conceivable that these stones grew practically spherically throughout developing eccentricity merely by melting at the ground. However, in order to determine minimum possible growth times they are analysed under the limiting assumption that negligible melting was incurred after reaching the ground.

From the numerous growth transitions in Fig. 4.8.2 it is clear

that stone α' grew persistently near the growth transitions whilst $0.22 < R < 0.62$ cm, or, since $X(\alpha') = 1.38$, whilst $0.15 < R_3 < 0.45$ cm. For $0.45 < R_3 < 0.93$ cm it grew with $T_s < -3^{\circ}C$, but Fig. 4.3.5 indicates that even a 20% decrease in updraught velocity when the stone was at an intermediate radius could only have accounted for a $3^{\circ}C$ departure at this radius. Consequently to a good approximation it may be assumed that growth occurred along the W/D line* whilst $0.15 < R_3 < 0.93$ cm. Similarly stone α may be considered as growing along the W/D line whilst $0.2 < R_3 < 1.06$ cm.

The position in the z-V plane of the W/D line depends on the value of the effective water content, (EW), but a comparison of Fig. 4.1.1 with the growth curves in Fig. 4.3.4 shows that, for any water content such that $(EW) > 3$ g m^{-3}, a stone may grow along the relevant W/D line only provided that $U_z(z) > \frac{3}{4} U_m$ for $R > 0.3$ cm. This is shown clearly in Fig. 4.3.5 for the particular case when $(EW) = 3$ g m^{-3}.

A lower limit to the possible growth time may be obtained using an effective (liquid) water content of 4 g m^{-3} corresponding to the mean adiabatic water content. Independent evidence of the unlikelihood of a higher value is provided by the subsequent analysis of stone β. Bearing in mind section 4.5, Fig. 4.1.1 shows that the time taken for the growth of stones α and α' along the relevant W/D

---

*Strictly, between the W/D line and the isopleth of $T_s = -3^{\circ}C$: however the difference is inappreciable.

line for $0.23 < R_3 < 1.06$ and 0.93 cm respectively is 390 and 345 sec, all of which must be accomplished whilst $U_z(z) > \frac{3}{4} U_m$ (especially at larger radii). This phase of growth is represented in Fig. 4.8.4 by the path A_1A_2.

For both stones the outermost layer comprises clear and transparent ice. The wet growth which this implies must have occurred either during a continued (but slower) ascent prior to rising above the -40°C level, or (more likely) during its descent through a diminishing updraught behind the updraught axis. This phase of growth is represented in Fig. 4.8.4 by the path A_2A_3 for stone α, where the radius at A_3 is taken to be 1 mm greater than that observed at the ground in order to take into account the melting incurred during the descent of the stone below the 0°C level. The time spent in growing along A_2A_3 is approximately 280 sec.

An explanation of the increase in the updraught profile experienced by the stone and for the subsequent decrease beyond A_2 may be found in the inclination of the updraught, which caused the stones to cross the axis of the updraught as shown in Fig. 2.12.1.

(2) Analysis of stone β.

Stone β (National Grid Ref. 745 595) had a mass 14.6 g and an axis/diameter ratio, $X(\beta)$, of 1.55. Fig. 4.8.3 shows photographs of a section through its plane of maximum eccentricity. These illustrate the presence of a circular ring of bubbles for $0.5 < R < 0.6$ cm indicating spherical growth at least out to a radius of 0.6 cm.

For lack of any other evidence the technique enunciated in section 4.5.(2) is used whereby a transformation to a spheroid with $X(\beta) = 1.55$ is assumed to have occurred whilst R_3 remained constant at 0.6 cm, so that the remaining growth was such as to maintain the axis/diameter ratio constant at 1.55.

Except when $0.5 < R < 0.6$ cm — when the presence of bubbles suggests growth near the W/D transition — stone β comprised clear ice. It is therefore concluded that it always grew wet, the possibility of spongy growth being disregarded as far as the estimation of the total growth-time is concerned (cf. section 4.6). A one-to-one correlation must therefore be expected between the crystallite size and the ice crystal concentration in the air-stream. Assuming that the crystallites approximated to radially orientated circular cylinders, their mean volume was about 0.004 cm^3, implying an ice crystal concentration of less than 1 per litre. According to Findeisen and Schulz (1944) such a concentration would be exceeded above the $-20^{\circ}C$ level ($z \approx 7$ km) solely as a result of heterogeneous nucleation within an updraught which reaches 5 m sec^{-1} at the cloud base, so that it appears that the growth of stone β was accomplished wholly below the 7 km level. Fig. 4.1.1 then shows that, for growth near the W/D line at R = 0.6 cm and at levels below 7 km, (EW) cannot exceed 3.5 g m^{-3}. However great reliance cannot be placed upon the predicted ice crystal concentrations and so, in order to estimate a lower limit to the possible time, (EW) will again be taken as 4 g m^{-3}. Moreover the limiting case is considered in which growth occurs along the relevant

W/D line whilst 0.2 < R < 0.6 cm. Fig. 4.1.1 then shows that the required growth-time was at least 240 sec, this phase of growth being represented by the path B_1B_2 in Fig. 4.8.4. It is clear from a comparison of the slopes of the W/D lines in Fig. 4.1.1 with those of the growth curves in Fig. 4.3.4 that, irrespective of the actual value of (EW), the wet growth of stone β whilst 0.2 < R < 0.5 cm and its subsequent growth near the W/D line whilst 0.5 < R < 0.6 cm can only be explained provided that $U_z(z) > \frac{3}{4} U_m$.

During the ensuing transition to a spheroid with X = 1.55, which occurs at B_2, R_3 remains at 0.6 cm whilst R increases to 0.93 cm. According to eq. 4.5.21 this takes 75 sec. In order that the stone might remain in the wet growth regime it must not continue to ascend, so that $U_z \leqslant V$ at this position: the linear profile required to satisfy this condition is $U_z(z) \leqslant 0.6\ U_m$. The subsequent wet growth along B_2B_3 (Fig. 4.8.4) with 0.6 < R < 1.2 cm could have been accomplished within about 430 sec if the stone descended through an updraught which steadily declined to about $\frac{1}{2} U_m$.

The minimum growth time (in sec) for stones α and β for (EW) = 4 g m^{-3} are summarized below in Table 4.8.1

TABLE 4.8.1

Stone α	$t(A_1A_2) = 390$	$t(A_2A_3) \sim 280$	$t(A_1A_3) \sim 670$
Stone β	$t(B_1B_2) = 240$	$t(B_2B_3) \sim 430$	$t(B_1B_3) \sim 665$
	$U_z(z) > \frac{3}{4} U_m$	$U_z(z) < \frac{3}{4} U_m$	

Thus although the total growth-times are comparable, stone α grew for a longer time within the core of the updraught.

For (EW) < 4 g m^{-3}, $t(A_2A_3)$ and $t(B_2B_3)$ do not differ appreciably from the above values: $t(A_1A_2)$ and $t(B_1B_2)$ on the other hand are increased in the inverse ratio of the effective water concentrations.

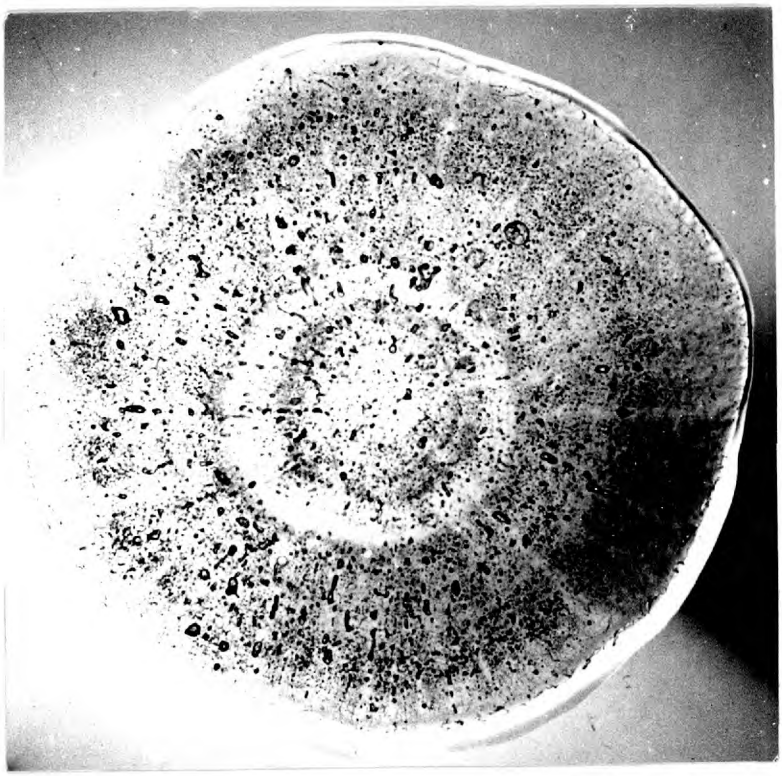

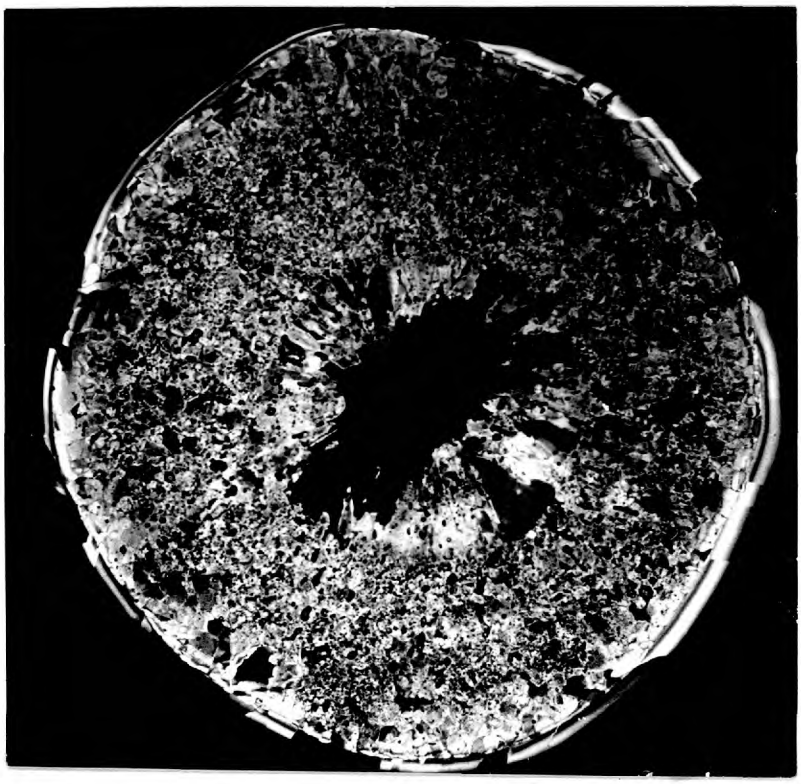

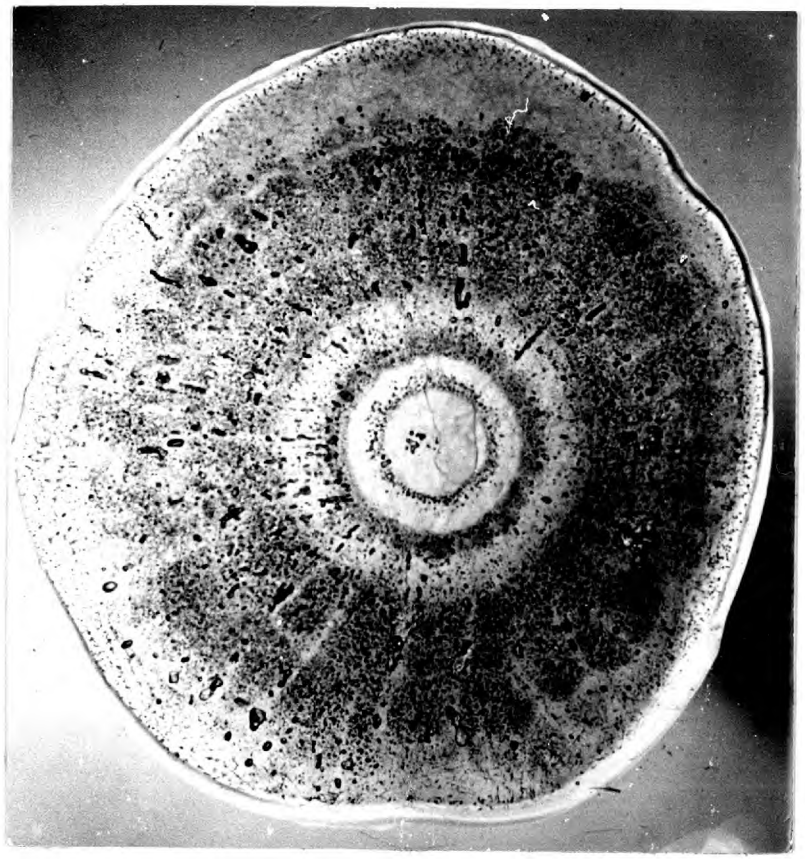

Figs. 4.8.1 and 4.8.2
Sections of stones α and α' in the plane of their longest axes photographed between crossed polaroids to show the constituent crystallites and by transmitted unpolarized light to show the bubble structures. Magnification: ~~x 5~~ × 3.25

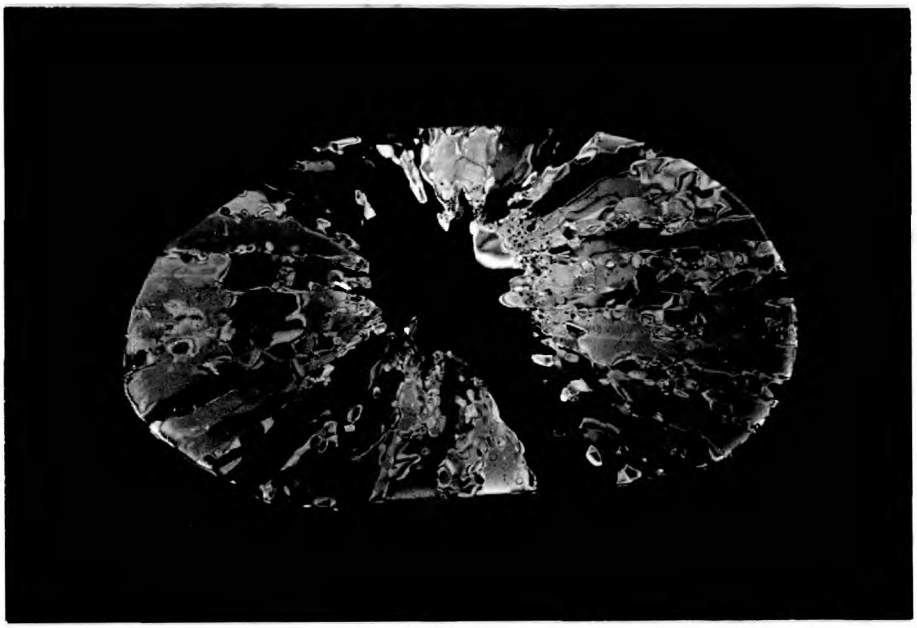

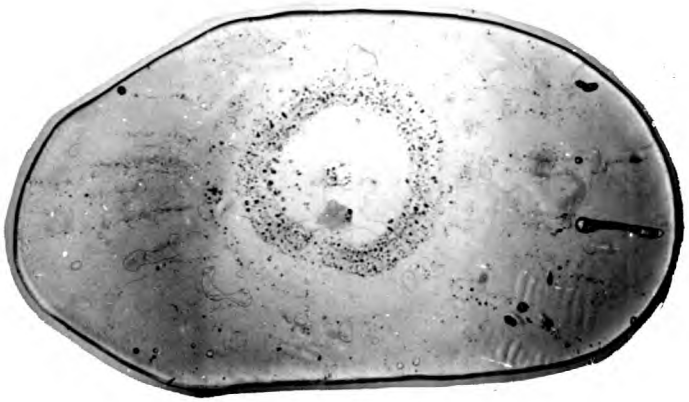

Fig. 4.8.3
Section of stone β in the plane of maximum eccentricity photographed between crossed polaroids to show the constituent crystallites and by transmitted unpolarized light to show the bubble structure. Magnification: x 2.5.

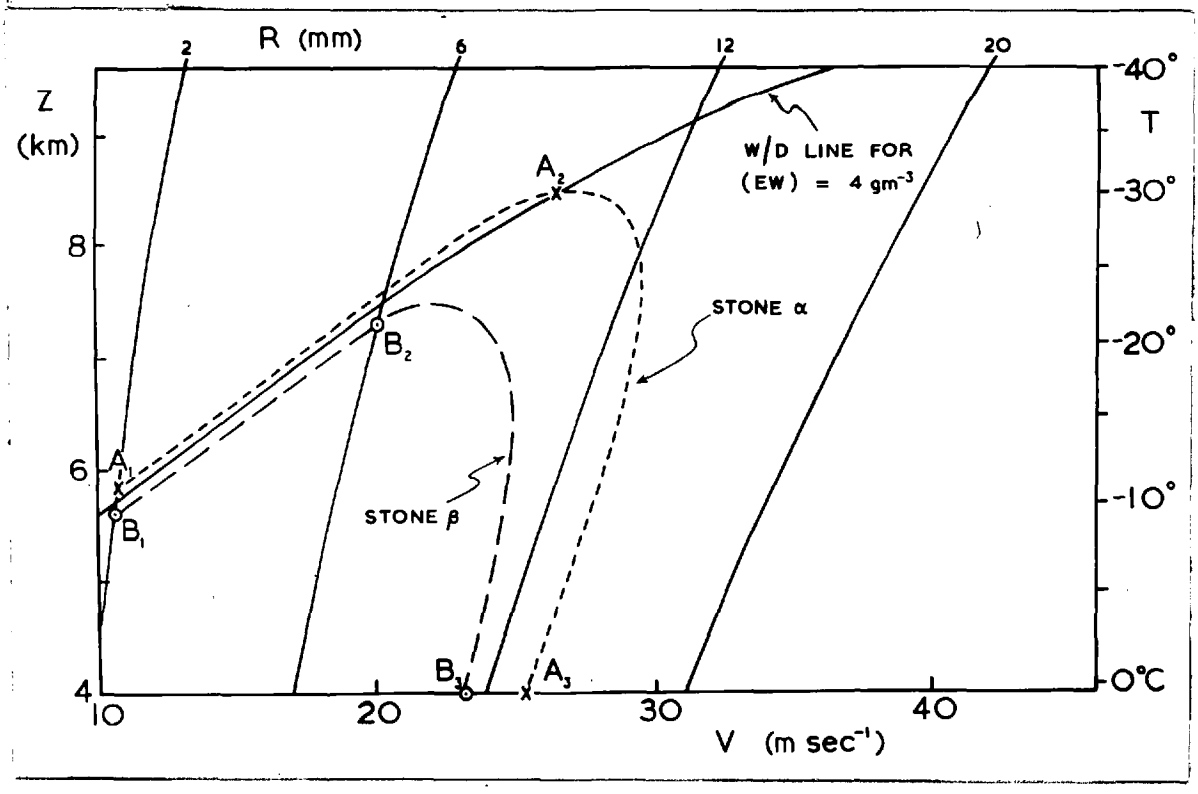

Fig. 4.8.4
The growth of the Wokingham hailstones α and β represented in the z-V plane assuming (EW) = 4 g m^{-3}.

9 An estimation of the inclination of the updraught within the Wokingham supercell

The radar data combined with a consideration of the structure of the largest hailstones have enabled the vertical updraught velocity above the forward overhang to be specified approximately (section 4.4), and continuity considerations have given an indication of the total updraught flux and hence its speed in this region (section 2.12). A further useful constraint upon the form of this part of the updraught is supplied by the analysis in section 4.8, as is now shown.

The radar data indicate that the updraught associated with the supercell was quasi-steady: it will therefore be assumed that $\frac{\partial U_z}{\partial t}$ was negligible. They also showed that there was a horizontal component of velocity within the updraught, U_x, directed towards the rear of the storm at all medium and low levels. Therefore, if it is assumed that the profile of vertical velocity, $U_z(z)$, along streamlines away from the updraught axis was linear and some fractional value of that along the axis, U_m, then any temporal rate of change in U_z for the local environment of the hailstones must have been due to a non-zero U_x given by

$$\frac{d}{dt} U_z(z) = U_x \frac{d}{dx} U_z(z) \qquad 4.9.1$$

Thus if a change of vertical velocity, ΔU_z, occurred in a time Δt and in a horizontal distance Δx, then the mean horizontal velocity over this distance is given by

$$\overline{U_x(x,z)} = \frac{\Delta x}{\Delta t} \qquad 4.9.2$$

Δx may be estimated to a first approximation from the two-dimensional model of the updraught obtained using a plausible updraught tilt; it can then be used to estimate $\overline{U}_x$ and hence an approximate updraught inclination; this in turn may be used to refine the initial model, from which a better estimate of Δx can be obtained, and so on. Δt can be estimated from the analysis of the internal structure of the hailstones (section 4.8). In order that reliable results may be obtained it is necessary to consider quite large increments of U_z, so that Δx and Δt are also large. Consequently in section 4.8 hailstone growth has been considered on either side of the updraught axis whilst $U(z) > \frac{1}{4}U_m$: during this phase z varied by several km, so that the horizontal velocity deduced is a mean value over a considerable height interval.

Of all the hailstones collected, α remained longest within the region where $U_z(z) > \frac{1}{4} U_m$, so that it is upon this stone that the estimate of an upper limit to $\overline{U}_x$ must be based. The phase of growth for which $U_z(z) > \frac{1}{4} U_m$ lasted for 390 secs (section 4.8): it is represented in Fig. 4.8.4 by the path A_1A_2, which shows that the stone was ascending in the interval $5.8 < z < 8.5$ km. Reference to Fig. 2.12.1 (applying a suitable correction to take into account additional flux entering the section at higher levels) then shows that $\Delta x = x(A_1) - x(A_2) \approx 3$ km. Consequently eq. 4.9.2 gives $\overline{U_x(A_1A_2)} \approx 8$ m sec^{-1}. This is an upper limit based upon an effective water concentration of 4 g m^{-3}: however it has been shown that 3 g m^{-3} is a more likely value, in which case $\overline{U_x(A_1A_2)} \approx 6$ m sec^{-1}. The model of the air-flow within the updraught presented in Fig. 2.12.1 is drawn accordingly.

CHAPTER V

SOME SIDE-EFFECTS OF THE GROWTH OF HAIL

1. Ice Crystal Production and charge separation within updraughts

Latham and Mason (1961a and b) have shown that in certain circumstances the freezing of supercooled droplets on an artificial pellet of soft hail is accompanied by the ejection of ice splinters. They find that the splinters normally carry away a ~~negative~~ positive charge leaving the hailstone with a net ~~positive~~ negative charge — an effect which they ascribe to the greater mobility of protons over that of hydroxyl ions, causing the preferential migration of protons under the influence of transient temperature gradients. They have shown that the rates of charging and splinter production are insensitive to variationsin the droplet radius (r) and their impact velocity (V), provided that $25 < r < 50\mu$ and $5 < V < 20$ m sec^{-1}, but that they rapidly decrease outside of these ranges. Latham and Mason have also investigated the dependence upon the air-temperature (T). (Actually the splinter production is a function of the surface temperature of the hailstone (T_s), but because of the slow rates of accretion employed in their experiments, T_s was practically equal to T). It appears that there is negligible splinter production when $T_s > -2^{\circ}C$, and that their rate of production increases rapidly at lower temperatures reaching an average of between 12 and 14 splinters per droplet at $-6^{\circ}C$ and below (for the ranges of r and V previously mentioned). These findings are now utilized to infer the variation with height of the steady state ice crystal concentration which might be expected to arise within a

virtually steady updraught of the kind associated with the Wokingham supercell.

Consider an updraught within which is evenly distributed an exponential size-spectrum of hailstones (at all levels above a height z_o) such that the concentration of stones within the radius interval (R, dR) is given by

$$N(R) = N_o \exp - \Lambda R \qquad 5.1.1$$

where N_o and Λ are constants, independent of position within the updraught.

The fractional volume swept out per unit time by hailstones in the size range $(0,R_1)$ at a height z is given by

$$F(R_1,z) = \int_o^{R_1} (\pi R^2) V(R,z) N(R) dR \qquad 5.1.2$$

where V(R,z) is the hailstone fall-speed. Assuming that the stones are spherical, and substituting in eq. 5.1.2 from eq. 4.1.10, as well as from 5.1.1, gives

$$F(R_1,z) = \int_o^{R_1} f(R,z) dR \qquad 5.1.3$$

where

$$f(R,z) = \pi N_o \left(\frac{8g\bar{s}}{3C_D\rho}\right)^{1/2} R^{5/2} \exp - \Lambda R \qquad 5.1.4$$

On integrating this becomes

$$F(G_1,z) = A\left\{\frac{15}{16}\sqrt{\pi}\, erf\, G_1 - (\exp - G_1^2)\left[\tfrac{1}{2}G_1^5 + \tfrac{5}{4}G_1^3 + \tfrac{15}{8}G_1\right]\right\} \qquad 5.1.5$$

where

$$A(z) = \frac{2\pi N_o}{\Lambda^{7/2}}\left(\frac{8g\bar{s}}{3C_D\rho}\right)^{1/2} \qquad 5.1.6$$

and

$$G_1 = (\Lambda R_1)^{1/2} \qquad 5.1.7$$

The fractional volume swept out per unit time by all hailstones

at height z is given by

$$F_\infty(z) = \lim_{G_1 \to \infty} F(G_1, z) = \frac{15}{16}\sqrt{\pi}\, A(z) \qquad 5.1.8$$

Consider droplets with $25 < r < 50\mu$ present in a concentration which in the absence of hail would have been constant at about n_o. In the presence of the exponential hail spectrum this is reduced to

$$n(z) = n_o \exp -L_\infty(z, z_o) \qquad 5.1.9$$

where
$$L_\infty = \int_{z_o}^{z} F_\infty(z) \,/\, U_z(z)\, dz \qquad 5.1.10$$

z_o being the height of the lowermost tip of the forward overhang in the case of the Wokingham storm.

The mean number of splinters ejected each time one of these is accreted by a hailstone, x_s, is a known function of the surface temperature of the hailstone, T_s, and hence of the effective water concentration (EW), R and z. Therefore, assuming the collection efficiency for the droplets to be unity, the number of splinters produced between z_1 and $z_1 + \delta z$ in time δt per unit horizontal cross-sectional area is given by

$$\left\{ F_s(z_1)\, n(z_1)\, \delta z\, \delta t \right\}$$

where
$$F_s(z_1) = \int_R f(R, z_1)\, x(T_s)\, dR, \qquad 5.1.11$$

$f(R, z_1)$ is given by eq. 5.1.4, and T_s is obtained as a function of R, z_1 and (EW) from eq. 4.1.7. This number of splinters will be contained within the volume of air ascending past the level z_1 per unit horizontal cross-sectional area during the same period, i.e. $U_z(z_1)\, \delta t$.

Thus the concentration of splinters at a height z ($\geq z_1$) owing to the splinters produced between z_1 and $z_1 + \delta z$ is given by

$$C(z,z_1)\,\delta z = \left\{ \frac{F_s(z_1)\,n(z_1)}{U_z(z_1)} \right\} \delta z \exp - L_w(z,z_1) \qquad 5.1.12$$

where the additional exponential term takes into account the subsequent loss of some of the splinters owing to collection by the wet hailstones, so that

$$L_w = \int_{z_1}^{z} \frac{F_w(z)}{U_z(z)}\, dz \qquad 5.1.13$$

where
$$F_w(z) = \int_{R_c}^{\infty} f(R,z)\, dR \qquad 5.1.14$$

and R_c is the critical radius at which the hailstone radius is just wet at the level z.

Finally, the total concentration of splinters at a height z arising from splinters produced at all levels above z_o is given by

$$S(z) = \int_{z_o}^{z} C(z,z_1)\, dz \qquad 5.1.15$$

The above analysis is now applied to the special case of the Wokingham supercell to determine the variation of splinter concentration along the updraught axis. The following assumptions are made;

(1) that the exponential spectrum of hail size, found by Ludlam and Macklin to apply to both the Horsham storm of 5 September 1958 and the Wokingham storm, was valid at all levels within the updraught above the tip of the forward overhang, so that $N_o = 8 \times 10^{-5}$ cm^{-4} and

$\Lambda = 4.54\ cm^{-1}$ for $z \geqslant 4$ km (Atlas and Ludlam, 1961); and (2) that the hailstones were spherical with a drag coefficient (C_D) of 0.6 and a mean density ($\bar{\rho}$) of 0.9 g cm^{-3}.

Using these two assumptions eq. 5.1.5 has enabled the calculation of $F(R_1,z)$, which is shown in Fig. 5.1.1 as a function of R_1 at a level. where the air density (ρ) is 10^{-3} g cm^{-3}.

A third assumption is that the critical radius (R_C) and the surface temperature (T_s) at other radii were those given by Fig. 4.1.2 assuming an effective liquid water content of 3 g m^{-3}. Using this further assumption eqs. 5.1.8 and 5.1.14 have enabled the derivation of Fig. 5.1.2 which shows as a function of height the fractional volumes swept out per unit time by all hailstones (F_∞), and also by the wet hailstones alone (F_w) and the dry hailstones alone, F_D.

Fig. 5.1.3 shows isopleths of T_s in the R-z plane derived from eq. 4.1.7 assuming (EW) = 3 g m^{-3}. On the right are tabulated as a function of T_s the values of x_s determined experimentally by Latham and Mason (1961b) for droplets in the size range $25 < r < 50\mu$. Together with values of $F(R_1,z)$ from Fig. 5.1.1 these have enabled the derivation of the contributions to F_s at 1 km height intervals from stones within various ranges of T_s (see also Fig. 5.1.3). The trend with height of the total value of F_s is shown in Fig. 5.1.4.

The profile of vertical velocity along the updraught axis is taken as that given by eq. 4.4.1. During their ascent within such an updraught the concentration of droplets is assumed to have decreased below that at the tip of the forward overhang owing to collection by

hail, which reduces their numbers by a factor $\exp\{-L_\infty\}$ given from eq. 5.1.10. Calculating this on the basis of the above assumptions leads to the variation with height shown by curve B of Fig. 5.1.5. The ratio (S/n_o) which results from the application of eq. 5.1.15 is plotted in curve B of Fig. 5.1.6.

Probably the least reliable parameters involved in the derivation of these two curves are N_o and $U_z(z)$. Now these always appear in the combination $(N_o/U_z(z))$, so that the effect upon the splinter concentration of a variation in each of these may be considered together. To this end curves A, C and D have been plotted in Figs. 5.1.5 and 5.1.6 for values of $(N_o/U_z(z))$ corresponding to 2, ½ and ¼ times the value assumed in the derivation of curve B. Now increasing this ratio increases the rate of production of splinters per unit droplet concentration, F_s, but it also increases the rate of depletion of the droplet concentration, n, (see Fig. 5.1.5) as well as the rate of collection of the splinters by wet hail. The net result of these opposing effects is that the splinter concentration decreases for values of $(N_o/U_z(z))$ on either side of that corresponding to curve C, the dependence not being a sensitive one. Curve C may therefore be taken as the upper limit to the ice splinter concentration that can be generated by this mechanism: evidently $S < n_o$, $1/3\, n_o$, $1/100\, n_o$ for $T > -30$, -20, and $-10^\circ C$ respectively.

The above splinter concentrations have been deduced on the assumption that the concentration of droplets decreased exponentially with height owing to collection by hail. However this probably underesti-

mates the concentration since it is likely that fresh droplets of radius approaching 25μ were continually appearing owing to their continued growth throughout their ascent within the updraught. Consequently curves A,B,C and D in Fig. 5.1.6 have been recomputed on the alternative assumption that the droplet concentration remained constant at η_o. The resulting curves (A',B',C' and D') are shown in Fig. 5.1.6: they represent an upper limit. Evidently however these values do not exceed those previously obtained by more than a factor of about 4 at the -20°C level, so that (S/η_o) is still unlikely to have significantly exceeded unity at this level.

The largest source of error in the estimation of the splinter concentration, S, lies in the value of η_o. This is because few observations of droplet concentrations within cumulonimbus have been made and the applicability of even these is uncertain owing to a lack of adequate knowledge as to the part of the updraught which has been sampled. Now the hypothesis was made in section 4.2 that every ice crystal accreted by a hailstone which is growing wet would create a fresh crystallite within the hailstone structure. From the analysis of actual hailstones it has been established that the water content in the growth region was about 3 and no more than 4 g m^{-3}, so that according to this hypothesis the mean volume of the individual crystallites within stones growing wet at the -20°C level was such as to imply a maximum ice crystal concentration in the free air of only 1 per litre at this level. (This assumes a collection efficiency of unity for ice particles with wet hailstones, which is reasonable in

view of the rapid growth which ice crystals undergo in an environment saturated with respect to water). This is no more than the concentration which Findeisen and Schulz (1944) have shown to arise at the same level solely as a result of heterogeneous nucleation in an updraught which attains a rising speed of 5 m sec^{-1} at cloud-base level. It therefore appears that if the splintering mechanism was operative then n_o cannot have significantly exceeded 1 per litre. Alternatively Fig. 5.1.3 shows that the low splinter concentration at the 7 km level could have arisen in the presence of larger concentrations of droplets if there had been a dearth of stones with $R < 4$ mm within the updraught below this level. This possibility cannot be ruled out since the supply of embryos of a suitable size at the foot of the updraught may have been restricted.

The rate of separation of charge per unit volume is given by $F_s(z)n(z)q$, where q is the average charge on a splinter ——— 2.5×10^{-7} e.s.u according to Latham and Mason (1961). Therefore substituting for $F_s(z)$ from Fig. 5.1.4 and taking the mean horizontal dimension of the updraught as 7 km, it follows that even a constant value of 1 per litre for n would give rise to the separation of a total charge of only 10^{-3} coulomb sec^{-1} throughout the whole updraught. This is inadequate by about 3 orders of magnitude to account for the observed (rather modest) rate of discharge of a few flashes per minute associated with the Wokingham storm as a whole. In order to account for the bulk of this charge separation it would seem necessary to consider the edges of the main updraught or any region where the updraughts

were of limited extent or duration. Here the concentration of liquid water is likely to have been smaller with the result that the proportion of stones growing dry would have been far larger, especially at low levels. For instance, a decrease in (EW) from 3 to 1 g m^{-3} at the $-5^{\circ}C$ level causes R_c to increase from about 1 to 5 mm with the result that F_D is enhanced by a factor of 170 at this level (neglecting any decrease in F_D owing to a smaller value of N_o).

However increasing F_D to account for the rate of separation of charge inevitably results in increased splinter concentrations in these regions, an effect which is magnified where the updraught velocities are small. Indeed a simple order of magnitude calculation indicates that there is no way of accounting for the observed rate of charge separation in terms of the splintering mechanism which does not involve the development of high concentrations of splinters in these regions. Thus if α_s and n are each taken to be independent of height, the total rate of charge separation is given by

$$\frac{dQ_c}{dt} = A q \alpha_s n \int_z F_D(z)\, dz \qquad 5.1.16$$

where the integration extends throughout the depth of the supercooled region. Moreover, neglecting sweeping up by wet hail[1], the splinter concentration near the top of this region is given by

$$S_{max} = \alpha_s n \int_z \frac{F_D(z)}{U_z(z)}\, dz \qquad 5.1.17$$

---

[1] Owing to the low concentration of wet hail at the high levels from which come the dominant contribution to S_{max}, sweeping up cannot account for more than a 4-fold diminution in S_{max} even for values of N_o as high as those corresponding to curve A in Fig. 5.1.6

Equations 5.1.16 and 5.1.17 then give an approximate mean value of the vertical updraught velocity as

$$\bar{u}_z \sim \int_z F_b(z)dz \Big/ \int_z \frac{F_b(z)dz}{u_z(z)} = \frac{dQ_c}{dt} \Big/ A\, q\, S_{max} \qquad 5.1.18$$

This shows that the separation of 1 coulomb sec^{-1} can only be accomplished provided $S_{max} \geqslant 10\ cm^{-3}$ if $\bar{u}_z \sim 10\ m\ sec^{-1}$ and $A \leqslant 100\ km^2$. The adiabatic water concentration distributed amongst such a concentration of splinters would give a population with a mean volume radius of less than 50μ. As this is unreasonable it seems doubtful whether the splintering mechanism (as conceived at present) can in any way account for the required total rate of charge separation.

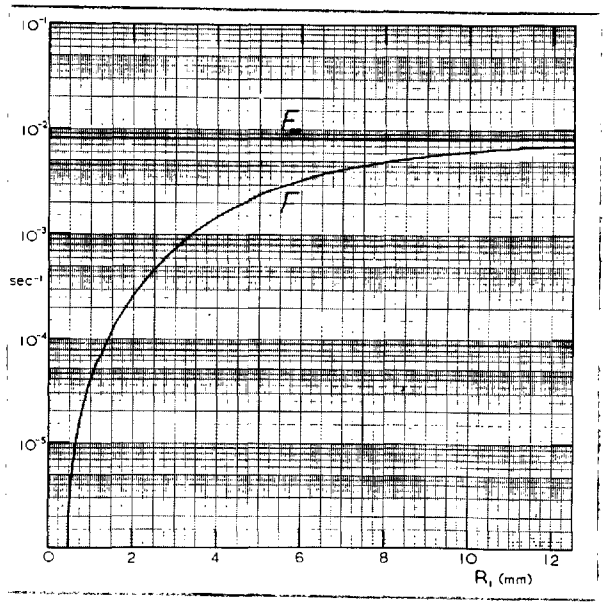

Fig. 5.1.1
The fractional volume F swept out per unit time by those hailstones within the exponential Horsham-Wokingham spectrum whose radii is less than R_1 (as a function of R_1 at a level where the air density (ρ) is 10^{-3} g cm^{-3}.

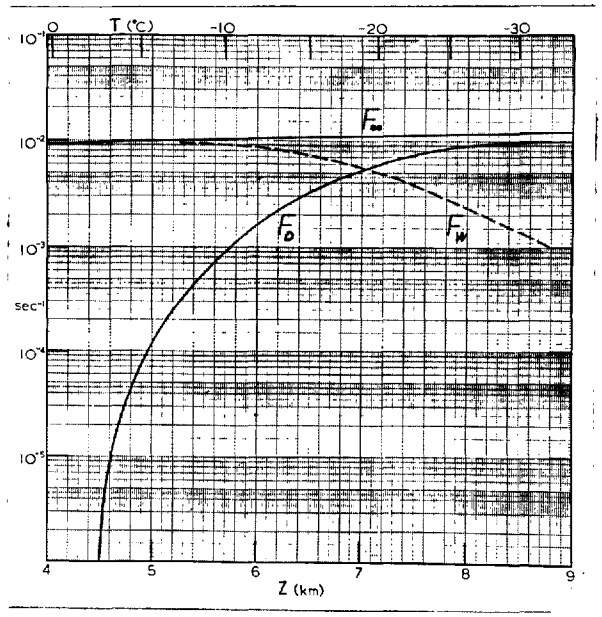

Fig. 5.1.2.
The fractional volumes swept out per unit time by all hailstones (F_∞), by the wet hailstones alone (F_W) and by the dry hailstones alone (F_D), as a function of height.

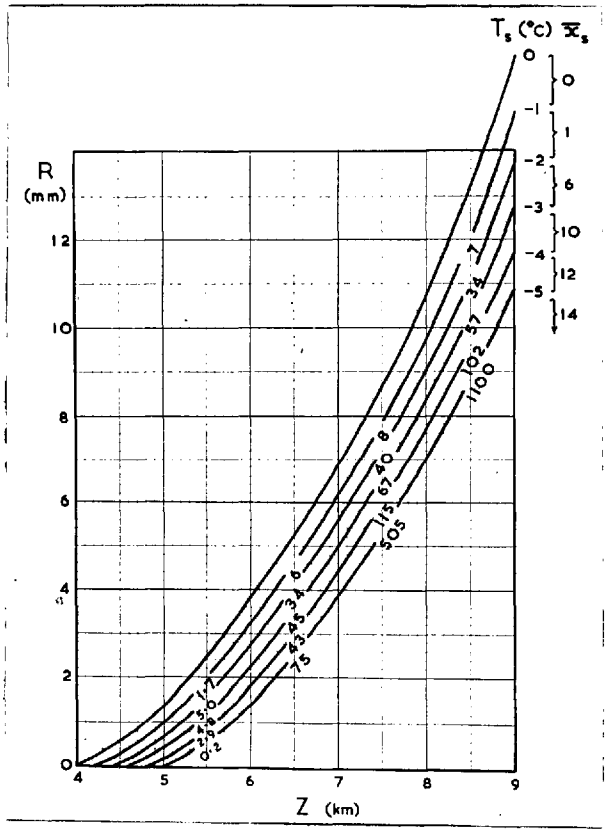

Fig. 5.1.3
Isopleths of T_s in the R-z plane for an effective liquid water concentration (EW) of 3 g m^{-3}. On the right are tabulated as a function of T_s the mean number of splinters ejected per accreted droplet ($\bar{x}_s$), as determined experimentally by Latham and Mason for droplets in the size range $25 < r < 50\mu$. Also indicated are the contributions at various levels towards F_s from stones with different surface temperatures.

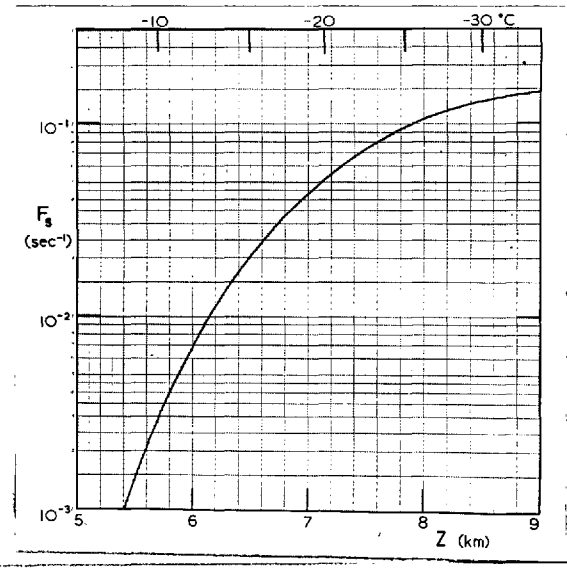

Fig. 5.1.4
Rate of splinter production per unit volume per unit concentration of droplets in the range $25 < r < 50\mu$ as a function of height.

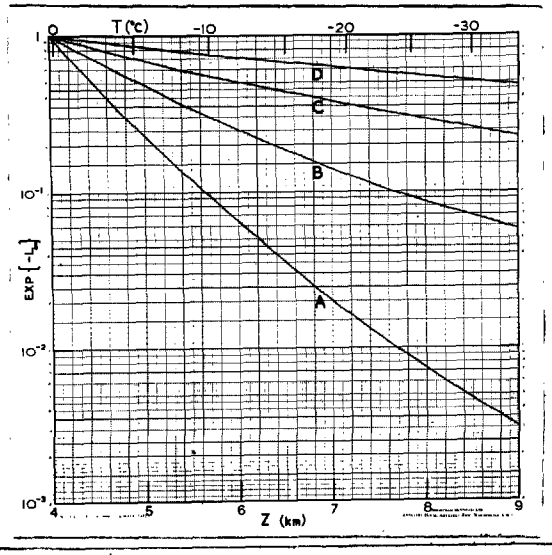

Fig. 5.1.5
Variation with height of the factor by which the concentration of droplets is reduced owing to sweeping up by hailstones. Curves A,B,C and D refer to different values of the ratio $N_o/U_z(z)$, (see p:213).

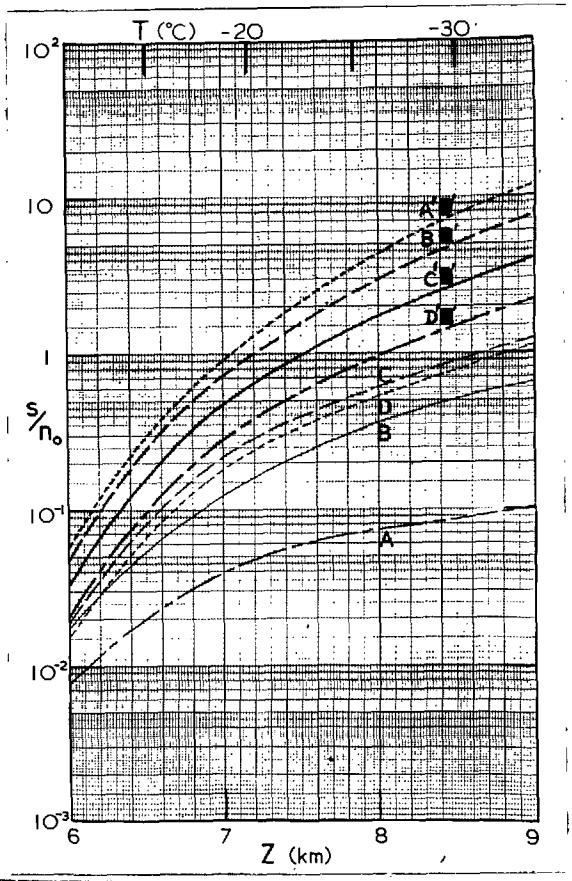

Fig. 5.1.6
Variation with height of the ratio of the concentration of splinters to that of droplets in the size range $25 < r < 50\mu$. The primed and unprimed series of curves respectively were derived assuming a constant droplet concentration and one which decreased exponentially with time. The various curves within each series refer to different values of the ratio $N_o/U_z(z)$, (see p. 213).

2. The quantity of water shed by hail growing wet

When all the accreted water is retained a hailstone grows according to the equation

$$\frac{dR}{dt} = \frac{(EW)\ V(z)}{4\bar{\delta}} \qquad 5.2.1$$

If it is assumed that all the water which cannot be frozen is shed, then a hailstone grows according to the equation

$$\frac{dR}{dt} = \frac{W_c(V,z)\ V(z)}{4\bar{\delta}} \qquad 5.2.2$$

where the critical water content, W_c, is given by eq. 4.1.12. The quantity of water shed in unit time by a hailstone of radius R is therefore given by

$$m_s(R,z) = 4\pi R^2 \frac{V(z)}{4\bar{\delta}} \left[(EW) - W_c(V,z)\right] \qquad 5.2.3$$

Substituting for V(z) from eq. 4.1.10 then gives

$$m_s(R,z) = \chi R^{5/2} \left[(EW) - W_c(R,z)\right] \qquad 5.2.4$$

where

$$\chi = \left(\frac{8\pi^2 g}{3C_D \rho \bar{\delta}}\right)^{1/2} \qquad 5.2.5$$

If the concentration of hailstones per unit size range is given by N(R) throughout an updraught whose profile of vertical velocity is $U_z(z)$, then (neglecting the fall-speed of the shed droplets) the concentration of water at a height z which has been shed between this level and some lower level, z_o, is given by

$$\int_{z_o}^{z} M_s\, dz = \int_{z_o}^{z} \int_{R=0}^{\infty} \frac{m_s(R,z)\, N(R)}{U_z(z)}\, dR\, dz \qquad 5.2.6$$

where M_s is the mass of water shed per unit volume of air during its ascent through a unit height interval.

During the intense phase of the Wokingham storm the lowermost tip of the forward overhang remained around the 4 km (0°C) level, so that $M_s(z,z_o)$ has been computed with z_o = 4 km. Consequently if $U_z(z)$ is given by eq. 4.4.1 and (EW), C_D and $\bar{\delta}$ respectively are taken as 3.5 g m^{-3}, 0.6 and 0.9 g cm^{-3}, then the quantity of water shed at various levels is that shown in Fig. 5.2.1. Evidently a large proportion of the liquid water content is swept up by the hail and shed again between the 0 and -10°C levels.

According to Weikmann and auf Kampe (1953) droplet concentrations much in excess of 100 cm^{-3} are unlikely to occur within cumulonimbus. However if an effective water content of 3.5 g m^{-3} is distributed evenly amongst this number of droplets their radius would be 20μ. Now it was shown in the previous section that a concentration of ice splinters would arise at the -20°C level which is comparable with that of the droplets in the range $25 < r < 50\mu$. Although zero at smaller radii, the mean number of splinters ejected by each accreted droplet of radius 15μ is still as much as ½ x_s, so that in the event of an even distribution of the water content amongst the droplet population an ice splinter concentration equal to more than half that of the droplets would result. Therefore in order to avoid excessive concentration of ice crystals, it is necessary to find a mechanism capable of reducing the numbers of droplets within this size range — and this must be accomplished within the 400 seconds taken by the updraught to rise from the cloud base to the -20°C level. Such a mechanism is available when the tip of the forward overhang lies as low as the

$0^{\circ}C$ level, for the presence of hail within the updraught at low levels causes the water content of the majority of the original small droplets to be redistributed amongst droplets whose predominant radius would almost certainly be greater than 50μ. In general, where no overhang is supported, precipitation descends through the updraught at much lower levels with the result that this mechanism is then even more important.

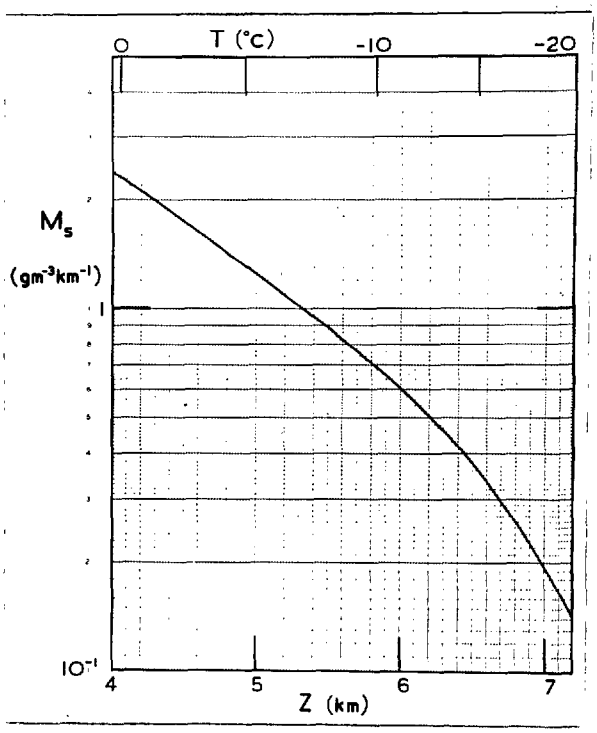

Fig. 5.2.1.
Vertical variation of the mass of water shed by the exponential Horsham-Wokingham hail spectrum into a unit volume of air during its ascent through a unit height interval. It has been assumed that (EW) = 3.5 g m^{-3} and that all unfrozen water is shed.

ACKNOWLEDGEMENTS

It is with the utmost pleasure that I acknowledge the friendly guidance of Dr. F.H. Ludlam during this research. I am also very grateful for the many helpful discussions with Drs. David Atlas and W.C. Macklin.

For financial support I am indebted to D.S.I.R.

The observational work was undertaken in collaboration with the British Meteorological Office at their East Hill Radar Station (Officer in Charge: W.G. Harper), and was supported by the Geophysics Research Directorate, Air Force Cambridge Research Center of the Air Research and Development Command, United States Air Force.

The British Rainfall Organisation kindly provided data from their observers: I am also grateful for the many painstaking records provided by a large number of voluntary hail observers, and to Mr. D.A. Rogers and Dr. W.C. Macklin who undertook most of the work of interrogation in the area severely affected by the Wokingham storm.

Finally I would like to thank Dr. W.C. Macklin for permission to reproduce photographs of hailstone sections.

REFERENCES

Atlas, D. & Ludlam, F.H.	1961	"Multi-wavelength radar reflectivity of hailstorms", Quart. J.R. Met. Soc., 87, p.523
Atlas, D., Harper W.G., Ludlam, F.H.	1960	"Radar scatter by large hail". Quart. J.R. Met. Soc., 86, p.468.
Atlas, D., & Mossop, S.C.	1959	"Calibration of a weather radar by using a standard target". Bull. Amer. Met. Soc., 41, p.377
Booker, H.G.	1951	"Meteorological aspects of propogation problems". Compendium of Meteorology, Amer. Met. Soc., pp. 1290-1296.
Byers, M.R. & Braham, R.R.	1949	"The Thunderstorm", Thunderstorm Project, Washington.
Craddock, J.M.	1949	"The development of cumulus cloud", Quart. J.R. Met. Soc., 75, p.147
Cunningham, R.M.	1960	"Hailstorm structure viewed from 32,000 ft", Geophys. Monograph No.5, Amer.Geophys. Un., Washington, D.C.
Dessens, H.	1960	"Severe hailstorms are associated with very strong winds between 6,000 and 12,000 m, Geophys. Monograph No.5, Amer. Geophys. Un., Washington, D.C.
Donaldson, R.J. Jr, Chmela A.C. & Shackford, C.R.	1960	"Some behaviour patterns of New England hailstorms", Geophys. Monograph No.5, Amer. Geophys. Un., Washington, D.C.
Findeisen, W. & Schulz, G.	1944	"Experimentelle untersuchunger über die atmosphärische eisteilchenbildung I", Forsch.u.Erfahr. Reichsamt f. Wetterdienst, A, 27.
Frössling, N.	1938	"Uber die Verdunstung fallender Tropfen", Beitr. Geophys. 52, p.170.

Fujita, T. & Byers, H.R.	1960	"Model of a hail cloud as revealed by photogrammetric analysis", Tech. Rep. 3 Contract Cwb 9762, Univ. of Chicago.
Gibson, W.S.	1863	"Hailstorms and their phenomena", Miscellanies, Longman, Green, Longman, Roberts and Green, London.
Hallett, J.	1960	"Crystal growth and the formation of spikes on the surface of supercooled water". J. Glaciol., 3, No.28, p.698
Howell, W.E.	1960	"Cloud seeding in the American Tropics", Geophys. Monograph No.5, Amer. Geophys. Un., Washington, D.C.
Jones, D.M.A.	1956	"Rainfall drop size-distribution and radar reflectivity", Met. Lab. Res. Rep. No.6, Illinois State Water Survey, Urbana, Illinois.
Jones, R.F.	1960	"Size-distribution of ice crystals in cumulonimbus clouds", Quart.J.R.Met. Soc., 86, p.187
Kramers, H.	1946	"Heat transfer from spheres to flowing media", Physica, 12, p.61
Latham, J. & Mason, B.J.	1961a	"Electric charge transfer associated with temperature gradients in ice", Proc. Roy., Soc., A, 260, p.523.
Latham, J. & Mason, B.J.	1961b	"Generation of electric charge associated with the formation of soft hail in thunderclouds", Proc. Roy. Soc. A, 260, p.537
Ligda, M.G.H. & Mayhew, W.A.	1954	"On the relationship between the velocities of small precipitation areas and the geostrophic winds". J. Met., 11, p.421.
List, R.	1961	"On the growth of hailstones", Nubila, 4, p.29

Ludlam, F.H.	1950	"The composition of coagulation — elements in cumulonimbus", Quart. J.R.Met. Soc., 76, p.52
Ludlam, F.H.	1958	"The hail problem", Nubila, 1, p.12.
Ludlam, F.H.	1960	"The role of radar in rainstorm forecasting", Nubila, 3, p.53.
Ludlam, F.H. & Macklin, W.C.	1959	"Some aspects of a severe storm in S.E. England". Nubila, 2, p.38.
Ludlam, F.H. & Saunders, P.M.	1956	"Shower formation in large cumulus", Tellus, 8, p.424.
Macklin, W.C.	1960	"The growth of hail", Ph.D. thesis, University of London.
Macklin, W.C. & Ludlam, F.H.	1961	"The fallspeeds of hailstones", Quart. J.R. Met. Soc., 87, p.72
Macklin, W.C. Strauch, E, & Ludlam, F.H.	1960	"The density of hailstones collected from a summer storm", Nubila, 3, p.12
Marriott, W.	1892	"Report on the thunderstorms of 1888 and 1889", Quart. J.R. Met. Soc., 18, p.23.
Mason, B.J.	1957	"The physics of clouds". Clarendon Press
Mathun, L.S., & Kulshrestha, S.M.	1961	"On super-refraction after the passage of a thunderstorm", Indian J. Met. Geophys., 12, 1, p.71.
Newton, C.W.	1960	"Morphology of thunderstorms and hailstorms as affected by vertical wind shear", Geophys. Monograph No.5, Amer. Geophys. Un., Washington, D.C.
Newton, C.W. & Katz, S.	1958	"Movement of large convective rainstorms in relation to winds aloft". Bull. Amer. Met. Soc., 39, p.129.

Normand, Sir Charles	1946	"Energy in the atmosphere", Quart. J.R. Met. Soc., 72, p.145
Prohaska, K.	1905	"The direction, strength and speed of hailstorms", Met. Zeit, 22, p.519
Prohaska, K.	1907	"The hail fall of 6 July, 1905 in the east Alps", Met. Zeit, 24, p.193
Ramaswamy, C.	1956	"On the sub-tropical jet stream and its role in the development of large-scale convection", Tellus, 8, p.26
Shelley, Percy Bysshe	1820	"The cloud", published with "Prometheus Unbound".
Thorkelsson, T.	1946	"Cloud and shower", Quart. J.R. Met. Soc., 72, p.332
Weickmann, H.K. & aufm Kampe, H.J.	1953	"Physical properties of cumulus clouds", J. Met. 10, p. 204.
Wichmann, H.	1948	"Grundprobleme der physik des Gewitters" Wolfenbütteler Verlagsanstalt, Hanover.